Discovery and ADME profiling of CNS-active natural products

Inauguraldissertation

zur

Erlangung der Würde eines Doktors der Philosophie

vorgelegt der

Philosophisch-Naturwissenschaftlichen Fakultät

der Universität Basel

von

Fahimeh Moradiafrapoli

aus Mazandaran, Iran

Basel, 2019

Genehmigt von der Philosophisch-Naturwissenschaftlichen Fakultät

auf Antrag von

Prof. Dr. Matthias Hamburger

Prof. Dr. Muriel Cuendet

Basel, den 22.05.2018

Prof. Dr. Martin Spiess

Dekan

Attribution-NonCommercial-NoDerivatives 3.0 Switzerland
(CC BY-NC-ND 3.0 CH)

You are free: to Share — to copy, distribute, and transmit the work

Under the following conditions:

Attribution — You must attribute the work in the manner specified by the author or licensor (but not in any way that suggests that they endorse you or your use of the work).

NonCommercial — You may not use this work for commercial purposes.

NoDerivatives — You may not alter, transform, or build upon this work.

With the understanding that:

- **Waiver** — Any of the above conditions can be **waived** if you get permission from the copyright holder.
- **Public Domain** — Where the work or any of its elements is in the **public domain** under applicable law, that status is in no way affected by the license.
- **Other Rights** — In no way are any of the following rights affected by the license:
  - Your fair dealing or **fair use** rights, or other applicable copyright exceptions and limitations;
  - The author's **moral** rights;
  - Rights other persons may have either in the work itself or in how the work is used, such as **publicity** or privacy rights.
- **Notice** — For any reuse or distribution, you must make clear to others the license terms of this work. The best way to do this is with a link to this webpage.

Source: https://creativecommons.org/licenses/by-nc-nd/3.0/ch/deed.en Date: 12.11.2013

Table of Contents

LIST OF ABREVIATIONS..... 3

SUMMARY..... 4

ZUSAMMENFASSUNG..... 6

1. AIM OF THE WORK..... 9

2. INTRODUCTION..... 13

2.1. Natural products in CNS-active drug discovery..... 14

Challenges and opportunities..... 14

Discovery of novel leads..... 16

Neuroactive leads..... 17

2.2. The $GABA_A$ receptor..... 22

Structure and pharmacology..... 22

In vitro $GABA_A$ receptor modulation models..... 23

In vivo GABAergic activity models..... 25

Promising NP-based $GABA_A$ receptor modulators..... 26

2.3. Zebrafish as a model organism in drug discovery and development..... 31

2.3.1. Zebrafish development and life cycle..... 31

2.3.2. Advantages of zebrafish as a model organism..... 34

Rapid life cycle and low-cost maintenance..... 34

Transparent embryos and larvae..... 34

Genetic homology to humans..... 35

Multi-organ system similar to humans..... 35

2.3.3. Zebrafish in drug discovery and development..... 37

Hit discovery and lead development..... 37

Target identification..... 38

ADME analysis..... 39

Toxicology studies..... 40

2.3.4. Rationale for neuroactive drug discovery with zebrafish..... 41

Complex brain..... 41

Functional blood-brain barrier..... 42

ADME principles..... 43

2.3.5. $GABA_A$ signaling system in zebrafish..... 44

2.3.6. Behavior-based assays with zebrafish..... 46

Photomotor response (PMR)..... 46

Locomotor activity..... 47

Escape and avoidance behavior..... 48
Habituation..... 49
2.4. ADME profiling in neuroactive drug discovery..... 54
2.4.1. Drug-like properties..... 54
2.4.2. Druggability assessment models..... 54
2.4.2.1. *In silico* prediction models..... 55
2.4.2.2. *In vitro* membrane permeability studies..... 56
Cell-based intestinal barrier model..... 57
Cell-based blood-brain barrier model..... 59
2.5. Bioanalysis..... 64
2.5.1. Bioanalytical method development..... 64
Sample preparation..... 64
LC-MS/MS instrument and detection optimization..... 65
2.5.2. Bioanalytical method validation..... 66
Selectivity and Specificity..... 67
Calibration model..... 68
Repeatability (precision) and Reproducibility..... 68
Stability..... 68
Accuracy..... 69
3. RESULTS AND DISCUSSION..... 72
3.1. HPLC-based activity profiling for $GABA_A$ receptor modulators in extracts – validation of an approach utilizing a larval zebrafish locomotor assay..... 73
3.2. HPLC-based activity profiling for $GABA_A$ receptor modulators in *Searsia pyroides* using a larval zebrafish locomotor assay..... 88
3.3. Validation of UHPLC-MS/MS methods for the determination of kaempferol and its metabolite 4-hydroxyphenyl acetic acid, and application to *in vitro* blood-brain barrier and intestinal drug permeability studies 100
4. CONCLUSION AND OUTLOOK..... 122

List of Abbreviations

4-HPAA	4-hydroxyphenylacetic acid
AChE	acetylcholinesterase
AD	Alzheimer's disease
ADME	absorption, distribution, metabolism and excretion
BBB	blood-brain barrier
BMP	bone morphogenetic protein
CNS	central nervous system
CRBN	cereblon
dpf	days post-fertilisation
EMA	European Medicines Agency
FDA	Food and Drug Administration
GABAA	γ-Aminobutyric acid type A receptor
GAD	glutamic acid decarboxylase
hBMEC	immortalized human brain microvascular endothelial cell line
HBSS	Hank's balanced salt solution
HPLC	high performance liquid chromatography
HTS	high throughput screening
i.o.	oral administration
i.p.	intraperitoneal application
IS	internal standards
KMF	kaempferol
LC-MS/MS	liquid chromatography coupled to triple (tandem) quadrupole mass spectrometry
LLOQ	lower limit of quantification
logP	octanol/water partition coefficient
MRM	multiple reaction monitoring
MTC	maximum tolerable concentration
NMR	nuclear magnetic resonance
NP	natural products
Papp	apparent permeability coefficient
P-gp	P-glycoprotein
PK	pharmacokinetics
PMR	photomotor response
PPT	protein precipitation
PSA	polar surface area
PTZ	pentylenetetrazol
QCH	quality control at a high level
QCL	quality control at a low level
QCM	quality control at a medium level
RBEC	rat brain endothelial cells
RHB	Ringer HEPES buffer
SAR	structure-activity-relationship
SPE	solid-phase extraction
TEER	transendothelial electrical resistance
UHPLC	ultra-high performance liquid chromatography
ULOQ	upper limit of quantification
VA	valerenic acid
VEGF	vascular endothelial growth factor

Summary

Gamma aminobutyric acid type A ($GABA_A$) receptors are the major inhibitory neurotransmitter receptors in the Central Nervous System (CNS). Several clinically important drugs used to treat anxiety, insomnia and epilepsy act *via* an allosteric modulation of postsynaptic $GABA_A$ receptors. The currently used drugs are associated with serious side-effects, mainly due to a lack of receptor subtype selectivity. This raises the medical need for discovery of novel types of $GABA_A$ receptor modulators.

We previously identified a series of allosteric $GABA_A$ receptor agonists with the aid of HPLC-based activity profiling, whereby activity was tracked with an electrophysiological assay in *Xenopus* oocytes expressing $GABA_A$ receptors of desired subunit composition. In an expansion of our investigations, aiming at acceleration of the activity profiling, an in-house assay was established using larval zebrafish locomotor activity model. In that, larval convulsions were provoked by the pro-convulsant $GABA_A$ receptor antagonist pentylenetetrazol (PTZ), and $GABA_A$ receptor agonistic extracts and compounds were identified through a decrease in larval locomotion. The assay was validated with the aid of known GABAergic compounds that had previously shown activity in the *Xenopus* oocyte assay. Assay validation was approached with respect to parameters relevant for the quality of results, including PTZ concentration, number of larvae, concentration of test samples, duration of incubation with test solutions and tracking of larval locomotion, as well as data visualization protocol. The validated protocol was subsequently translated into an HPLC-based activity profiling protocol using ethyl acetate extracts of *Valeriana officinalis* and *Magnolia officinalis*.

The zebrafish larvae locomotor assay was later employed for activity profiling of South African medicinal plants traditionally used for the treatment of epilepsy and other neurological disorders. An initial screening of medicinal plants in *Xenopus* oocytes patch clamp assay revealed GABAergic activity of a dichloromethane extract from leaves of *Searsia pyroides*. The extract significantly lowered PTZ-provoked locomotion in zebrafish larvae when tested at 4 µg/mL. HPLC-based profiling followed by targeted isolation of phytochemicals in the active time-window, revealed identification of three anacardic acid derivatives (**1-3**). Also, three structurally related compounds (**4-6**) were purified from inactive areas. After assessment of the isolated compounds with both *Xenopus* oocyte and larval zebrafish models, $GABA_A$ receptor modulation

activity of the extract was successfully correlated with the phytochemicals in the active time-window.

Additionally, in the zebrafish larval assay a series of $GABA_A$ receptor agonistic natural products, previously identified by the *Xenopus* oocyte assay, were tested. Lowering of locomotor activity was found for these compounds with exception of sanggenone C. Physicochemical and biochemical properties (PSA, cLogP, number of H-donor and acceptor sites, and number of rotatable bonds) of tested compounds were calculated *in silico*. A lack of permeability across the blood-brain-barrier (BBB) was concluded for sanggenone C, inferring its lack of activity *in vivo*, which also remarked the exclusivity of the zebrafish larvae assay for discovery of BBB-permeable natural products.

The last part of our research focused on the membrane permeability of kaempferol (KMF), a sedative flavonoid which targets $GABA_A$ receptors, and its major intestinal metabolite, 4-hydroxyphenylacetic acid (4-HPAA). In previous studies, KMF induced sedative effects in mice only after oral administration (i.o.) but not after intraperitoneal application (i.p.). However, 4-HPAA, the biotransformation product of KMF by intestinal microflora, induced behavioral changes after i.p. injection. To further explore the relation between KMF and 4-HPAA bioactivities and their route of administration, their ability to cross biological barriers has been examined. Intestinal barrier permeability studies were performed with Caco-2 cells, and blood-brain barrier transport studies were done with an immortalized mono-culture human model and a primary triple-co-culture rat model. UHPLC–MS/MS quantification methods for bioanalysis of KMF and 4-HPAA in the corresponding transport media were developed and validated according to international guidelines. The fundamental validation parameters included accuracy, precision, specificity, selectivity, sensitivity, repeatability, reproducibility, short-term and long-term stabilities. Data obtained with all barrier models were indicative of high intestinal and BBB permeation of KMF, and no permeation for 4-HPAA when compared with the fluorescent barrier integrity markers. In all experiments efflux ratios were below two, indicating that no active transport processes were involved for both compounds. Within a calcein-AM uptake assay in porcine brain capillary endothelial cells, kaempferol and 4-HPAA were found neither P-glycoprotein substrates nor P-glycoprotein inhibitors. Our *in vitro* data supported the previous described *in vivo* CNS effects of KMF while the role of 4-HPAA needs to be further studied.

Zusammenfassung

Die Gamma-Aminobuttersäure-A-Rezeptoren ($GABA_A$) sind die wichtigsten inhibitorischen Neurotransmitter-Rezeptoren im Zentralnervensystem (ZNS). Mehrere klinisch wichtige Medikamente zur Behandlung von Angstzuständen, Schlaflosigkeit und Epilepsie wirken über eine allosterische Modulation postsynaptischer $GABA_A$-Rezeptoren. Die gegenwärtig verwendeten Arzneimittel sind mit ernsthaften Nebenwirkungen verbunden, hauptsächlich aufgrund eines Mangels an Rezeptorsubtypselektivität. Dies erhöht den medizinischen Bedarf für die Entdeckung neuer Arten von $GABA_A$-Rezeptormodulatoren.

Wir identifizierten zuvor einige allosterische $GABA_A$-Rezeptor-Agonisten unter Verwendung von HPLC-gestützter Aktivitätsprofilierung, wobei die Aktivität mit einem elektrophysiologischen Test in *Xenopus*-Oozyten verfolgt wurde, die $GABA_A$-Rezeptoren der gewünschten Untereinheiten-Zusammensetzung exprimieren. In einer Erweiterung unserer Untersuchungen, die auf eine Beschleunigung des Aktivitätsprofils abzielte, wurde ein In-House-Assay unter Verwendung des Larven-Zebrafisch-Bewegungsaktivitätsmodells erstellt. Dabei wurden Larvenkonvulsionen durch den prokonvulsiven $GABA_A$-Rezeptor-Antagonisten Pentylentetrazol (PTZ) hervorgerufen, und $GABA_A$-Rezeptor-Agonisten-Extrakte und -Verbindungen wurden durch eine Abnahme der Larvenbewegung identifiziert. Der Test wurde durch bekannte GABAerge Verbindungen validiert, die zuvor eine Aktivität im *Xenopus*-Oocyten-Assay gezeigt hatten. Die Testvalidierung wurde hinsichtlich der für die Qualität der Ergebnisse relevanten Parameter, einschließlich PTZ-Konzentration, Anzahl der Larven, Konzentration der Testproben, Dauer der Inkubation mit Testlösungen und Verfolgung der Larvenfortbewegung, sowie Datenvisualisierungsprotokoll angegangen. Das validierte Protokoll wurde anschließend in ein HPLC-gestütztes Aktivitätsprofil-Protokoll unter Verwendung von Ethylacetat-Extrakten von *Valeriana officinalis* und *Magnolia officinalis* übersetzt.

Der Zebrafisch-Larven-Bewegungs-Assay wurde später zur Aktivitäts-Profilierung von südafrikanischen Heilpflanzen verwendet, die traditionell zur Behandlung von Epilepsie und anderen neurologischen Störungen verwendet werden. Ein erstes Screening von medizinischen Pflanzen im *Xenopus*-Oozyten-Patch-Clamp-Assay zeigte die GABAerge Aktivität eines Dichlormethan-Extrakts aus Blättern von *Searsia pyroides*. Der Extrakt mit 4 µg/ml senkte signifikant die PTZ-provozierte Fortbewegung in Zebrafischlarven. HPLC-basierte Profilierung gefolgt von einer gezielten Isolierung von Phytochemikalien im aktiven Zeitfenster ergab die Identifizierung von drei Anacardinsäurederivaten (1-3). Außerdem wurden drei strukturell verwandte Verbindungen (4-6) aus inaktiven Bereichen gereinigt. Nach Bewertung der isolierten Verbindungen mit *Xenopus*-Oocyten- und Zebrafisch-Larvenmodellen wurde die $GABA_A$-

Rezeptormodulationsaktivität des Extrakts erfolgreich mit den Phytochemikalien im aktiven Zeitfenster korreliert.

Zusätzlich wurde eine Reihe von $GABA_A$-Rezeptor-agonistischen Naturprodukten, die zuvor durch den *Xenopus*-Oocyten-Assay identifiziert wurden, im Zebrafisch-Larval-Assay getestet. Für diese Verbindungen wurde mit Ausnahme von Sanggenon C eine Verringerung der lokomotorischen Aktivität gefunden. Physikalisch-chemische und biochemische Eigenschaften (PSA, cLogP, Anzahl der H-Donor- und Akzeptorstellen und Anzahl der rotierbaren Bindungen) der Verbindungen wurden in silico berechnet. Ein Mangel an Permeabilität über die Blut-Hirn-Schranke (BHS) wurde für Sanggenon C vorgeschlagen, was auf seine fehlende Aktivität in vivo hinweist, was auch die Exklusivität des Zebrafisch-Larven-Assays für die Entdeckung von BBBpermeablen Naturprodukten anzeigte.

Der letzte Teil unserer Forschung konzentrierte sich auf die Membranpermeabilität von Kaempferol (KMF), einem sedativen Flavonoid, das auf $GABA_A$-Rezeptoren abzielt, und auf seinen Hauptmetaboliten 4-Hydroxyphenylessigsäure (4-HPAA). In früheren Studien induzierte KMF bei Mäusen nur nach oraler Verabreichung (i.o.), jedoch nicht nach intraperitonealer Verabreichung (i.p.) sedative Wirkungen. Jedoch induzierte 4-HPAA, das Biotransformationsprodukt von KMF, das durch die Darmflora produziert wurde, Verhaltensänderungen nach i.p. Injektion. Um die Beziehung zwischen den Bioaktivitäten von KMF und 4-HPAA und deren Verabreichungsweg weiter zu erforschen, wurde ihre Fähigkeit, biologische Barrieren zu überwinden, untersucht. Darmpermeabilitätsstudien wurden an Caco-2-Zellen durchgeführt, und Blut-Hirn-Schranke-Transportstudien wurden an einem immortalisierten Monokultur-Humanmodell und einem primären Dreifach-Co-Kultur-Rattenmodell durchgeführt. UHPLC-MS/MS-Quantifizierungsmethoden für die Bioanalytik von KMF und 4-HPAA in den Transportmedien wurden nach internationalen Richtlinien entwickelt und validiert. Zu den grundlegenden Validierungsparametern gehörten Genauigkeit, Präzision, Spezifität, Selektivität, Empfindlichkeit, Wiederholbarkeit, Reproduzierbarkeit sowie Kurzzeit- und Langzeitstabilität. Daten, die mit allen Barrierenmodellen erhalten wurden, zeigten eine hohe Darm- und BBB-Permeation von KMF und keine Permeation für 4-HPAA im Vergleich zu den Markern der Fluoreszenzbarriereintegrität. In allen Experimenten lagen die Efflux-Verhältnisse unter zwei, was darauf hindeutete, dass keine aktiven Transportprozesse beteiligt waren. Innerhalb eines Calcein-AM-Aufnahmeassays in porcinen Hirnkapillarendothelzellen wurden Kaempferol und 4-HPAA nicht als Pglycoprotein-Substrate und nicht als P-Glycoprotein-Inhibitoren befunden. Unsere In-vitro-Daten unterstützten die zuvor beschriebenen in vivo ZNS-Wirkungen von KMF, während die Rolle von 4-HPAA weiter untersucht werden muss.

1. Aim of the Work

Nature provides a rich source of small molecules with huge structural diversity, and keeps offering promising bioactive chemical hints. In recent years, various natural products with new scaffolds targeting $GABA_A$ receptors have been reported. In our research group, HPLC-time-based activity profiling was used as a successful approach for rapid localization and characterization of $GABA_A$ receptor modulators in natural extracts [1, 2]. A semi-automated patch clamp assay with *Xenopus* oocyte was applied for the corresponding bioactivity screenings in collaboration with our external research colleagues [3]. In HPLC-based activity profiling, the turnaround time of bioassay data is believed to be the limiting step. Therefore, in the present study, we aimed to establish an in-house assay to accelerate the discovery and de-replication process by reducing the turnaround time of bioactivity data. A larval zebrafish locomotor activity model has been developed for this purpose with respect to the fact that the GABAergic system of zebrafish develops during embryogenesis and is functional in larvae.

In larval zebrafish locomotor activity model, seizure-like behavior is triggered with the $GABA_A$ receptor antagonist pentylenetetrazol (PTZ) [4]. Following exposure to PTZ, zebrafish larvae exhibit concentration-dependent stereotypic swimming behavior which starts with increased motility, progresses to rapid circular movements, and later, to brief clonus-like convulsions and body-stiffening. Finally, it leads to loss of movement [5]. Quantitative assessment of the seizure behavior is based on calculation of distance traveled by larvae in a defined period after exposure to PTZ [6]. The PTZ-provoked locomotor activity model has been previously used by some research groups for examination of natural products. However, the reported assay protocols differed significantly between each other with respect to key parameters for assay performance as well as data interpretation. Aiming at the production of reliable data, in this study, the assay has been further optimized and validated with the aid of known GABAergic compounds and extracts. Finally, the assay was translated into an HPLC-based profiling protocol using the extracts which previously showed activity in the same bioassay.

The second part of the thesis aimed at application of the validated zebrafish locomotor assay for discovery of new scaffolds targeting the $GABA_A$ receptor. A selection of traditional South African medicinal plants which primarily showed activity in *Xenopus* oocyte patch clamp assay was examined in zebrafish larvae. Promising extracts were submitted to HPLC-based profiling for targeted isolation and characterization of their active principles. The constituents in the active micro-fractions were purified with the aid of diverse chromatographic techniques and elucidated

by means of spectroscopic methods. Bioactivity of the isolated compounds was reassessed in zebrafish larvae. The activity had to be confirmed with *Xenopus* oocyte model in order to make sure that lowering of PTZ-provoked locomotor activity was not *via* targets other than $GABA_A$ receptors.

With regards to bioactive compounds targeting the CNS, druggability of the molecule comes into consideration, along with potency and selectivity studies, during the early exploratory stages of drug development. Druggability is interpreted with satisfactory physicochemical and biochemical characteristics which enable a candidate drug molecule to reach adequate concentrations at its site of action. In this PhD thesis, beyond the screening of $GABA_A$ receptor modulators, we evaluated drug-like properties for compounds of interest. Physicochemical and biochemical properties of GABAergic natural products were calculated *in silico* aiming at justification of their *in vivo* activity/inactivity in zebrafish model.

In addition, in the last part of the thesis, we dug into membrane permeability of a sedative flavonoid that targets $GABA_A$ receptors and its major intestinal metabolite: kaempferol (KMF) and 4-hydroxyphenylacetic acid (4-HPAA), respectively. Anxiolytic-like activities of KMF and 4-HPAA have been previously verified in pharmacological studies by our research colleagues. Route of administration appeared to be decisive for pharmacologic activity of the compounds as KMF induced sedative effects in mice only after oral administration (i.o.) but not after intraperitoneal application (i.p.). The intestinal metabolite of that, 4-HPAA, was active after i.p. application [7]. For expanding our understanding on ADME principles of KMF and 4-HPAA, their membrane permeability was studied in cell-based models. Orally administered neuroactive compounds need to be absorbed from the gut *via* intestinal epithelium into systemic circulation, and cross the BBB to reach the CNS. Considering this fact, an intestinal barrier model with Caco-2 cell-line, and two BBB models with immortalized human and rat cells were utilized for the transport studies.

The compounds had to be analyzed in transport matrices for determination of their permeability coefficients across the cell monolayers. In this regard, quantitative ultra-high performance liquid chromatography tandem mass spectrometry (UHPLC-MS/MS) methods were developed. The quantification methods were validated with respect to selectivity, precision, and reliability, according to international guidelines.

References:

[1] Potterat, O., Hamburger, M., Concepts and technologies for tracking bioactive compounds in natural product extracts: generation of libraries, and hyphenation of analytical processes with bioassays. Natural Product Reports. 30 (2013) 546-64.

[2] Potterat, O., Hamburger, M., Combined Use of Extract Libraries and HPLC-Based Activity Profiling for Lead Discovery: Potential, Challenges, and Practical Considerations. Planta Medica. (2014).

[3] Zaugg, J., et al., HPLC-based activity profiling: discovery of piperine as a positive $GABA_A$ receptor modulator targeting a benzodiazepine-independent binding site. Journal of Natural Products. 73 (2010) 185-91.

[4] Baraban, S., et al., Pentylenetetrazole induced changes in zebrafish behavior, neural activity and c-fos expression. Neuroscience. 131 (2005) 759-68.

[5] Baraban, S. C., Zebrafish as a simple vertebrate organism for epilepsy research. Animal Models of Epilepsy: Methods and Innovations. (2009) 59-74.

[6] Afrikanova, T., et al., Validation of the zebrafish pentylenetetrazol seizure model: locomotor versus electrographic responses to antiepileptic drugs. PLoS One. 8 (2013) e54166.

[7] Grundmann, O., et al., Kaempferol from the leaves of *Apocynum venetum* possesses anxiolytic activities in the elevated plus maze test in mice. Phytomedicine. 16 (2009) 295-302.

2. Introduction

2.1. Natural products in CNS-active drug discovery

Challenges and opportunities

Minerals and natural extracts were the only source of medicines for thousands of years until the development of experimental procedures in the nineteenth century provided the ability to isolate and characterize active principles from these extracts. A revolution in the chemistry of natural products started with the commercial availability of powerful spectrometers especially NMR and MS, which allowed the determination of the structure of biologically active principles. Gradually, synthetic methods were introduced; allowing the semi-synthesis of clinically useful analogues of natural compounds, and purely synthetic agents appeared towards the end of the nineteenth century [1, 2]. Throughout the twentieth century, organic synthesis became increasingly important to the point that large-scale synthesis of drug candidates played a leading role in drug development [1, 3]. In the late twentieth century advances in combinatorial chemistry, along with invention of biological techniques for simultaneous examination of thousands of compounds and appearance of sophisticated robotics, encouraged the creation of enormous synthetic libraries of small molecules by pharmaceutical companies [1, 3, 4]. In contrast, NPs were supposed to be incompatible with contemporary HTS platforms. Additional challenges such as the lengthy purification and identification process of bioactive components from the raw material, complexity of correlating bioactivity profiles of natural extracts with their chemical profiles, concerns about repeated isolation of known compounds, and the supply problems for preclinical/clinical developmental studies as well as translation of laboratory-scale discoveries to commercial items, all together, scaled back the NP-based discovery programs [2, 5]. However, shortly after, the output of high-throughput screenings of synthetic libraries appeared below expectations. The de-emphasis in natural product drug discovery correlated with the overall reduction of new leads in the drug development pipeline and the substantial decline in new drug approval [1, 3-5]. Retrospective analysis of industrial HTS campaigns indicated that the selection of plates containing natural products would have significantly improved hit rates [6]. The main reason has been realized to be a lack of true chemical diversity of synthetic scaffolds. It has been understood that diversity within the ‘chemical space’ was more important than the library size, and that synthetic libraries could not compete with the diversity of natural products [6, 7]. The phenomenon of chemical diversity in natural products is a consequence of a rich variety of

organisms in the ecosphere, their interaction with each other and with their environment, resulting in the evolution of complex natural chemicals in the organisms, to enhance their survival and competitiveness [8]. In fact, nature has been doing combinational chemistry for ages, not just a decade or two, and has been selecting products from that combinational library that have specific biological advantages [8]. Structural diversity, however, was not the only reason for interest in natural products. An important additional feature was the possession of highly selective and specific bio-activities, often observed, based on mechanisms of action. The HMG-CoA reductase inhibition exhibited by statins and the tubulin-assembly promotion activity of paclitaxel are, only, two examples of these [2]. Therefore, attitudes were redirected from ignorance or replacement of natural products towards engagement of technological advances to facilitate the challenges of the discovery process from this wealth of novel leads. The innovative approaches, including automated coupling of HPLC and MS enabled separation and discrimination of closely related compounds in complex extracts, eluting in a narrow chromatographic area [4, 9, 10]. Combination of micro-fractionation procedures with spectroscopic methods and high-throughput bioassays enabled the rapid generation of bioactivity information along with dereplication of well-studied NPs, while NMR cryoprobes with significantly improved sensitivity increased the speed of generating structural information from limited amounts of study material [4, 9]. The current toolbox of synthetic chemists and biologists, expanded with the aid of bio-catalysis and combinatorial bio-synthesis would address the supply problems inherent with this source material, by production of therapeutic NPs at commercially viable yields [2, 4, 6, 8, 11, 12].

The study by Newman and Cragg, that reviewed approved therapeutic agents between 1981 and 2014, clearly demonstrates the continuing role that natural products and structures derived from or related to natural products play in the development of current therapeutic products [12]. Indeed, the new era of NP discovery benefits the advent of bioinformatics, pharmacogenomics, *in silico* modelling, and combinatorial chemistry [2, 8, 13]. Thus, NPs based approaches can be seen as a provider of initial lead compounds of pharmacological interest with a potential for structure optimization, in a multidisciplinary approach, to obtain desired efficacy, selectivity and ADME properties [2, 12].

Discovery of novel leads

Natural extracts are highly complex mixtures. An efficient approach to obtain bioactive principles in an extract requires a targeted isolation following an early-stage localization of activity in the crude mixture. In this regard, bringing together biological data and chemo-analytical information of the extract is the most challenging step [14].

The classical strategy for purification of bioactive NPs was activity-guided isolation, in which, bioactive extracts underwent successive chromatographic steps with increasing separation performance. Isolation of active principles was guided by intermediate testing of chromatographic fractions in the corresponding bioassay [15, 16]. This historically successful approach is not, any more, compatible with modern drug research strategies, running with minute amounts of raw material and limited timelines. Following development of highly sensitive and miniaturized assays along with technological advances in chromatography and spectroscopy, over the last two decades, more efficient methodologies have been developed. Among those, HPLC-based activity profiling is used as one of the most successful approaches, in which, bioactivity can be tracked in complex mixtures without isolation of compounds. It involves time-based fractionation of micrograms of bioactive extracts in 96-deep well plates by means of analytical or semi-preparative scale HPLC. The bioactivity for each micro-fraction is assessed with the corresponding micro-scaled bioassays. Subsequently, correlation of the activity profile with the chromatogram reveals identification of active peaks. The on-line or off-line spectroscopic information of the activity-assigned peaks are available and, in combination with database searches such as the Dictionary of Natural Products (DNP), allow early dereplication of known compounds and tracking potentially new molecules in crude mixtures [17, 18].

Complementary investigations of promising metabolites are pursued by preparative-scale isolation and purification of the compounds, mainly, with the aid of various chromatographic techniques, followed by precise structure elucidation. Hyphenation of HPLC separation with different spectroscopic detection methods such as PDA and MS offers primary structural information of constituents, simultaneous to their isolation. A PDA detector provides the spectral profile of compounds bearing UV-active chromophores. Pattern of maximal absorptions can often be related to characteristic chromophores and, consequently, to classes of secondary metabolites. High resolution mass spectrometric (HR-MS) data provide accurate masses to

calculate the molecular formula of a compound while detailed and precise constitutional information of the molecule is, ultimately, achieved by NMR measurements. The covalent structure of the molecule is determined with One-dimensional ^{1}H and ^{13}C NMR and two-dimensional COSY, HSQC and HMBC experiments [19].

The complete structure elucidation of a new bioactive NP comprises assignment of the absolute configuration, considering that many NPs, being generated by stereospecific reagents and catalysts, have several chiral centers. In many cases, the presence of such chiral centers contributes to the stereospecific binding sites and, consequently, selectivity of these molecules for their bioactivities [20]. Stereo-chemical information are obtained with NOESY and ROESY experiments, displaying through space correlations, to determine the complete 3D-structure of a molecule (relative configuration) [19], while chiroptical methods, such as electronic circular dichroism (ECD), and X-ray crystallography are employed for assignment of absolute configurations [21].

Neuroactive leads

NPs are anticipated to play a significant role in the development of new bioactive leads for various therapeutic areas, from which, the CNS disorders are not excluded. This may be attributable to the fact that NPs are natural metabolites. In other words, such compounds are more likely to be substrates for one or more transporter systems to be delivered to their intracellular site of action [6]. Neuroactive leads have to bear a proper combination of physicochemical properties that enables them to penetrate the blood-brain barrier (BBB). In a study by Joyner and Cichewicz, physiochemical properties of natural product leads, prior to any type of structure optimization, were compared to clinical drugs known to interact with CNS targets. This comparison revealed that, overall, natural products met many of the basic requirements for CNS-active drugs (Figure 2.1-1) and can be regarded as a lead pool with high probability to provide drug candidates compatible with the BBB penetration needs of CNS-active agents. In that comparison, molecular weight, ClogP, topological polar surface area, ClogD, number of hydrogen bond donors, and pK_a were considered as parameters that define BBB permeability of compounds. Some deviations were observed in molecular weight and total polar surface area as NPs tend to be larger and have greater polar surface areas. It remarked the potential of NPs for structure optimization, driven by medicinal chemistry, and an expanded

space to introduce new generations of therapeutics [10].

The major research on small molecule NPs for the neuroactive drug development focused on neurodegenerative diseases. Among those, Alzheimer's disease (AD) received the most intense studies, accounting for about 70% of the described leads [10]. The promising application of natural acetylcholinesterase inhibitors as CNS-active therapeutics was exemplified by galantamine and rivastigmine. Galantamine was originally isolated from Caucasian snowdrops (*Galanthus nivalis*) in the 1950s. The compound is also produced by *Galanthus woronowii* Losinsk., some species of *Narcissus* and *Leucojum aestivum* L. (Amaryllidaceae) and is currently in clinical use for the treatment of Alzheimer's disease [22]. Rivastigmine is a semisynthetic analogue of the pyrroloindole alkaloid physostigmine (eserine), which was isolated from *Physostigma venenosum* Balf. (Leguminosae), and underwent structure optimization for an improved pharmacokinetic profile. Rivastigmine is currently used for treatment of mild to moderate AD and Parkinson's [22].

Extensive research has been directed towards the identification of AChE inhibitors following approval of the two NP-derived AChE inhibitors. While structurally diverse, these compounds are primarily alkaloids such as huperzine A, isolated from *Huperzia serrata* (Thunb.) Trevis. (Lycopodiaceae). A total synthesis of huperzine A has been developed. The compound has been

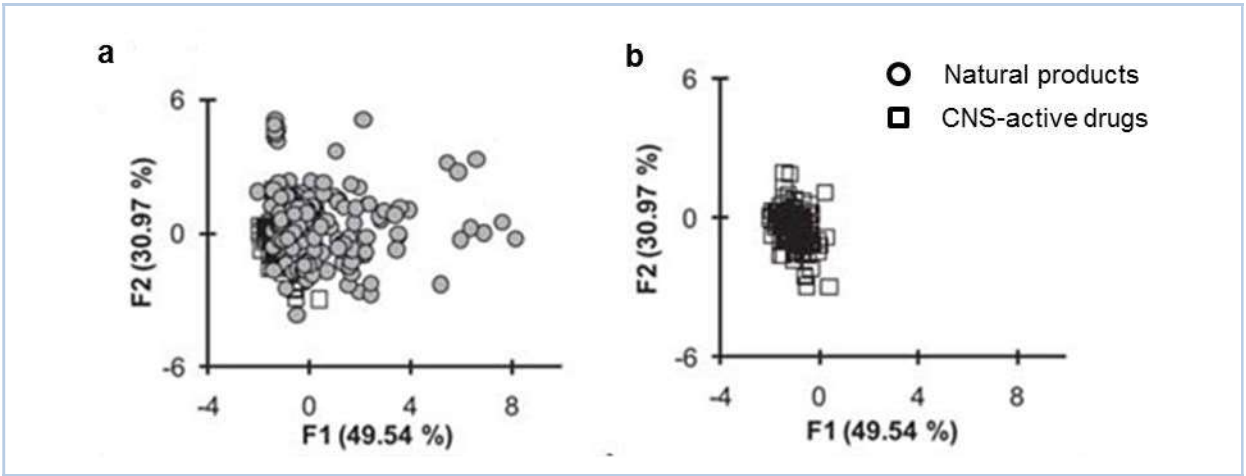

Fig. 2.1-1: Scatter plots from principal components analysis of the chemical properties exhibited by CNS-active drugs and natural products with bioactivity relevant to neurodegenerative disease. Data points that cluster together have similar chemical properties, including molecular weight, C logP, topological polar surface area, C logD, number of hydrogen bond donors and the strongest basic pKa. a) Data points for clinical drugs and natural products, showing the large amount of overlap between the two groups. b) Data points representing only clinical drugs [10].

approved in China to treat AD symptoms [23]. Indole alkaloid derivatives (infractopicrin and 10-hydroxy-infractopicrin) of the fungus *Cortinarius infractus* Berk. (Cortinariaceae) are other promising examples with greater selectivity than galantamine and predicted BBB permeability [22, 23].

Indole alkaloids of ergot (*Claviceps purpurea*) are NPs with psycho- and neuro-activities known for nearly two centuries. To varying degrees, these agents act as partial agonists or antagonists at R-adrenergic, serotoninergic, and dopaminergic receptors. Cabergoline, a selective and long-lasting agonist of dopamine D2 receptor, is an ergot alkaloid analogue launched in several European countries and the U.S for the symptomatic treatment of Parkinson's disease, as adjuvant therapy with levodopa, allowing reduction in levodopa dosage [24]. Another member of the ergoline family, terguride, is a serotonin receptor antagonist and dopamine receptor agonist. Terguride was first marketed for the treatment of schizophrenia and Parkinson's disease [25]. Later, it was granted orphan drug status for the treatment of pulmonary arterial hypertension [26]. Some of the ergoline derivatives, such as ergotamine, are used clinically for the purpose of vasoconstriction and in the treatment and alleviation of migraines [27], and others, such as LSD, are psychedelic substances [28].

With regards to therapeutic $GABA_A$ receptor modulators, as the main focus of studies in this thesis, the currently prescribed drugs are synthetic compounds, mostly, derived from the benzodiazepine scaffold [12]. However, several scientific investigations have been performed in academia reporting on structurally diverse NPs that act on $GABA_A$ receptors. Some examples of these compounds are provided in Section 2.2.

References:

[1] Patrick, G.L., History of Drug Discovery, 2013, in: eLS. John Wiley & Sons, Ltd: Chichester. DOI: 10.1002/9780470015902.a0003090.pub2.

[2] Cragg, G. M., Newman, D. J., Natural products: a continuing source of novel drug leads, Biochimica et Biophysica Acta (BBA)-General Subjects. 1830 (2013) 3670-95.

[3] http://pharmsci.uci.edu/history.php, A short history of drug discovery, Pharmaceutical Sciences University of California, Irvine.

[4] Gonzalez-Sabin, J., Natural products: Back to the future in drug discovery. Biochemical Pharmacology. 1 (2012) 1-3.

[5] Shen, B., A new golden age of natural products drug discovery. Cell. 163 (2015) 1297-300.

[6] Harvey, A. L., Edrada-Ebel, R., Quinn, R. J., The re-emergence of natural products for drug discovery in the genomics era. Nature Reviews Drug Discovery. 14 (2015) 111.

[7] Peterson, R. T., Fishman, M. C., Designing zebrafish chemical screens. Methods in Cell Biology. 105 (2011) 525-41.

[8] McChesney, J. D., Venkataraman, S. K., Henri, J. T., Plant natural products: back to the future or into extinction?. Phytochemistry. 68 (2007) 2015-22.

[9] Challal, S., et al., Zebrafish bioassay-guided microfractionation for the rapid *in vivo* identification of pharmacologically active natural products. CHIMIA. 66 (2012) 229-32.

[10] Joyner, P. M., Cichewicz, R. H., Bringing natural products into the fold–exploring the therapeutic lead potential of secondary metabolites for the treatment of protein-misfolding-related neurodegenerative diseases. Natural Product Reports. 28 (2011) 26-47.

[11] Awan, A. R., Shaw, W. M., Ellis, T., Biosynthesis of therapeutic natural products using synthetic biology. Advanced Drug Delivery Reviews. 105 (2016) 96-106.

[12] Newman, D. J., Cragg, G. M., Natural products as sources of new drugs from 1981 to 2014, Journal of Natural Products. 79 (2016) 629-61.

[13] Al-Ali, H., The evolution of drug discovery: from phenotypes to targets, and back. MedChemComm. 7 (2016) 788-98.

[14] Potterat, O., Targeted approaches in natural product lead discovery. CHIMIA International Journal for Chemistry. 60 (2006) 19-22.

[15] Potterat, O., Hamburger, M., Natural products in drug discovery-concepts and approaches for tracking bioactivity. Current Organic Chemistry. 10 (2006) 899-920.

[16] Zhu, Y. Z., Natural products: essential resources for human survival: 2007, World Scientific.

[17] Potterat, O., Hamburger, M., Combined use of extract libraries and HPLC-based activity profiling for lead discovery: potential, challenges, and practical considerations. Planta Medica. 80 (2014) 1171-81.

[18] Potterat, O., Hamburger, M., Concepts and technologies for tracking bioactive compounds in natural product extracts: generation of libraries, and hyphenation of analytical processes with bioassays. Natural Product Reports. 30 (2013) 546-64.

[19] Bross-Walch, N., et al., Strategies and tools for structure determination of natural products using modern methods of NMR spectroscopy. Chemistry and Biodiversity. 2 (2005) 147-77.

[20] Feher, M., Schmidt, J. M., Property distributions: differences between drugs, natural products, and molecules from combinatorial chemistry. Journal of Chemical Information and Computer Sciences. 43 (2003) 218-27.

[21] Kondru, R. K., Wipf, P., Beratan, D. N., Theory-assisted determination of absolute stereochemistry for complex natural products via computation of molar rotation angles. Journal of the American Chemical Society. 120 (1998) 2204-5.

[22] Williams, P., Sorribas, A., Howes, M. J. R., Natural products as a source of Alzheimer's drug leads. Natural Product Reports. 28 (2011) 48-77.

[23] Geissler, T., et al., Acetylcholinesterase inhibitors from the toadstool *Cortinarius infractus*. Bioorganic and Medicinal Chemistry. 18 (2010) 2173-7.

[24] Shu, Y. Z., Recent natural products based drug development: a pharmaceutical industry perspective, Journal of Natural Products. 61 (1998) 1053-71.

[25] Shen, W. W., A history of antipsychotic drug development. Comprehensive Psychiatry. 40 (1999) 407-14.

[26] Norman, P., Pulmonary arterial hypertension: a rare disease that encourages the development of multiple treatments. Expert Opinion on Orphan Drugs. 2 (2014) 1137-45.

[27] Ong, J. J. Y., De Felice, M., Migraine Treatment: Current acute medications and their potential mechanisms of action. Neurotherapeutics. (2017) 1-17.

[28] Larsen, J. K., Neurotoxicity and LSD treatment: a follow-up study of 151 patients in Denmark. History of Psychiatry. 27 (2016) 172-89.

2.2. The $GABA_A$ receptors

Structure and pharmacology

Treatment of emotional disturbances, cognitive and motor impairments resulting from neurodegenerative and genetic abnormalities are aided by modulation of neurotransmitter systems in the Central Nervous System (CNS). The most widely distributed neurotransmitter systems in the humans brain are the excitatory glutamate, and the inhibitory γ-aminobutyric acid (GABA) systems, which along with a large number of other slower acting transmitters, modulators, and ion channels keep the chemical balance in the CNS [1].

GABA is the main inhibitory neurotransmitter in the brain. Approximately 20% of all neurons in the CNS are GABAergic [3]. The GABA system exerts its influence through increase of postsynaptic membrane permeability to chloride ions. In mature neurons, under normal conditions, the activation of GABA receptors leads to hyperpolarization of cell membrane potential and inhibition of neuronal activity [1, 2]. Altered GABAergic synaptic transmission is associated with panic, anxiety, impaired learning and sleep abnormalities. It also contributes to deficits associated with schizophrenia, bipolar disorder, major depression, and autism [1, 3].

There are two classes of GABA receptors: $GABA_A$ and $GABA_B$, which differ in terms of composition, pharmacology, and action [3]. The $GABA_A$ receptors and the associated chloride ion channels in the CNS are part of a complex pentameric protein-structure. A total of 19 mammalian genes coding for $GABA_A$-receptor subunits have been cloned, belonging to 8 subunit classes: α1-α6, β1-β3, γ1-γ3, δ, ε, θ, π, ρ1-ρ3. Each of the receptor subunits displays a unique distribution in the brain. The most abundant $GABA_A$-receptor subtype in the mammals consists of two α_1, two β_2 and one γ_2 subunits ($2\alpha_1 2\beta_2\gamma_2$), and is present in most brain regions [1, 4]. $GABA_B$ receptors are heterodimeric receptors coupled *via* G-proteins to potassium and calcium channels as well as adenylate cyclase. Thus, the action of $GABA_B$ receptors is slower than $GABA_A$ receptors. Presynaptically, $GABA_B$ receptors facilitate neurotransmitter release including glutamate and GABA, while postsynaptically, they generate inhibitory potentials [3].

$GABA_A$ receptors are particularly important from a pharmacological point of view as they are the target for a wide range of therapeutic agents [1, 5]. Benzodiazepines, barbiturates, neurosteroids, and anesthetics are some of the main $GABA_A$ receptor modulators [4]. A long-

term therapeutic use of $GABA_A$ receptor modulators is restricted by problems related to the loss of efficacy, development of tolerance, and dependence, the mechanisms of which are still poorly known [1]. Additionally, a lack of receptor-subtype selectivity associated with the current drugs may result in undesired experiences such as reduced coordination, and cognitive impairments [6]. Thus, the need for discovery and development of new GABAergic therapeutics is remained unmet.

In vitro $GABA_A$ receptor modulation models

Exploration of the GABAergic system has been enabled by various biological assays contributing to understanding receptor assembly, structure and functions. Expression of various $GABA_A$ receptor subunits by pharmacological manipulations are mainly studied with mouse or rat primary-cell-based models, such as cortical neurons cultures (expressing $\alpha_1\alpha$-$_5\beta$ $_{,2}$, $\beta_3\gamma$ $_{,2}$, and δsubunits), cerebellar granule cell cultures (expressing $\alpha_1\alpha$-$_6\beta$ $_{,1}\beta$-$_3\gamma$ $_{,1}\gamma$-$_3$, and δsubunits), and hippocampal neuron cultures (expressingα $_1\alpha$-$_5\beta$ $_{,1}\beta$-$_3\gamma$ $_{,1}\gamma$-$_3$, and δ subunits of the $GABA_A$-receptors) [1]. Pharmacological and allosteric modulation of the receptors can be examined by ligand binding techniques in which a radio-labelled or fluorescent reference ligand is displaced in the cell lines overexpressing the desired receptors. The receptor affinities of test compounds are examined in competition with that specific ligand [4, 7, 8]. Such assays target a known specific binding site depending on the labelled ligand used. Thus, they cannot provide information on scaffolds for unknown binding sites. Binding assays measure only affinity, but do not allow to differentiate between agonistic or antagonistic activities. To acquire functional

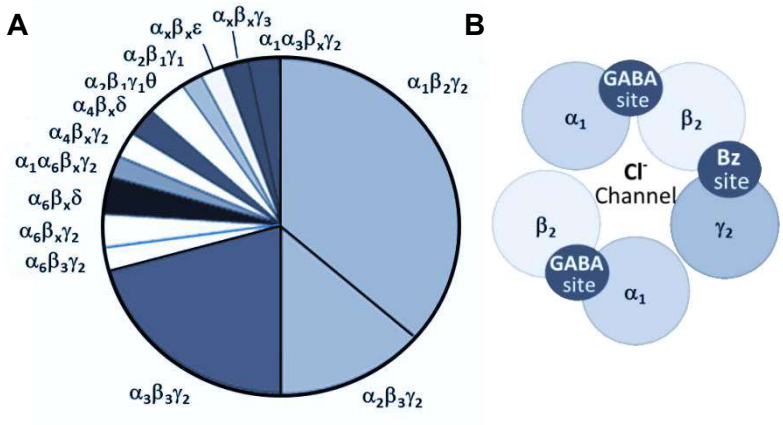

Figure 2.1-1: A pie chart representing an approximate abundance of $GABA_A$ receptor subtypes in the rat brain (**A**); The most abundant mammalian $GABA_A$-receptor subtype (**B**) [4].

insights, based on the principle of allosteric modulation on the receptor, other complementary techniques are required.

Discovery of new $GABA_A$ receptor modulators with novel scaffolds, possibly targeting binding sites other than those of current drugs, has been facilitated with various functional assays. A variety of quinoline-based fluorescent dyes such as MEQ and MQAE which are sensitive to chloride ions can be used to examine $GABA_A$-receptor responses by measurement of intracellular chloride concentrations [4, 9, 10]. When using these assays, one has to be aware of the probability to pick false-positives or -negatives due to significant leakage of the utilized dyes from the cells. The leakage needs to be minimized by use of efflux pump inhibitors. Also, a key disadvantage of the quinoline-based fluorescent dyes is the tendency to strong bleaching, limiting the utility of these dyes for robust studies [4]. Radioactivity-based ion flux assays, measuring $^{36}Cl^-$ influx in stable cell lines overexpressing the receptors, can also directly examine the chloride permeability and therefore, the ion channel functions [11]. Activation of the $GABA_A$-receptors leads to a fall in intracellular pH, associated with an alkalinisation at the extracellular surface of the cell membrane. These techniques, known as microphysiometry, can also contribute to the ion channel function studies by measuring the changes in extracellular acidification rate in live cells with potentiometric silicon-based sensors [4, 12].

One of the most direct and widely used methods of measuring ion channels functions is the patch clamp electrophysiology study in which charge transfer is recorded directly and quantitatively [13, 14]. The earlier studies were performed with native tissue preparations including brain slices, and isolated neurons. In recent studies, larger cells such as the egg progenitor cells (oocytes) of the African frog, *Xenopus laevis*, expressing cloned cDNA or synthetic RNA are utilized. The *Xenopus* oocyte is widely used for this purpose due to its large size, its faithful expression of channel proteins in the cell membrane, and the relative absence of endogenous channels which might complicate analysis of electrophysiology measurements [15]. Automated high-throughput electrophysiology methods are useful for determination of efficacy in primary screenings of small molecule and extract libraries, as well as secondary screening of identified compounds for receptor-subtype selectivity [15].

In vivo GABAergic activity models

Vertebrates and invertebrates both have GABA as a major inhibitory neurotransmitter [16]. Behavioral changes mediated by the GABAergic system are studied with various animal models. The rodent behavior-based anxiety models such as the elevated plus maze model, the open field and the light/dark assays, explore natural spontaneous reactions namely escape, avoidance, and freezing, and are highly sensitive to $GABA_A$ receptor modulating compounds [17]. The punishment based assays such as the four-plate test and the Vogel conflict test are used for studying conditioned anxiety-like behaviors, which are observed as suppression of a simple innate ongoing behavior (passive avoidance) [18].

The other behavioral models which can be applied to $GABA_A$ modulations discovery include locomotor activity assessments such as motor coordination assays (rotarod, horizontal bar, static rods and parallel bars [19], beam walking assay [20], actimeter test [21]), and epilepsy models in which the $GABA_A$ receptor antagonists picrotoxin, bicuculline, strychnine, or pentylenetetrazole (PTZ) are utilized to induce seizure-like behaviors [22].

The more complex rodent and mammalian models likely have greater relevance to the human condition and provide valuable information regarding the functional roles of $GABA_A$ receptors and their specific subunits. However, these models do not support large-scale screenings of extracts and active compounds due to the expense and time required for animal maintenance, breeding, and behavioral analyses [23]. In contrast, the simpler model organisms such as the nematode *Caenorhabditis elegans*, the arthropod *Drosophila melanogaster* (fruit fly), and the vertebrate *Danio rerio* (zebrafish) provide a potential for high-throughput analysis and are used in early drug discovery research [24]. Fruit flies exhibit social behaviors, associative learning and sensorimotor integration [23]. In many instances drug actions at the mammalian $GABA_A$ receptors parallel those at the arthropod receptor whereas sites of action of benzodiazepines, steroids and convulsants on the insect ionotropic GABA receptors have been described [25, 26].

Invertebrate animals are lacking some developmental characteristics specific to vertebrates such as the presence of the BBB [27]. In this respect, to compromise between physiological complexity and throughput, the zebrafish (*Danio rerio*) has recently emerged as an ideal model for neurobehavioral studies [28]. Zebrafish offers a combination of genetic tractability, close homology with higher vertebrates and accessible experimental methodologies such as behavioral

analysis and electrophysiological (EEG) recording [29]. In the section 2.3, further descriptions on the zebrafish model organism are provided.

Promising NP-based $GABA_A$ receptor modulators

There is an impressive array of NP scaffolds, including coumarins, terpenoids, alkaloids, phenylpropanes, lignans, etc., that influence the function of ionotropic receptors for GABA [30-43]. Flavonoids are the most extensively studied $GABA_A$ receptor modulators from plant origin, demonstrating anxiolytic-like, sedative-like, and anticonvulsant-like properties [44]. Apigenin, hesperidin and (-)-epigallocatechin gallate are among the widely occurring flavonoids which have shown the ability to enhance activity of diazepam, the clinically used benzodiazepine [44]. More than one binding site on the $GABA_A$ receptor was suggested for the flavonoids, and their mode of action on the receptor varies strongly with their substitution pattern; which originates from different hydroxylation, C-prenylation, O-methylation, C- and O-glycosidation, and/or polymerization [44-47]. However, bioavailability of flavonoids, their systemic distribution and their ability to cross the BBB are not well understood, and the information available is sometimes controversial [48]. Pharmacological investigations demonstrated routes of administration to be decisive for bioactivities of flavonoids, which raised the hypothesis that flavonoids act as prodrugs [49].

One of the well-known GABAergic terpenoids is valerenic acid (VA), a major constituent of *Valeriana officinalis* L.. VA showed anxiolytic-like activities in various *in vivo* models. Allosteric modulation of $GABA_A$ receptors by VA was observed, selectively, at the receptors comprising β2 or β3 subunits (but not β1 subunit). Within structure-activity relationship studies, VA was converted into various amides with differing lipophilicity and bulkiness at the carboxyl site, and novel $GABA_A$ receptor modulators with higher efficacy than the natural parent compound were achieved [50].

Honokiol is a neolignan isolated from *Magnolia officinalis*. It is a positive modulator of $GABA_A$ receptor with proven *in vivo* anxiolytic effects [51, 52]. Honokiol has shown selective interaction with the β2 or β3 subunits of the receptor, similar to VA [53].

In our research group, several studies focused on identification of GABAergic NPs, and positive modulators of $GABA_A$ receptors belonging to various structural classes were reported [30-43].

Compounds, such as piperine, have been shown to interact at a benzodiazepine independent allosteric binding site [39]. Piperine is the main pungent component of black pepper (*Piper nigrum* L.) fruits. It has already served for medicinal chemistry efforts, and *in vivo* active analogues of that with improved selectivity and biopharmaceutical properties were achieved [30]. Additionally, BBB permeability of piperine and its bioactive analogues was found compatible with the needs of CNS-active agents [54], thereby supporting the validity of natural products in the search for novel $GABA_A$ receptor modulators.

A significant number of NPs are valuable for their antagonist interaction at $GABA_A$ receptors. Some of these compounds are employed as control drugs or compounds which qualify as lead structures, in various bioassays for discovery of GABAergic leads. Picrotoxin, the well-known proconvulsant used in animal convulsion studies, is mixture of two sesquiterpene lactones: picrotoxinin and picrotin. The individual pure components, as well as the mixture, are potent $GABA_A$ receptor channel blockers [55]. Bicuculline, a phtalide isoquinoline, is also a convulsant compound which served for many years as the reference for $GABA_A$ receptor research [56].

References:

[1] Uusi-Oukari, M., Korpi, E. R., Regulation of $GABA_A$ receptor subunit expression by pharmacological agents. Pharmacological Reviews. 62 (2010) 97-135.

[2] Olsen, R. W., GABA-benzodiazepine-barbiturate receptor interactions. Journal of Neurochemistry. 37 (1981) 1-13.

[3] Fatemi, S. H., Folsom, T. D., GABA receptor subunit distribution and FMRP–mGluR5 signaling abnormalities in the cerebellum of subjects with schizophrenia, mood disorders, and autism. Schizophrenia Research. 167 (2015) 42-56.

[4] Whiting, P. J., $GABA_A$ receptor subtypes in the brain: a paradigm for CNS drug discovery?. Drug Discovery Today. 8 (2003) 445-50.

[5] Smith, A. J., Simpson, P. B., Methodological approaches for the study of $GABA_A$ receptor pharmacology and functional responses. Analytical and Bioanalytical Chemistry. 377 (2003) 843-51.

[6] Rudolph, U., Knoflach, F., Beyond classical benzodiazepines: novel therapeutic potential of $GABA_A$ receptor subtypes. Nature Reviews Drug Discovery. 10 (2011) 685-97.

[7] Bylund, D. B., Toews, M. L., Radioligand binding methods: practical guide and tips, American Journal of Physiology-Lung Cellular and Molecular Physiology. 265 (1993) L421-L9.

[8] Möhler, H., Richards, J., Agonist and antagonist benzodiazepine receptor interaction in vitro. Nature. 294 (1981) 763-765.

[9] Marandi, N., Konnerth, A., Garaschuk, O., Two-photon chloride imaging in neurons of brain slices. Pflügers Archiv. 445 (2002) 357-65.

[10] Kuner, T., Augustine, G. J., A genetically encoded ratiometric indicator for chloride: capturing chloride transients in cultured hippocampal neurons. Neuron. 27 (2000) 447-59.

[11] Smith, A. J., et al., Effect of α subunit on allosteric modulation of ion channel function in stably expressed human recombinant γ-aminobutyric acid A receptors determined using ^{36}Cl ion flux. Molecular Pharmacology. 59 (2001) 1108-18.

[12] Smith, A. J., McKernan, R. M., Atack, J. R., Benzodiazepine modulation of recombinant α1β3γ2 $GABA_A$ receptor function efficacy determination using the Cytosensor microphysiometer. European Journal of Pharmacology. 359 (1998) 261-9.

[13] Kvist, T., Hansen, K. B., Bräuner-Osborne, H., The use of *Xenopus* oocytes in drug screening, Expert Opinion on Drug Discovery. 6 (2011) 141-53.

[14] Baburin, I., Beyl, S., Hering, S., Automated fast perfusion of *Xenopus* oocytes for drug screening. Pflügers Archiv. 453 (2006) 117-23.

[15] Papke, R. L., Smith-Maxwell, C., High throughput electrophysiology with *Xenopus* oocytes, Combinatorial Chemistry and High Throughput screening. 12 (2009) 38-50.

[16] Ffrench-Constant, R. H., et al., A point mutation in a Drosophila GABA receptor confers insecticide resistance. Nature. 363 (1993) 449.

[17] Rodgers, R., et al., Animal models of anxiety: an ethological perspective. Brazilian Journal of Medical and Biological Research. 30 (1997) 289-304.

[18] Griebel, G., Holmes, A., 50 years of hurdles and hope in anxiolytic drug discovery. Nature Reviews Drug Discovery. 12 (2013) 667.

[19] Deacon, R.M., Measuring motor coordination in mice, JoVE (Journal of Visualized Experiments). (2013) e2609-e.

[20] Stanley, J. L., et al, The mouse beam walking assay offers improved sensitivity over the mouse rotarod in determining motor coordination deficits induced by benzodiazepines. Journal of Psychopharmacology. 19 (2005) 221-7.

[21] HascoëT, M., Bourin, M., A new approach to the light/dark test procedure in mice. Pharmacology Biochemistry and Behavior. 60 (1998) 645-53.

[22] Akdogan, I., Yonguc, N. G., Experimental epilepsy models and morphologic alterations of experimental epilepsy models in brain and hippocampus. in: Underlying Mechanisms of Epilepsy, 2011: InTech Open Access Publisher.

[23] Kaun, K. R., Devineni, A. V., Heberlein, U., Drosophila melanogaster as a model to study drug addiction. Human Genetics. 131 (2012) 959-75.

[24] Kaletta, T., Hengartner, M. O., Finding function in novel targets: C. elegans as a model organism. Nature Reviews Drug Discovery. 5 (2006) 387-99.

[25] Grolleau, F., Sattelle, D. B., Single channel analysis of the blocking actions of BIDN and fipronil on a Drosophila melanogaster GABA receptor (RDL) stably expressed in a Drosophila cell line. British Journal of pharmacology. 130 (2000) 1833-42.

[26] Zhang, H. G., A unique amino acid of the Drosophila GABA receptor with influence on drug sensitivity by two mechanisms. The Journal of Physiology. 479 (1994) 65.

[27] Tropepe, V., Sive, H. L., Can zebrafish be used as a model to study the neurodevelopmental causes of autism?. Genes, Brain and Behavior. 2 (2003) 268-81.

[28] Santana, S., Rico, E. P., Burgos, J. S., Can zebrafish be used as animal model to study Alzheimer's disease, Amarican Journal of Neurodegenerative Disease. 1 (2012) 32-48.

[29] Baraban, S. C., Emerging epilepsy models: insights from mice, flies, worms and fish. Current Opinion in Neurology. 20 (2007) 164.

[30] Khom, S., et al., $GABA_A$ receptor modulation by piperine and a non-TRPV1 activating derivative. Biochemical Pharmacology. 85 (2013) 1827-36.

[31] Kim, H. J., HPLC-based activity profiling approach for the discovery of $GABA_A$ receptor ligands using an automated two microelectrode voltage clamp assay on *Xenopus* oocytes. Planta Medica. 74 (2008) 521.

[32] Kim, H. J., et al., HPLC-based activity profiling--discovery of sanggenons as $GABA_A$ receptor modulators in the traditional Chinese drug Sang bai pi (*Morus alba* root bark). Planta Medica. 78 (2012) 440-7.

[33] Li, Y., et al., HPLC-based activity profiling for $GABA_A$ receptor modulators: a new dihydroisocoumarin from *Haloxylon scoparium*. Journal of Natural Products. 73 (2010) 768-70.

[34] Rueda, D. C., et al., HPLC-Based Activity Profiling for $GABA_A$ Receptor Modulators in Adenocarpus cincinnatus. Journal of Natural Products. 77 (2014) 640-9.

[35] Rueda, D.C., et al., Identification of dehydroabietc acid from *Boswellia thurifera* resin as a positive $GABA_A$ receptor modulator. Fitoterapia. 99 (2014) 28-34.

[36] Rueda, D.C., et al., Identification of dihydrostilbenes in *Pholidota chinensis* as a new scaffold for $GABA_A$ receptor modulators. Bioorganic and Medicinal Chemistry. 22 (2014) 1276-84.

[37] Rueda, D.C., et al., Discovery of $GABA_A$ Receptor Modulator Aristolactone in a Commercial Sample of the Chinese Herbal. Ethnomedicine-Based Discovery and Characterization of Plant-Derived $GABA_A$ Receptor Modulators with New Scaffolds. 78 (2012) 63.

[38] Schramm, A., et al., Phytochemical profiling of *Curcuma kwangsiensis* rhizome extract, and identification of labdane diterpenoids as positive $GABA_A$ receptor modulators. Phytochemistry. 96 (2013) 318-29.

[39] Zaugg, J., et al., HPLC-based activity profiling: discovery of piperine as a positive $GABA_A$ receptor modulator targeting a benzodiazepine-independent binding site. Journal of Natural Products. 73 (2010) 185-91.

[40] Zaugg, J., et al, Identification of $GABA_A$ receptor modulators in *Kadsura longipedunculata* and assignment of absolute configurations by quantum-chemical ECD calculations. Phytochemistry. 72 (2011) 2385-95.

[41] Zaugg, J., et al., Positive $GABA_A$ receptor modulators from *Acorus calamus* and structural analysis of (+)-dioxosarcoguaiacol by 1D and 2D NMR and molecular modeling. Journal of Natural Products. 74 (2011) 1437-43.

[42] Zaugg, J., et al., HPLC-based activity profiling of *Angelica pubescens* roots for new positive $GABA_A$ receptor modulators in *Xenopus* oocytes, Fitoterapia. 82 (2011) 434-40.

[43] Zaugg, J., et al., Identification and characterization of $GABA_A$ receptor modulatory diterpenes from *Biota orientalis* that decrease locomotor activity in mice, Journal of Natural Products. 74 (2011) 1764-72.

[44] Jäger, A. K., Saaby, L., Flavonoids and the CNS. Molecules. 16 (2011) 1471-85.

[45] Hanrahan, J. R., Chebib, M., Johnston, G. A., Flavonoid modulation of $GABA_A$ receptors. British Journal of Pharmacology. 163 (2011) 234-45.

[46] Marder, M., et al., Detection of benzodiazepine receptor ligands in small libraries of flavone derivatives synthesized by solution phase combinatorial chemistry. Biochemical and Biophysical Research Communications. 249 (1998) 481-5.

[47] Yang, X., et al., HPLC-based activity profiling for $GABA_A$ receptor modulators from the traditional Chinese herbal drug Kushen (*Sophora flavescens* root). Molecular Diversity. 15 (2011) 361-72.

[48] Manach, C., Donovan, J.L., Pharmacokinetics and metabolism of dietary flavonoids in humans. Free Radical Research. 38 (2004) 771-85.

[49] Vissiennon, C., et al., Route of administration determines the anxiolytic activity of the flavonols kaempferol, quercetin and myricetin – are they prodrugs?. Journal of Nutritional Biochemistry. 23 (2012) 733-40.

[50] Khom, S., et al., Valerenic acid derivatives as novel subunit-selective $GABA_A$ receptor ligands–*in vitro* and *in vivo* characterization. British Journal of Pharmacology. 161 (2010) 65-78.

[51] Kuribara, H., Stavinoha, W. B., Maruyama, Y., Honokiol, a putative anxiolytic agent extracted from magnolia bark, has no diazepam-like side-effects in mice. Journal of Pharmacy and Pharmacology. 51 (1999) 97-103.

[52] Maruyama, Y., et al., Identification of magnolol and honokiol as anxiolytic agents in extracts of saiboku-to, an oriental herbal medicine. Journal of Natural Products. 61 (1998) 135-8.

[53] Baburin, I., et al., Honokiol modulates $GABA_A$ receptors subunit specifically. Scientia Pharmaceutica. 77 (2009) 225.

[54] Eigenmann, D.E., et al., *In vitro* blood-brain barrier permeability predictions for $GABA_A$ receptor modulating piperine analogs. European Journal of Pharmaceutics and Biopharmaceutics. 103 (2016) 118-126.

[55] Jarboe, C. H., Porter, L. A., Buckler, R. T., Structural aspects of picrotoxinin action. Journal of Medicinal Chemistry. 11 (1968) 729-31.

[56] Johnston, G., $GABA_A$ receptor pharmacology. Pharmacology and Therapeutics. 69 (1996) 173-98.

2.3. Zebrafish as a model organism in drug discovery and development

Zebrafish (*Danio rerio*), a fresh water vertebrate of the Cyprinidae family, has been a popular aquarium fish for decades. It was first proposed as a model for small molecule discovery in 1957 [1]. The use of zebrafish for research has been rapidly increasing in the 1990s and 2000s to a point that in 2003 it was ranked by the National Institute of Health (NIH) as the third most important experimental organism after rats and mice [2]. Over the past decade the zebrafish has emerged as a vertebrate model adaptable to large-scale studies in a wide range of biological topics, from early developmental process to genetic analysis, to complex behavioral research [3, 4]. The stage of the animals used can range from single cell stage for early development screens to late larval stages for physiology or behavior screens, and adult fish for exploring complex social interactions [4]. In the present section an overview of zebrafish life-cycle and developmental stages is given. The characteristics which make zebrafish a favorite model for drug discovery and, the contribution of zebrafish-based assays to drug discovery and development are discussed afterwards.

2.3.1. Zebrafish development and life cycle

Natural populations of zebrafish are found in rivers, small streams, and rice paddies with temperatures between 27 and 34 °C. Zebrafish are photoperiodic breeders mating in silt-bottomed well-vegetated pools right after sunrise [5]. Under standard laboratory conditions, adult zebrafish are housed in rack systems with a controlled temperature at about 28 °C and a photoperiod of 14 h light/10 h dark. Mating crosses are set up in the early evening and the natural spawning starts when the lights are turned on in the morning. A successful

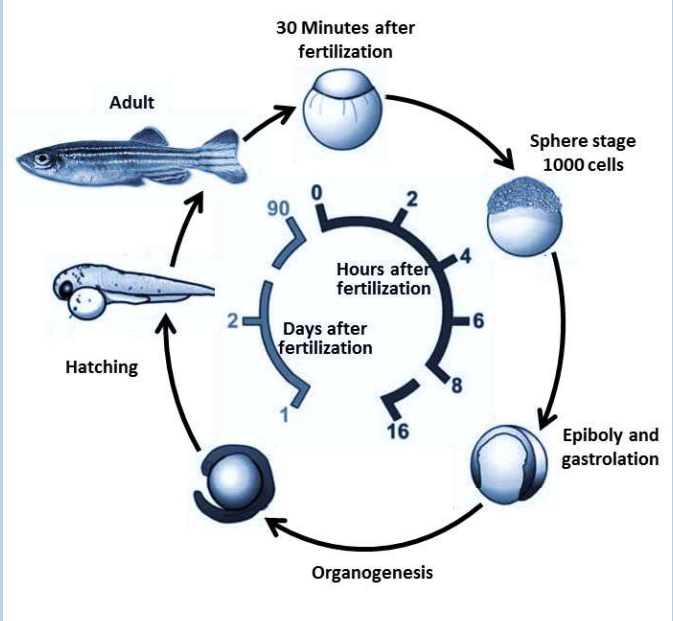

Figure 2.3-1: Zebrafish life cycle from a fertilized egg to an adult fish is 90 days [8].

mating can yield 200-300 embryos per day per adult pair [6]. The zebrafish life cycle starts with a fertilized egg (zygote). The zygote at the time of fertilization is about 0.7 mm in diameter [7]. It has a yolk which provides nutrients for embryonic development, and a chorion as a protective membrane surrounding the embryo [8]. The full life cycle from a fertilized egg to an adult fish is 90 days and is divided into four major periods including embryonic, larval, juvenile, and adult stages [8]. Embryonic development for zygotes of the same batch fertilized simultaneously exhibit slightly differing rates. Therefore, the embryonic stage is described based on the morphological criteria rather than the age, and is divided into six periods:

I) Cleavage period. Shortly after fertilization, the cytoplasm moves toward one pole of the egg inflating a single cell called blastodisc. The first cleavage in the zygote occurs about 40 minutes after fertilization and continues at about 15-minute intervals within 6 cleavage cycles. The cells formed during cleavage period (blastomeres) undergo rapid, synchronized cell division with no cell growth [7, 8].

II) Blastula period. Is the embryonic development between the 8^{th} and 14^{th} cell cycle ($2^{1/4}$ – $5^{1/4}$ h) in which the embryo begins to make its own RNA. The cell cycles are thus longer. In this period a dramatic movement of cells begins over the surface of the yolk, known as epiboly, and a tightly sealed epithelial monolayer and a deep cell multilayer are formed over the yolk [7, 8].

III) Gastrula period. Transition from 50% epiboly (the moment which the cells cover about half of the yolk) to the somite appearance is named gastrula period [7, 8]. The embryos produce two primary germ layers, each of them giving rise to different lineage-specific fates restricted to one tissue or organ ($5^{1/4}$ – 10 h).

IV) Segmentation period. The first day of embryonic development ends with the segmentation period (10 – 24 h). During that, the somites develop, the rudiments of the primary organs become visible, the tail grows, and the first body movements appear. The overall body length of the embryo increases very rapidly as the tail extends [7, 8].

V) Pharingula period. During the second day of embryonic development (24 – 48 h), the pharyngeal arches develop rapidly, the fins begin to form, the pigment cells differentiate, and the heart begins to beat along with the head-straitening. Moreover, some marked behavioral developments are observed such as spontaneous side-to-side contractions of the embryo, tactile

sensitivity, and reflexive movements after light touches to the head or body of the dechorionated embryo. However, the embryo cannot yet effectively move its body through the water [7, 8].

VI) Hatching period. On the third day of embryonic development (48 – 72 h), morphogenesis of many of the organ rudiments is rather complete, with some notable exceptions including the gut and its associated organs [7, 8].

The hatched larva at three days post fertilization (3dpf) is 3.1 – 3.5 mm long [9] and continues to grow rapidly. The larva consumes energy stores of the yolk during the next 4 days (until 7dpf) and has no need to be fed. The main changes during the early larval stage include anterior-dorsal protrusion of the mouth, the ventrally drop of the gut, and the inflation of the swim bladder [7, 8]. Some significant behavioral developments are also observed during the larval stage. The hatched larva initially lies on the side, on the bottom of the tank, and occasionally darts forward or circles around. It displays a startle response when exposed to abrupt stimuli including touch, sound, water flow, or light. Between 4 and 5dpf, by inflation of the swim bladder, the larva starts swimming around. At the same time, it can follow moving objects with the eyes, a behavior that is referred to as the optokinetic response. At 5dpf, the larval vision progresses; it is actively hunting for food. At 5, 6 and 7dpf, larva displays diurnal rhythms in activity that is higher activity during the day than at night [9].

After 7dpf, during the juvenile stage, the fish are fully mobile. Their abilities to hunt and swim increase, and after 2-3 months, the fish reach adulthood [8].

2.3.2. Advantages of zebrafish as a model organism

Zebrafish has increasingly attracted attention as a biological model in a wide range of scientific areas such as biomedicine, pharmacology and toxicology [1]. Several characteristics of zebrafish at different developmental stages, namely physiological attributes, genetic homology and structure similarity to humans, rapid life cycle and low cost maintenance, can explain its superiority as a model organism in research [11].

Rapid life cycle and low-cost maintenance

The adult zebrafish grows to an average size of only 3 – 4 cm, making it feasible to maintain a large number of them in a relatively small laboratory area with low husbandry costs [11-13]. Zebrafish has a relatively short generation time (3 months) and rapid development. The fish breeds all year round and a modest colony of fish can produce hundreds of fertilized eggs daily. A fertilized egg develops into an embryo with a beating heart in just 24 h; organ progenitors appear by 36 h post-fertilization, and hatching occurs by the third day after fertilization [9, 11, 12]. The large number of embryos spawned per week along with the rapid embryonic development provides the opportunity for large-scale mutagenesis and small molecule screens [14, 15]. Zebrafish embryos and larvae are small enough to fit into 96-well plates, enabling high-throughput screening with only minute quantities of chemicals [16].

Transparent embryos and larvae

Zebrafish eggs are fertilized outside the body. Also, due to the sequestration of the yolk granules into a single giant yolk cell, the eggs and embryos are transparent. The extra uterine transparent embryos are accessible to experimental manipulations such as DNA, RNA, protein, or morpholino oligonucleotide microinjections which provide the opportunity to determine gene functions, and provide insights into the genetic control of complex developmental processes [1, 8, 9, 11, 13]. In addition, the possibility of live visualization of the entire embryonic development from the early cleavage stage, and tracking of the fate of individual cells as they divide, migrate and differentiate makes zebrafish embryo ideal for developmental investigations [11]. Accurate developmental assessments facilitate adoption of automated screening platforms for time-limited studies restricted to the embryonic stages [14, 15].

Observation of the internal organs in older larvae at real time has become feasible by depigmentation of larvae with the tyrosinase inhibitor 1-phenyl-2-thiourea supplemented in the media. As for the adult fish, transparent Casper lines with no pigmentation have been developed, and they can be crossed with any mutant or transgenic fish of interest [6]. *In vivo* live imaging studies of adult vertebrate have been enabled with transparent lines of zebrafish which transgenically express a fluorescent protein [17, 18].

Genetic homology to humans

Humans and zebrafish share a common ancestor that lived around 400 million years ago [19]. Zebrafish has the largest gene set sequenced so far among vertebrates [20, 21]. 71% of human proteins and 82% of disease-associated human proteins have an obvious orthologue in zebrafish [16, 19, 22]. Similarities of the enzymes, channels and receptors are even greater at the active sites (the main targets of drugs) than the entire protein. For example, the zebrafish glucocorticoid receptor, which is only about 50% identical to the human receptor overall, is 74% identical in the carboxy-terminal region containing the ligand-binding domain [22]. Moreover, transgenic zebrafish are continuously increasing in number, and are used to model the humans' diseases [14, 23]. Thousands of mutant lines of zebrafish with targeted loss-of-function have been generated [19, 22]. Any lines that produce a disease-relevant phenotype can be quickly expanded and used to screen chemical suppressors of the disease-associated phenotypes [12, 22].

Multi-organ system similar to humans

When it comes to drug discovery research, the zebrafish holds an important advantage over yeast and cultured cells that is possession of organs and behavior [4]. Zebrafish larvae possess functional organs such as liver, pancreas, kidney, or blood-brain barrier. Each organ communicates with all other organs around it [22, 24]. To exhibit activity in zebrafish assays, compounds must have the ability to be absorbed, reach the target tissue, and avoid rapid metabolism and excretion. Rather than the conserved partitioning of drugs into different passive compartments based on physicochemical characteristics, there is strong evidence of the regulation of drug distribution across active physiological boundaries such as the blood-brain barrier, and by tissue-specific transporters [22, 24]. Despite some major differences resulting in adaptation to aquatic life, most zebrafish organs perform the same functions as their human counterparts. For example, zebrafish

pancreas contains islets comprising α, β, δ, and ε cells that regulate glucose homeostasis by secreting glucagon, insulin, somatostatin and ghrelin. Drugs that modulate glucose homeostasis in humans have been shown to have the same effects in zebrafish [24]. The zebrafish hematopoietic system is highly similar to the human system and consists of the same cell types including erythrocytes, neutrophils, eosinophils, lymphocytes, and macrophages, along with the similar hematopoietic processes namely, globin switching and hepcidin-ferroportin pathways. In fact, the key components of these processes were first discovered in zebrafish [24]. Cardiovascular physiology is also highly conserved between humans and zebrafish at anatomical, cellular and membranal levels [19, 24]. Interestingly, the cardiac electrophysiology of humans is more similar to that of zebrafish than rodents. Many human cardiovascular drugs have been shown to have identical effects on zebrafish physiology [24]. The zebrafish immune system shows many points of conservation with that of mammals. Zebrafish have both an adaptive (B- and T-cell-mediated) immune response, and a well-developed innate immune system. Adult zebrafish have been used as hosts for *Listeria monocytogenes*, *Streptococcus* sp., *Mycobacterium marinum* and *Edwardsiella tarda* in infectious disease studies [19]. An additional example of high level similarity between the human and zebrafish is the glucocorticoid system. The main endogenous glucocorticoid hormone in zebrafish is cortisol, as it is in humans. In contrast, in the most commonly used rodent models it is corticosterone [19]. Some efforts have been made to characterize the parallels between different stages of zebrafish development and those of humans. It has been observed that the key molecular transitions in each of the organs relevant for disease modelling or drug metabolism take place in sequence, but often much more rapidly in zebrafish than in humans. For example, the sequential electrophysiological maturation of the zebrafish heart takes place within 96 h post-fertilization, whereas in humans some of the parallel events are not completed until adolescence [24]. Overall, zebrafish, as a model organism, provides a unique platform for *in vivo* screens comprising the biological complexity associated with multi-organ development and function of a whole animal [6].

2.3.3. Zebrafish in drug discovery and development

A drug discovery program initiates because there is a disease or clinical condition without suitable medical products available [25]. Discovery of lead compounds starts with an intensive search to find a drug-like small molecule or biological therapeutic which can progress into preclinical and, if successful, into clinical development. The hit-to-lead starting point usually involves a high throughput assay to establish the activity of the compounds on the molecular target. Compounds which meet basic criteria are subjected to intensive structure-activity-relationship (SAR) studies and medicinal chemistry efforts to produce more potent and selective compounds. Detailed physicochemical analysis and *in vitro* ADME profiling are carried out in parallel to ensure appropriate PK properties which enable the *in vivo* efficacy. Finally, compounds which meet the target potency and selectivity, and most of the desired physicochemical and ADME properties will be submitted to mammalian models prior to progression into clinical development [25].

The zebrafish-based bioassays focus on either a specific organ, a molecular target, or the whole organism, fit into multiple stages of the drug discovery process from the hit identification to the lead optimization, to ADME profiling and toxicity studies [6]. A reasonable number of human drugs have been tested for conserved effects in zebrafish, suggesting a high probability of direct correlation between effects in humans and those in zebrafish [6]. Several of the molecules discovered by zebrafish-based screens are progressing toward clinical studies [4].

Hit discovery and lead development

Zebrafish embryos and larvae are rapidly gaining favor in numerous small molecule screens against human diseases such as cancer [26], kidney disorders [27], cardiovascular disease [28], hearing loss [29], muscular dystrophy [30], as well as neurological diseases [6, 14, 31-35], thanks to their several advantages as a model organism compared to the similar scale *in vitro* and cell-based models (section 2.3.2). Wild type fish have mainly been used for observing the effects of compounds on the development, morphology, and function of specific organs and tissues [36, 37], while the newly available mutant lines were adapted to genetically enhanced disease-like models such as atherosclerosis, hyperlipidemia, blood vessel inflammation and many others [6, 38]. Invention and power of several high-throughput screens owe the transparency of embryos

and larvae which allows live imaging of alterations in various tissues [39-41]. Antiangiogenic compound screening using fluorescently marked blood vessels is one of the well-known examples of such assays [6, 42, 43]. One of the major utilities of zebrafish in drug discovery, not possible with simpler screening systems, has been the search for compounds affecting complex behaviors [6, 9, 13, 35]. The recent high-throughput studies to identify compounds impacting sleep behavior (periods of rest and wake cycles) [44], and photomotor response of embryos [6, 32] are examples of successful drug screens in zebrafish. The latter has resulted in creation of activity barcodes on the basis of phenotypic similarity [32]. Pain, sedation, tumor metastasis, vascular tone, and gut motility are other examples of disease-relevant phenotypes that are observable in zebrafish yet simply inaccessible to modelling in cultured cells [22]. Also, zebrafish-based screenings have the capability to uncover prodrug activities, which are otherwise missed when utilizing *in vitro* assays [6, 35].

The discovery of a hit compound is generally followed by intensive SAR studies to generate related entities with greater potency, and less side effects. Zebrafish provides a powerful *in vivo* tool for the simultaneous assessment of efficacy and toxicity of the modified compounds. Hence, it can open a new gate to hit-to-lead development process by facilitating the SAR studies. This strategy has been used, for instance, in modification of dorsomorphin, an inhibitor of bone morphogenetic protein (BMP) in abnormal dorsoventral patterning, to its highly selective analogues [6, 22, 45]. Dorsomorphin itself was not applicable as a therapeutic agent due to a significant inhibition of vascular endothelial growth factor (VEGF) signaling. Medicinal chemistry efforts around dorsomorphin followed by angiogenesis screens in embryos led to the discovery of several highly selective BMP signaling inhibitors with no observable off-target VEGF inhibition [45].

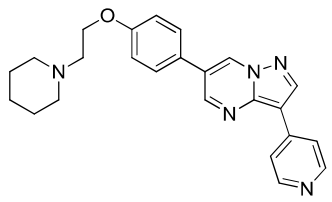

Dorsomorphin

Target identification

Targets are a range of biological entities (proteins, genes and RNA) accessible to the potential drug molecules which, upon binding, elicit a biological response [25]. Compounds with similar effects, discovered in large-scale screens, may be acting through different targets. The vast arsenal of molecular biology and genetic approaches available for zebrafish can be utilized for

rapid target identification or confirmation after identification of a lead compound [6]. An example of target confirmation using zebrafish-based assays is that of thalidomide. Thalidomide was widely prescribed in the 1950s and 1960s to pregnant women suffering from morning sickness. This resulted in serious developmental birth defects including severe shortening or absence of limbs in over ten thousand children. The mechanism behind those developmental defects was unknown for a long time, as the commonly utilized animal models (mice and rats) are insensitive to thalidomide teratogenicity. Later, zebrafish embryos were recognized sensitive to thalidomide teratogenicity and provided an *in vivo* vertebrate model for the corresponding studies. The embryos which were treated with thalidomide exhibited developmental defects such as pectoral fin malformations. Cereblon (CRBN) was confirmed as a thalidomide target since the effects of the drug was recapitulated in zebrafish when CRBN was knocked down [6, 12].

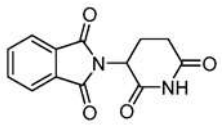

Thalidomide

Beyond the generic approaches, there are some zebrafish-specific tools to aid target identification such as the large collection of zebrafish phenotypes associated with specific gene mutations and knockdowns [4]. Identifying similarities between a drug-induced phenotype and a genetic phenotype can provide clues to the principal drug target [22].

ADME analysis

Absorption, distribution, metabolism and excretion (ADME) of drugs might also be accessible in zebrafish modelling. There is strong evidence that aqueous exposure is a practical route of drug administration in zebrafish as numerous drug compounds have been shown to be active in larvae and adult fish by this route of administration [24]. Oral absorption is followed by water ingestion in the gastrointestinal tract [24]. In addition, passive membrane transport is likely to be similar in fish and humans. In a screening of dozens of hits with zebrafish-based assays, it was observed that compounds with low octanol/water partition coefficient (log P) (values < 1) rarely had bioactivity. Thus, log P has been introduced as a physicochemical factor that affects bioactivity in zebrafish by influencing absorption [4]. Rather than conserved partitioning of drugs into different passive compartments, the regulation of drug distribution in zebrafish is clearly influenced by active physiological boundaries such as the blood-brain barrier and retinal barrier, as well as by conserved tissue-specific transporters [24].

Another important factor in the conservation of drug activity is drug metabolism. The phase I biotransforming cytochromes P450 (CYP) monooxygenases are an important means of drug metabolism in zebrafish. Zebrafish possesses a full complement of CYP450 genes. The dioxin inducible CYP1A gene is well characterized in the zebrafish and can be induced in many tissues of the embryo [12]. Constitutive and xenobiotics induced expression of zebrafish CYP3A gene is also conserved [13]. Also, they express several phase II metabolic enzymes similar to mammalian glutathione-S-transferase (GST), uridine diphosphoglucuronyl transferases (UGTs) and sulfotransferases (SULTs) [46-50]. These findings demonstrate similar metabolic capabilities in the zebrafish as those observed in mammalian species.

Finally, drug excretion is clearly regulated in the zebrafish despite the fact that few studies of drug filtration, reabsorption or excretion have been undertaken to date. As mass spectroscopy techniques advance, more generalized approaches to ADME in the zebrafish are emerging [24].

Toxicology studies

Mammalian toxicology is performed in preclinical development to determine the safety of lead compounds and drug candidates. Such studies are done at relatively late stages due to the cost and effort associated with them [22]. The high-throughput zebrafish models can unravel toxicity issues early on and, therefore, save time and money by enabling toxic compounds to fail fast before substantial investments on their preclinical advancement are made [6, 22].

Traditionally, zebrafish models have been used in environmental toxicology studies focusing on acute toxicity of chemicals, pesticides, and pharmaceuticals [6]. Recently, zebrafish has been shown to be a highly predictive model for several types of drug toxicities. External development of embryos affords advantages over mammalian models in teratogenicity studies [19]. Cardiotoxicity appears to be highly conserved between zebrafish and humans. Systematic studies of drugs that cause QT prolongation in humans showed > 95% conservation of effect in zebrafish [22]. Likewise, close correlations have been observed for hepatotoxicity, nephrotoxicity and reproductive toxicity, in which all of the known toxicants in preclinical mammalian models or humans have similar effects in zebrafish [22]. Other categories of toxicity which can be specifically assessed in the zebrafish includes various types of neurotoxicity such as ototoxicity, locomotor effects, gastrointestinal and visual toxicity [6].

2.3.4. Rationale for neuroactive drug discovery with zebrafish

Many neuroactive drugs available today are the analogues of behavior-altering prototypes which have been discovered by chance in the 1940s and 50s [12]. The lack of available relevant models to screen large numbers of active compounds has been one of the main reasons for the lack of newer neuroactive drugs. The *in vitro* models cannot reflect the complex networks of the brain, and the mammalian models are not able to support high-throughput screenings due to the high expense and ethical issues [12]. Some invertebrate organisms such as the nematode *Caenorhabditis elegans*, as well as the insects *Drosophila melanogaster* (fruit fly) and *Locusta migratoria* (grass hopper) have been used to explore the genetic aspects of neurogenesis, and provided important insights into neurodegenerative diseases. However, invertebrate animals lack many developmental characteristics specific to vertebrates [11] which limits their application in modelling complex CNS disorders [23, 51]. In this respect, zebrafish has recently emerged as an ideal model for neurobehavioral studies providing a reasonable compromise between physiological complexity and throughput [23]. Rather than the general advantages of zebrafish for large-scale small molecule studies (described in section 2.1.2), they possess a number of features that offer the rationale for their utilities, particularly in neuroactive drug discovery:

i) Possessing a complex brain with significant physiological homology to mammals [11, 23]
ii) Functional and size exclusive BBB [52]
iii) Complex network of multiple organs requiring appropriate bioavailability and ADME properties [22]

Complex brain

Brain organization, neuroanatomical and neurochemical pathways in zebrafish show an overall homology with humans [11, 23]. Zebrafish CNS contains the main cellular types found in the mammalian brain, such as microglia, oligodendrocytes and myelin, cerebellar purkinje cells and astrocytes [11]. Primary neurogenic and basic helix-loop-helix genes necessary to generate a highly organized central nervous system (CNS) in mammals have been shown to guide the brain development in zebrafish, as well. Zebrafish encephalon has fore-, mid- and hind-brain structures including diencephalon, telencephalon and cerebellum [13, 23]. The major neurotransmitter paths such as the excitatory glutamatergic and the inhibitory GABAergic paths as well as the

muscarinic cholinergic neurotransmission have been demonstrated to exist in the zebrafish brain. The associated neurotransmitters namely GABA, dopamine, serotonin, histamine, glutamate and acetylcholine [11, 13] are also present along with their transporters and synaptic vesicle proteins [11, 13]. Similar to other vertebrates, zebrafish have all of the classical sense modalities including vision, olfaction, taste, tactile, balance and hearing, and their sensory pathways share an overall homology with humans [11]. The optic tectum, in zebrafish brain has defined areas such as the hypothalamus and olfactory bulb which appear to be homologous to the mammalian hippocampus [23]. The topographical projection of the retinotectal pathway for visual processing is highly conserved among all vertebrates. In larval zebrafish, the second order motion perception (similar to processing of complex visual information in human's visual cortex) has been additionally observed suggesting a higher-level of cortical-like visual processing [11].

In summary, production, differentiation and connectivity of neurons in the developing zebrafish CNS require molecular mechanisms similar to those in mammals [11], enabling preparation of neuropathological and behavioral phenotypes, and corresponding screening models [11, 23].

Functional blood-brain barrier

The CNS has developed specialized barriers that isolate neurons from the blood stream, assisting maintenance of the homeostasis and proper neuronal function in the CNS [53]. Blood-brain barrier (BBB), choroid plexus, and arachnoid barrier are the three CNS barriers [15]. The BBB regulates ionic balance and nutrient transport in the brain, and provides a protection layer from pathogens and harmful materials circulating in the blood [52]. However, tightness of the BBB also causes significant problems for delivery of therapeutic drugs to the brain [52, 53]. It has been estimated that > 98% of small molecules cannot penetrate the BBB [15], and most of the neuroactive drugs fail in clinical trials due to inadequate BBB permeability [54]. The tight junctions between endothelial cells of the vasculature, providing the first level of barrier [52, 55], make the BBB an essentially vertebrate system [52, 53]. Invertebrates do not possess a complex circulatory system and therefore have no endothelial-based BBB.

Several studies have demonstrated that zebrafish at the early larval stage gradually develop endothelial-based BBB with similar histologic and functional properties to those of higher vertebrates [52, 55, 56]. The BBB against large molecules is formed by 2dpf [53]. In 3dpf zebrafish embryos, the BBB is resistant to horseradish peroxidase (44 kDa) and rhodamine

dextran (10 kDa), which are similar in size to most plasma proteins, suggesting a comparable BBB permeability in 3dpf zebrafish embryos with that of mammals [52]. The BBB tight junctions consist of several proteins which contribute to the physiological properties of the BBB. The major constituents of endothelial tight junctions are claudin-5 and zonula occludens-1 [54]. Their expression has been observed in zebrafish embryos as early as 3dpf. The restriction to small molecules is considered to develop by this stage [52, 53]. In addition, function of the BBB in mammals is tied to the presence of active transport systems such as the P-glycoprotein (P-gp) transporters [15, 54]. In zebrafish, active transport of molecules across the BBB has been demonstrated with anatomical and functional evidences [55]. Taken together, these features formulate a selective permeable barrier which makes zebrafish a superior model in neuroactive drug discovery.

ADME principles

In drug development process, a highly selective and potent compound may not simply end up as a therapeutic agent, due to its poor ADME properties [54]. As mentioned in section 2.3.3, zebrafish larvae can provide a prediction tool for compounds' absorption and distribution. They are equipped with both passive diffusion and active transport systems [55], and the key phase I and phase II enzymes for drug metabolism [12, 13, 46-50]. Therefore, physiochemical and biological properties of the circulating metabolites in the body, metabolic inactivation/activation of pharmacologically active compounds, as well as their excretion are determinative factors for compounds activities in zebrafish-based screens. Compounds which exhibit activity in zebrafish models are assumed to have reasonable bioavailability and ADME properties [22]. These features provide rationale for employment of zebrafish-based models for various bioactivity screens including neuroactivity studies.

2.3.5. $GABA_A$ signaling system in zebrafish

In mammalian species, GABA is produced *via* α-decarboxylation of glutamic acid catalyzed by glutamic acid decarboxylase (GAD). The two different forms of GAD described in mammals and birds are GAD65 and GAD67, in which 65 and 67 refer to the molecular weight of each protein in kilodaltons. Expression of GAD65 and GAD67 in the zebrafish embryo has been reported during the axonogenesis period. The corresponding cDNAs have been described with over 84% identity to those of the humans [57]. Both GAD genes are expressed in the forebrain, midbrain, hindbrain and spinal cord neurons, and catalyze the production of GABA in the developing embryo. Production of GABA is detectable at all sites of GAD expression [57].

The zebrafish genome comprises 22 genes encoding for $GABA_A$ receptor subunits. Based on the gene expression in the GABA signaling system of zebrafish, the proposed $GABA_A$ receptors are $\alpha_1\beta_2\gamma_2$, $\alpha_1\beta_2\delta$, $\alpha_{2b}\beta\varepsilon\gamma_2$, $\alpha_{2b}\beta_3\delta$, $\alpha_4\beta_2\gamma_2$, $\alpha_4\beta_2\delta$, $\alpha_{6b}\beta_2\gamma_2$ and $\alpha_{6b}\beta_2\delta$ [58]. In addition, rather than the $GABA_A$ receptors in zebrafish brain, presence of $GABA_A$ and $GABA_C$ receptors has been revealed on zebrafish retinal bipolar cells by electrophysiological studies [59]. The α_{6a} is more abundant in retinas while the α_{6b} is more abundant in the brain [58]. $GABA_B$ receptors have been found in the cerebellum, and were linked to three zebrafish genes homologous to the human genes for subunit β_1 and β_2 [58].

The whole-cell patch-clamp electrophysiology studies with Mauthner cells (the largest neurons in the zebrafish CNS) of embryonic zebrafish disclosed the properties of $GABA_A$ mediated postsynaptic currents. Accordingly, there are three general groups of $GABA_A$ receptor-containing synapses: group I expresses a homogeneous type of receptor with a broad distribution and a single exponential decay time peaking around 40 – 60 ms; group II expresses $GABA_A$ receptors with a single decay time peaking around 120 – 160 ms, and group III appears to express a combination of the first two groups [60].

Understanding of zebrafish GABAergic neurotransmission has been partly achieved through the investigations on environmental toxins. The GABA antagonist pentylenetetrazole (PTZ) induces a concentration-dependent sequence of behavioral changes in zebrafish culminating in clonus-like convulsions which can be inhibited by common antiepileptic drugs such as benzodiazepines

[23]. Zebrafish larvae exposed to this chemoconvulsant exhibit epileptiform electrographic discharges on field potential recordings from the optic tectum. Epileptiform activities recorded from zebrafish brains include interictal- and ictal-like discharges, and are similar to the neural activities described for hippocampal-slice recordings from rodent brains [61]. These observations indicate that the GABAergic system can be impaired in zebrafish, being a relevant target for the study of the balance between neuronal circuits, and for the evaluation of antiepileptic drugs and neuroprotectants [23].

2.3.6. Behavior-based assays with zebrafish

Zebrafish has been gaining favor as a behavioral model at various developmental stages (embryos, larvae and adult fish) [62]. Several classes of known neuroactive drugs have shown distinctive and reproducible behavioral signatures in zebrafish behavioral assays [22], proposing the zebrafish behavior models as a bridge to the study of human disease in mammalian models [62]. Zebrafish larvae possess a broad range of behaviors from simple stimulus responses to more complex learning and sleeping behaviors, many of which are amenable to assessments in 96-well format [22]. Along with the automated systems developed for imaging in multi-well plates, zebrafish larvae are well suited for high-throughput analyses of behavior [9]. The major behavior-based assays with zebrafish can be classified into photomotor response models, locomotor activity models, escape-and-avoidance behaviors and habituation.

Photomotor response (PMR)

The high-intensity light stimulants elicit a stereotypic series of motor behaviors in embryonic and larval zebrafish known as the photomotor response (PMR). The PMR in embryos is divided into four phases: a pre-stimulus background phase, a latency phase, an excitation phase and a refractory phase [9, 35]. Zebrafish embryos are mostly inactive during the pre-stimulus phase, showing low basal activity characterized by spontaneous and infrequent body flexions within their chorions. Presentation of a light stimulus elicits a robust motor excitation phase (lasting 5 – 7 s) characterized by vigorous shaking. This excitation phase is preceded by a latency phase (lasting 1 – 2 s) and is followed by a refractory phase during which basal activity is suppressed and embryos do not respond to a second light

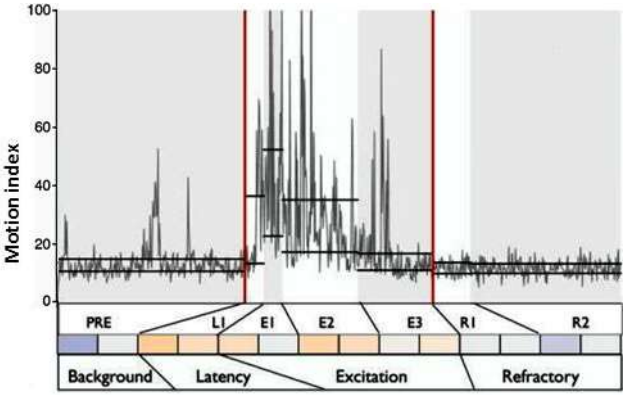

Figure 2.3-2: High-intensity light-stimulus elicits a stereotypic series of motor behaviors, known as the photomotor response (PMR). The PMR can be divided into four broad phases: a pre-stimulus background phase, a latency phase, an excitation phase and a refractory phase [35].

pulse (Fig. 2.3-2) [9, 35]. Zebrafish larvae display a startle response when exposed to a sudden light intensity. The startle response is characterized by a brief period of elevated activity and can be induced when the light is abruptly turned on or off. When the light is turned off at 6dpf, locomotion initially increases to a maximum at 4 minutes and then decreases to a low level at 20 minutes (Fig. 2.3-3) [9, 63].

Small molecules with different mechanisms of action (adrenergic, dopaminergic and serotonergic, for instance) produce distinct changes in the PMR assay, suggesting the involvement of multiple neurotransmitter pathways in the various components of the PMR. The motor activity throughout the PMR is increased with isoproterenol, a psychostimulant, and is lowered by the anxiolytic compound diazepam. The dopamine agonist apomorphine lengthens the PMR latency period [35]. To separate anxiolytic effects from defects in vision or defects in muscle contractions, investigators often show that zebrafish with reduced anxiety still have normal functioning sensory and motor systems [9]. Moreover, like humans and other mammals, zebrafish have wake and sleep-like states characterized by periods of activity and rest (the rest-wake cycle). During the day, zebrafish display increased locomotor activity for longer periods while their night activity is characterized by short periods of infrequent movements and increased arousal thresholds to a mechanical stimulus (Fig. 2.3-4) [12, 64]. The rest-wake cycle is established in zebrafish larvae as early as 4dpf. The quantitative measurements comprise variations of frequency and duration of rest and wake periods, and the latency between different states for individual larva over three days [12, 64].

Locomotor activity

In normal bathing medium, zebrafish larvae move infrequently and in small dart-like motions. Larval locomotion might be altered by various neuroactive chemicals. For instance, GABA antagonists (i.e. picrotoxin and PTZ) increase larval locomotion in a stepwise progression including a period of increased swim activity (Stage I), followed by rapid whirlpool-like swimming (Stage II), and finally, brief violent clonus-like convulsions accompanied by a short post-ictal loss of posture (Stage III) [13]. Locomotion tracking assays serve as a rapid method to screen large numbers of antiepileptic candidates and/or proconvulsant compounds [13]. The quantitative measurements comprise speed and direction of the movements, distance traveled by the larvae, and duration of the mobility and/or immobility [65].

Escape and avoidance behavior

Emotional states such as fear and anxiety may be induced when larvae are exposed to the stimuli they would normally avoid or escape from. Escape and avoidance behavior develop early and are observed at the larval stage. The larvae display a startle response when exposed to tactile, acoustic, or visual stimuli. The escape response can also be triggered by water flow at 3 – 4dpf. Zebrafish larvae avoid dark areas, moving objects, conspecifics, and open spaces [9].

The 7dpf larvae are phototactic. They prefer a lighter section of the tank over a darker section. However, adult fish display an opposite response to light as they prefer darker sections in a tank. Assays for measuring larval phototaxis were recently optimized by dimming a uniform field of illumination, followed by a 10-fold weaker spot of light. The larvae display a routine turn towards the light followed by a series of slow swims in the direction of the light source [9].

Zebrafish larvae are also thigmotactic (position-choice along the wall). They prefer the edge over the center in multi-well plates [66]. In nature, open areas may expose zebrafish larvae to predators and this exposure could induce an anxiety-like state in the larvae

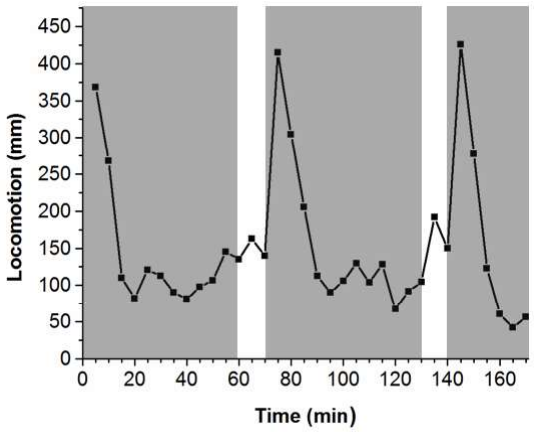

Figure 2.3-3: Effect of alternating light–dark periods on locomotion in 6dpf larval zebrafish. A 60-min period of darkness was followed by two alternating cycles of 10-min light (white areas) and 60-min dark (grey areas). When the light is turned off, locomotion rapidly increases to a maximum and then decreases to a low level within 20 minutes. Data are presented as distance moved in 5-min intervals(mm). (Performed as an inhouse experiment)

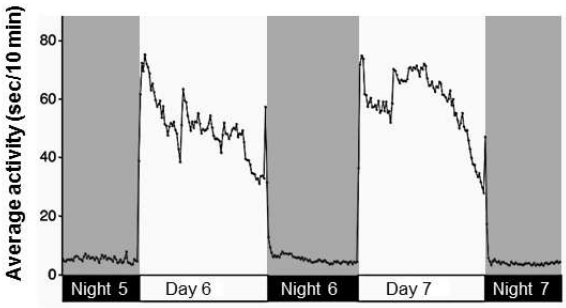

Figure 2.3-4: Rest-wake cycle of larval zebrafish after 6dpf. Wake-like states, characterized by periods of activity, are signified with white areas. The grey areas signify the rest or sleep-like states. [64]

similar to the anxiogenic effects of open areas in rodents. This behavior may be used for the discovery of novel drugs with anxiolytic properties [9].

Adult zebrafish may respond to the threatening stimuli by diving, freezing, jumping, erratic movements, or shoaling. In fish tanks with various colors and shapes, adult zebrafish prefer dark areas over light areas and blue over red color [9, 67, 68]. They also avoid dark spots on a white background, and a dark line on a rotating drum. Zebrafish display freezing behavior as an anxiety-like response when confined to the white background that they would normally avoid. Adult fish, similar to the rodents, may exhibit thigmotaxis. When the fish are placed in a novel tank, they dive to the bottom and gradually explore higher levels of the tank over time. This behavior is quantitatively measured in the model of stress response named Novel Tank Diving Test alike the rodent anxiety model of Novel Open Field Test [9, 66, 69]. Several classes of anxiolytic drugs (serotonergic, benzodiazepines and nicotinic) attenuate the diving behavior [9, 67, 69]. Diazepam reduces the time that the fish spend at the bottom of the tank [66].

Habituation

Several recent studies suggest that zebrafish can habituate to various stimuli, including conditioned place preference, light/dark locomotion and the startle reflex testing [70]. Figure 2.3-5 presents habituation of 6dpf larvae to alternating dark–light periods in one of our in-house experiments. Analysis of habituation is used to characterize animal cognitive phenotypes and their modulation. Impaired habituation can also be associated with increased anxiety. Therefore, habituation models provide insight into anxiety-memory interplay. Stress-inducing alarm pheromone and anxiogenic drugs such as caffeine attenuate zebrafish habituation while chronic ethanol and fluoxetine treatments improve this behavior [70].

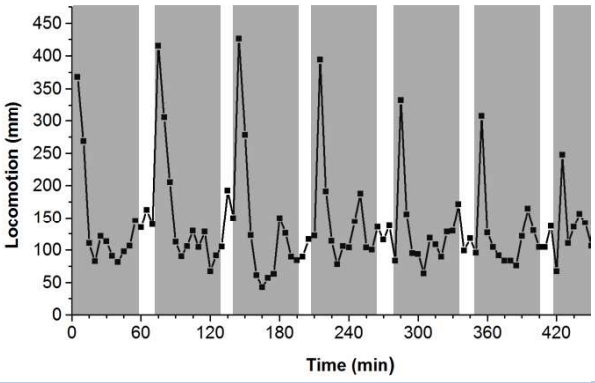

Figure 2.3-5: Habituation of 6dpf larvae to alternating light–dark periods. A 60-min period of darkness was followed by cycles of 10-min light (white areas) and 60-min dark (grey areas). When the light is turned off, locomotion rapidly increases to a maximum level and then decreases to a low level within 20 minutes. Garadually adaptation of the larvae to the stimulie is observed after the third cycle. Data are presented as distance moved in 5-min intervals (mm). (Performed as an inhouse experiment)

References:

[1] Vallverdú-Queralt, A., et al., Identification of phenolic compounds in red wine extract samples and zebrafish embryos by HPLC-ESI-LTQ-Orbitrap-MS. Food Chemistry. 181 (2015) 146-151.

[2] US Food and Drug Administration, http://www.fda.gov/forconsumers/consumerupdates/ucm343940.htm, in FDA Consumer Health Information. 2013.

[3] Bowman, T. V. Zon, L. I., Swimming into the future of drug discovery: *in vivo* chemical screens in zebrafish. ACS Chemical Biology. 5 (2010) 159-161.

[4] Peterson, R. T., Fishman, M.C., Designing zebrafish chemical screens. Methods in Cell Biology. 105 (2011) 525-541.

[5] Engeszer, R. E., et al., Zebrafish in the wild: a review of natural history and new notes from the field. Zebrafish. 4 (2007) 21-40.

[6] Delvecchio, C., Tiefenbach, J., Krause, H. M., The zebrafish: a powerful platform for in vivo, HTS drug discovery. Assay and Drug Development Technologies. 9 (2011) 354-361.

[7] Westerfield, M., The zebrafish book: a guide for the laboratory use of zebrafish Danio (*Brachydanio rerio*): 2007, Eugene: University of Oregon Press, Institute of Neuroscience.

[8] JoVE Science Education Database Essentials of Biology 2: Mouse, Zebrafish, and Chick. Zebrafish Reproduction and Development. 2016. DOI: 10.3791/5151.

[9] Colwill, R. M. Creton, R., Imaging escape and avoidance behavior in zebrafish larvae. Reviews in the Neurosciences. 22 (2011) 63-73.

[10] D'Costa, A., Shepherd, I. T., Zebrafish development and genetics: introducing undergraduates to developmental biology and genetics in a large introductory laboratory class. Zebrafish. 6 (2009) 169-177.

[11] Tropepe, V., Sive, H. L., Can zebrafish be used as a model to study the neurodevelopmental causes of autism?. Genes, Brain and Behavior. 2 (2003) 268-281.

[12] Taylor, K. L., et al., Small molecule screening in zebrafish: an in vivo approach to identifying new chemical tools and drug leads. Cell Communication and Signaling. 8 (2010) 1.

[13] Baraban, S. C., Zebrafish as a simple vertebrate organism for epilepsy research. in: Animal Models of Epilepsy: Methods and Innovations. 2009: 59-74, Humana Press.

[14] Tamplin, O. J., et al., Small molecule screening in zebrafish: swimming in potential drug therapies. Developmental Biology. 1 (2012) 459-468.

[15] Umans, R., Taylor, M., Zebrafish as a model to study drug transporters at the blood–brain barrier. Clinical Pharmacology and Therapeutics. 92 (2012) 567-570.

[16] Truong, L., et al., Multidimensional in vivo hazard assessment using zebrafish. Toxicological Sciences. 137 (2014) 212-233.

[17] Dray, N., et al., Large-scale live imaging of adult neural stem cells in their endogenous niche. Development. 142 (2015) 3592-3600.

[18] Blackburn, J. S., et al., High-throughput imaging of adult fluorescent zebrafish with an LED fluorescence macroscope. Nature Protocols. 6 (2011) 229-241.

[19] Brittijn, S. A., et al., Zebrafish development and regeneration: new tools for biomedical research. International Journal of Developmental Biology. 53 (2009) 835-850.

[20] Howe, K., et al., The zebrafish reference genome sequence and its relationship to the human genome. Nature. 496 (2013) 498-503.

[21] Key, B., Devine, C. A., Zebrafish as an experimental model: strategies for developmental and molecular neurobiology studies. Methods in Cell Science. 25 (2003) 1-6.

[22] MacRae, C. A., Peterson, R. T., Zebrafish as tools for drug discovery. Nature Reviews Drug Discovery. 14 (2015) 721-731.

[23] Santana, S., Rico, E. P., Burgos, J. S., Can zebrafish be used as animal model to study Alzheimer's disease. Amarican Journal of Neurodegenerative Disease. 1 (2012) 32-48.

[24] Murphey, R., Zon, L., Small molecule screening in the zebrafish. Methods. 39 (2006) 255-261.

[25] Hughes, J., et al., Principles of early drug discovery. British Journal of Pharmacology. 162 (2011) 1239-1249.

[26] White, R., K. Rose, and L. Zon, Zebrafish cancer: the state of the art and the path forward. Nature Reviews Cancer. 13 (2013) 624-636.

[27] McKee, R. A., Wingert, R. A., Zebrafish renal pathology: emerging models of acute kidney injury. Current Pathobiology Reports. 3 (2015) 171-181.

[28] Chico, T. J., Ingham, P. W., Crossman, D. C., Modeling cardiovascular disease in the zebrafish. Trends in Cardiovascular Medicine. 18 (2008) 150-155.

[29] Ou, H. C., et al., Drug screening for hearing loss: using the zebrafish lateral line to screen for drugs that prevent and cause hearing loss. Drug Discovery Today. 15 (2010) 265-271.

[30] Bassett, D. I., Currie, P. D., The zebrafish as a model for muscular dystrophy and congenital myopathy. Human Molecular Genetics. 12 (2003) 265-270.

[31] Ali, S., Champagne, D. L., Richardson, M. K., Behavioral profiling of zebrafish embryos exposed to a panel of 60 water-soluble compounds. Behavioural Brain Research. 228 (2012) 272-283.

[32] Kokel, D., Peterson, R. T., Using the zebrafish photomotor response for psychotropic drug screening. Methods in Cell Biology. 105 (2011) 517.

[33] Rihel, J., Schier, A. F., Behavioral screening for neuroactive drugs in zebrafish. Developmental Neurobiology. 72 (2012) 373-385.

[34] Wang, Y. N., et al., Behavioural screening of zebrafish using neuroactive traditional Chinese medicine prescriptions and biological targets. Scientific Reports. 4 (2014).

[35] Kokel, D., et al., Rapid behavior-based identification of neuroactive small molecules in the zebrafish. Nature chemical biology. 6 (2010) 231-237.

[36] Langheinrich, U., Vacun, G., Wagner, T., Zebrafish embryos express an orthologue of HERG and are sensitive toward a range of QT-prolonging drugs inducing severe arrhythmia. Toxicology and Applied Pharmacology. 193 (2003) 370-382.

[37] Hentschel, D. M., et al., Rapid screening of glomerular slit diaphragm integrity in larval zebrafish. American Journal of Physiology-Renal Physiology. 293 (2007) 1746-1750.

[38] Miller, Y., K. Stoletov, Klemke, R., Models of atherosclerosis, hyperlipidemia, lipoprotein oxidation and blood vessel inflammation and methods for making and using them. Google Patents. (2015).

[39] Lieschke, G. J., Currie, P. D., Animal models of human disease: zebrafish swim into view. Nature Reviews Genetics. 8 (2007) 353-367.

[40] Lawson, N. D., Weinstein, B. M., *In vivo* imaging of embryonic vascular development using transgenic zebrafish. Developmental Biology. 248 (2002) 307-318.

[41] Mathias, J. R., et al., Resolution of inflammation by retrograde chemotaxis of neutrophils in transgenic zebrafish. Journal of Leukocyte Biology. 80 (2006) 1281-1288.

[42] Childs, S., et al., Patterning of angiogenesis in the zebrafish embryo. Development. 129 (2002) 973-982.

[43] Tran, T.C., et al., Automated, quantitative screening assay for antiangiogenic compounds using transgenic zebrafish. Cancer Research. 67 (2007) 11386-11392.

[44] Rihel, J., et al., Zebrafish behavioral profiling links drugs to biological targets and rest/wake regulation. Science. 327 (2010) 348-351.

[45] Hao, J., et al., *In vivo* structure activity relationship study of dorsomorphin analogs identifies selective VEGF and BMP inhibitors. ACS Chemical Biology. 5 (2010) 245.

[46] Hu, G., et al., Metabolism of calycosin, an isoflavone from *Astragali Radix*, in zebrafish larvae. Xenobiotica. 42 (2012) 294-303.

[47] Chen, B., et al., Metabolism of ginsenosides Rk3 and Rh4 from steamed notoginseng in zebrafish by ultraperformance liquid chromatography/quadrupole-time-of-flight mass spectrometry. Archives of Pharmacal Research. 38 (2015) 1468-1476.

[48] Jones, H. S., et al., Metabolism of ibuprofen in zebrafish larvae. Xenobiotica. 42 (2012) 1069-1075.

[49] Li, Y., et al., Metabolic profiling analysis of berberine, palmatine, jatrorrhizine, coptisine and epiberberine in zebrafish by ultra-high performance liquid chromatography coupled with LTQ Orbitrap mass spectrometer. Xenobiotica. 45 (2015) 302-311.

[50] Wei, Y., et al., Metabolism of tanshinone IIA, cryptotanshinone and tanshinone I from Radix *Salvia Miltiorrhiza* in zebrafish. Molecules. 17 (2012) 8617-8632.

[51] Cole, G. J., et al., Effects of ethanol exposure on nervous system development in zebrafish. International Review of Cell and Molecular Biology. 299 (2011) 255-315.

[52] Jeong, J. Y., et al., Functional and developmental analysis of the blood–brain barrier in zebrafish. Brain Research Bulletin. 75 (2008) 619-628.

[53] Xie, J., et al., A novel transgenic zebrafish model for blood-brain and blood-retinal barrier development. BMC Developmental Biology. 10 (2010) 1.

[54] Geldenhuys, W. J., Allen, D. D., Bloomquist, J. R., Novel models for assessing blood–brain barrier drug permeation. Expert Opinion on Drug Metabolism and Toxicology. 8 (2012) 647-653.

[55] Fleming, A., Diekmann, H., Goldsmith, P., Functional characterisation of the maturation of the blood-brain barrier in larval zebrafish. PLoS One. 8 (2013) e77548.

[56] Eliceiri, B. P., Gonzalez, A. M., Baird, A., Zebrafish model of the blood-brain barrier: morphological and permeability studies. The Blood-Brain and Other Neural Barriers: Reviews and Protocols. (2011) 371-378.

[57] Martin, S. C., Heinrich, G., Sandell, J. H., Sequence and expression of glutamic acid decarboxylase isoforms in the developing zebrafish. Journal of Comparative Neurology. 396 (1998) 253-266.

[58] Cocco, A., et al., Characterization of the γ-aminobutyric acid signaling system in the zebrafish (*Danio rerio* Hamilton) central nervous system by reverse transcription-quantitative polymerase chain reaction. Neuroscience. 343 (2017) 300-321.

[59] Connaughton, V. P., Nelson, R., Bender, A. M., Electrophysiological evidence of $GABA_A$ and $GABA_C$ receptors on zebrafish retinal bipolar cells. Visual neuroscience. 25 (2008) 139-153.

[60] Roy, B., Ali, D.W., Multiple types of $GABA_A$ responses identified from zebrafish Mauthner cells. Neuroreport. 25 (2014) 1232-1236.

[61] Afrikanova, T., et al., Validation of the zebrafish pentylenetetrazol seizure model: locomotor versus electrographic responses to antiepileptic drugs. PLoS One. 8 (2013) e54166.

[62] Huuskonen, H., New models and molecular markers in evaluation of developmental toxicity. Toxicology and Applied Pharmacology. 207 (2005) 495-500.

[63] MacPhail, R. C., et al., Locomotion in larval zebrafish: Influence of time of day, lighting and ethanol. NeuroToxicology. 30 (2009) 52-58

[64] Prober, D. A., et al., Hypocretin/orexin overexpression induces an insomnia-like phenotype in zebrafish. The Journal of Neuroscience. 26 (2006) 13400-13410.

[65] Airhart, M. J., et al., Movement disorders and neurochemical changes in zebrafish larvae after bath exposure to fluoxetine (PROZAC). Neurotoxicology and Teratology. 29 (2007) 652-664.

[66] Richendrfer, H., et al., On the edge: pharmacological evidence for anxiety-related behavior in zebrafish larvae. Behavioural Brain Research. 228 (2012) 99-106.

[67] Pagnussat, N., et al., One for all and all for one: the importance of shoaling on behavioral and stress responses in zebrafish. Zebrafish. 10 (2013) 338-342.

[68] Blaser, R., L. Chadwick, McGinnis, G., Behavioral measures of anxiety in zebrafish (*Danio rerio*). Behavioural Brain Research. 208 (2010) 56-62.

[69] Bencan, Z., Sledge, D., Levin, E. D., Buspirone, chlordiazepoxide and diazepam effects in a zebrafish model of anxiety. Pharmacology Biochemistry and Behavior. 94 (2009) 75-80.

[70] Wong, K., et al., Analyzing habituation responses to novelty in zebrafish (Danio rerio). Behavioural Brain Research. 208 (2010) 450-457.

2.4. ADME profiling in neuroactive drug discovery

2.4.1. Drug-like properties

With regard to bioactive compounds targeting the CNS, druggability of the molecule comes into consideration, along with potency and selectivity studies, during the early exploratory stages of drug discovery and development.

Sets of rules and criteria are applied to rank druggability of a candidate compound whereas there are no absolute definitions for the concept. The main characteristics that define druggability of a molecule are categorized into structural properties, including molecular weight, lipophilicity (Log *P*), ionization constant (pK_a), pH stability and hydrogen bonding; physicochemical properties, such as solubility and chemical stability; and biochemical properties including metabolic stability and transporter interaction. These characteristics are decisive for absorption, distribution, metabolism and elimination (ADME) of the compound [1].

Structural properties are intrinsic characteristics of the molecule and determine its physicochemical properties, whereas physicochemical properties are closely linked to the biochemical properties and ADME behavior of the molecule [2]. Inappropriate Log *P*, pK_a and product pH may increase chemical instability, cost and complexity of product development [3]. Solubility is influenced by the pK_a of the molecule and the solution pH. Low solubility results in a low concentration of free drug molecules at the biologic membranes and may, consequently, decrease the bioavailability [1]. Metabolic stability, referring to the susceptibility of compounds to biotransformation, has a relation with secondary pharmacokinetic parameters such as bioavailability and half-life, and can assist with defining the pharmacological and toxicological profiles of the new drug candidate [3]. Transporters may influence ADME by enhancing uptake or efflux of the molecules at the tissue membranes [1].

In general, druggability can be interpreted as the possession of satisfactory physicochemical and biochemical characteristics which enable a candidate drug molecule to reach adequate concentration in its site of action.

2.4.2. Druggability assessment models

Property prediction has been started with the “Rule of 5” elaborated by Christopher A. Lipinski in 1997 [1]. This set of rules was introduced based on structural properties that encompassed

90% of the orally administered chemical entities with acceptable safety and pharmacokinetic (PK) behaviors for human. Lipinski's rule states that compounds are more likely to have poor absorption or permeation if they have more than five H-bond donors, more than 10 H-bond acceptors, MW greater than 500, and *C*log*P* above five [1]. The rule-of-five values are set at the 90^{th} percentile of the compound set. Exceeding one of the parameters puts the compound into only 10% of the successful compound set. Exceeding more than one parameter further increases the risk [1]. The prediction rules have evolved gradually and other rule sets were developed later. "Veber rules" were developed based on a compound set that had rat oral bioavailability, and suggested that oral absorption of a molecule is favored if the sum of rotatable bonds is ≤ 10, and the polar surface area (PSA) is ≤ 140 $Å^2$ or the total H-bonds (acceptor plus donor) is ≤ 12. "Waring rules" were developed using a compound set with available Caco-2 data, and "Golden triangle" was explained by considering permeability and metabolic stability as the drug-like properties of interest [1].

Drug-like properties are, nowadays, evaluated by different approaches such as *in silico* prediction models, high-throughput *in vitro* assays for measurement of fundamental physicochemical and biochemical properties, and *in vivo* PK assessments using model organisms [1, 4]. *In silico* and *in vitro* models enabled ADME profiling much earlier in the discovery process while *in vivo* models, known as low-throughput, costly and labor-intensive approaches, are mainly applied at later stages of the drug development [5].

In our studies, *in silico* models were applied to predict druggability of GABAergic natural products. Also, *in vitro* cell-based models were used to measure membrane permeability of a GABAergic flavonoid, kaempferol, and the major intestinal metabolite of that, 4-hydroxyphenylacetic acid (4-HPAA). In the upcoming sections, an overview on the *in silico* prediction models, *in vitro* gastrointestinal and blood-brain barrier permeability assays, and approaches to accurate and precise bioanalytical methods are provided.

2.4.2.1. In silico prediction models

In silico prediction of compounds druggability is an area of ongoing investigation, and part of many drug discovery programs [4, 6-8]. Multiple molecular properties of the compounds, mentioned in various rule-sets, such as H-bond donors/acceptors and MW are simply defined by counting while some others such as *C*Log*P* and polar surface area (PSA) are determined by

computation [1]. Therefore, numerous computational models have been developed and applied for prediction of structural and physicochemical properties, such as the QikProp [9], the Schrodinger [10, 11] and the ACD/Labs Percepta Drug Profiler [12]. QikProp model which was applied in our studies is among the earliest ADME programs that predicted a substantial array of pharmacologically relevant properties [4]. The first version of the program provided predictions for intrinsic aqueous solubility, Caco-2 cell permeability and several partition coefficients including octanol/water. Updated QikProp versions covered additional quantities including log *BB* for brain-blood partitioning, log K_{hsa} for serum albumin binding and primary metabolites. Based on the QikProp predictions, a compound would be seen potentially problematic if it does not satisfy a "rule-of-three" which is predicted log S > -6, P Caco > 30 nm/s, and number of primary metabolites ≤ 6. For the bioactivities which require blood-brain barrier penetration, the predicted log *BB* should also be positive [4].

The *in silico* prediction models serve as faster and less expensive substitutes to *in vitro* or *in vivo* assays. However the existing *in silico* methods, despite their broad range of complexity from relatively simple quantitative models to complex pharmacokinetics and/or pharmacodynamics models, are still not accurate enough to fully replace *in vitro* and *in vivo* approaches [6].

2.4.2.2. In vitro membrane permeability studies

The term permeability originated from Fick's first law that relates the diffusive flux to the concentration gradient. The flux goes from regions of high concentration to regions of low concentration. Permeability represents an experimentally determined transport coefficient of the compound under study [13]. Different mechanisms are known for membrane permeation including passive transcellular diffusion, efflux transport, uptake transport, para-cellular transport and endocytosis, as shown in figure 2.4-1 [1].

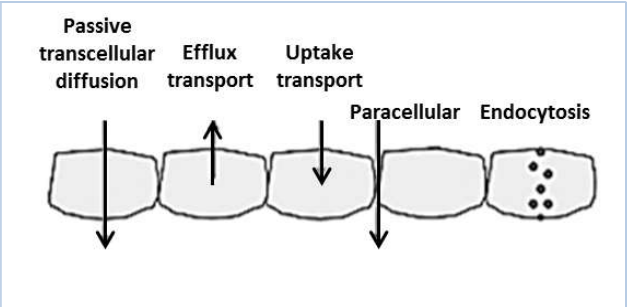

Figure 2.4-1. Major permeability mechanisms [1].

In vitro approaches to study membrane permeability are divided into physicochemical and cell-based models. The physicochemical assays such as the Parallel Artificial Membrane Permeability Assay

(PAMPA) [14, 15] and the Immobilized Artificial Membrane High Performance Liquid Chromatography (IAM-HPLC) [6, 16] can predict passive diffusions. They can be used in high-throughput scale with low costs and relatively high reproducibility. However, artificial membranes are lacking para-cellular pores, influx and efflux transporters, and metabolic enzymes, all of which influence the extent of drug absorptions in biological membranes [6]. In contrast to artificial membranes, the cell-based models can provide information, at a cellular level, on absorption and metabolism of drug molecules across tissue barriers. They can also provide estimations on transporter-mediated routes of absorption rather than prediction of passive diffusions [17].

Membrane permeability is a key feature for compounds that need to be orally absorbed, and/or need to reach sanctuary tissues such as the CNS [18, 19]. Intestinal barrier permeability and the ability to cross the BBB are among the main ADME challenges for those drug candidates, respectively.

Cell-based intestinal barrier model

Compounds intended for oral administration can achieve therapeutic concentrations if they have adequate aqueous solubility and intestinal permeability [20]. Methods used to investigate intestinal permeability mainly include *in situ* perfusion of the intestinal tract [20], *in vitro* everted tract experiments, and *in vitro* monolayer cell-based models [21].

The cell-based models are developed using immortalized cells that grow rapidly into confluent monolayers and undergo spontaneous differentiation [6]. The Madin Darby Canine Kidney (MDCK), TC-7, HT29-MTX, 2/4/A1, and the Caco-2 cells are some of the cell lines in use for modelling intestinal absorption [6]. Among those, the Caco-2 cell monolayer assay has emerged as one of the standard *in vitro* tools, and is recognized in the US FDA's Biopharmaceutics Classification System (BCS) Guidance [13].

The Caco-2 cells, derived from a human colon carcinoma, have the potential to differentiate during a 3-week culture period, and acquire characteristics of intestinal epithelial cells [6, 17, 22]. They form tight junctions between cells, and express transporter proteins for bile acids, amino acids, and sugars [6, 17]. Also, efflux proteins such as P-glycoprotein (P-gp) and the multidrug resistance-associated protein (MRP), drug metabolizing enzymes such as hydrolases,

carboxylesterases, uridine diphosphoglucuronosyl transferases, glutathione-*S*-transferases, and Phase II conjugation enzymes including sulfotransferases and glucuronyl transferases are expressed on the cells [6, 17, 22]. Presence of phase II metabolizing enzymes, particularly, benefits bioavailability studies of the orally administered compounds [6, 22]. One of the functional deficiencies in Caco-2 cells, in comparison with normal cells, is absence of cytochrome P450 isozymes, especially CYP3A4 which is normally expressed at high levels in the intestine. However, some specific treatments of the cells, such as exposure to vitamin D3 have been shown to induce a higher level of CYP3A4 expression in the Caco-2 cells [6]. Therefore, Caco-2 cell monolayers can be employed for simultaneous elucidation of transport mechanisms and metabolic transformation of bioactive compounds [6, 17, 22].

To establish a membrane model, Caco-2 cells are cultured on inserts with semipermeable polycarbonate surfaces fitted into a multi-well plate. The inserts introduce an apical and a basolateral chamber which are connected only through the cells monolayer and their semipermeable substrate. The apical chamber represents luminal side of the gastrointestinal tract while the basolateral chamber represents its blood side (Figure 2.4-2) [6]. Permeability of a test compound can be traced in two directions, from apical to basolateral side or vice versa [22]. The transport rate for a particular concentration of the test compound is expressed as apparent permeability coefficient (P_{app}) value [6, 22].

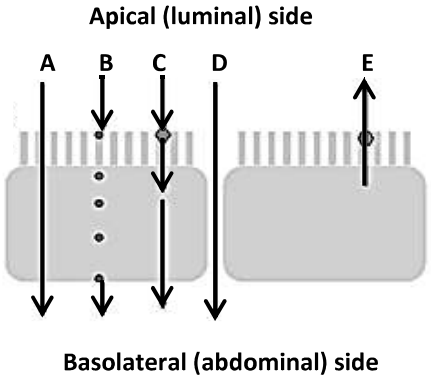

Figure 2.4-2: Caco-2 cells cultured on semipermeable polycarbonate surfaces establish apical and basolateral chambers representing the luminal side and the blood side of the gastrointestinal tract, respectively. Permeation of the investigated compounds may follow each of the passive transcellular diffusion (A), endocytosis (B), efflux transport (C), para-cellular transport (D) and/or uptake (E) mechanisms. Permeability of a test compound can be traced in both directions, apical to the basolateral side or vice versa [6].

Caco-2 cell based barriers, similar to many other *in vitro* models, are accompanied with significant limitations for full replacement of animal experiments:

i) The tight junctions in differentiated Caco-2 cell monolayers are more characteristic of those in the colon than in the small intestine. As a result, a higher transendothelial electrical resistance (TEER) is observed in the model than that normally found across the small intestinal epithelium. *ii*) The mucus layer normally found on the intestinal epithelium is absent in the Caoco-2 model due to the absence of mucin producing cells, and finally, *iii*) the barrier model is lacking physiological parameters such as intestinal motility or transit time [17]. These limitations need to be considered when interpreting the transport data.

Cell-based blood-brain barrier model

BBB is an active interface between blood circulation and the CNS. It strictly controls the molecular and cellular traffic between blood and the brain, and therefore, takes an important share in providing the steady state environment needed for a proper neuronal function [23]. The BBB protects the CNS by preventing xenobiotics, toxic metabolites and some drugs with unwanted effects from crossing the CNS [24]. However, despite its beneficial role, the BBB introduces an extra challenge in development of drugs acting on the CNS [25, 26]. It is estimated that more than 98% of small molecules are unable to cross the BBB [25, 26]. Thus, a significant number of potential drugs fail as they may not reach relevant concentrations in the CNS [23, 26].

The BBB is formed by endothelial cells of cerebral capillary blood vessels coming in close contact with neighboring pericytes and glial cells [23]. The barrier does not permit para-cellular permeation due to impenetrable tight junctions between membrane cells [1, 24]. Tight junctions make a network of strands, composed of a row of transmembrane proteins with extracellular domains, joining together and sealing the intercellular cleft. By preventing the free diffusion of ions, the continuous line of tight junctions defines a transendothelial electrical resistance (TEER) which is considered as the most sensitive marker for estimation of the junctions' tightness [23, 27]. Due to the unlikely para-cellular permeation, the molecular traffic is forced to take the transcellular route through individual endothelial cells [23]. Only substances that are very lipophilic in nature may succeed crossing the cell membranes [24]. Still, the penetrated molecules have to overcome the efflux transporters which are highly expressed in the membrane of brain endothelial cells, and actively remove the penetrated molecules from inside the cells [1,

23, 24]. Unfortunately, a large number of potential drug candidates are substrates of efflux transporters, severely limiting their usefulness in the therapy of CNS disorders. Therefore, the ability of the compounds to cross the BBB has become one of the key features to be studied at the exploratory stages of neuroactive-drug discovery and development.

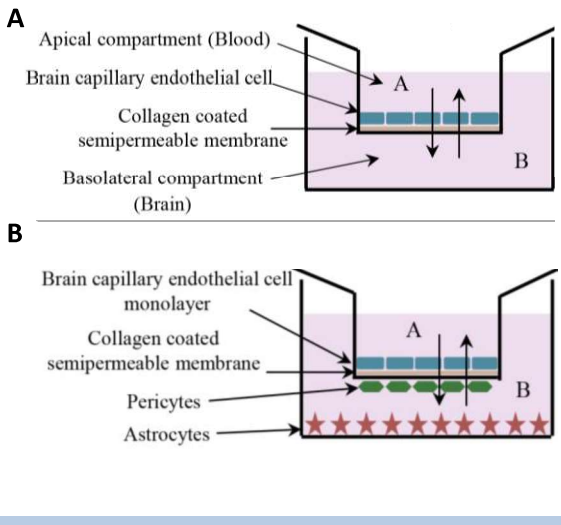

Figure 2.4-3: The models used for BBB permeability studies might be simply mono-cultured cerebral endothelial cells on microporous membranes (A), or more complex co-cultures of endothelial cells with astrocytes and/or pericytes (B) [33].

The cell-based models which exhibit reproducible solute permeability, restrictive paracellular pathway, functional expression of transporters, and ease of culture have the potential to be useful techniques for medium/high-throughput BBB permeability studies [23]. The BBB models might be simple mono-cultured cerebral endothelial cells on microporous membranes, or more complex co-cultures of endothelial cells with astrocytes and/or pericytes (Figure 2.4-3) [27]. Endothelial cells on the microporous membrane provide the two CNS compartments separated by the BBB: the circulation side (apical) and the brain side (basolateral). The pores in the membrane allow exchange of solutes between the apical and the basolateral compartments. Astrocytes and pericytes in co-culture models provide the *in vivo* anatomic properties of a neurovascular unit. It is believed that astrocytes affect development of inter-endothelial junctions during the cells adulthood. They also play a significant role in upregulation of efflux transporters [23, 28-30].

Tightness of inter-endothelial junctions in cell-based BBB models is controlled by measurement of the TEER value, and the apparent permeability of marker molecules such as mannitol, sucrose, and inulin which should be as close as possible to the values measured *in vivo* [23, 27]. Engagement of the efflux transporters can be characterized by measurement of efflux ratio for the test compounds [23, 31, 32]. The efflux ratio is calculated by performing bidirectional (i.e., apical-to-basolateral and basolateral-to-apical) permeability assays. The efflux ratio that is below 0.5 or above 2 is indicative of an active efflux or uptake, respectively [23].

Primary-cells are the first choice for establishing mono- or co-cultured BBB models in respect to the tightness of the barrier. Primary cells from rat, murine, porcine, and bovine are the most accepted cells, rather than those of the human origin. However, due to the species differences which could lead to misinterpretations during development of new human drugs, considerable effort has been made in the past decades to establish human cell based models. Isolation and culture of primary cells is often complicated and costly. The cells might differ from batch to batch, and are usually not enough for high-throughput studies. Therefore, immortalized brain endothelial cell lines have been established by transfection of the primary cells with tumor genes [23].

In our investigations on BBB permeability of neuroactive natural products, we have employed a human cell based model using immortalized hBMEC cells. The hBMEC cell line has been selected among four currently available immortalized human brain capillary endothelial cell lines (hCMEC/D3, hBMEC, TY10, and BB19) following a comparative study performed by our colleagues. The comparison was in terms of tightness of the barrier being established by each cell line in the 24-well transwell system, where the hBMEC cell line showed a better performance amongst all [34].

References:

[1] Di, L., Kerns, E. H., Drug-like properties: concepts, structure design and methods from ADME to toxicity optimization. 2015: Academic Press.

[2] Jensen, H., et al., Physicochemical profiling of drug candidates using capillary-based techniques. Journal of Drug Delivery Science and Technology. 23 (2013) 333-345.

[3] Masimirembwa, C. M., Bredberg, U., Andersson, T. B., Metabolic stability for drug discovery and development. Clinical pharmacokinetics. 42 (2003) 515-528.

[4] Ortega, S. S., Cara, L. C. L., Salvador, M.K., *In silico* pharmacology for a multidisciplinary drug discovery process. Drug Metabolism and Drug Interactions. 27 (2012) 199-207.

[5] Paiva, A., Shou, W. Z., Recent developments in software tools for high-throughput *in vitro* ADME support with high-resolution MS. Bioanalysis. 8 (2016) 1723-1733

[6] Van Breemen, R. B., Li, Y., Caco-2 cell permeability assays to measure drug absorption. Expert Opinion on Drug Metabolism & Toxicology. 1 (2005) 175-185.

[7] Tao, L., et al., Recent progresses in the exploration of machine learning methods as *in-silico* ADME prediction tools. Advanced Drug Delivery Reviews. 86 (2015) 83-100.

[8] Eddershaw, P. J., Beresford, A. P., Bayliss, M. K. ADME/PK as part of a rational approach to drug discovery. Drug Discovery Today. 5 (2000) 409-414.

[9] Ioakimidis, L., et al., Benchmarking the reliability of QikProp. Correlation between experimental and predicted values. Molecular Informatics, 27 (2008) 445-456.

[10] Butina, D., Segall, M. D., Frankcombe, K., Predicting ADME properties *in silico*: methods and models. Drug Discovery Today. 7 (2002) 83-88.

[11] Katritzky, A. R., et al., Quantitative correlation of physical and chemical properties with chemical structure: utility for prediction. Chemical Reviews. 110 (2010) 5714-5789.

[12] Tait, S., Perugini, M., et al., Relative toxicological ranking of eight polybrominated diphenyl ether congeners using cytotoxicity, chemical properties and exposure data. Food and Chemical Toxicology. 108 (2017) 74-84.

[13] Chen, M.-L., et al., The BCS, BDDCS, and regulatory guidances. Pharmaceutical research. 28 (2011) 1774.

[14] Ottaviani, G., Martel, S., Carrupt, P. A., Parallel artificial membrane permeability assay: a new membrane for the fast prediction of passive human skin permeability. Journal of Medicinal Chemistry. 49 (2006) 3948-3954.

[15] Masungi, C., et al., Parallel artificial membrane permeability assay (PAMPA) combined with a 10-day multiscreen Caco-2 cell culture as a tool for assessing new drug candidates. Die Pharmazie-An International Journal of Pharmaceutical Sciences. 63 (2008) 194-199.

[16] Tsopelas, F., Vallianatou, T., Tsantili-Kakoulidou, A., The potential of immobilized artificial membrane chromatography to predict human oral absorption. European Journal of Pharmaceutical Sciences. 81 (2016) 82-93.

[17] Gan, L. S. L., Thakker, D. R., Applications of the Caco-2 model in the design and development of orally active drugs: elucidation of biochemical and physical barriers posed by the intestinal epithelium. Advanced Drug Delivery Reviews. 23 (1997) 77-98.

[18] Kansy, M., Avdeef, A., Fischer, H., Advances in screening for membrane permeability: high–resolution PAMPA for medicinal chemists. Drug Discovery Today: Technologies. 1 (2004) 349-355.

[19] Yamamoto, T., Suzuki, H., Hisaka, A., Principles of Pharmacokinetics: Predicting Human Pharmacokinetics in Drug Discovery. in: Mass Spectrometry in Drug Metabolism and Disposition: Basic Principles and Applications. 2011: 197-228, John Wiley & Sons. Inc.

[20] Balimane, P. V., Chong, S., Morrison, R. A., Current methodologies used for evaluation of intestinal permeability and absorption. Journal of Pharmacological and Toxicological Methods. 44 (2000) 301-312.

[21] Deferme, S., Annaert, P., Augustijns, P., *In vitro* screening models to assess intestinal drug absorption and metabolism. in: Drug absorption studies. 2008: 182-215, Springer.

[22] Hubatsch, I., Ragnarsson, E. G., Artursson, P., Determination of drug permeability and prediction of drug absorption in Caco-2 monolayers. Nature Protocols. 2 (2007) 2111-2119.

[23] Wilhelm, I. Krizbai, I. N. A., *In vitro* models of the blood–brain barrier for the study of drug delivery to the brain. Molecular Pharmaceutics. 11 (2014) 1949-1963.

[24] Shou, W. Z., Zhang, J., Recent development in high-throughput bioanalytical support for in vitro ADMET profiling. Expert Opinion on Drug Metabolism and Toxicology. 6 (2010) 321-336.

[25] Pardridge, W. M., Blood-brain barrier drug targeting: the future of brain drug development. Molecular Interventions. 3 (2003) 90.

[26] Pardridge, W. M., Blood–brain barrier delivery. Drug Discovery Today. 12 (2007) 54-61.

[27] Wilhelm, I., Fazakas, C., Krizbai, I. A., *In vitro* models of the blood-brain barrier. Acta Neurobiology Experimentalis. 71 (2011) 113-28.

[28] Gaillard, P. J., et al., Establishment and functional characterization of an *in vitro* model of the blood–brain barrier, comprising a co-culture of brain capillary endothelial cells and astrocytes. European Journal of Pharmaceutical Sciences. 12 (2001) 215-222.

[29] Nakagawa, S., et al., Pericytes from brain microvessels strengthen the barrier integrity in primary cultures of rat brain endothelial cells. Cellular and Molecular Neurobiology. 27 (2007) 687-694.

[30] Kirkpatrick, C. J., Fuchs, S., Unger, R. E., Co-culture systems for vascularization-learning from nature. Advanced Drug Delivery Reviews. 63 (2011) 291-299.

[31] Kikuchi, R., de Morais, S. M., Kalvass, J. C., *In vitro* P-glycoprotein efflux ratio can predict the *in vivo* brain penetration regardless of biopharmaceutics drug disposition classification system class. Drug Metabolism and Disposition. 41 (2013) 2012-2017.

[32] Summerfield, S. G., et al., Improving the *in vitro* prediction of *in vivo* central nervous system penetration: integrating permeability, P-glycoprotein efflux, and free fractions in blood and brain. Journal of Pharmacology and Experimental Therapeutics. 316 (2006) 1282-1290.

[33] Moradi-Afrapoli, F., et al., Validation of UHPLC–MS/MS methods for the determination of kaempferol and its metabolite 4-hydroxyphenyl acetic acid, and application to *in vitro* blood–brain barrier and intestinal drug permeability studies. Journal of Pharmaceutical and Biomedical Analysis. 128 (2016) 264-274.

[34] Eigenmann, D. E., et al., Comparative study of four immortalized human brain capillary endothelial cell lines, hCMEC/D3, hBMEC, TY10, and BB19, and optimization of culture conditions, for an in vitro blood–brain barrier model for drug permeability studies. Fluids and Barriers of the CNS. 10 (2013) 1-17.

2.5. Bioanalysis

Bioanalysis is a term used to describe the quantitative determination of a compound or its metabolite in biological fluids such as blood, plasma, serum, urine or tissue extracts [1-3]. Analysis of biological samples for ADME property evaluations and PK interpretations is a challenging task due to complexity of biological matrices and the need to determine minute quantities of the analytes in such complex samples [4]. Therefore, development of a proper analytical procedure with adequate sensitivity and selectivity is an integral part of PK/PD characterization for new chemical entities. Bioanalytical methods should be robust, precise, and reproducible, with capability of generating accurate and reliable data [5]. For this purpose, it is essential to develop, optimize and fully validate the bioanalytical methods for each compound prior to sample analysis [5-7].

Recently, by the application of more sensitive and more selective liquid chromatography-mass spectrometry (LC-MS) and LC-tandem mass spectrometry (LC-MS/MS) techniques, quantification of chemicals in biological samples has been improved considerably. Taking advantage of the sensitivity and speed of mass spectrometric detections, and by application of fast chromatographic techniques, such as UHPLC, a noticeable increase in the throughput of analyses (up to 10 folds routine HPLC separations) may be achieved [8-10]. Within the following sections, development and validation of LC-MS/MS based quantification methods, the employed technique in our studies, are described.

2.5.1. Bioanalytical Method development

Development of a bioanalytical method consists of two main compartments: sample preparation and instrumental/detection optimization [11, 12].

Sample preparation

Sample preparation mainly aims to clean up the samples before analysis and to enrich the analytes of interest by transferring them from a complex biologic matrix into a more hospitable medium [3, 4]. Selection of a proper sample preparation technique would help to minimize interferences from biological matrices which can affect (suppress or enhance) the signal of the analyte (matrix effect) [10, 13]. Consequently, a smoother baseline due to the noise reduction and therefore, a lower limit of detection (LOD), a lower limit of quantification (LOQ) and an improved accuracy

of measurement would be achieved [3, 11, 14-16]. Protein precipitation (PPT) based methods, solid phase extractions (SPE), and liquid-liquid extractions (LLE) are the most commonly used approaches for sample preparation [4, 10, 11, 13]. In our studies we have employed a PPT technique as the first choice of sample clean up. The PPT technique is considered relatively easy, fast, and inexpensive [3, 11]. Through that, proteins present in the biological matrices are removed by denaturation and the consequent precipitation caused by an external stress such as strong acid/base, heat or, most commonly, organic solvents (methanol, acetonitrile) [1]. The denatured proteins can be removed by centrifugation while the desired analytes remain in the supernatant liquid [1]. Prior to any sample processing, a suitable internal standard (IS) is added to the samples so that the preparation recovery can be easily monitored [11, 17].

Bioanalytical assays rely heavily on the use of stable internal standards which can correct variations of the analytes occurring during sample preparation (extraction and/or transfer losses) or during LC-MS analysis [10, 18]. The ISs have similar physicochemical properties as the analyte of interest, and can mimic closely the performance of the analyte in every stage of the analysis [18]. The best ISs are stable isotopic-labeled (e.g. ^{2}H, ^{13}C, ^{15}N) compounds due to the highest physicochemical similarities to analytes, however the high synthesis cost limits their wide application [17, 18].

LC-MS/MS instrument and detection optimization

Quality of LC performance is optimized by selecting the suitable LC columns, elution solvents and conditions (pH adjustments, isocratic versus gradient elution, reverse versus normal phase), needle wash solvents, and instrumentation [11, 18]. Rather than selection of a proper IS and an efficient sample preparation technique, a well-developed chromatographic separation would play a significant role in reduction of matrix effects by separation of the matrix constituents from the analyte of interest [10, 13].

As for the detection, LC-MS/MS in multiple reactions monitoring (MRM) scan mode is the highly recommended technique for drug quantitation in biological samples [9, 19, 20]. The MRM scan provides high sensitivity and superior selectivity owing to filtering out background ions [9]. When the mass spectrometer is operated in MRM mode, high selectivity can be achieved at two levels. First, the precursor ions of the analyte and co-eluted components are resolved in Q1 by their mass-to-charge ratios. Subsequently, the analyte is differentiated from

interfering components in Q3 based on unique product-ions whose formation by collision-induced fragmentation is highly structure-specific. Therefore, interference is expected to be rare in such LC-MS/MS analysis [12]. Figure 2.5-1 shows schematic MRM transition of kaempferol (KMF).

During the method development, all tuning parameters are optimized to achieve the best intensity and resolution [11, 20]. One of the key parameters that is extremely compound dependent is the collision energy. Fragments or product-ions of the parent compounds are obtained at different collision energy levels. This information can be used to approximate the optimal collision energy required to generate the most abundant product ion [11].

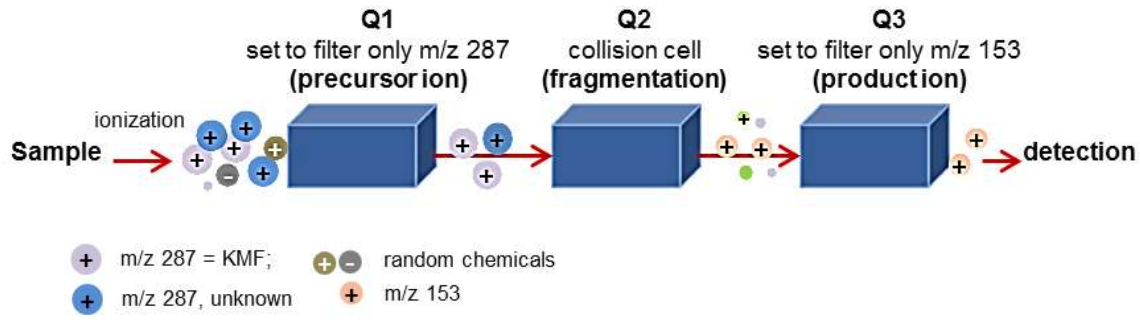

Figure 2.5-1: MRM transition of kaempferol (KMF). The MRM scan mode provides high selectivity owing to filtering out the complicated background ions at two levels. In Q1, the precursor ions of analyte and co-eluted components are resolved by their mass-to-charge ratios. In Q3, the analyte is differentiated from interfering components based on the unique product-ions formed by collision-induced fragmentation.

2.5.2. Bioanalytical method validation

Validation of a bioanalytical method involves documentations justifying that the performance characteristics of the method are suitable and reliable for the intended analytical applications in a particular biological matrix [3, 5]. Validation of quantification methods may follow the guidelines provided by international health authorities such as the United States Food and Drug Administration (FDA) [21] and/or European Medicine Agency (EMA) [22]. According to the FDA and EMA guidelines, the validation parameters to be evaluated for quantitative procedures include selectivity, calibration model, limit of quantification, short-term and long-term stabilities, and accuracy. Additional parameters which might have to be evaluated include limit of

quantification (LOQ), recovery, reproducibility and robustness [3, 5, 23]. In medium-/high-throughput investigations for drug discovery, the method validations are mainly focused on specificity, linearity and precision, and it is usually not necessary to perform all of the various validation studies [3].

Based on the background and actual situation of each investigation, different levels and types of method validations, namely Full Validation, Partial Validation, and Cross Validation, are recommended [5, 21]. Full validation is necessary when a bioanalytical method is being developed and implemented for the first time, and within that, the entire validation parameters are established for each analyte [5]. A partial validation is a modification of a validated bioanalytical method that does not necessarily require full revalidation. Partial Validation can range from as little as one intra-assay accuracy and precision determination to a nearly full validation. A typical bioanalytical method change which falls into this category is change of the study matrix/species/anti-coagulant/change of analytical instrumentation or software [5]. As in our membrane-permeability studies of kaempferol and 4-HPAA, partial method validations for quantification of analytes in HBSS buffer (Caco-2 transport medium) followed the previously full validations in RHB (BBB transport medium) [24]. Cross Validation is a comparison of validation parameters of two or more bioanalytical methods, and are necessary when more than one bioanalytical methods are used to generate data within the same study [5].

Selectivity and specificity

There should be evidence that the substance being quantified is the intended analyte, and no endogenous interferences exist at the retention time of analyte peak using the optimized chromatographic conditions [7]. One approach to establish method selectivity is to prove the lack of response in blank matrix [25]. Assessment of method selectivity requires evaluation during method development and validation and may continue throughout application of the method in actual study samples [5].

The method specificity is established using multiple independent sources of the same matrix [5, 21]. In hyphenated mass spectrometry based methods, investigating one of the two parameters matrix effect and specificity (as described in the FDA and EMA guidelines) can be used to ensure precision, selectivity and sensitivity of the method.

Calibration curve

The accuracy of the measured concentrations relative to the nominal analyte concentrations is evaluated with a calibration curve. This can be done by analyzing known samples (calibrators) and plotting the resulting responses versus the corresponding concentrations [26]. The curve fitting is determined by applying the simplest algorithm (model) which best describes the concentration response relationship using appropriate weighting and statistical tests for "goodness of fit" requirement. It must be continuous and reproducible, and should be based on minimizing the percent relative error in the back calculated values [5]. The concentration range over which the analyte in the study samples would be reliably and reproducibly quantified, known as limit of quantification, is defined based on the calibration curve [5]. The lower limit of quantification (LLOQ) serves as the lowest concentration on the standard curve which can be measured with acceptable accuracy and precision. The highest standard will define the upper limit of quantification (ULOQ) of a bioanalytical method [5, 26].

Repeatability and reproducibility

The repeatability expresses the closeness of a series of analyte measurements obtained from replicates of the same homogenous sample [5]. In order to evaluate the precision of measurements within one round of analysis, quality control samples (QCs) at five levels (LLOQ, QCL, QCM, QCH and ULOQ) are analyzed in six replicates in one validation run. Reproducibility of the analysis is justified by the observations from three validation runs within three different days [5, 26].

Stability

Instability of an analyte in any stage of the bioanalysis process, including sample collection, processing, storage, extraction and LC-MS/MS analysis, can result in under- or over-estimation [12, 23]. Instability of some analytes that contain certain chemically or biologically labile moieties, such as ester, thiol, and catechol is readily predictable for the specific precautions throughout the bioanalysis process. However, the instability of many other analytes is not readily predictable [10]. Therefore, evaluations need to be conducted before proceeding with the analysis of the study samples to define the compound-specific actions which should be taken to preserve the integrity of the molecule throughout the bioanalysis process especially during

sample collection and storage [5, 10, 12]. For instance, when enzymes are the main cause of the analyte instability, properly control of the solutions pH and/or addition of a finite amount of enzyme inhibitors to the matrix would be the effective approaches to retard the degradation [12]. A simple addition of antioxidants such as ascorbic acid has been found very effective for stabilizing those analytes which can be readily oxidized [12].

Analyte stability in biological samples should be established for multiple freeze–thaw cycles (freeze–thaw cycle stability), short-term (e.g. 4 h) stay on the bench-top (room temperature stability), long-term storage at a defined temperature (long-term stability), and reconstituted sample extracts (autosampler stability) [12, 17, 23]. The stability results are obtained by comparison of the analyte concentrations in freshly prepared samples with the values obtained from QC samples (mainly QCL and QCH) after various storage conditions [12, 23].

Accuracy

Accuracy, sometimes termed as trueness, is the degree of closeness of the determined value to the nominal value under prescribed conditions [5]. The inaccuracy in validation tests is expressed as the relative error (RE%). FDA and EMA guidance stipulate that in all validation tests, the inaccuracy has to be within ± 15% of the nominal values at all levels excluding the LLOQ. The inaccuracy at LLOQ should not exceed 20% of the nominal value [21]. When analyzing the study samples, the QC samples are used to accept or reject the run. Values falling outside the inaccuracy limit can be discarded provided they do not exceed 33% of the QC samples and not all replicates are at the same concentration.

References:

[1] Kole, P.L., et al., Recent advances in sample preparation techniques for effective bioanalytical methods. Biomedical Chromatography. 25 (2011) 199-217.

[2] FDA (Draft Guidance September 2013) Guidance for Industry: Bioanalytical Method Validation.

[3] Pandey, S., et al., Bioanalysis in drug discovery and development. Pharmaceutical methods. 1 (2010) 14-24.

[4] Nazario, C. E. D., et al., New materials for sample preparation techniques in bioanalysis. Journal of Chromatography B. 1043 (2016) 81-95.

[5] Shah, V. P., et al., Bioanalytical method validation—a revisit with a decade of progress. Pharmaceutical Rsearch. 17 (2000) 1551-1557.

[6] Paiva, A., Shou, W. Z., Recent developments in software tools for high-throughput in vitro ADME support with high-resolution MS. 2016.

[7] Srinivas, N. R., Applicability of bioanalysis of multiple analytes in drug discovery and development: review of select case studies including assay development considerations. Biomedical Chromatography, 20 (2006) 383-414.

[8] Van Breemen, R. B., Li, Y. Caco-2 cell permeability assays to measure drug absorption. Expert Opinion on Drug Metabolism & Toxicology. 1 (2005) 175-185.

[9] Xu, L., Klunk L. J., Prakash, C., Common liquid chromatography–mass spectrometry (LC–MS) methodology for metabolite identification, in: Mass Spectrometry in Drug Metabolism and Disposition: Basic Principles and Applications, John Wiley & Sons, Inc., 2011: 291-319.

[10] Xu, R. N., et al., Recent advances in high-throughput quantitative bioanalysis by LC–MS/MS. Journal of Pharmaceutical and Biomedical Analysis. 44 (2007) 342-355.

[11] Hayward, M., et al., Techniques to facilitate the performance of mass spectrometry: sample preparation, liquid chromatography, and non- mass- spectrometric detection. In: Mass Spectrometry in Drug Metabolism and Disposition: Basic Principles and Applications, 2011: 353-381, John Wiley & Sons, Inc.

[12] Li, W., J. Zhang, Tse, F. L., Strategies in quantitative LC- MS/MS analysis of unstable small molecules in biological matrices. Biomedical Chromatography. 25 (2011) 258-277.

[13] Van Eeckhaut, A., et al., Validation of bioanalytical LC-MS/MS assays: evaluation of matrix effects. Journal of Chromatography B. 877 (2009) 2198-2207.

[14] Soltani, S., Jouyban, A., Biological sample preparation: attempts on productivity increasing in bioanalysis. Bioanalysis. 6 (2014) 1691-1710.

[15] Prabu, S. L., Suriyaprakash, T. N. K., Extraction of drug from the biological matrix: a review, in: Applied Biological Engineering-Principles and Practice. 2012: InTech Open Access Publisher.

[16] Chiu, M. L., et al., Matrix effects-a challenge toward automation of molecular analysis. Journal of Laboratory Automation. 15 (2010) 233-242.

[17] Fluhler, E., et al., White Paper on recent issues in bioanalysis: a full immersion in bioanalysis (Part 1-small molecules by LCMS). Bioanalysis. 6 (2014) 3039-3049.

[18] Xu, Q. A. Madden, T. L., LC-MS in Drug Bioanalysis, 2012, Springer Science & Business Media.

[19] Zhang, N., et al., Integrated sample collection and handling for drug discovery bioanalysis. Journal Of Pharmaceutical And Biomedical Analysis. 23 (2000) 551-560.

[20] Shou, W. Z., Zhang, J., Recent development in high-throughput bioanalytical support for in vitro ADMET profiling. Expert Opinion On Drug Metabolism & Toxicology. 6 (2010) 321-336.

[21] FDA, C., Guidance for industry: bioanalytical method validation. US Department of Health and Human Services, 2001, Food and Drug Administration, Center for Drug Evaluation and Research (CDER), Center for Veterinary Medicine (CV).

[22] EMA, Guideline on bioanalytical method validation. 2011, European Medicines Agency (EMEA/CHMP/EWP/192217/2009): London.

[23] Haug, K. G., et al., Nonlinear pharmacokinetics of visnagin in rats after intravenous bolus administration. European Journal of Pharmaceutical Sciences, 45 (2012) 79-89.

[24] Moradi-Afrapoli, F., et al., Validation of UHPLC–MS/MS methods for the determination of kaempferol and its metabolite 4-hydroxyphenyl acetic acid, and application to *in vitro* blood-brain barrier and intestinal drug permeability studies. Journal Of Pharmaceutical and Biomedical Analysis, 128 (2016) 264-274.

[25] Peters, F. T., Drummer, O. H., Musshoff, F., Validation of new methods. Forensic Science International. 165 (2007) 216-224.

[26] Peters, F. T., Maurer, H. H., Bioanalytical method validation and its implications for forensic and clinical toxicology-a review, in: Validation in Chemical Measurement. 2002: 1-9, Springer.

3. Result and Discussion

3.1. HPLC-based activity profiling for $GABA_A$ receptor modulators in extracts – validation of an approach utilizing a larval zebrafish locomotor assay

Fahimeh Moradi-Afrapoli, Samad Ebrahimi, Martin Smiesko, Matthias Hamburger

Journal of Natural Products, 128 (2017) 264–274, **DOI:** 10.1021/acs.jnatprod.7b00081

Gamma aminobutyric acid type A ($GABA_A$) receptors are the target for numerous clinically important drugs used to treat anxiety, insomnia and epilepsy. Various assay formats have been used for the discovery of $GABA_A$ receptor ligands *in vitro* and *in vivo*. In recent years, zebrafish (*Danio rerio*) has become an increasingly important model organism in drug discovery. With respect to the fact that the GABAergic system in the zebrafish develops during embryogenesis and is functional in larvae, in the present study we have established and validated an in-house assay utilizing a behavioral model with zebrafish larvae.

The assay uses 7day old larvae in a 96-well format, and automated tracking of larval movements with an IR-sensitive camera. Larval convulsions are provoked by the pro-convulsant $GABA_A$ receptor antagonist pentylenetetrazol (PTZ), and $GABA_A$ receptor agonistic extracts and compounds are identified through a decrease in locomotor activity. The assay was validated with the aid of compounds with known GABAergic activity and subsequently translated into an HPLC-based profiling protocol. Various assay parameters were optimized for the purpose, such as PTZ concentration, number of larvae, incubation time, data analysis and visualization. In addition, the effects of selected compounds in the zebrafish model were compared with data from *in silico* BBB permeability predictions, to validate the use for discovery of BBB-permeable natural products.

My contributions to this publication: Establishment of the zebrafish larnae locomotor activity model, validation of the assay and translation into the HPLC-based activity profiling, sample preparation and analysis, writing the manuscript draft, and preparation of figures and tables.

Fahimeh Moradiafrapoli

JOURNAL OF NATURAL PRODUCTS

Article

pubs.acs.org/jnp

HPLC-Based Activity Profiling for $GABA_A$ Receptor Modulators in Extracts: Validation of an Approach Utilizing a Larval Zebrafish Locomotor Assay

Fahimeh Moradi-Afrapoli,[†] Samad Nejad Ebrahimi,[†,‡] Martin Smiesko,[§] and Matthias Hamburger*[,†]

[†]Pharmaceutical Biology and [§]Division of Molecular Modeling, Department of Pharmaceutical Sciences, University of Basel, Klingelbergstrasse 50, 4056 Basel, Switzerland

[‡]Department of Phytochemistry, Medicinal Plants and Drugs Research Institute, Shahid Beheshti University, G. C., Evin, Tehran, Iran

Supporting Information

ABSTRACT: Gamma-aminobutyric acid type A ($GABA_A$) receptors are major inhibitory neurotransmitter receptors in the central nervous system and a target for numerous clinically important drugs used to treat anxiety, insomnia, and epilepsy. A series of allosteric $GABA_A$ receptor agonists was identified previously with the aid of HPLC-based activity profiling, whereby activity was tracked with an electrophysiological assay in *Xenopus laevis* oocytes. To accelerate the discovery process, an approach has been established for HPLC-based profiling using a larval zebrafish (*Danio rerio*) seizure model induced by pentylenetetrazol (PTZ), a pro-convulsant $GABA_A$ receptor antagonist. The assay was validated with the aid of representative GABAergic plant compounds and extracts. Various parameters that are relevant for the quality of results obtained, including PTZ concentration, the number of larvae, the incubation time, and the data analysis protocol, were optimized. The assay was then translated into an HPLC profiling protocol, and active compounds were tracked in extracts of *Valeriana officinalis* and *Magnolia officinalis*. For selected compounds the effects in the zebrafish larvae model were compared with data from in silico blood–brain barrier (BBB) permeability predictions, to validate the use for discovery of BBB-permeable natural products.

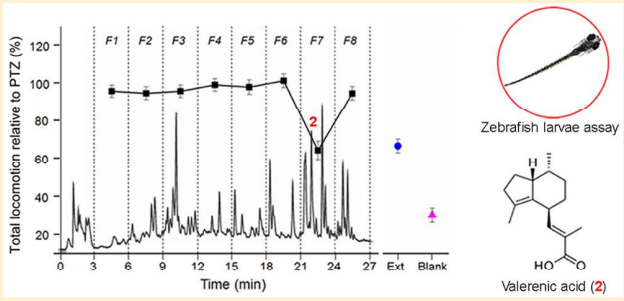

Gamma-aminobutyric acid type A ($GABA_A$) receptors are the key inhibitory neurotransmitter receptors in the central nervous system (CNS). They are heteropentamers composed of different subunits forming a central pore permeable to chloride and bicarbonate ions. The most abundant $GABA_A$ receptor subtype in the mammalian CNS is an assembly of two $\alpha 1$, two $\beta 2$, and one $\gamma 2$ subunit.[1] $GABA_A$ receptors are targets for numerous clinically important drugs used to treat anxiety, panic, insomnia, and epilepsy.[2,3] However, current drugs such as the benzodiazepines and nonbenzodiazepines (the so-called Z-drugs) are associated with side-effects due to a lack of receptor-subtype selectivity.[2] Also, the scaffold diversity of synthetic drugs and experimental compounds targeting $GABA_A$ receptors is very limited. The need for the discovery of allosteric $GABA_A$ receptor modulators with novel scaffolds that possibly target binding sites other than the benzodiazepine binding site is thus apparent. Various natural products with scaffolds that are new for $GABA_A$ receptors have been reported in recent years,[4−8] and compounds such as piperine have been shown to interact at a benzodiazepine-independent allosteric binding site.[9] Medicinal chemistry efforts starting from piperine led to in vivo active analogues with improved selectivity and biopharmaceutical properties,[10−12] thereby supporting the validity of natural products directed efforts in the search for novel $GABA_A$ receptor modulators.

Various assay formats have been used for the discovery of $GABA_A$ receptor ligands, such as radioimmunoassays and fluorescent labels to identify compounds interacting at the benzodiazepine binding site,[13,14] while radioactivity-based ion flux assays,[15] microphysiometry,[16] and the use of fluorescent dyes that are sensitive to chloride ions have been used to examine ion channel function.[17,18] Patch clamp and two-microelectrode electrophysiological assays have been employed with *Xenopus laevis* oocytes and HEK cells in which $GABA_A$ receptors were transiently or stably expressed.[19,20] A semi-automated assay with *Xenopus* oocytes has been successfully used for the screening of extract libraries, HPLC activity profiling for hits, and subsequent structural optimization of active hits.[8,9,11,12,20−32]

In HPLC-based activity profiling of extracts, the turnaround time of bioassay data is the limiting step.[33,34] To accelerate the discovery and dereplication process, we have established and validated in the present work an in-house assay utilizing a

Received: January 26, 2017
Published: May 9, 2017

DOI: 10.1021/acs.jnatprod.7b00081
J. Nat. Prod. 2017, 80, 1548−1557

behavioral model with zebrafish larvae. In recent years, zebrafish (*Danio rerio*) has become an increasingly important model organism in drug discovery,[35−38] being ranked by the National Institutes of Health (NIH) as the third most important experimental organism after rats and mice.[39] It has a high genetic homology (<70%) to humans and the largest gene set sequenced so far among vertebrates.[40] High fecundity of adult fish, a fast ex utero development of embryos, development of all major organs within 36 h of fertilization, and their small size render zebrafish larvae suitable for in vivo medium- to high-throughput screening in a 96-well format.[36,41] Moreover, given that in zebrafish larvae the test compounds have to be absorbed and systemically distributed to reach the target tissues at relevant concentrations, the model is reasonably predictive for later translation into mammalian models.[35] With regard to compounds targeting the CNS, the presence of a complex brain and of a blood−brain barrier (BBB) expressing various drug transporters provides a strong rationale for using zebrafish larvae for the discovery of CNS drugs.[42,43] The GABAergic system of zebrafish develops during embryogenesis and is functional in larvae.[44,45] Pentylenetetrazol (PTZ), a $GABA_A$ receptor antagonist[46] that has been extensively used in rodent models for acute seizure and anxiety, also leads to concentration-dependent seizures in zebrafish larvae.[47] PTZ induces stereotypic behavior in three stages, starting from increase of swimming activity (stage I), to rapid whirlpool-like movement (stage II), and to brief clonus-like convulsions leading to body stiffening that renders larva immobile (stage III).[47] The total distance of larval movement provoked by PTZ has been used for a quantitative assessment of the seizure behavior.[47−49] The PTZ-provoked locomotor activity model has been validated with the aid of known antiepileptic drugs,[44,48,49] and zebrafish larval assays have been used by some research group for the testing of natural products.[50−55] However, the assay protocols used have differed substantially from each other with respect to PTZ concentration used to induce convulsive movements in larvae and in the incubation time of larvae with test compounds, the number of larvae used per data point, and data capturing and analysis. Therefore, in some cases compounds such as cardenolides and other glycosides were reported as active, even though their BBB permeation is highly unlikely.[50,51,55] Also, bioassay data presented often did not allow for a detailed analysis of movement patterns and, hence, for a critical assessment of findings. Such an assessment is essential, given that reduced motility due to toxicity can be misinterpreted as a sedative effect mediated by $GABA_A$ receptors.

Therefore, the assay has been developed further for routine use in HPLC-based activity profiling for $GABA_A$ receptor modulators in plant extracts, whereby various parameters were optimized, such as PTZ concentration, the number of larvae, the incubation time, and also the data analysis protocol. The assay was then validated with the aid of compounds with known GABAergic activity (diazepam, valerenic acid (**1**), magnolol (**2**), and piperine (**3**), and additional $GABA_A$ receptor agonistic compounds (**4**−**7**) that had been previously identified with the aid of the *Xenopus* oocyte assay), and the effects in the zebrafish larvae model were then compared with data from in silico BBB permeability predictions. Finally, the assay was translated into an HPLC profiling protocol, using extracts of *Magnolia officinalis* and *Valeriana officinalis*.

Chart 1

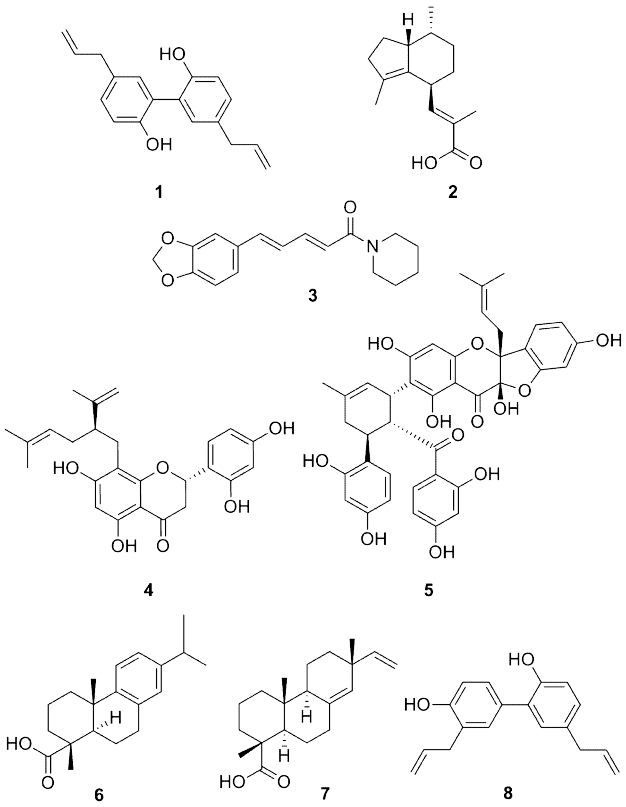

RESULTS AND DISCUSSION

Optimization of PTZ Concentration. A first issue was with the selection of an appropriate concentration of PTZ needed to induce larval convulsions. In previous locomotor behavior studies, concentrations of 20,[44,48,49,52,53] 15,[47] 10,[50,54] and 7.5 mM[51] have been used, but we could not find a systematic assessment evaluating the influence of PTZ concentration on the outcome of a screening for $GABA_A$ receptor modulators. However, it was reasonable to assume that the transition of larval movements from stage I to stage III would be shortened significantly with increasing PTZ concentrations and that this had to be taken into account when selecting an appropriate recording time of larval movements.

Therefore, locomotor activity was first assessed as induced by increasing concentrations of PTZ (2.5, 5, 7.5, 10, 12.5, 15, 17.5, and 20 mM) in 7-day postfertilization (dpf) larvae (n = 32 for each test concentration). Total distance traveled (mm) within 30 min (min 0 to 30) was recorded for each concentration, summed for 5 min intervals, and compared with untreated larvae (blank; 0 mM PTZ) (Figure 1A). A linear concentration−response relationship was observed for PTZ concentrations up to 10 mM, while a quadratic relationship was found when higher PTZ concentrations (>10 mM) were also included (Figure 1A).

Patterns of larval response to different PTZ concentrations were visualized by plotting movement vs time, whereby total distance traveled in 5 min intervals was summed (Figure 1B). Locomotor activity increased following exposure to 5 mM PTZ and remained constant within 30 min. The movement induced by 10 mM PTZ gradually increased within 15 min due to the increasing frequency of whirlpool-like movements (stage II)

DOI: 10.1021/acs.jnatprod.7b00081
J. Nat. Prod. 2017, 80, 1548−1557

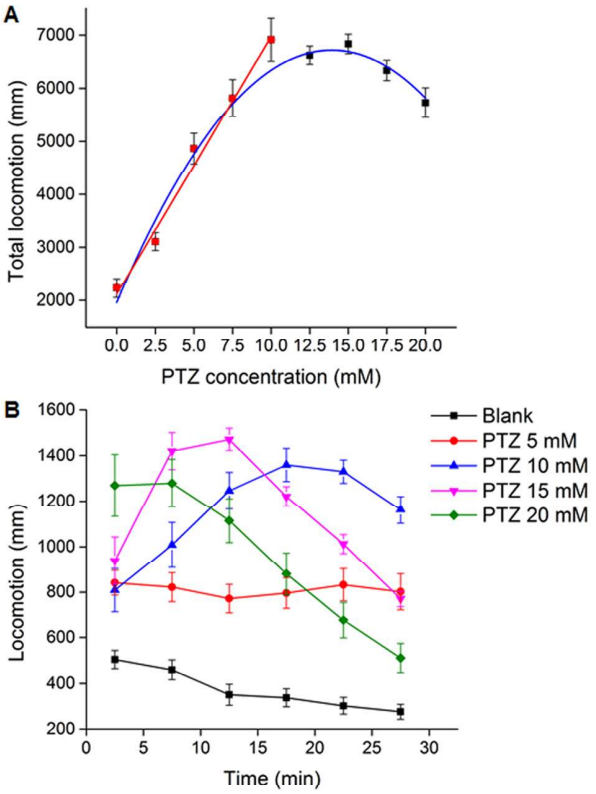

Figure 1. Locomotor activity of zebrafish larvae provoked by various PTZ concentrations over a 30 min tracking period. (A) Concentration response relationship for 0 to 20 mM PTZ. (B) Patterns of larval movements expressed as average distance traveled over 5 min intervals ± SEM (n = 32). For clarity, only four PTZ concentrations are presented, along with the blank (0 mM PTZ).

and remained at a high level for the next 15 min, prior to loss of movement (stage III of seizure behavior). PTZ at 15 mM shortened the latency to the stages II and III of seizure, by provoking a rapid increase of locomotor activity and a subsequent, rapid decline of movement after minute 15. At 20 mM PTZ, the progress of seizure behavior to stage III was even faster.

Since the larval locomotor activity model is based on the increase of total larval movement after exposure to PTZ,[32] the evaluations were started with 10 mM PTZ, inducing the highest level of locomotion. Total distance traveled between minute 5 and 30 after exposure to PTZ, along with the pattern of larval movements during the tracking period, was analyzed in the activity assessment of the test samples.

Assay Validation with Known $GABA_A$ Receptor Modulators. Absorption of test compounds may be through the gastrointestinal tract or across the skin, given that larvae are able to swallow and are not yet covered by scales.[49] Incubation of larvae with test compounds in previously published studies varied from 1 to 24 h.[48−53] A higher incubation time increases the risk of decomposition of test compounds in the aqueous medium and also may favor metabolism of test compounds in the larvae. Both could thus lead to false positive or negative results.

The effects of diazepam and natural products **1**−**7** with known GABAergic activity were therefore examined on PTZ-provoked locomotor activity in zebrafish larvae, utilizing increasing incubation times. The toxicity of each test compound was assessed prior to screening for activity. Signs of toxicity were monitored between 1.5 and 24 h of incubation. The toxicity rate (total number of impaired and dead larvae) did not change significantly between 3 and 24 h (data not shown). It was thus assumed that an exposure of 3 h was sufficient for the compounds to be absorbed and to exhibit toxicity and/or activity. The maximal tolerated concentration (MTC) of each compound, as determined in the toxicity assessment (Table 1), was then used as the highest test concentration. Lower test concentrations were prepared by serial dilutions.

Table 1. Maximum Tolerated Concentrations (MTC) of Pure Compounds and Plant Extracts

compound	MTC (μM)	compound	MTC (μM)	extract	MTC (μg/mL)
diazepam	20	sophoraflavanone G (**4**)	10	*M. officinalis*	4
magnolol (**1**)	4	sanggenon C (**5**)	2	*V. officinalis*	12
valerenic acid (**2**)	10	dehydroabietic acid (**6**)	6		
piperine (**3**)	12	sandaracopimaric acid (**7**)	2		

Benzodiazepines are the most frequently prescribed $GABA_A$ receptor modulators and are highly effective inhibitors of PTZ-evoked seizures in rodents.[47] Therefore, the assay protocol was evaluated first with diazepam (Figure 2). Diazepam (MTC 20 μM) lowered PTZ-provoked locomotor activity in zebrafish larvae in a concentration-dependent manner at concentrations of <4 μM. Patterns of larval movements indicated that diazepam increased the latency to different seizure stages (Figure 2A). These findings were in line with earlier studies reporting a suppression of PTZ-evoked epileptiform electrographic discharges in larval zebrafish by diazepam in a concentration-dependent manner.[47] Diazepam was used as the positive control in subsequent experiments.

Magnolol (**1**), valerenic acid (**2**), and piperine (**3**) have been previously identified as allosteric modulators of $GABA_A$ receptors.[9,25,56,57] The effects of **1**−**3** on PTZ-induced locomotor activity were assessed at four concentrations starting from MTC, whereby concentration−response curves (Figure 3) showed statistically significant and concentration-dependent lowering of locomotor activity in test groups compared to the PTZ-only group. An additional series of $GABA_A$ receptor modulators was then tested that had been previously identified with the aid of the *Xenopus* oocyte assay, namely, sophoraflavanone G (**4**),[21] sanggenon C (**5**),[22] dehydroabietic acid (**6**),[23] and sandaracopimaric acid (**7**).[8] Lowering of locomotor activity was found for these compounds (Figure 4A−C, Figures S1 and S2, Supporting Information), with the exception of **5** (Figure 4D−F). Physicochemical descriptors relevant to BBB permeability (PSA, cLogP, number of H-donor and acceptor sites, and number of rotatable bonds) were calculated for these compounds (Table 2), which, in the case of **5**, predicted a lack of BBB permeability. Hence, its lack of activity appeared to correlate with the presence of a functional and size-exclusive BBB in the zebrafish larvae.

Evaluation of Plant Extracts. Next, plant extracts with known GABAergic constituents, namely, ethyl acetate (EtOAc) extracts of *M. officinalis* bark (containing magnolol **1**) and

DOI: 10.1021/acs.jnatprod.7b00081
J. Nat. Prod. 2017, 80, 1548−1557

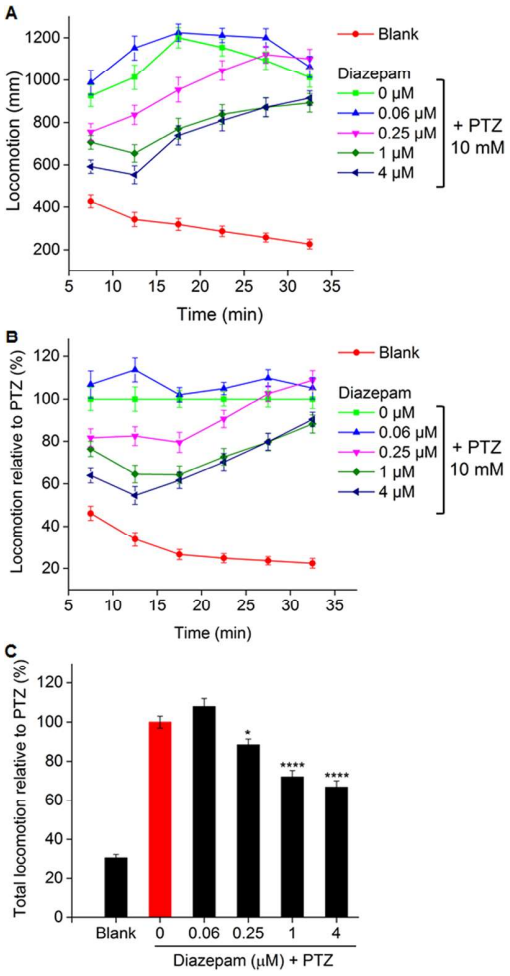

Figure 2. PTZ-induced locomotor activity of zebrafish larvae pretreated for 3 h with different concentrations of diazepam. (A) Patterns of movements expressed as average distance traveled over 5 min intervals (means ± SEM) during the observation period of 30 min. Tracking of larval movements started 5 min after exposure to PTZ. (B) Distance traveled by larvae over 5 min intervals, normalized against the PTZ-only group (0 μM diazepam) (mean % ± SEM). (C) Total distance traveled by larvae in 25 min (minute 5 to 30) relative to PTZ (mean % ± SEM, n = 48, significant difference from PTZ-only group: *p < 0.05, ****p < 0.0001, one-way ANOVA).

V. officinalis roots (containing valerenic acid **2**) were tested in the zebrafish locomotor assay. Toxicity assessments prior to screening for activity revealed MTC values of 4 and 12 μg/mL, respectively (Table 1).

The *M. officinalis* extract significantly suppressed PTZ-provoked locomotor activity in a concentration-dependent manner between 1 and 4 μg/mL (Figure 5A–C). Increase of latency to seizure stage III was observed in larvae pretreated with 4 μg/mL extract. Pretreatment of zebrafish larvae with *V. officinalis* extract at 12 and 10 μg/mL significantly lowered the PTZ-induced locomotion, but the extract was not active at the lower test concentrations (Figure 5D–F).

HPLC-Based Activity Profiling of Extracts. The larval locomotor activity assay was translated into an HPLC-based activity profiling protocol, and its applicability to localize the active compounds in analytical HPLC separations of *M. officicinalis* and *V. officinalis* extracts was tested. The amount of each extract needed for a time-based microfractionation was calculated on the assumption that (i) active compounds might elute in one or two microfractions and (ii) a 50% loss of compound might occur during chromatography.[33,34] Extracts were submitted to gradient elution on an analytical HPLC column, and 3 min microfractions were collected and submitted to the bioassay.

The EtOAc extract of *M. officinalis* was selected as a first simple case, given that the HPLC chromatogram of the extract showed two major UV-absorbing peaks of honokiol (**8**) and magnolol (**1**) (Figure 6A). Lowering of PTZ-provoked locomotor activity (tested at 2 × MTC) of 3 min microfractions is shown by the curve above the chromatogram, whereby F6 (minute 18 to 21) decreased locomotion. Patterns of movements are shown in Figure S3, Supporting Information. Next, a peak-based fractionation of the time window of F5 and F6 was performed (Figure 6B; patterns of movements are given in Figure S4, Supporting Information). Peak *e* corresponding to **1** correlated with major activity, whereas peak *c* (corresponding to **8**) only slightly reduced PTZ-provoked locomotor activity.

Next, *V. officinalis* extract was separated as an example of a highly complex extract containing valepotriates and other isoprenoids, lignans, and flavonoids.[58,59] The HPLC profile and the activity of corresponding microfractions are shown in Figure 7A (the patterns of movements are given in Figure S5, Supporting Information), whereby testing was performed at 2 × MTC. The major activity was localized in fraction F7. A peak-based microfractionation of F7 was carried out (Figure 7B; patterns of movements are given in Figure S6, Supporting Information). Lowering of the larval locomotor activity was observed for fractions *b* and *d*, whereby peak *b* corresponded to valerenic acid, a known $GABA_A$ receptor modulator in *V. officinalis*.[7,25] The ESIMS data of the major peak in fraction *d* indicated the presence of several compounds with m/z = 202, 204, 260, 292, 362, and 374, and identification of the active compound(s) was not further pursued in this study.

Concluding Remarks. We previously identified a series of allosteric $GABA_A$ receptor agonists with the aid of HPLC-based activity profiling, whereby activity was tracked with a semiautomated electrophysiological assay in *Xenopus* oocytes expressing $GABA_A$ receptors. To accelerate the discovery process, an in-house approach has now been established and validated for HPLC activity profiling utilizing a zebrafish behavioral model instead. The assay uses 7-dpf larvae in a 96-well format and automated tracking of larval movements with an IR-sensitive camera.

In contrast to previous publications using zebrafish larvae for the discovery of CNS-active natural products, various parameters were optimized that are relevant for the quality of data, such as PTZ concentration, concentration of test extracts/compounds, incubation time with test extract/compound, duration of the recording of larval motility, and data analysis. In the final protocol used, larvae were incubated with the test samples for 3 h, and larval movements were afterward provoked by 10 mM PTZ. $GABA_A$ receptor modulators were identified through a decrease in total larval movement (distance traveled, mm) during the tracking period (25 min). With respect to test concentrations, it was found that determination of an MTC for each extract was critical and that for HPLC activity profiling of extracts an extract amount corresponding in the bioassay to a 2- or 4-fold concentration (2 × MTC or 4 × MTC) was appropriate. With respect to data analysis, it was determined that movement patterns normalized against the PTZ-only treated group could lead to erroneous data interpretation. Thus,

DOI: 10.1021/acs.jnatprod.7b00081
J. Nat. Prod. 2017, 80, 1548–1557

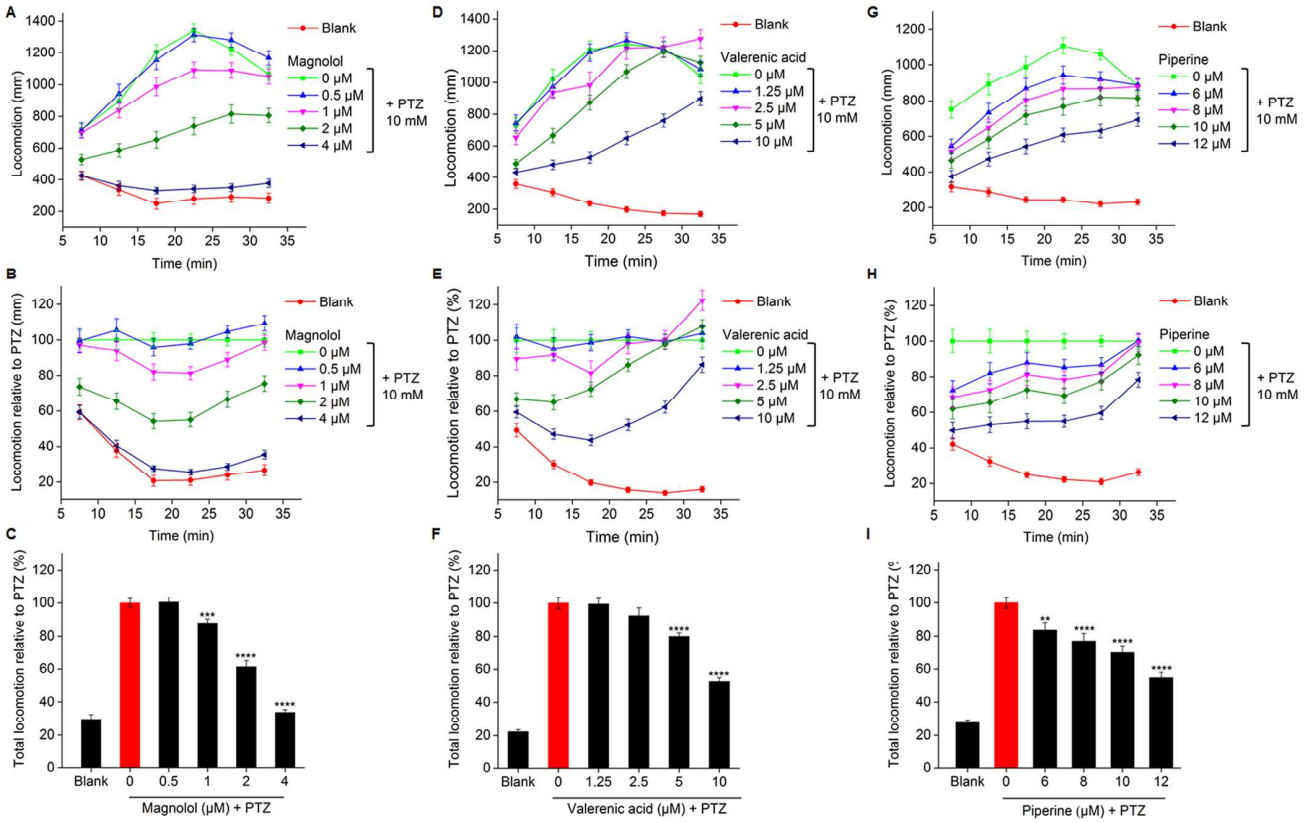

Figure 3. PTZ-induced locomotor activity of zebrafish larvae pretreated for 3 h with different concentrations of magnolol **1** (A–C), valerenic acid **2** (D–F), and piperine **3** (G–I). (A, D, and G) Patterns of movements expressed as total distance traveled over 5 min intervals (mean ± SEM) during the observation period of 30 min. (B, E, and H) Distance traveled by larvae over 5 min intervals, normalized against the PTZ-only group (0 μM magnolol) (mean % ± SEM). (C, F, and I). Total distance traveled by larvae in 25 min (minute 5 to 30) relative to PTZ (mean % ± SEM, n = 48, significant difference from PTZ-only group: **p < 0.01, ***p < 0.001, ****p < 0.0001, one-way ANOVA).

the original larval movement patterns should be first analyzed, in order to identify the appearance of different seizure stages. The assay was validated with compounds of known GABAergic activity. The apparent lack of BBB permeation for sanggenone C (**5**) (confirmed by in silico property assessment) corroborated the utility of the zebrafish larvae assay for discovery of BBB-permeable and, thus, high-quality natural product hits that have a good potential for translation into mammalian models and further optimization by medicinal chemistry. The assay was translated into a HPLC profiling protocol and successfully tested with representative plant extracts.

However, PTZ-induced seizures in zebrafish may also be prevented by compounds acting on targets other than $GABA_A$ receptors.[44,47,48] Therefore, the *Xenopus* oocyte model may be used for the primary screening of extract libraries for $GABA_A$ receptor modulation, and only extracts testing as active in the *Xenopus* oocyte assay would undergo HPLC activity profiling using the zebrafish larval assay described herein. Mechanistic studies identifying the binding site of compounds, or subunit selectivity, should then be performed in cell-based functional assays. The described protocol is now being employed for HPLC-based activity profiling of South African medicinal plants traditionally used for treatment of epilepsy and other neurological disorders.

EXPERIMENTAL SECTION

General Experimental Procedures. Larval zebrafish locomotor activity was tracked with a DanioVision observation chamber (Noldus Information Technology) equipped with an IR-sensitive camera and a temperature controller unit. HPLC-PDA-MS analyses were performed with a Binary Gradient Prominence LC-MS/MS (Shimadzu) consisting of a degasser, quaternary pump (LC-20AD), column oven (CTO-20AC), PDA detector (SPD-M20A), and triple quadrupole mass spectrometer (LCMS-8030), connected to an ELSD 3300 detector (Alltech). Data acquisition and processing were performed using Labsolutions software (Shimadzu). Evaporation of micro-fractions was performed with a Genevac EZ-2 Plus vacuum centrifuge (Avantec). HPLC-grade CH_3CN (Scharlau Chemie) and H_2O (obtained by a Barnstead EASY-pure II water purification system) were used for HPLC separations. HPLC solvents contained 0.1% HCOOH (Scharlau) for analytical separations. DMSO (Scharlau) was used for dissolving the samples. Solvents used for extraction were of technical grade (Romil Pure Chemistry) and were purified by distillation. PTZ and piperine (**3**) were purchased from Sigma-Aldrich, magnolol (**1**) from Tokyo Chemical Industry, and valerenic acid (**2**) from Phytolab. Diazepam was from Lipomed. Sophoraflavanone G (**4**),[21] sanggenon C (**5**),[22] dehydroabietic acid (**6**),[23] and sandaracopimaric acid (**7**)[8] were isolated in earlier work.

Plant Material. Dried bark of *Magnolia officinalis* Rehd. et Wils. (Magnoliaceae) was purchased from Peter Weinfurth, Germany, and roots of *Valeriana officinalis* L. (Valerianaceae) (Valerianae Radix, Ph. Eur.) were from Dixa, Switzerland. Voucher specimens (00216 and 07891, respectively) have been deposited at the Institute of Pharmaceutical Biology, University of Basel.

DOI: 10.1021/acs.jnatprod.7b00081
J. Nat. Prod. 2017, 80, 1548–1557

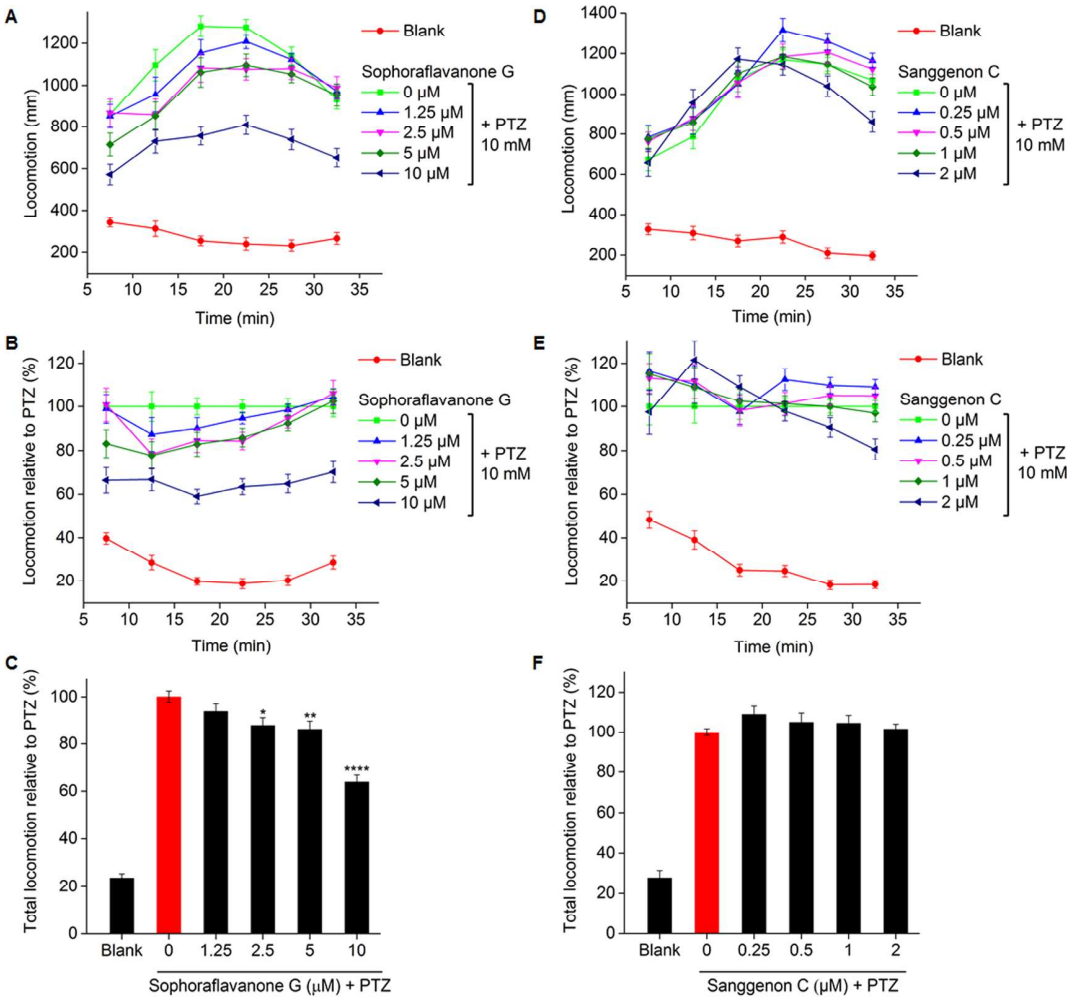

Figure 4. PTZ-induced locomotor activity of zebrafish larvae pretreated for 3 h with different concentrations of sophoraflavanone G (**4**) (A–C) and sanggenon C (**5**) (D–F). (A and D) Patterns of movements expressed as total distance traveled over 5 min intervals (mean ± SEM) during the observation period of 30 min. (B and E) Distance traveled by larvae over 5 min intervals, normalized against the PTZ-only group (0 μM testing compounds) (mean % ± SEM). (C and F) Total distance traveled by larvae in 25 min (minute 5 to 30) relative to PTZ (mean % ± SEM, $n = 32$, significant difference from PTZ-only group: $^{**}p < 0.01$, $^{****}p < 0.0001$, one-way ANOVA).

Table 2. Mean Values of in Silico Physicochemical Descriptors of Compounds

	QikProp									Marvin	
compound	#acid	#rotor[a]	MW[b]	donor HB[c]	accpt HB[d]	logP o/w[e]	log BB[f]	PMDCK[g]	PSA[h]	logD 7.4[i]	PSA[h]
magnolol (**1**)	0	5	266.3	2	2	4.96	−0.55	1045.2	37.8	5.19[j]	40.5
valerenic acid (**2**)	1	2	234.3	1	2	3.62	−0.46	145.2	49.5	1.28	37.3
piperine (**3**)	0	3	285.3	0	3	3.27	−0.13	2165.0	48.0	2.78	38.8
sophoraflavanone G (**4**)	0	6	424.5	4	6	3.94	−1.87[j]	51.7	113.1[j]	5.74[j]	107.2
sanggenon C (**5**)	0	6	708.7[j]	8[j]	12[j]	4.21	−3.06[j]	5.3[j]	204.2[j]	7.39[j]	214.4[j]
dehydroabietic acid (**6**)	1	2	300.4	1	2	4.95	−0.24	273.3	42.9	2.98	37.3
sandaracopimaric acid (**7**)	1	2	302.5	1	2	4.90	−0.21	270.1	43.0	2.52	37.3

[a]Rotatable bonds. [b]Molecular weight. [c]Hydrogen bond donors. [d]Hydrogen bond acceptors. [e]Oil/water partition coefficient. [f]Blood/brain partition coefficient. [g]MDCK cell permeability. [h]Polar surface area. [i]Distribution coefficient at pH 7.4. [j]Values that are not in favor of BBB permeability.

Extraction. Plant extracts were prepared by pressurized liquid extraction at 70 °C and 120 bar, by sequential extraction with petroleum ether and ethyl acetate, utilizing an ASE 200 extraction system with solvent module (Dionex).[34] Solvents were evaporated at reduced pressure, and extracts stored at −20 °C until use.

Zebrafish. The animal experiments were approved by the Kantonales Veterinaeramt Basel-Stadt and conducted in accordance with EU directive 2011/63/EU. Wild-type zebrafish of the ABC×TU strain were provided by Dr. Heinz-Georg Belting (Department of Cell Biology, Biozentrum, University of Basel). The fish were kept under standard conditions.[60] The photoperiod was set to 12 h light and 12 h darkness. Fertilized eggs were collected via natural spawning. Embryos were incubated at 28.5 °C in E3 medium containing 5 mM NaCl, 0.17 mM KCl, 0.33 mM CaCl, and 0.33 mM $MgSO_4$ in water (0.5 mL of methylene blue 0.05% w/v was added to 1 L of medium as a disinfectant; pH was corrected to 7.4 by 0.5 M K_2CO_3). The medium

DOI: 10.1021/acs.jnatprod.7b00081
J. Nat. Prod. 2017, 80, 1548–1557

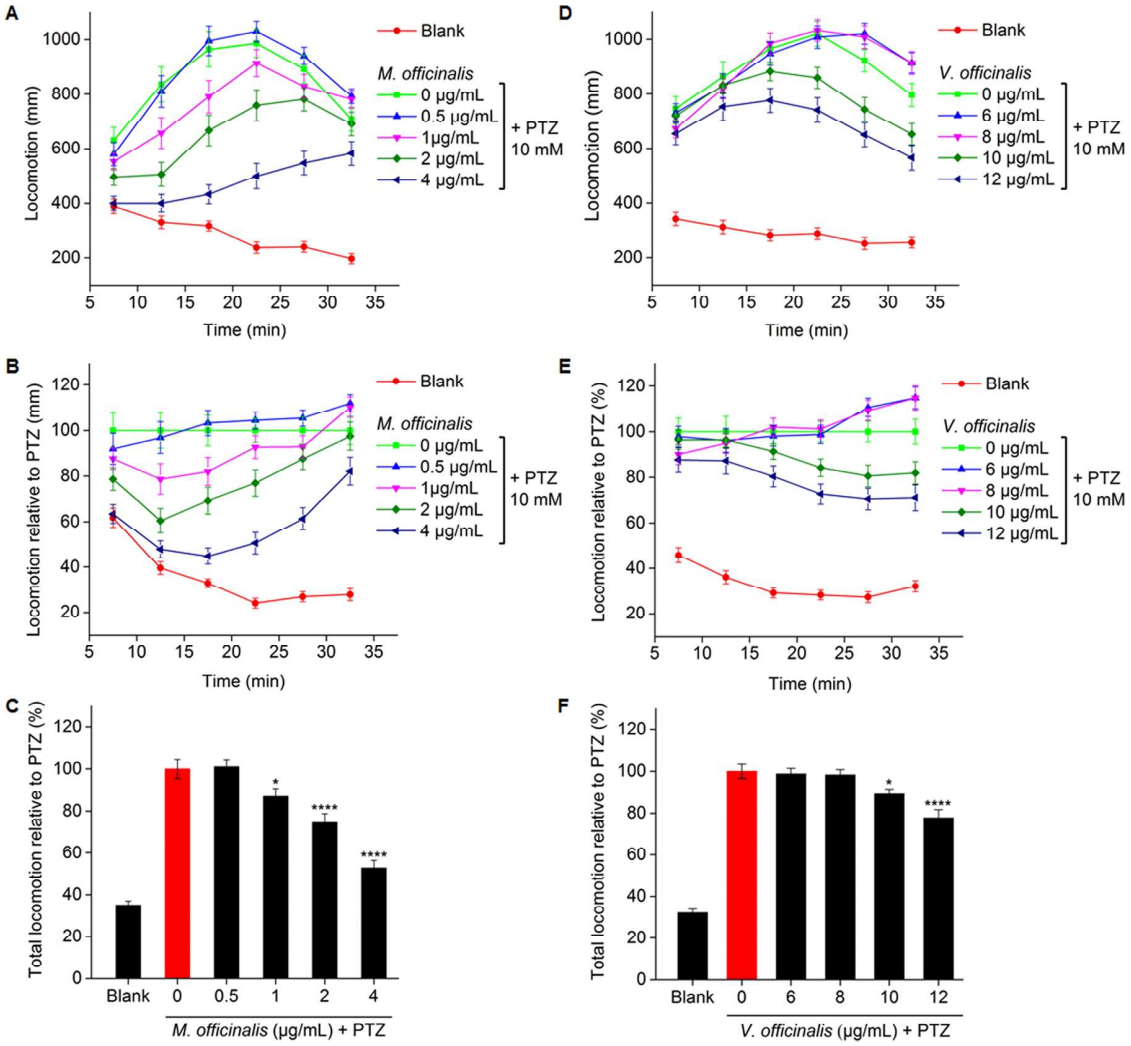

Figure 5. PTZ-induced locomotor activity of zebrafish larvae pretreated for 3 h with different concentrations of EtOAc extracts from *Magnolia officinalis* bark (A–C) and *Valeriana officinalis* roots (D–F). (A and D) Patterns of movements expressed as total distance traveled over 5 min intervals (mean ± SEM) during the observation period of 30 min. (B and E) Distance traveled by larvae over 5 min intervals, normalized against the PTZ-only group (0 μM testing extracts) (mean % ± SEM). (C and F) Total distance traveled by larvae in 25 min (minute 5 to 30) relative to PTZ (mean % ± SEM, n = 48, significant difference from PTZ-only group: *p < 0.05, ****p < 0.0001, one-way ANOVA).

was changed every day for 7 days, and unfertilized eggs and dead larvae were removed.

Toxicity Assessment. Prior to the activity screening, an assessment of toxicity was performed for each test sample at 50, 25, 12.5, and 6.25 μM (for pure compounds) or 50, 25, 12.5 and 6.25 μg/mL (for extracts). Larvae were incubated with test samples (n = 12) and individually checked under a microscope (×30 magnification) at four time points (1.5, 3, 6, and 24 h). The locomotor impairment including loss of larval response after a light touch of the tail, loss of posture, body deformation, and death was monitored and compared with the blank (same number of untreated larvae). After the first toxicity assessments intermediate test concentrations were examined to define accurately the maximal tolerated concentration at which not more than two out of 12 larvae were impaired.[48] The MTC was selected as the highest test concentration in activity assessment.

Locomotor Activity Measurement. Zebrafish larvae at 7 days postfertilization (dpf) were used in the 96-well format assay (1 larva per well, 200 μL of E3 medium). Several concentrations of PTZ (2.5, 5, 7.5, 10, 12.5, 15, 17.5, and 20 mM) were tested initially to find the best suited concentration for the studies. The recording of larval movement over 35 min started immediately after addition of PTZ.

To perform the activity screening, stock solutions of test compounds and extracts were prepared at 5 and 10 mg/mL DMSO, respectively. Working solutions were prepared in E3 medium at concentrations corresponding to 5-fold MTC values (20–100 μg/mL). Aliquots of 50 μL working solutions were added to each well, and larvae were incubated for 3 h at 28.5 °C (16 wells per sample per plate). Afterward, 20 μL of PTZ stock solution (in E3 medium) was added to each well to reach a 10 mM PTZ concentration in the assay. Microplates were then placed in the movement-tracking chamber (DanioVision). Larvae were left for 5 min to habituate, and the movement was tracked with the IR-sensitive camera for the following 30 min. Total locomotor activity within 25 min (minute 5 to 30) was recorded and then quantified for 5 min intervals by EthoVision XT software. The medium, test solutions, and the room temperature were maintained at 28 °C to minimize external stimuli, given that rapid temperature variation affects larval locomotor activity (data not shown). Diazepam was used as the positive control. A PTZ-only group (16 larvae treated only with PTZ) and a blank group (16 larvae maintained only with the E3 medium) were placed in each microplate. To assess the reproducibility of data between different batches of larvae, all samples were tested at least in two independent assays on

DOI: 10.1021/acs.jnatprod.7b00081
J. Nat. Prod. 2017, 80, 1548–1557

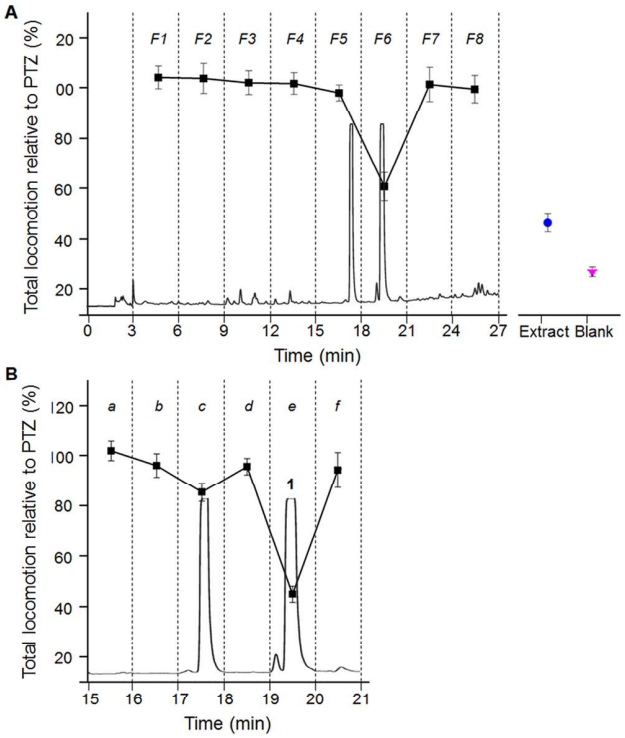

Figure 6. HPLC-based activity profiling of an EtOAc extract of *Magnolia officinalis* bark at a concentration equivalent to 2 × MTC. (A) Chromatogram (254 nm) for a separation of 360 μg of extract on an analytical HPLC column. Eight microfractions (F1–F8) were collected in 3 min time windows (indicated with dashed lines), and lowering of PTZ (10 mM)-induced locomotor activity by microfractions is shown above (expressed as % activity relative to the PTZ-only group, n = 32). Locomotor activity with extract and blank is shown to the right of the chromatogram. (B) Peak-based fractionation of the time window of 15 to 21 min. Activity in fraction *e* corresponds to magnolol (**1**).

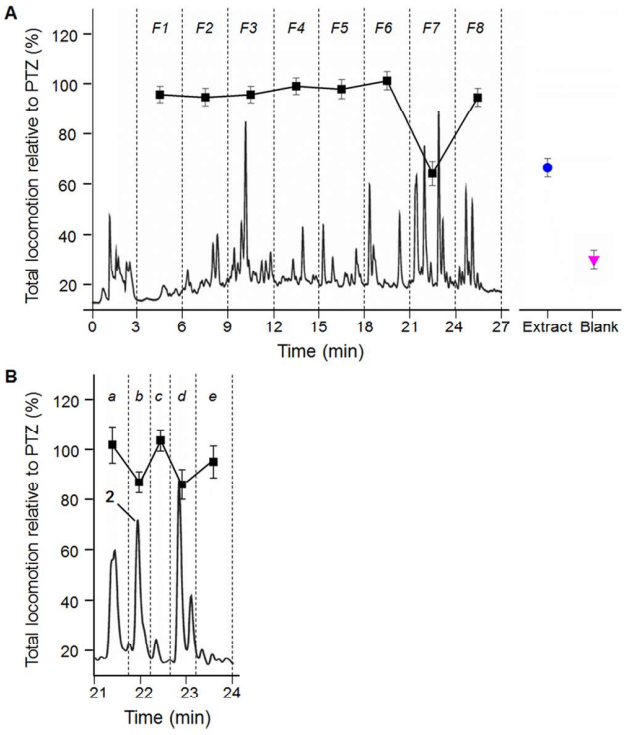

Figure 7. HPLC-based activity profiling of an EtOAc extract of *Valeriana officinalis* roots at a concentration equivalent to 2 × MTC. (A) HPLC chromatogram (254 nm) for a separation of 360 μg of extract on an analytical HPLC column. Eight microfractions (F1–F8) were collected in 3 min time windows (indicated with dashed lines), and lowering of PTZ (10 mM)-induced locomotor activity by microfractions is shown above (expressed as % activity relative to the PTZ-only group, n = 32). Locomotor activity with extract and blank is shown to the right of the chromatogram. (B) Peak-based fractionation (*a*–*e*) of the active time window (minute 21–24). Lowering of locomotor activity in fraction *b* corresponds to valerenic acid (**2**).

separate days (n = 32). Final DMSO concentration in the assay did not exceed 0.5%.

HPLC-Based Microfractionation of Extracts. HPLC time-based activity profiling[33,34] was adapted to the zebrafish larvae model to localize active compounds in plant extracts. The amount of extract to be microfractionated by HPLC was calculated by taking into account the requirements of the bioassay and the MTC of each extract. Final test concentration of the microfractions was calculated as equivalent to 4 times the MTC of the corresponding extract, based on the assumption that each active constituent might elute in one or two microfractions and that a 50% loss of compound during chromatography and redissolution would occur.[34] Larvae were examined after 3 h of incubation with microfractions. If toxicity and larval death were observed, experiments were performed at half-concentration (equal to 2 times the MTC). If the MTC was ≤10 μg/mL, the 360 μg extract (36 μL of 10 mg/mL solution in DMSO) was submitted to analytical HPLC (SunFire C_{18} column, 3.5 μm, 3 × 150 mm; Waters) with H_2O (A) and CH_3CN (B) containing 0.1% formic acid. The EtOAc extract of *M. officinalis* was separated using the following gradient: 30% → 100% B (0–26 min), 100% B (26–30 min); separation of the EtOAc extract of *V. officinalis* was with the following gradient: 5% → 100% B (0–24 min), 100% B (24–30 min). The flow rate was 0.4 mL/min. The extract of *V. officinalis* was microfractionated two times in a row, given the MTC = 12 μg/mL. Three-minute fractions between minute 3 and 27 were collected in 96-well deep-well plates. Plates were dried in an EZ-2 Plus evaporator (GeneVac). Dried microfractions in the 96-well plate were redissolved with 45 μL of DMSO, and the plate was shaken at 1400 rpm for 30 min for complete dissolution. Corresponding microfractions from the two separations were combined (stock solution). Afterward, the stock solutions [18 μL for *M. officinalis* (MTC = 4 μg/mL), 54 μL for *V. officinalis* (MTC = 12 μg/mL)] were added to E3 medium up to the final volume of 1800 μL to obtain the appropriate working solutions. Aliquots of 50 μL were added to each well containing one zebrafish larva in 200 μL of E3 medium (16 wells per sample per plate, duplicate, n = 32).

Data Analysis. Larval locomotor activity was recorded as total distance traveled (mm) by each treatment group during 25 min (minute 5–30 after exposure to PTZ) and given as the mean ± SE. Patterns of larval movements were provided by calculation of total distance traveled over 5 min intervals (mean ± SEM). Statistical analysis was performed using SPSS Statistics version 20 (IBM). Average total movements of test groups were compared with the PTZ-only group by one-way ANOVA, followed by Dunnet's multiple comparison test. To facilitate the comparison between different treatment groups, total distance traveled (summed between min 5 and 30) is presented as bar graphs normalized against the PTZ-only group (%).

In Silico Prediction of BBB Penetration. Three-dimensional computer models of the structures were built in the Maestro modeling environment (Maestro, version 9.3, Schrödinger, LLC, New York, 2012), and the most favorable conformers were identified by the conformational search in MacroModel (MacroModel, version 9.9, Schrödinger, LLC, New York, 2012) using the OPLS-2005 force-field, implicit solvent conditions (water), and 1000 iterations of the mixed serial/low-mode sampling method. For each isomer, the conformers

DOI: 10.1021/acs.jnatprod.7b00081
J. Nat. Prod. 2017, 80, 1548–1557

within 5 kcal/mol from the corresponding global minimum were used as input for the QikProp application (QikProp, version 3.5, Schrödinger, LLC, New York, 2012), to evaluate various descriptors relevant for drug permeability. For comparison, the polar surface area (PSA) and the logarithm of partition coefficient (cLogP) descriptors were calculated also using the Calculator plugin of Chemaxon Marvin Web-application (http://www.chemaxon.com/marvin/sketch/index.php) requiring only the 2D structural formula as input.

■ ASSOCIATED CONTENT

Supporting Information

The Supporting Information is available free of charge on the ACS Publications website at DOI: 10.1021/acs.jnatprod.7b00081.

PTZ-induced locomotor activity of zebrafish larvae pretreated with dehydroabietic acid and sandaracopimaric acid; patterns of movements corresponding to PTZ-induced locomotion of zebrafish larvae pretreated with 3 min microfractions from EtOAc extracts of *M. officinalis* and *V. officinalis*, together with their corresponding peak-based microfractions (PDF)

■ AUTHOR INFORMATION

Corresponding Author

*Tel: +41-61-267-1425. Fax: +41-61-267-1474. E-mail: matthias.hamburger@unibas.ch.

ORCID

Matthias Hamburger: 0000-0001-9331-273X

Notes

The authors declare no competing financial interest.

■ ACKNOWLEDGMENTS

Thanks are due to Dr. H.-G. Belting (Department of Cell Biology, Biozentrum, University of Basel) for provision of access to the Zebrafish Facility and for the zebrafish strain. O. Fertig is acknowledged for technical assistance.

■ REFERENCES

(1) Uusi-Oukari, M.; Korpi, E. R. *Pharmacol. Rev.* **2010**, *62*, 97−135.
(2) Rudolph, U.; Knoflach, F. *Nat. Rev. Drug Discovery* **2011**, *10*, 685−697.
(3) Möhler, H. J. *J. Recept. Signal Transduction Res.* **2006**, *26*, 731−740.
(4) Johnston, G. A.; Hanrahan, J. R.; Chebib, M.; Duke, R. K.; Mewett, K. N. *Adv. Pharmacol.* **2006**, *54*, 285−316.
(5) Tsang, S.; Xue, H. *Curr. Pharm. Des.* **2004**, *10*, 1035−1044.
(6) Hanrahan, J. R.; Chebib, M.; Johnston, G. A. *Br. J. Pharmacol.* **2011**, *163*, 234−245.
(7) Kopp, S.; Baur, R.; Sigel, E.; Möhler, H.; Altmann, K. *ChemMedChem* **2010**, *5*, 678−681.
(8) Zaugg, J.; Khom, S.; Eigenmann, D.; Baburin, I.; Hamburger, M.; Hering, S. *J. Nat. Prod.* **2011**, *74*, 1764−1772.
(9) Zaugg, J.; Baburin, I.; Strommer, B.; Kim, H. J.; Hering, S.; Hamburger, M. *J. Nat. Prod.* **2010**, *73*, 185−191.
(10) Eigenmann, D. E.; Dürig, C.; Jähne, E. A.; Smieško, M.; Culot, M.; Gosselet, F.; Cecchelli, R.; Helms, H. C. C.; Brodin, B.; Wimmer, L. *Eur. J. Pharm. Biopharm.* **2016**, *103*, 118−126.
(11) Schöffmann, A.; Wimmer, L.; Goldmann, D.; Khom, S.; Hintersteiner, J.; Baburin, I.; Schwarz, T.; Hintersteininger, M.; Pakfeifer, P.; Oufir, M. *J. Med. Chem.* **2014**, *57*, 5602−5619.
(12) Khom, S.; Strommer, B.; Schöffmann, A.; Hintersteiner, J.; Baburin, I.; Erker, T.; Schwarz, T.; Schwarzer, C.; Zaugg, J.; Hamburger, M. *Biochem. Pharmacol.* **2013**, *85*, 1827−1836.
(13) Smith, A. J.; Simpson, P. B. *Anal. Bioanal. Chem.* **2003**, *377*, 843−851.
(14) Möhler, H.; Richards, J. *Nature* **1981**, *294*, 763−765.
(15) Smith, A. J.; Alder, L.; Silk, J.; Adkins, C.; Fletcher, A. E.; Scales, T.; Kerby, J.; Marshall, G.; Wafford, K. A.; McKernan, R. M. *Mol. Pharmacol.* **2001**, *59*, 1108−1118.
(16) Smith, A. J.; McKernan, R. M.; Atack, J. R. *Eur. J. Pharmacol.* **1998**, *359*, 261−269.
(17) Marandi, N.; Konnerth, A.; Garaschuk, O. *Pfluegers Arch.* **2002**, *445*, 357−365.
(18) Kuner, T.; Augustine, G. *Neuron* **2000**, *27*, 447−459.
(19) Kvist, T.; Hansen, K. B.; Bräuner-Osborne, H. *Expert Opin. Drug Discovery* **2011**, *6*, 141−153.
(20) Baburin, I.; Beyl, S.; Hering, S. *Pfluegers Arch.* **2006**, *453*, 117−123.
(21) Yang, X.; Baburin, I.; Plitzko, I.; Hering, S.; Hamburger, M. *Mol. Diversity* **2011**, *15*, 361−372.
(22) Kim, H. J.; Baburin, I.; Zaugg, J.; Ebrahimi, S. N.; Hering, S.; Hamburger, M. *Planta Med.* **2012**, *78*, 440−447.
(23) Rueda, D. C.; Raith, M.; De Mieri, M.; Schöffmann, A.; Hering, S.; Hamburger, M. *Fitoterapia* **2014**, *99*, 28−34.
(24) Zaugg, J.; Eickmeier, E.; Rueda, D. C.; Hering, S.; Hamburger, M. *Fitoterapia* **2011**, *82*, 434−440.
(25) Kim, H. J.; Baburin, I.; Khom, S.; Hering, S.; Hamburger, M. *Planta Med.* **2008**, *74*, 521−526.
(26) Rueda, D. C.; de Mieri, M.; Hering, S.; Hamburger, M. *J. Nat. Prod.* **2014**, *77*, 640−649.
(27) Rueda, D. C.; Schöffmann, A.; de Mieri, M.; Raith, M.; Jähne, E. A.; Hering, S.; Hamburger, M. *Bioorg. Med. Chem.* **2014**, *22*, 1276−1284.
(28) Schramm, A.; Ebrahimi, S. N.; Raith, M.; Zaugg, J.; Rueda, D. C.; Hering, S.; Hamburger, M. *Phytochemistry* **2013**, *96*, 318−329.
(29) Rueda, D. C.; Zaugg, J.; Quitschau, M.; Reich, E.; Hering, S.; Hamburger, M. *Planta Med.* **2012**, *78*, 207−210.
(30) Zaugg, J.; Ebrahimi, S. N.; Smiesko, M.; Baburin, I.; Hering, S.; Hamburger, M. *Phytochemistry* **2011**, *72*, 2385−2395.
(31) Zaugg, J.; Eickmeier, E.; Ebrahimi, S. N.; Baburin, I.; Hering, S.; Hamburger, M. *J. Nat. Prod.* **2011**, *74*, 1437−1443.
(32) Li, Y.; Plitzko, I.; Zaugg, J.; Hering, S.; Hamburger, M. *J. Nat. Prod.* **2010**, *73*, 768−770.
(33) Potterat, O.; Hamburger, M. *Planta Med.* **2014**, *80*, 1171−1181.
(34) Potterat, O.; Hamburger, M. *Nat. Prod. Rep.* **2013**, *30*, 546−564.
(35) MacRae, C. A.; Peterson, R. T. *Nat. Rev. Drug Discovery* **2015**, *14*, 721−731.
(36) Delvecchio, C.; Tiefenbach, J.; Krause, H. M. *Assay Drug Dev. Technol.* **2011**, *9*, 354−361.
(37) Kokel, D.; Bryan, J.; Laggner, C.; White, R.; Cheung, C. Y. J.; Mateus, R.; Healey, D.; Kim, S.; Werdich, A. A.; Haggarty, S. *Nat. Chem. Biol.* **2010**, *6*, 231−237.
(38) Rihel, J.; Prober, D. A.; Arvanites, A.; Lam, K.; Zimmerman, S.; Jang, S.; Haggarty, S. J.; Kokel, D.; Rubin, L. L.; Peterson, R. T. *Science* **2010**, *327*, 348−351.
(39) He, J. H.; Gao, J. M.; Huang, C. J.; Li, C. Q. *Neurotoxicol. Teratol.* **2014**, *42*, 35−42.
(40) Howe, K.; Clark, M. D.; Torroja, C. F.; Torrance, J.; Berthelot, C.; Muffato, M.; Collins, J. E.; Humphray, S.; McLaren, K.; Matthews, L. *Nature* **2013**, *496*, 498−503.
(41) Crawford, A. D.; Esguerra, C. V.; de Witte, P. A. *Planta Med.* **2008**, *74*, 624−632.
(42) Jeong, J. Y.; Kwon, H. B.; Ahn, J. C.; Kang, D.; Kwon, S. H.; Park, J. A.; Kim, K. W. *Brain Res. Bull.* **2008**, *75*, 619−628.
(43) Fleming, A.; Diekmann, H.; Goldsmith, P. *PLoS One* **2013**, *8*, e77548.
(44) Baxendale, S.; Holdsworth, C. J.; Santoscoy, P. L. M.; Harrison, M. R. M.; Fox, J.; Parkin, C. A.; Ingham, P. W.; Cunliffe, V. T. *Dis. Models & Mech.* **2012**, *5*, 773−784.
(45) Mueller, T.; Vernier, P.; Wullimann, M. F. *J. Comp. Neurol.* **2006**, *494*, 620−634.
(46) Huang, R. Q.; Bell-Horner, C. L.; Dibas, M. I.; Covey, D. F.; Drewe, J. A.; Dillon, G. H. *J. Pharmacol. Exp. Ther.* **2001**, *298*, 986−995.

DOI: 10.1021/acs.jnatprod.7b00081
J. Nat. Prod. 2017, 80, 1548−1557

(47) Baraban, S. C.; Taylor, M. R.; Castro, P. A.; Baier, H. *Neuroscience* **2005**, *131*, 759−768.
(48) Afrikanova, T.; Serruys, A. S. K.; Buenafe, O. E.; Clinckers, R.; Smolders, I.; de Witte, P. A.; Crawford, A. D.; Esguerra, C. V. *PLoS One* **2013**, *8*, e54166.
(49) Berghmans, S.; Hunt, J.; Roach, A.; Goldsmith, P. *Epilepsy Res.* **2007**, *75*, 18−28.
(50) Li, X.; Zhang, M.; Xiang, C.; Li, B. C.; Li, P. *J. Asian Nat. Prod. Res.* **2015**, *17*, 724−732.
(51) Li, J. L.; Zhou, J.; Chen, Z. H.; Guo, S. Y.; Li, C. Q.; Zhao, W. M. *J. Nat. Prod.* **2015**, *78*, 1548−1555.
(52) Orellana-Paucar, A. M.; Serruys, A. S. K.; Afrikanova, T.; Maes, J.; De Borggraeve, W.; Alen, J.; León-Tamariz, F.; Wilches-Arizábala, I. M.; Crawford, A. D.; de Witte, P. A. *Epilepsy Behav.* **2012**, *24*, 14−22.
(53) Buenafe, O. E.; Orellana-Paucar, A.; Maes, J.; Huang, H.; Ying, X.; De Borggraeve, W.; Crawford, A. D.; Luyten, W.; Esguerra, C. V.; de Witte, P. *ACS Chem. Neurosci.* **2013**, *4*, 1479−1487.
(54) Long, S. M.; Liang, F. Y.; Wu, Q.; Lu, X. L.; Yao, X. L.; Li, S. C.; Li, J.; Su, H.; Pang, J. Y.; Pei, Z. *Mar. Drugs* **2014**, *12*, 3307−3322.
(55) Challal, S.; Buenafe, O. E. M.; Queiroz, E. F.; Maljevic, S.; Marcourt, L.; Bock, M.; Kloeti, W.; Dayrit, F. M.; Harvey, A. L.; Lerche, H. *ACS Chem. Neurosci.* **2014**, *5*, 993−1004.
(56) Khom, S.; Baburin, I.; Timin, E.; Hohaus, A.; Trauner, G.; Kopp, B.; Hering, S. *Neuropharmacology* **2007**, *53*, 178−187.
(57) Maruyama, Y.; Kuribara, H.; Morita, M.; Yuzurihara, M.; Weintraub, S. T. *J. Nat. Prod.* **1998**, *61*, 135−138.
(58) Navarrete, A.; Avula, B.; Choi, Y. W.; Khan, I. A. *J. AOAC Int.* **2006**, *89*, 8−15.
(59) Wang, P. C.; Hu, J. M.; Ran, X. H.; Chen, Z. Q.; Jiang, H. Z.; Liu, Y. Q.; Zhou, J.; Zhao, Y. X. *J. Nat. Prod.* **2009**, *72*, 1682−1685.
(60) Westerfield, M. *The Zebrafish Book. A Guide for the Laboratory Use of Zebrafish (Danio rerio)*; University of Oregon Press: Eugene, OR, 2007.

DOI: 10.1021/acs.jnatprod.7b00081
J. Nat. Prod. 2017, 80, 1548−1557

Supporting Information

Journal of Natural Products

Validation of a larval zebrafish locomotor assay for discovery of $GABA_A$-receptor modulators *via* HPLC-based activity profiling of extracts

Fahimeh Moradi-Afrapoli,[†] Samad Nejad Ebrahimi,[†,‡] Martin Smiesko,[§] and Matthias Hamburger[†*]

[†]Pharmaceutical Biology, Department of Pharmaceutical Sciences, University of Basel, Klingelbergstrasse 50, 4056 Basel, Switzerland

[‡]Department of Phytochemistry, Medicinal Plants and Drugs Research Institute, ShahidBeheshti University, G. C., Evin, Tehran, Iran

[§]Division of Molecular Modeling, Department of Pharmaceutical Sciences, University of Basel, Klingelbergstrasse 50, 4056 Basel, Switzerland

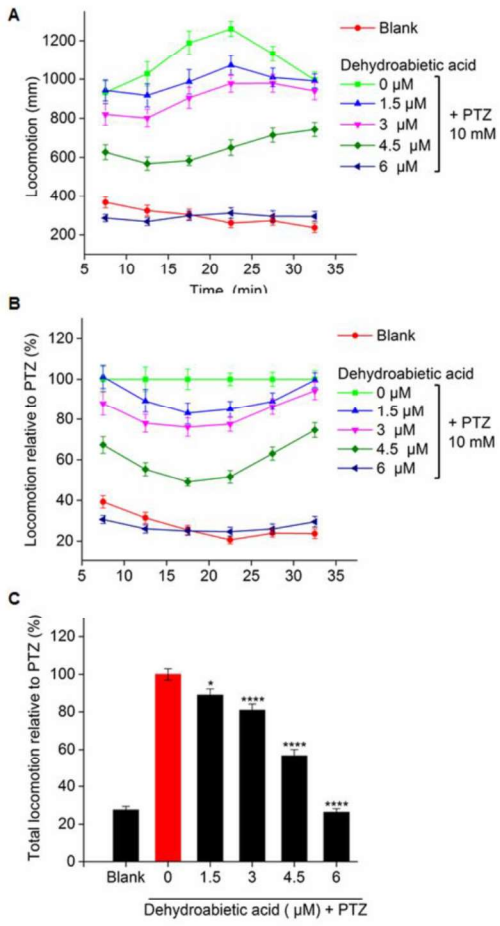

Figure S1. PTZ-induced locomotor activity of zebrafish larvae pretreated for three hours with different concentrations of dehydroabietic acid (**6**). (A) Patterns of movements expressed as average distance travelled over 5-min intervals (mean ± SEM) during the observation period of 30 min. (B) Distance travelled by larvae over 5-min intervals, normalized against the PTZ-only group (0 µM dehydroabietic acid) (mean % ± SEM). (C) Total distance travelled by larvae in 25 min (min 5 to 30) relative to PTZ (mean % ± SEM, n = 32, significant difference from PTZ-only group: * $p < 0.05$, **** $p < 0.0001$, one way ANOVA).

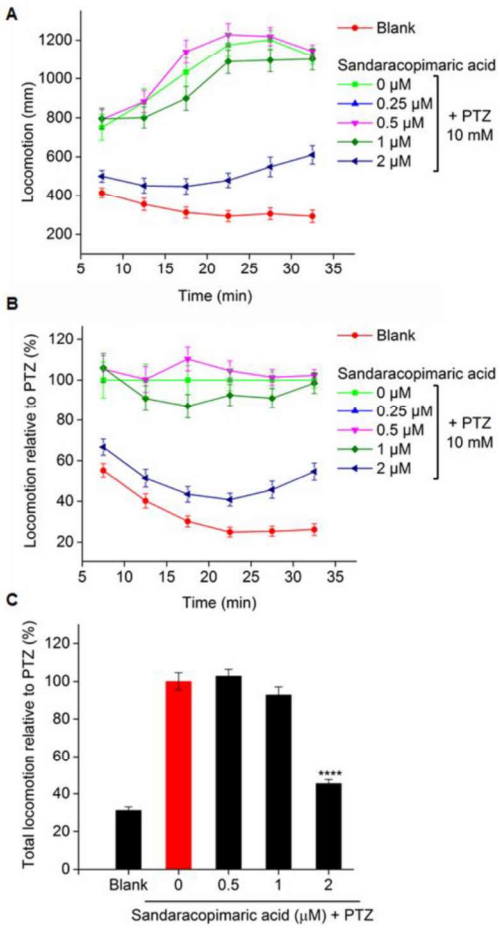

Figure S2. PTZ-induced locomotor activity of zebrafish larvae pretreated for three hours with different concentrations of sandaracopimaric acid (**7**). (A) Patterns of movements expressed as average distance travelled over 5-min intervals (mean ± SEM) during the observation period of 30 min. (B) Distance travelled by larvae over 5-min intervals, normalized against the PTZ-only group (0 µM sandaracopimaric acid) (mean % ± SEM). (C) Total distance travelled by larvae in 25 min (min 5 to 30) relative to PTZ (mean % ± SEM, n = 48, significant difference from PTZ-only group: **** $p < 0.0001$, one way ANOVA).

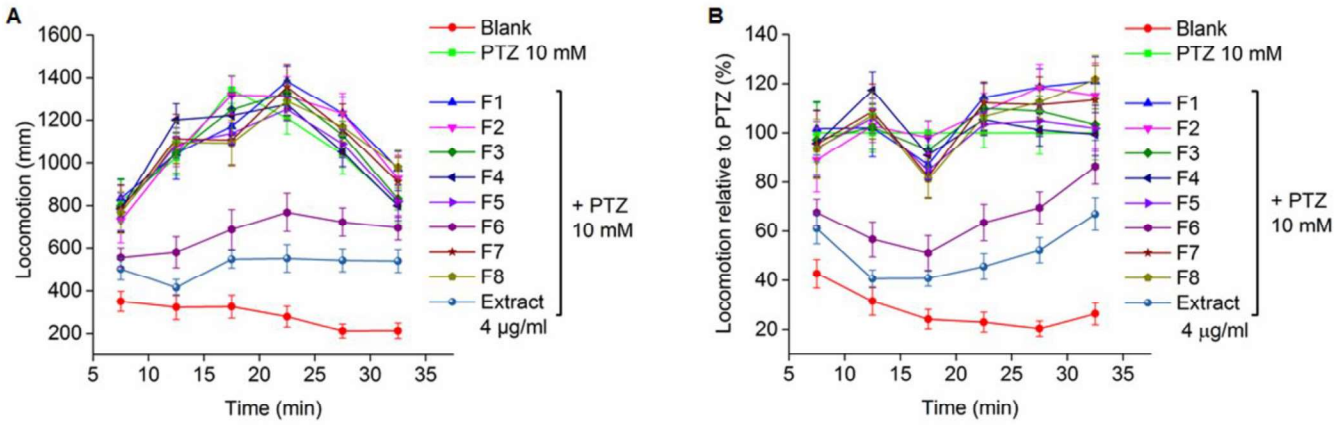

Figure S3. PTZ-induced locomotor activity of zebrafish larvae pretreated for three hours with 3-min microfractions (F1 to F8) from the HPLC separation of an EtOAc extract of *Magnolia officinalis*. (A) Patterns of movements expressed as average distance travelled over 5-min intervals (mean ± SEM) during the observation period of 30 min. (B) Distance travelled by larvae over 5-min intervals, normalized against the PTZ-only group (mean % ± SEM).

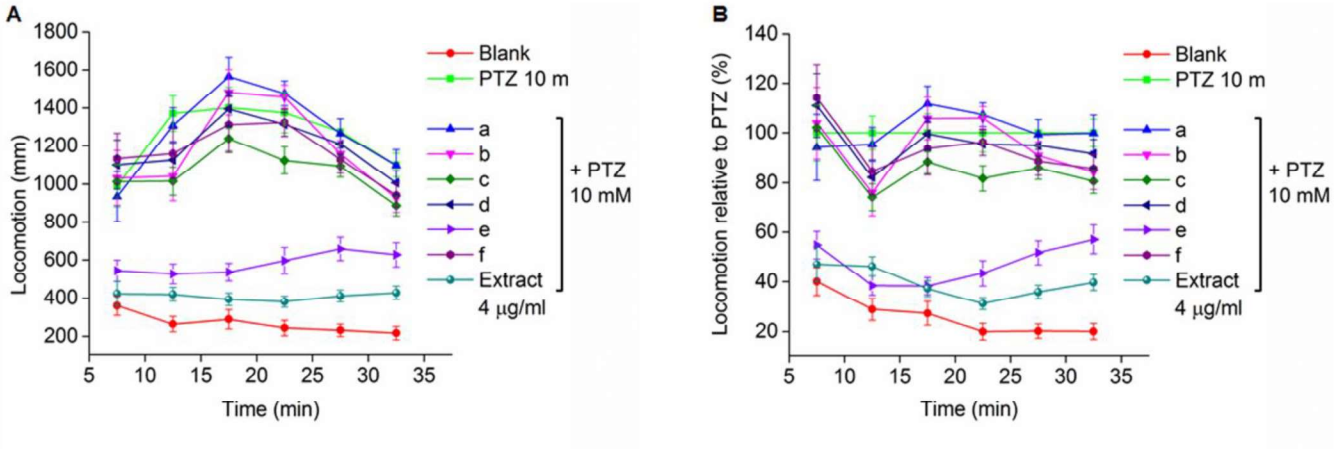

Figure S4. PTZ-induced locomotor activity of zebrafish larvae pretreated for three hours with peak-based microfractions (*a* to *f*) from the HPLC separation of an EtOAc extract of *Magnolia officinalis* (min 15-21). (A) Patterns of movements expressed as average distance travelled over 5-min intervals (mean ± SEM) during the observation period of 30 min. (B) Distance travelled by larvae over 5-min intervals, normalized against the PTZ-only group (mean % ± SEM).

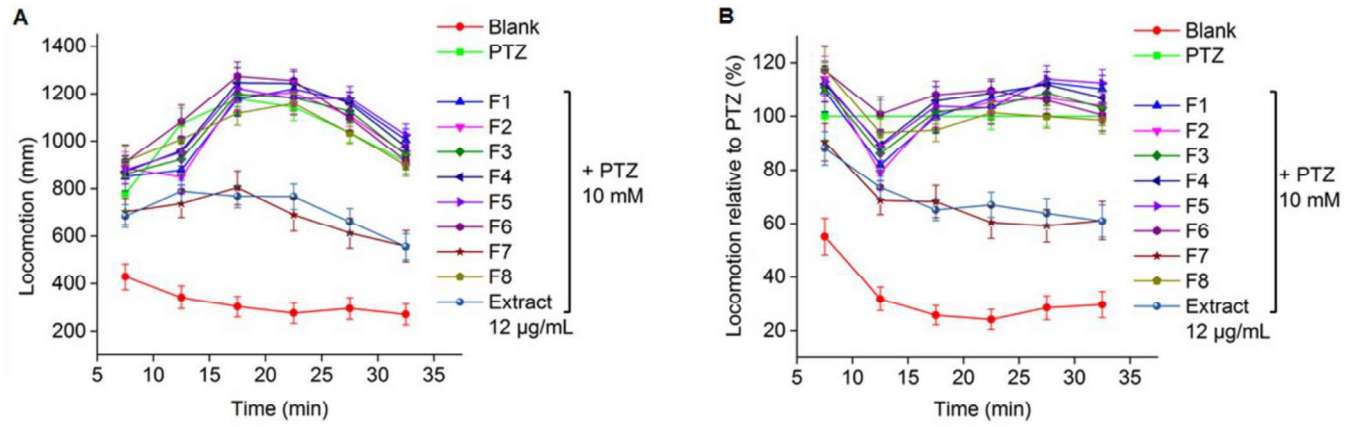

Figure S5. PTZ-induced locomotor activity of zebrafish larvae pretreated for three hours with 3-min microfractions (F1 to F8) from the HPLC separation of an EtOAc extract of *Valeriana officinalis*. (A) Patterns of movements expressed as average distance travelled over 5-min intervals (mean ± SEM) during the observation period of 30 min. (B) Distance travelled by larvae over 5-min intervals, normalized against the PTZ-only group (mean % ± SEM).

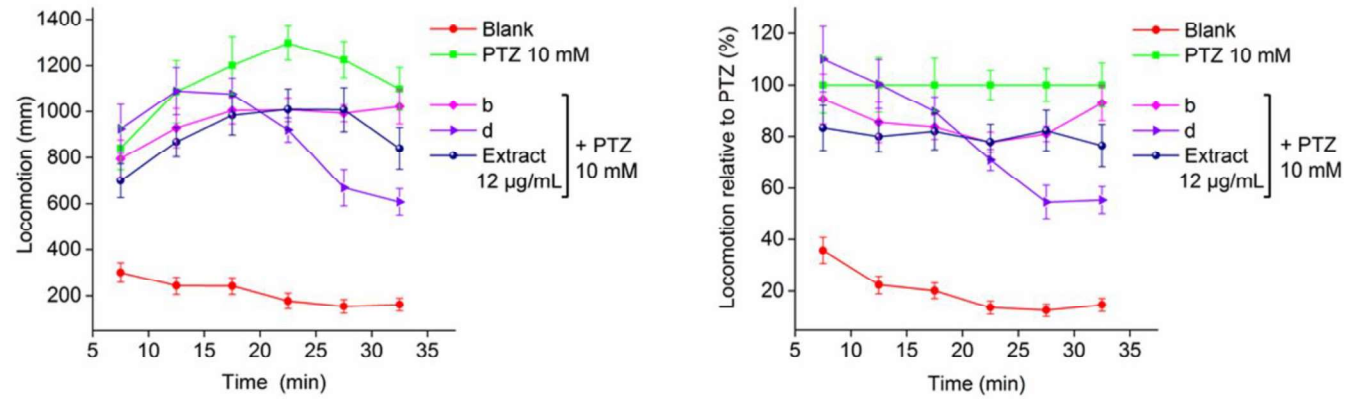

Figure S6. PTZ-induced locomotor activity of zebrafish larvae pretreated for three hours with peak-based microfractions from the HPLC separation of an EtOAc extract of *Valeriana officinalis*. For clarity, only data of fractions *b* and *d*, showed lowering effect on the larval movements, are exhibited along with the crude extract. (A) Patterns of movements expressed as average distance travelled over 5-min intervals (mean ± SEM) during the observation period of 30 min. (B) Distance travelled by larvae over 5-min intervals, normalized against the PTZ-only group (mean % ± SEM).

3.2. HPLC-based activity profiling for $GABA_A$ receptor modulators in *Searsia pyroides* using a larval zebrafish locomotor assay

Fahimeh Moradi-Afrapoli, Hannes van der Merwe, Maria De Mieri, Anke Wilhelm, Marco Stadler, Pieter. C. Zietsman, Steffen Hering, Kenneth Swart, Matthias Hamburger

Planta Medica, 83 (2017) 1–7, **DOI:** 10.1055/s-0043-11068

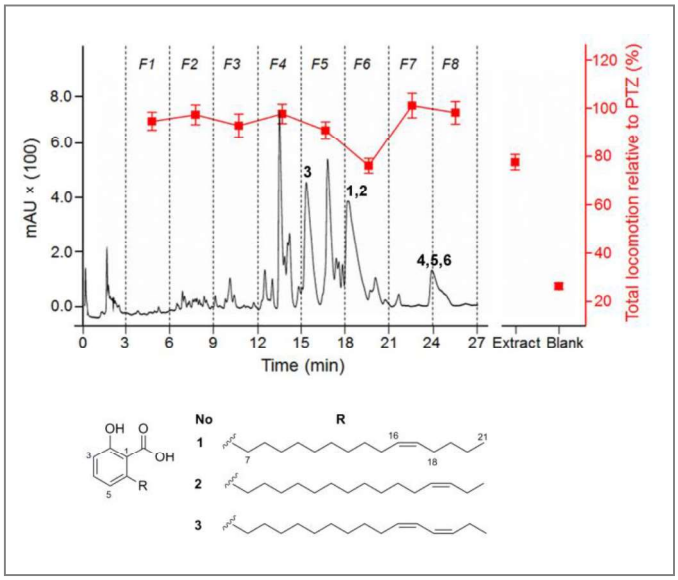

Searsia pyroides (Burch.) Moffett (syn. *Rhus pyroides*, Anacardiaceae) is a South African medicinal plant traditionally used for treatment of CNS disorders.

In the present study we performed a screening of leaf extracts from *S. pyroides* for GABAergic activity with the *Xenopus* oocyte model expressing $GABA_A$ receptors of $\alpha_1\beta_2\gamma_2$s subunits and with the zebrafish larval locomotor assay. The corresponding active constituents were subsequently isolated with the HPLC-based activity profiling. With the aid of NMR and high resolution mass spectrometry, the structures were identified as analogues of anacardic acid. Compounds **1-3** exhibited concentration dependent decrease of PTZ-provoked locomotions in the zebrafish larvae model and enhancement of GABA-induced chloride currents (I_{GABA}) in the *Xenopus* oocytes assay.

My contributions to this publication: Activity assessments with the zebrafish larvae locomotor assay, HPLC-based activity profiling of the active extract, purification and identification of the phytochemicals, writing the manuscript draft, and preparation of figures and tables.

Fahimeh Moradiafrapoli

Thieme

HPLC-Based Activity Profiling for $GABA_A$ Receptor Modulators in *Searsia pyroides* Using a Larval Zebrafish Locomotor Assay*

Authors
Fahimeh Moradi-Afrapoli[1], Hannes van der Merwe[2], Maria De Mieri[1], Anke Wilhelm[2], Marco Stadler[3], Pieter C. Zietsman[4], Steffen Hering[3], Kenneth Swart[2,5], Matthias Hamburger[1]

Affiliations
1 Pharmaceutical Biology, Department of Pharmaceutical Sciences, University of Basel, Basel, Switzerland
2 Faculty of Natural and Agricultural Sciences, University of the Free State, Bloemfontein, Republic of South Africa
3 Institute of Pharmacology and Toxicology, Pharmaziezentrum, University of Vienna, Vienna, Austria
4 National Museum, Bloemfontein, Republic of South Africa
5 FARMOVS-PAREXEL, University of the Free State, Bloemfontein, South Africa

Key words
Searsia pyroides, Anacardiaceae, $GABA_A$ receptor, zebrafish larvae, *Xenopus* oocytes, pentylenetetrazole, HPLC-based activity profiling

received February 20, 2017
revised May 4, 2017
accepted May 4, 2017

Bibliography
DOI https://doi.org/10.1055/s-0043-110768
Published online May 16, 2017 | Planta Med 2017; 83: 1169–1175 | ISSN 0032-0943

Correspondence
Prof. Matthias Hamburger
Pharmaceutical Biology, Department of Pharmaceutical Sciences, University of Basel
Klingelbergstrasse 50, 4056 Basel, Switzerland
Phone: +41 61 267 14 25, Fax: +41 61 267 14 74
matthias.hamburger@unibas.ch

Supporting information available online at http://www.thieme-connect.de/products

ABSTRACT

A dichloromethane extract from leaves of *Searsia pyroides* potentiated gamma aminobutyric acid-induced chloride currents by 171.8 ± 54% when tested at 100 µg/mL in *Xenopus* oocytes transiently expressing gamma aminobutyric acid type A receptors composed of $\alpha_1\beta_2\gamma_2$s subunits. In zebrafish larvae, the extract significantly lowered pentylenetetrazol-provoked locomotion when tested at 4 µg/mL. Active compounds of the extract were tracked with the aid of HPLC-based activity profiling utilizing a previously validated zebrafish larval locomotor activity assay. From two active HPLC fractions, compounds **1–3** were isolated. Structurally related compounds **4–6** were purified from a later eluting inactive HPLC fraction. With the aid of ^{1}H and ^{13}C NMR and high-resolution mass spectrometry, compounds **1–6** were identified as analogues of anacardic acid. Compounds **1–3** led to a concentration-dependent decrease of pentylenetetrazol-provoked locomotion in the zebrafish larvae model, while **4–6** were inactive. Compounds **1–3** enhanced gamma aminobutyric acid-induced chloride currents in *Xenopus* oocytes in a concentration-dependent manner, while **4–6** only showed marginal enhancements of gamma aminobutyric acid-induced chloride currents. Compounds **2**, **3**, and **5** have not been reported previously.

ABBREVIATIONS

6/7dpf	6/7-day post-fertilization
$GABA_A$	gamma aminobutyric acid type A
MTC	maximum tolerable concentration
PTZ	pentylenetetrazole

Introduction

$GABA_A$ receptors are the major inhibitory neurotransmitter receptors in the central nervous system. They are heteropentamers forming a central pore permeable for chloride ions. When acti-

* Dedicated to Professor Dr. Max Wichtl in recognition of his outstanding contribution to pharmacognosy research.

vated, a rapid increase of chloride ion flux into the cells occurs, leading to an inhibitory hyperpolarizing response of neurons [1, 2]. The most abundant subtype of $GABA_A$ receptors in the mammalian brain consists of two α1, two β2, and one γ2 subunit(s) [1, 3]. Benzodiazepines and several other clinically important drugs used to treat anxiety, insomnia, and epilepsy act via an allosteric modulation of postsynaptic $GABA_A$ receptors [4, 5]. However, the drugs used currently are associated with side effects that are mainly due to a lack of receptor subtype selectivity. Thus, the need for discovery of novel types of $GABA_A$ receptor modulators is apparent. In recent years, a broad range of GABAergic natural products with scaffolds new to the target has been reported. With the aid of HPLC-based activity profiling [6, 7] utilizing a two-microelectrode voltage clamp assay with *Xenopus laevis* oocytes transiently expressing $GABA_A$ receptors, we previously identified a series of structurally differing allosteric $GABA_A$ receptor agonists from our in-house extract library [8–22]. A notable finding was that piperine interacted with a benzodiazepine-independent allosteric binding site of the $GABA_A$ receptor and showed anxiolytic-like effects in mice [21].

In HPLC-based activity profiling, the turnaround time of bioassay data is the rate-limiting step in the identification of active moleculeS. To accelerate the discovery of new $GABA_A$ receptor modulators, we recently developed and validated an HPLC-based activity profiling approach using a locomotor activity model with zebrafish (*Danio rerio*) larvae [23]. In this assay, larval convulsions are provoked with the $GABA_A$ receptor antagonist PTZ, and GABAergic activity of the extracts and HPLC microfractions can be tracked via their lowering of PTZ-provoked larval locomotion [24, 25].

Searsia pyroides (Burch.) Moffett (syn. *Rhus pyroides* Burch., Anacardiaceae) is used in South African traditional medicine for treatment of CNS disorders, such as delirium, epilepsy, and pediatric seizures, whereby infusions prepared from the roots are most widely used [26–29]. In a previous study, an ethanolic extract from leaves of *S. pyroides* was found to interact *in vitro* with the benzodiazepine binding site of $GABA_A$ receptors [30], and antagonistic activity at N-methyl-D-aspartic acid (NMDA) receptors was also reported [26]. However, these studies remained at the stage of extract screening, since the compounds responsible for the pharmacological activity were not identified. We here report on the initial screening of *S. pyroides* leaf extracts for GABAergic activity in a functional screen in *Xenopus* oocytes, and on the subsequent identification of active compounds by HPLC-based activity profiling utilizing a zebrafish larval locomotor assay. Finally, we confirmed the activity of pure compounds in both zebrafish larval and *Xenopus* assays.

Results and Discussion

In *Xenopus* oocytes transiently expressing $GABA_A$ receptors composed of $\alpha_1\beta_2\gamma_2$s subunits, a dichloromethane extract from leaves of *S. pyroides* enhanced the GABA-induced chloride ion current (I_{GABA}) by 171.8 ± 54 % when tested at a concentration of 100 µg/mL. The extract was subsequently tested in the zebrafish larvae locomotor activity assay. First, toxicity of the extract was assessed prior to the activity screening in order to determine the MTC, which was 4 µg/mL. The MTC was then used as the highest test concentration, and lowering of PTZ-induced larval locomotion by the extract was determined at 1, 2, and 4 µg/mL. Total distance (mm) travelled by the larvae within 25 min (min 5 to 30 after exposure to PTZ) was recorded and compared with that of the PTZ only group (▶ **Fig. 1 A**). The larvae pretreated with 4 µg/mL extract showed significantly lower locomotion. Patterns of larval movements were visualized by plotting the total distance travelled over 5-min intervals vs. time (▶ **Fig. 1 B**). The extract at the highest test concentration (4 µg/mL) lowered PTZ-provoked larval locomotion over the entire tracking period and increased the latency of seizures to progress to the later stages [25]. Diazepam (4 µM) was used as a positive control.

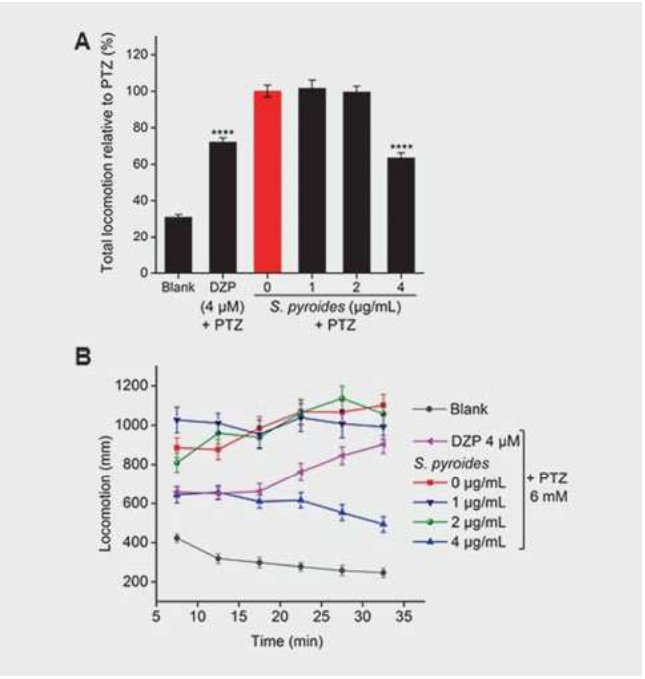

▶ **Fig. 1** PTZ-induced (6 mM) locomotor activity of zebrafish larvae pretreated for 3 h with a dichloromethane extract from *S. pyroides* leaves at concentrations of 0, 1, 2, and 4 µg/mL. **A** Locomotion (total distance travelled) of larvae in 25 min (min 5 to 30) relative to PTZ (mean % ± SEM, n = 32, significant difference from PTZ only group: **** $p < 0.0001$, Kruskal-Wallis test followed by the Mann-Whitney test). Diazepam (DZP, 4 µM) was used as a positive control. **B** Locomotion expressed as average distance travelled over 5-min intervals (mean ± SEM) during the observation period of 30 min. Tracking of larval movements started 5 min after exposure to PTZ.

As a next step, HPLC-based activity profiling of the dichloromethane extract was performed with the aid of a previously validated protocol [23]. The HPLC-UV chromatogram (254 nm) and the corresponding activity profile are shown in ▶ **Fig. 2**. A decrease of larval locomotion was found for HPLC fractions 5 (min 15–18) and 6 (min 18–21). Compounds in the active time windows were obtained by a targeted isolation combining vacuum liquid chromatography on a C18 cartridge with a final purification by semipreparative HPLC.

Compounds **1** and **2** were isolated from the active fraction 6, while **3** was obtained from fraction 5 as the major constituent (60% by NMR) of an inseparable mixture of positional isomers. Structurally related **4–6** were purified from a later eluting inactive HPLC fraction 8. By means of 1D and 2D NMR spectra and HRMS data, the structures were identified as anacardic acid analogues (▶ **Fig. 3**). For NMR and MS data of **1–6**, see **Tables S1–S3**, Supporting Information.

Compound **1** had a molecular formula $C_{22}H_{34}O_3$, as calculated from the HR ESIMS spectrum (*m/z* 345.25 measured for $[M - H]^-$, calcd. 345.24 for $C_{22}H_{34}O_3$). The ^{1}H NMR spectrum of **1** showed resonances at 6.60 ppm (*d, J* = 7.5 Hz, H-3), 7.20 ppm (*dd, J* = 7.5, 7.5 Hz, H-4), and 6.63 ppm (*d, J* = 7.5 Hz, H-5), which were indicative of a 1,2,6-trisubstituted aromatic ring. The nature and location of substituents on the aromatic ring were deduced from HMBC correlations of the aromatic spin system to quaternary carbons at 160.3 ppm (C-2, oxygenated), 114.6 ppm (C-1, bearing a carboxylic acid), and 147.1 ppm (C-6, substituted by an alkyl residue). The compound was thus a salicylic acid derivative bearing an alkyl chain at C-6. The low amount of compound precluded measurement of a ^{13}C NMR spectrum, and in the HMBC spectrum, no four-bond heteronuclear correlation to H-3, H-5, or H_2-7 could be detected, even in an experiment optimized for J_{CH} of 4 Hz. However, the presence of a salicylic acid moiety was supported by a broad signal at 8.18 ppm in the ^{1}H NMR spectrum, which was indicative of a proton involved in hydrogen bonding. The side chain at C-6 was identified as follows: A benzylic methylene was observed at 3 ppm (*m*, H-7), along with resonances of a chain of methylene groups at around 1.3 ppm (broad, H-9 to H-14) and 1.27 ppm (m, H-19 and H-20), and a terminal methyl group at 0.84 ppm (*t, J* = 7.5 Hz, H-21). Allylic protons at 1.96 and 1.97 ppm (m, H-15, H-18) and the corresponding two vinylic protons were observed at 5.29 ppm (m, H-16, H-17). The location of the double bond at C-16/C-17 of the side chain was established by COSY and HMBC correlations observed in the C-16/C-21 fragment. The *Z* configuration of the olefin was inferred from the chemical shift of allylic and homoallylic protons [31], which matched well with those predicted by ACD Labs software [32] for the *cis* isomer. ^{13}C-NMR shifts predicted for the C-16/C-21 fragment corroborated the assignment (**Figs. S1** and **S2**, Supporting Information). Finally, the length of the side chain was established by the molecular formula obtained from the HR ESIMS spectrum. Compound **1** was thus identified as (*Z*)-2-hydroxy-6-(pentadec-10-en-1-yl)-benzoic acid, a compound that had been previously reported from *Pelargonium* × *hortorum* L. H. Bailey [33].

Compound **2** had the same molecular formula as **1** and was a positional isomer of the latter. With the aid of COSY and HMBC correlations in the C-16/C-21 fragment, the position of the double bond in the side chain was located at C-18/C-19, while its *Z* stereochemistry was established as described for **1**. The amount of **2** was sufficient to measure a ^{13}C-NMR spectrum, and the presence of a carboxylic acid was supported by the signal of a quaternary carbon at 171.1 ppm. Compound **2** was thus identified as (*Z*)-2-hydroxy-6-(pentadec-12-en-1-yl)-benzoic acid.

Compound **3** had a molecular formula of $C_{22}H_{32}O_3$. In contrast to **1** and **2**, the NMR data of **3** revealed the presence of two pairs of olefinic protons at 5.42 ppm (*m*, H-16 and H-18) and 6.20 ppm (*m*, H-17 and H-19), and two allylic methylene groups at 2.10 ppm (*m*, H_2-15) and 2.12 ppm (*q, J* = 7.5 Hz, H_2-20). The chemical shifts were diagnostic of two conjugated double bonds with a *Z,Z* configuration [34]. The location of the conjugated diene was established by COSY and HMBC correlations in the C-14/C-21 fragment, and unequivocally confirmed by the key HMBC correlation from the terminal methyl group to the olefinic proton at C-19. Hence, compound **3** was (*Z,Z*)-2-hydroxy-6-(pentadec-10,12-dien-1-yl)-benzoic acid.

The structures of **4–6** were established in the same way. Compound **4** was identified as 6-pentadecylsalicylic acid, a compound that has been previously reported as a minor component in crude cashew nut shell liquid [35]. According to their molecular formula derived from the HR ESIMS spectrum (**Table S3**, Supporting Information), compounds **5** and **6** both contained heptadecenyl side chains. Compound **5** showed NMR data that were virtually superimposable to those of **2**. Considering the molecular formula of $C_{24}H_{38}O_3$ derived from the HR ESIMS spectrum, compound **5**

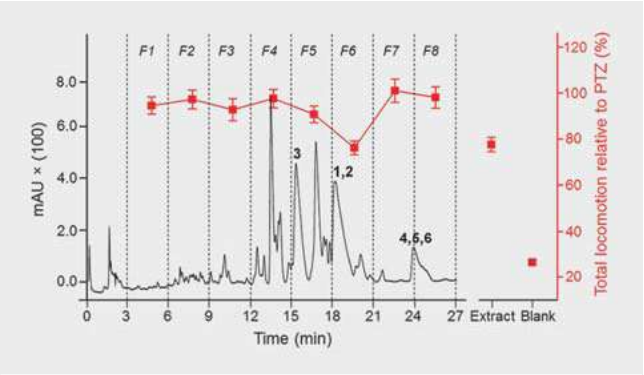

▶ **Fig. 2** HPLC-based activity profiling of the dichloromethane extract. Chromatogram (254 nm) for a separation of 120 µg extract on an analytical HPLC column. Eight microfractions (*F1–F8*) were collected in 3-min time windows (indicated with dashed lines), and lowering of PTZ-induced locomotor activity by microfractions is shown above (expressed as % activity relative to the PTZ only group, n = 32). Locomotor activities with extract and blank are shown to the right of the chromatogram.

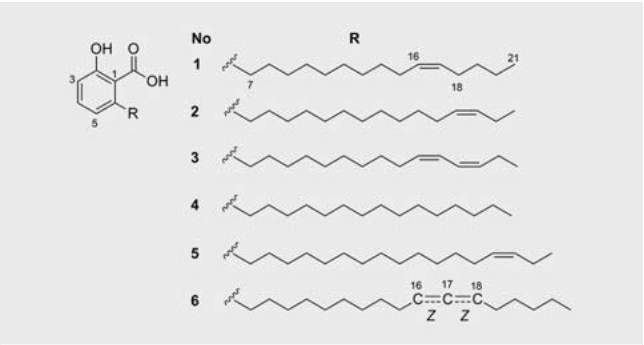

▶ **Fig. 3** Anacardic acid derivatives identified in the dichloromethane extract. In **6**, the location of the double bond (*cis*-D16 or *cis*-D17) could not be established unambiguously.

was thus (*Z*)-2-hydroxy-6-(heptadec-14-en-1-yl)-benzoic acid. In compound **6**, the *Z*-configured double bond had to be located at either C-16/C-17 or C-17/C-18, but could not be unambiguously assigned due to its distance from the terminal methyl group.

Compounds **1–6** were tested in the zebrafish larvae locomotor activity model at 0 to 4 µM. The corresponding concentration-response data are shown in ▶ **Fig. 4**. Pretreatment of larvae with compounds **1–3** led to a concentration-dependent decrease of PTZ-provoked locomotion. In contrast, compounds **4, 5**, and **6** did not show activity at the same test concentrations, while the positive control diazepam (4 µM) reduced the larval locomotion to 72.0 ± 2.4%. To confirm that the lowering of locomotor activity in the zebrafish larval assay was due to an interaction with $GABA_A$ receptors, compounds **1–6** were tested in the *Xenopus* oocyte assay at concentrations of 10 and 100 µM (▶ **Fig. 5A**). The GABA-induced chloride ion current (I_{GABA}) was increased by **1** (80.2 ± 9.8%), **2** (126.5 ± 23.8%), and **3** (307.6 ± 17.5%) when tested at 100 µM, while only a marginal enhancement was seen with **4–6**. Active compounds **1–3** were then evaluated at five test concentrations ranging from 3 to 300 µM (▶ **Fig. 5B**). The positive control diazepam (1 µM) enhanced I_{GABA} by 231.3 ± 22.6%.

The $GABA_A$ receptor modulatory activity of a dichloromethane extract from the traditional South African medicinal plant *S. pyroides* could be linked to anacardic acid derivatives. Given that only some of the isolated compounds showed activity indicated that certain structural features, such as length of the side chain and the presence as well as position of double bonds, were relevant for activity. Compounds **2, 3**, and **5** are reported here for the first time, while compounds **1, 4**, and **6** have been previously identified in *Gingko biloba* L. [36], *Schoepfia californica* Brandegee [37], *Ozoroa mucronata* (Bernh. Ex Krauss) R. Fern. & A. Fern. [38], and some *Knema* species [39–41]. However, this is the first report of anacardic acid analogues from *Searsia* species.

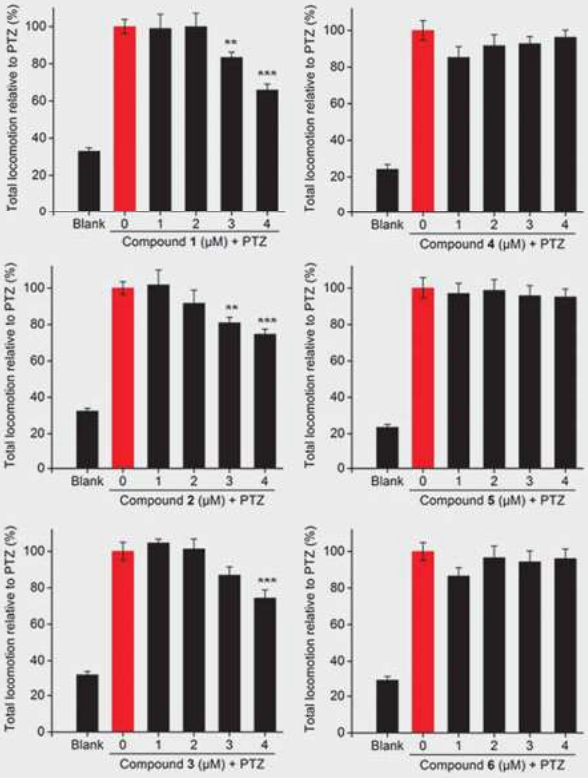

▶ **Fig. 4** PTZ-induced locomotor activity of zebrafish larvae pretreated for 3 h with anacardic acid derivatives **1–6** at concentrations of 0, 1, 2, and 4 µg/mL. Locomotion of larvae in 25 min (min 5 to 30) relative to PTZ (6 mM) is displayed as mean % ± SEM (n = 32, significant difference from PTZ only group: * $p < 0.05$, **** $p < 0.0001$, Kruskal-Wallis followed by the Mann-Whitney test). The positive control diazepam (4 µM) lowered the total distance travelled to 72.0 ± 2.4%.

Material and Methods

General experimental procedures

HPLC-PDA-MS analyses were performed with an HPLC-MS/MS system consisting of a degasser, quaternary pump (LC-20AD), column oven (CTO-20AC), PDA detector (SPD-M20A), and an LCMS-8030 triple quadrupole mass spectrometer (all Shimadzu) connected to an ELSD 3300 detector (Alltech). Data acquisition and processing were performed with LabSolutions software (Shimadzu). Evaporation of microfractions was done with a Genevac EZ-2 plus vacuum centrifuge (Avantec). Semipreparative HPLC was carried out with an Agilent 1100 series instrument equipped with a degasser, binary high-pressure mixing pump, column oven, and PDA detector. 1D and 2D NMR spectra were recorded on an AVANCE III 500 MHz spectrometer equipped with a 1-mm TXI microprobe (Bruker BioSpin). HRESI-TOF-MS spectra in positive and negative ion modes (scan range of *m/z* 200–1500) were recorded on a microTOF ESI-MS system (Bruker). The movement of zebrafish larvae was tracked with a DanioVision observation chamber equipped with an IR sensitive camera and a temperature controller unit (Noldus Information Technology). The locomotor activity was quantified by EthoVision XT11 software (Noldus Information Technology).

PTZ (purity ≥ 98%) was purchased from Sigma-Aldrich. Diazepam (purity ≥ 98%) was obtained from Lipodmed. Solvents used for extraction were of technical grade (Romil Pure Chemistry) and were purified by distillation. HPLC grade acetonitrile (MeCN) was from Scharlau Chemie, and HPLC grade H_2O was obtained from an EASY-pure II water purification system (Barnstead). HPLC solvents contained 0.1% HCOOH (Scharlau) and 1% THF (tetrahydrofuran, Scharlau). DMSO (Scharlau) was used for dissolving the samples. DMSO-d_6 (100 atom % D) was from Armar Chemicals.

Plant material

Leaves of *S. pyroides* were collected in December 2011 at Tussendie-riviere Nature Reserve, Free State, South Africa. The plant was identified by Dr. P. C. Zietsman, and a voucher specimen (PC & LE Zietsman 5147) has been deposited at the Herbarium of the National Museum, Bloemfontein (NMB), South Africa.

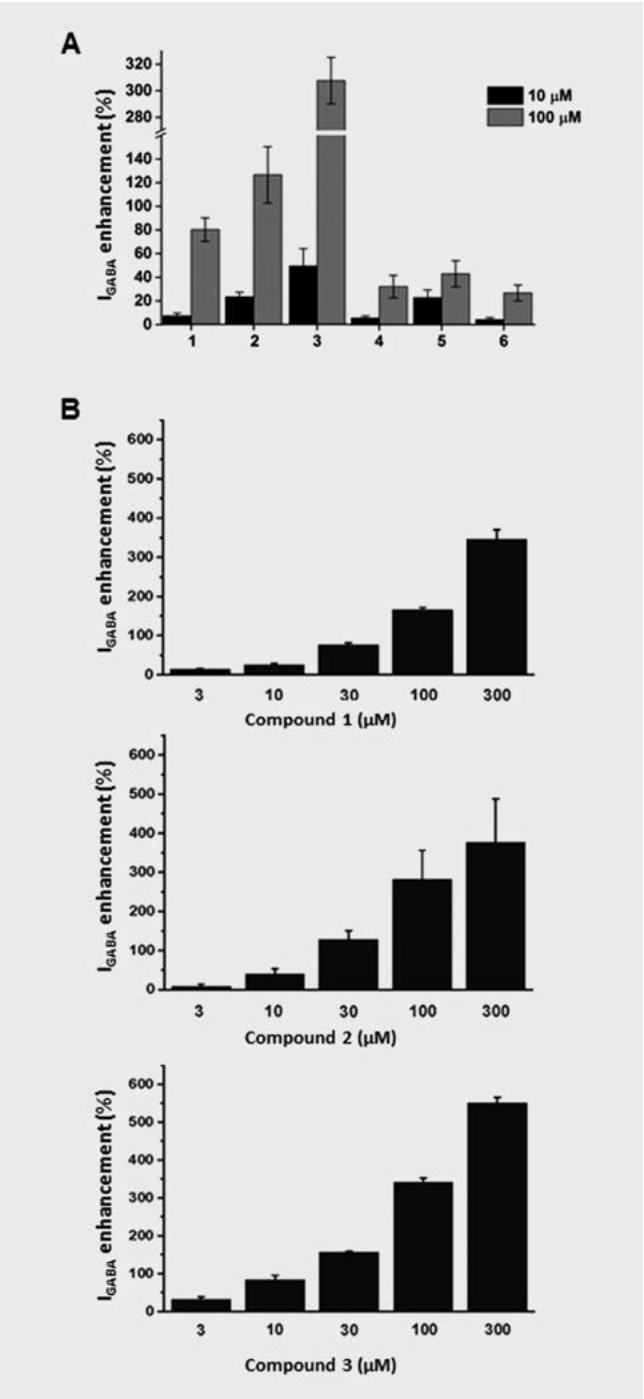

▶ **Fig. 5** Modulation of I_{GABA} in two-microelectrode voltage clamp assay with *X. laevis* oocytes expressing $GABA_A$ receptors of $\alpha_1\beta_2\gamma_{2S}$ subunit composition. **A** Preliminary activity evaluations performed at 10 and 100 µM. **B** Concentration-response curves for active compounds (**1**–**3**) between 3 and 300 µM, displayed as the mean ± SEM of at least two oocytes from two different batches. The positive control diazepam (1 µM) increased I_{GABA} by 231.3 ± 22.6% (n = 3).

Microfractionation for activity profiling

HPLC time-based activity profiling of the dichloromethane extract was performed with a zebrafish larvae locomotor activity assay as previously described [6, 7, 23], with minor modifications. The extract (10 mg/mL in DMSO) was submitted to analytical HPLC (SunFire® C18 column, 3.5 µm, 3 × 150 mm) in two portions of 120 µg (12 µL). The mobile phase was H_2O (A) and MeCN (B), both containing 0.1% formic acid and 1% THF, and the following gradient was used: 50% → 90% B (0–5 min), 90% → 100% B (5–20 min), 100% B (20–30 min). The flow rate was 0.4 mL/min. Three-min fractions (between min 3 and 27) were collected into a 96-well deep well plate. After drying of the plate in a vacuum centrifuge, microfractions in the wells were dissolved with 15 µL of DMSO, and the plate was shaken at 1400 rpm for 30 min for complete dissolution (stock solutions). Corresponding microfractions from the two separations were combined. Afterwards, 18 µL of each stock solution were added separately to E3 medium up to the final volume of 1800 µL (working solutions). Aliquots of 50 µL of working solutions were added to each well of a 96-well microtiter plate containing one zebrafish larva and 200 µL of E3 medium. Sixteen larvae were used per each microfraction, and the activity was assessed in duplicate experiments (n = 32).

Extraction and preparative isolation

Dried ground plant material (180 g) was exhaustively extracted with dichloromethane under stirring at room temperature. The extract was filtered and dried under reduced pressure to afford 220 mg of solid residue. The extract (220 mg) was dissolved in chloroform, adsorbed to C18 silica gel 100 (Fluka), and dried. The adsorbed extract was loaded onto an SPE cartridge (Chromabond C18 ec, 10 g) and submitted to vacuum liquid chromatography using a Visiprep™ SPE vacuum manifold (Sigma-Aldrich). The cartridge was eluted with a step gradient of H_2O/MeCN/EtOAc: 80:20:0 (150 mL), 50:50:0 (150 mL), 40:60:0 (150 mL), 30:70:0 (200 mL), 20:80:0 (150 mL), 0:100:0 (150 mL), 0:50:50 (150 mL), and 0:0:100 (150 mL) at a flow rate of 5 mL/min. Fractions corresponding to each gradient step were collected separately (F_1–F_8) and dried at reduced pressure and by freeze-drying. Fractions were monitored by HPLC-PDA-MS analysis on a SunFire C18 column (3.5 µm, 3 × 150 mm; Waters) to track peaks previously seen in the active time windows of the activity profile. A gradient of H_2O (solvent A) and MeCN (solvent B), both containing 0.1% HCOOH and 1% THF, was used at a flow rate of 0.4 mL/min: 50% → 90% B (0–5 min), 90% → 100% B (5–20 min), and 100% B (20–30 min). F_4 (32.5 mg) was dissolved in DMSO at 20 mg/mL and submitted in aliquots of 100 µL to semipreparative RP-HPLC (SunFire C18 column, 5 µm, 10 × 150 mm). Elution was with 20% A and 80% B (both containing 0.1% formic acid and 8% THF). A flow rate of 4 mL/min and UV detection at 254 nm were used. Compounds **1** (t_R = 47 min, 4 mg), **2** (t_R = 48 min, 6 mg), and **3** (t_R = 30 min, 6 mg) were obtained. A portion of F_5 (12 mg) was dissolved in DMSO (20 mg/mL) and separated in aliquots of 100 µL by semipreparative RP-HPLC (SunFire C18 column, 5 µm, 10 × 150 mm). A step gradient of A and B (both containing 0.1% formic acid and 8% THF): 80% B (0–30 min) → 85% B (30–60 min) → 100% B (60–70 min) was used at a flow rate of 4 mL/min, and UV detection was at 250 nm. Compounds **4** (t_R = 56 min,

510 µg), **5** (t_R = 57 min, 800 µg), and **6** (t_R = 58 min, 550 µg) were obtained.

Two-microelectrode voltage clamp assay with *Xenopus laevis* oocytes

Recombinant $GABA_A$ receptors ($\alpha_1\beta_2\gamma_2$s) were expressed in *X. laevis* oocytes by cRNA injection, as previously described [10]. Two-microelectrode voltage clamp measurements were performed between days 1 and 5 after cRNA injection, using a TURBO TEC 03X amplifier (npi Electronic GmbH) at a holding potential of − 70 mV and pCLAMP 10 data acquisition software (Molecular Devices). Currents were low-pass filtered at 1 kHz and sampled at 3 kHz. The bath solution contained 90 mM NaCl, 1 mM KCl, 1 mM $MgCl_2$, 1 mM $CaCl_2$, and 5 mM HEPES (pH 7.4). Electrode filling solution contained 2 M KCl. Test solutions (100 µL) were applied to the oocytes at a speed of 300 µL/s by means of the ScreeningTool (npi electronic) automated fast perfusion system. GABA $EC_{4–6}$ was determined through a concentration-response experiment with 0.1 to 1 mM GABA solutions. Stock solutions of tested extracts (10 mg/mL) and pure compounds (100 mM) in DMSO were diluted with a bath solution containing GABA $EC_{4–6}$ to obtain appropriate working solutions according to a validated protocol. Enhancement of the I_{GABA} was defined as $(I_{(GABA + Comp)}/I_{GABA}) - 1$, where $I_{(GABA + Comp)}$ is the current response in the presence of a given compound, and I_{GABA} is the control of the GABA-induced chloride current. Data were analyzed using Origin 7.0 SR0 software (OriginLab Corporation) and are given as the mean ± SE of at least two oocytes from ≥ 2 batches. Diazepam (purity ≥ 98%; Sigma) was used as a positive control at 1 µM.

Zebrafish larvae locomotor activity model

Zebrafish larvae experiments were approved by the Kantonales Veterinaeramt Basel-Stadt (licence number 1995 continuation; approval date 03.02.2015) and conducted in accordance with EU directive 2011/63/EU. Wild-type zebrafish of the ABC × TU strain were kept under standard conditions [42]. Fertilized eggs were collected via natural spawning and incubated at 28.5 °C in E3 medium containing 5 mM NaCl, 0.17 mM KCl, 0.33 mM CaCl, and 0.33 mM $MgSO_4$ in water (0.5 mL methylene blue 0.05% w/v was added to 1 liter medium as a disinfectant, and pH was corrected to 7.4 by K_2CO_3 0.5 M). Stock solutions of the extract and pure compounds (10 and 5 mg/mL, respectively, in DMSO) were diluted with E3 medium to obtain the appropriate working solutions. Toxicity assessments were performed for each test sample prior to the activity screening. Larvae (6dpf) were placed in 96-well plates, and aliquots of 50 µL working solutions were spiked into each well to afford a final volume of 250 µL. Larvae (n = 12) were incubated with the extract at 50, 25, 12.5, and 6.25 µg/mL, and with pure compounds at 25, 12.5, 6.25, and 3.12 µM. Locomotor impairments, including loss of larval response after a light touch of the tail, loss of posture, body deformation, and death were monitored and compared with the blank (same number of untreated larvae) after 3, 6, and 24 h. After the first toxicity assessment, intermediate concentrations were tested to accurately define the MTC at which not more than 2 of 12 larvae were impaired.

For activity screening, MTC was considered as the highest test concentration. The lower concentrations were obtained by serial dilutions. Larvae (7dpf, n = 16) were incubated for 3 h at 28.5 °C with the test solutions. Then, 20 µL of PTZ solution were added to each well to reach a final concentration of 6 mM. Microplates were placed in the movement-tracking chamber. Tracking of the larval movements started after 5 min, and continued until 30 min. Total distance travelled by the larvae within 25 min (between min 5 and 30) was considered as the total locomotor activity. Patterns of larval movements were obtained by plotting movement vs. time, whereby total distance traveled was calculated over 5-min intervals. A PTZ only group (16 larvae treated only with PTZ) and a blank group (16 larvae maintained only in the medium) were placed in each microplate. Diazepam (4 µM) was used as the positive control. All tests were repeated in two independent experiments (n = 32). Statistical analyses were performed with IBM SPSS Statistics version 20 using the Kruskal-Wallis test followed by the Mann-Whitney test to determine significant differences between treatment groups and the PTZ only group.

Supporting information

^{1}H-NMR data, ^{13}C-NMR data (extracted from HSQC-DEPT and HMBC spectra for compounds **1** and **3–6**), HR ESIMS data of **1–6**, and ^{13}C and ^{1}H-NMR shifts for *E* and *Z* isomers of compound **1** (DMSO-d_6) calculated with ACDLabs software are available as Supporting Information.

Acknowledgements

Access to the zebrafish facility of the Biozentrum (H. G. Belting and M. Affolter) is gratefully acknowledged. Financial support to S. K. was provided by the National Research Foundation (NRF) from South Africa, and to S. H. by the Austrian Science Fund (FWF). M. S. is a fellow of the FWF-funded doctoral program "Molecular Drug Targets" W 1232.

Conflict of Interest

None.

References

[1] Uusi-Oukari M, Korpi ER. Regulation of GABAA receptor subunit expression by pharmacological agents. Pharmacol Rev 2010; 62: 97–135

[2] Kash TL, Jenkins A, Kelley JC, Trudell JR, Harrison NL. Coupling of agonist binding to channel gating in the GABAA receptor. Nature 2003; 421: 272–275

[3] Barrera NP, Edwardson JM. The subunit arrangement and assembly of ionotropic receptors. Trends Neurosci 2008; 31: 569–576

[4] Rudolph U, Knoflach F. Beyond classical benzodiazepines: novel therapeutic potential of GABAA receptor subtypes. Nat Rev Drug Discov 2011; 10: 685–697

[5] Möhler H. GABA A receptors in central nervous system disease: anxiety, epilepsy, and insomnia. J Recept Signal Transduct Res 2006; 26: 731–740

[6] Potterat O, Hamburger M. Concepts and technologies for tracking bioactive compounds in natural product extracts: generation of libraries,

and hyphenation of analytical processes with bioassays. Nat Prod Rep 2013; 30: 546–564

[7] Potterat O, Hamburger M. Combined use of extract libraries and HPLC-based activity profiling for lead discovery: potential, challenges, and practical considerations. Planta Med 2014; 80: 1171–1181

[8] Kim HJ, Baburin I, Khom S, Hering S, Hamburger M. HPLC-based activity profiling approach for the discovery of GABAA receptor ligands using an automated two microelectrode voltage clamp assay on *Xenopus* oocytes. Planta Med 2008; 74: 521–526

[9] Rueda DC, Raith M, De Mieri M, Schöffmann A, Hering S, Hamburger M. Identification of dehydroabietic acid from *Boswellia thurifera* resin as a positive GABAA receptor modulator. Fitoterapia 2014; 99: 28–34

[10] Rueda DC, De Mieri M, Hering S, Hamburger M. HPLC-based activity profiling for GABAA receptor modulators in *Adenocarpus cincinnatus*. J Nat Prod 2014; 77: 640–649

[11] Rueda DC, Schöffmann A, De Mieri M, Raith M, Jähne EA, Hering S, Hamburger M. Identification of dihydrostilbenes in *Pholidota chinensis* as a new scaffold for GABAA receptor modulators. Bioorg Med Chem 2014; 22: 1276–1284

[12] Schramm A, Ebrahimi SN, Raith M, Zaugg J, Rueda DC, Hering S, Hamburger M. Phytochemical profiling of *Curcuma kwangsiensis* rhizome extract, and identification of labdane diterpenoids as positive GABAA receptor modulators. Phytochemistry 2013; 96: 318–329

[13] Khom S, Strommer B, Schöffmann A, Hintersteiner J, Baburin I, Erker T, Schwarz T, Schwarzer C, Zaugg J, Hamburger M. GABAA receptor modulation by piperine and a non-TRPV1 activating derivative. Biochem Pharmacol 2013; 85: 1827–1836

[14] Rueda DC, Zaugg J, Quitschau M, Reich E, Hering S, Hamburger M. Discovery of GABAA receptor modulator Aristolactone in a commercial sample of the Chinese herbal drug "Chaihu" (*Bupleurum chinense* roots) unravels adulteration by nephrotoxic *Aristolochia manshuriensis* roots. Planta Med 2012; 78: 207–210

[15] Kim HJ, Baburin I, Zaugg J, Ebrahimi SN, Hering S, Hamburger M. HPLC-based activity profiling-discovery of sanggenons as GABAA receptor modulators in the traditional Chinese drug Sang bai pi (*Morus alba* root bark). Planta Med 2012; 78: 440–447

[16] Zaugg J, Ebrahimi SN, Smiesko M, Baburin I, Hering S, Hamburger M. Identification of GABAA receptor modulators in *Kadsura longipedunculata* and assignment of absolute configurations by quantum-chemical ECD calculations. Phytochemistry 2011; 72: 2385–2395

[17] Zaugg J, Khom S, Eigenmann D, Baburin I, Hamburger M, Hering S. Identification and characterization of GABAA receptor modulatory diterpenes from *Biota orientalis* that decrease locomotor activity in mice. J Nat Prod 2011; 74: 1764–1772

[18] Zaugg J, Eickmeier E, Ebrahimi SN, Baburin I, Hering S, Hamburger M. Positive GABA(A) receptor modulators from *Acorus calamus* and structural analysis of (+)-dioxosarcoguaiacol by 1D and 2D NMR and molecular modeling. J Nat Prod 2011; 74: 1437–1443

[19] Zaugg J, Eickmeier E, Rueda DC, Hering S, Hamburger M. HPLC-based activity profiling of *Angelica pubescens* roots for new positive GABAA receptor modulators in *Xenopus* oocytes. Fitoterapia 2011; 82: 434–440

[20] Yang X, Baburin I, Plitzko I, Hering S, Hamburger M. HPLC-based activity profiling for GABAA receptor modulators from the traditional Chinese herbal drug Kushen (*Sophora flavescens* root). Mol Divers 2011; 15: 361–372

[21] Zaugg J, Baburin I, Strommer B, Kim HJ, Hering S, Hamburger M. HPLC-based activity profiling: discovery of piperine as a positive GABAA receptor modulator targeting a benzodiazepine-independent binding site. J Nat Prod 2010; 73: 185–191

[22] Li Y, Plitzko I, Zaugg J, Hering S, Hamburger M. HPLC-based activity profiling for GABAA receptor modulators: a new dihydroisocoumarin from *Haloxylon scoparium*. J Nat Prod 2010; 73: 768–770

[23] Moradi-Afrapoli F, Ebrahimi SN, Smiesko M, Hamburger M. HPLC-based activity profiling for $GABA_A$ receptor modulators in extracts – validation of an approach utilizing a larval zebrafish locomotor assay. J Nat Prod 2017; DOI: 10.1021/acs.jnatprod.7b00081

[24] Afrikanova T, Serruys ASK, Buenafe OE, Clinckers R, Smolders I, de Witte PAM, Crawford AD, Esguerra CV. Validation of the zebrafish pentylenetetrazol seizure model: locomotor versus electrographic responses to antiepileptic drugs. PLoS One 2013; 8: e54166

[25] Baraban SC, Taylor MR, Castro PA, Baier H. Pentylenetetrazole induced changes in zebrafish behavior, neural activity and c-fos expression. Neuroscience 2005; 131: 759–768

[26] Jäger A, Knap D, Nielsen B, Stafford GI, van Staden J. *Searsia* species with affinity to the N-methyl-D-aspartic acid (NMDA) receptor. S Afr J Bot 2012; 78: 312–314

[27] Marchetti C, Gavazzo P, Stafford GI, van Staden J. South African plants used in traditional medicine to treat epilepsy have an antagonistic effect on NMDA receptor currents. J Ethnopharmacol 2011; 137: 382–388

[28] Pedersen ME, Baldwin RA, Niquet J, Stafford GI, van Staden J, Wasterlain CG, Jäger AK. Anticonvulsant effects of *Searsia dentata* (Anacardiaceae) leaf extract in rats. Phytother Res 2010; 24: 924–927

[29] Stafford GI, Pedersen ME, van Staden J, Jäger AK. Review on plants with CNS-effects used in traditional South African medicine against mental diseases. J Ethnopharmacol 2008; 119: 513–537

[30] Svenningsen AB, Madsen KD, Liljefors T, Stafford GI, van Staden J, Jäger AK. Biflavones from *Rhus* species with affinity for the GABAA/benzodiazepine receptor. J Ethnopharmacol 2006; 103: 276–280

[31] Frost DJ, Gunstone FD. The PMR analysis of non-conjugated alkenoic and alkynoic acids and esters. Chem Phys Lipids 1975; 15: 53–85

[32] ACD/Structure Elucidator, version 16.1.1, Advanced Chemistry Development, Inc., Toronto, ON, Canada

[33] Schultz DJ, Olsen C, Cobbs GA, Stolowich NJ, Parrott MM. Bioactivity of anacardic acid against Colorado potato beetle (*Leptinotarsa decemlineata*) larvae. J Agric Food Chem 2006; 54: 7522–7529

[34] Jie LK, Marcel SF. Analysis of conjugated linoleic acid esters by nuclear magnetic resonance spectroscopy. Eur J Lipid Sci Technol 2001; 103: 628–632

[35] Malik MA, O'Brien P, Tuna F, Pritchard R, Buchweishaija J, Kimambo E, Mubofu EB. The synthesis, spectroscopy and X-ray single crystal structure of catena-[(μ-anacardato)-copper(II)-bipyridine][Cu_2{(μ-$O_2CC_6H_3$(*o*-OH)(*o*-$C_{15}H_{31}$)}$_4$-(NC_5H_5)$_2$]. Dalton Trans 2013; 42: 14438–14444

[36] Choi YH, Choi HK, Peltenburg-Looman A, Lefeber AW, Verpoorte R. Quantitative analysis of ginkgolic acids from *Ginkgo* leaves and products using 1H-NMR. Phytochem Anal 2004; 15: 325–330

[37] Chen J, Zhang YH, Wang LK, Sucheck SJ, Snow AM, Hecht SM. Inhibitors of DNA polymerase *β* from *Schoepfia californica*. Chem Commun 1998; 24: 2769–2770

[38] Kubo I, Kim M, Naya K, Komatsu S, Yamagiwa Y, Ohashi K, Sakamoto Y, Hirakawa S, Kamikawa T. Prostaglandin synthetase inhibitors from the African medicinal plant *Ozoroa mucronata*. Chem Lett 1987; 16: 1101–1104

[39] Gény C, Rivière G, Bignon J, Birlirakis N, Guittet E, Awang K, Litaudon M, Roussi F, Dumontet V. Anacardic acids from *Knema hookeriana* as modulators of Bcl-xL/Bak and Mcl-1/Bid interactions. J Nat Prod 2016; 79: 838–844

[40] Akhtar MN, Lam KW, Abas F, Ahmad S, Shah SAA, Choudhary MI, Lajis NH. New class of acetylcholinesterase inhibitors from the stem bark of *Knema laurina* and their structural insights. Bioorg Med Chem Lett 2011; 21: 4097–4103

[41] Spencer GF, Tjarks LW, Kleiman R. Alkyl and phenylalkyl anacardic acids from *Knema elegans* seed oil. J Nat Prod 1980; 43: 724–730

[42] Westerfield M. The Zebrafish Book. A Guide for the Laboratory Use of Zebrafish (*Danio rerio*), 5th edition. Eugene: University of Oregon Press; 2007

Supplementary data

Planta Medica

HPLC-based activity profiling for $GABA_A$ receptor modulators from *Searsia pyroides* leaves using a validated larval zebrafish locomotor assay

Fahimeh Moradi-Afrapoli[1], Hannes van der Merwe[2], Maria De Mieri[1], Anke Wilhelm[2], Marco Stadler[3], Pieter.C. Zietsman [4], Steffen Hering[3], Kenneth Swart[2,5], Matthias Hamburger[1]

1. Pharmaceutical Biology, Department of Pharmaceutical Sciences, University of Basel, Klingelbergstrasse 50, 4056 Basel, Switzerland.
2. Faculty of Natural and Agricultural Sciences, University of the Free State, Bloemfontein 9300, Republic of South Africa
3. Institute of Pharmacology and Toxicology, University of Vienna, Althanstrasse 14, 1090 Vienna, Austria
4. National Museum, Bloemfontein, Republic of South Africa
5. FARMOVS-PAREXEL, University of the Free State, Bloemfontein, South Africa

*corresponding author: Prof. Matthias Hamburger, Pharmaceutical Biology, Department of Pharmaceutical Sciences, University of Basel, Klingelbergstrasse 50, CH-4056 Basel, Switzerland, Phone: +41-61-267-1425 Fax: +41-61-267-1474
E-Mail: matthias.hamburger@unibas.ch

Table S1. ^{1}H-NMR data (500 MHz, DMSO-d_6) of compounds **1 - 6**

No	1	2	3	4	5	6
3	6.60 (*d*, 7.5)	6.61 (*d*, 7.5)	6.62 (*d*, 7.5)	6.62 (*d*, 7.5)	6.62 (*d*, 7.5)	6.60 (*d*, 7.5)
4	7.20 (*dd*, 7.5, 7.5)	7.20 (*dd*, 7.5, 7.5)	7.22 (*dd*, 7.5, 7.5)	7.22 (*dd*, 7.5, 7.5)	7.22 (*dd*, 7.5, 7.5)	7.16 (*dd*, 7.5, 7.5)
5	6.63 (*d*, 7.5)	6.62 (*d*, 7.5)	6.64 (*d*, 7.5)	6.64 (*d*, 7.5)	6.64 (*d*, 7.5)	6.67 (*d*, 7.5)
6	-	-	-	-	-	-
7	3.0 (*m*)	3.0 (*m*)	3.0 (*m*)	3.0 (*m*)	3.0 (*m*)	2.72 (*m*)
8	1.49 (*m*)	1.49 (*m*)	1.51 (*m*)	1.50 (*m*)	1.50 (*m*)	1.51 (*m*)
9	1.29 (*m*)	1.29 (*m*)	1.28 (*m*)	1.30 (*m*)	1.30 (*m*)	1.26 (*m*)
10	a	b	c	d	e	f
11	a	b	c	d	e	f
12	a	b	c	d	e	f
13	a	b	c	d	e	f
14	1.29 (m)	b	1.32 (*m*)	d	e	f
15	1.97 (*m*)	b	2.10 (*m*)	d	e	f
16	5.29 (*m*)	1.28 (*m*)	5.42 (*m*)	d	e	1.98 (*m*)
17	5.29 (*m*)	1.96 (*m*)	6.20 (*m*)	d	e	5.31 (*m*)
18	1.96 (*m*)	5.25-5.33 (*m*)	6.20 (*m*)	d	1.25 (*m*)	5.31 (*m*)
19	1.27 (*m*)	5.25-5.33 (*m*)	5.42 (*m*)	d	1.98 (*m*)	1.98 (*m*)
20	1.27 (*m*)	1.96 (*m*)	2.12 (*m*)	d	5.23-5.37 (*m*)	1.26 (*m*)
21	0.84 (*t*, 7.5)	0.88 (*t*, 7.5)	0.93 (*t*, 7.5)	1.23 (*m*)	5.23-5.37 (*m*)	1.26 (*m*)
22	-	-	-	1.24 (*m*)	1.98 (*m*)	1.26 (*m*)
23	-	-	-	0.85 (*t*, 7.5)	0.9 (*t*, 7.5)	0.85 (*t*, 7.5)
OH	8.18	8.18	8.18	8.16	8.16	8.20

[a-f] Designations with the same letter are indicative of overlapping signals: [a] 1.18-1.30 ppm, [b] 1.18-1.30 , [c] 1.17-1.30 ppm, [d] 1.10-1.42 ppm, [e]1.15-1.36 ppm , [f]1.15-1.36 ppm

Table S2. ^{13}C-NMR data (125 MHz, DMSO-d_6) of compounds **1– 6**

No	1[a]	2[b]	3[a]	4[a]	5[a]	6[a]
1	114.6 (C)	114.2 (C)	114.2 (C)	114.1 (C)	114.1 (C)	113.9 (C)
2	160.7 (C)	157.5 (C)	160.8 (C)	160.6 (C)	159.6 (C)	158.4 (C)
3	116.6 (CH)	114.1 (CH)	116.5 (CH)	116.5 (CH)	115.6 (CH)	113.3 (CH)
4	133.5 (CH)	130.7 (CH)	133.2 (CH)	133.4 (CH)	132.4 (CH)	130.0 (CH)
5	121.9 (CH)	120.3 (CH)	121.6 (CH)	121.7 (CH)	120.8 (CH)	119.4 (CH)
6	147.1 (C)	146.9 (C)	149.9 (C)	146.9 (C)	142.6 (C)	143.3 (C)
7	34.9 (CH_2)	34.8 (CH_2)	33.9 (CH_2)	34.8 (CH_2)	33.9 (CH_2)	33.6 (CH_2)
8	31.8 (CH_2)	31.7 (CH_2)	31.6 (CH_2)	31.7 (CH_2)	30.9 (CH_2)	30.8 (CH_2)
9	29.7 (CH_2)	29.6 (CH_2)	29.5 (CH_2)	29.4 (CH_2)	28.9 (CH_2)	28.5 (CH_2)
10	[c]	[d]	[e]	[f]	[g]	[h]
11	[c]	[d]	[e]	[f]	[g]	[h]
12	[c]	[d]	[e]	[f]	[g]	[h]
13	[c]	[d]	[e]	[f]	[g]	[h]
14	[c]	[d]	29.9(CH_2)	[f]	[g]	[h]
15	27.1 (CH_2)	[d]	27.2 (CH_2)	[f]	[g]	[h]
16	130.0 (CH)	29.5 (CH_2)	132.0 (CH)	[f]	[g]	26.1 (CH_2)
17	130.0 (CH)	27.1 (CH_2)	123.7 (CH)	[f]	[g]	129.1 (CH)
18	27.1 (CH_2)	130.0 (CH_2)	123.4 (CH)	[f]	28.6 (CH_2)	129.1 (CH)
19	32.2 (CH_2)	131.7 (CH_2)	133.4 (CH)	[f]	26.1 (CH_2)	26.1 (CH_2)
20	22.4 (CH_2)	20.3 (CH_2)	20.7 (CH_2)	[f]	128.8 (CH)	28.7 (CH_2)
21	14.3 (CH_3)	14.7 (CH_3)	14.3 (CH_3)	31.4 (CH_2)	131.2 (CH)	30.8 (CH_2)
22	-	-	-	22.4 (CH_2)	19.6 (CH_2)	21.7 (CH_2)
23	-	-	-	14.2 (CH_3)	13.9 (CH_3)	13.4 (CH_3)
COOH	[i]	171.1 (C)	[i]	[i]	[i]	[i]

[a] Data extracted from HSQC-DEPT and HMBC spectra
[b] Data from ^{13}C-NMR spectrum
[c-h] Designations with the same letter are indicative of overlapping signals: [c] 29.5-31.8 ppm (CH_2), [d] 29.5-31.8ppm (CH_2), [e] 28.2-29.6 ppm (CH_2), [f] 29.0-31.7 ppm (CH_2), [g] 28.0-31.0 ppm (CH_2), [h] 28.0-31.0 ppm (CH_2)
[i] No HMBC crosspeak for a four-bond correlation observed in HMBC spectra.

Table S3. HRESI-TOFMS data of compounds **1-6**.

compound	acc. mass found $[M-H]^-$	acc. mass calculated $[M-H]^-$	calcd formula
1	345. 25	345.24	$C_{22}H_{34}O_3$
2	345.25	345.24	$C_{22}H_{34}O_3$
3	343.20	343.23	$C_{22}H_{32}O_3$
4	347.30	347.26	$C_{22}H_{36}O_3$
5	373.30	373.27	$C_{24}H_{38}O_3$
6	373.30	373.27	$C_{24}H_{38}O_3$

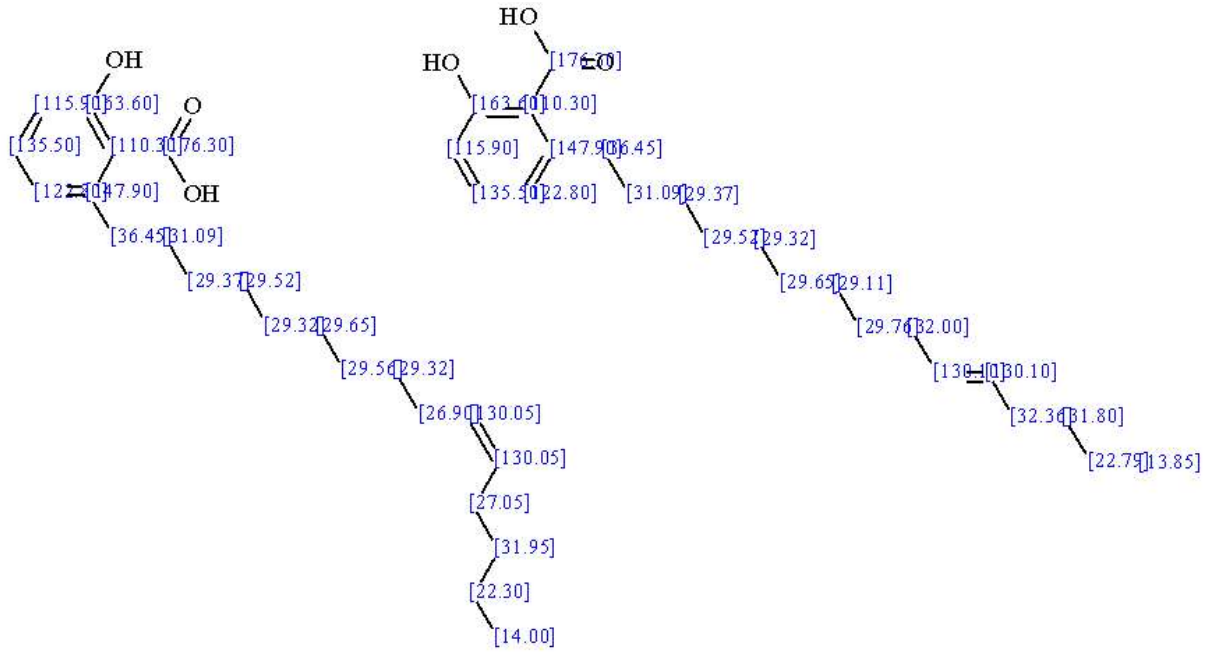

Figure S1. ^{13}C-NMR shifts for *E* and *Z* isomers of compound **1** (DMSO-d_6, 125 MHz), as calculated by ACDLabs software.

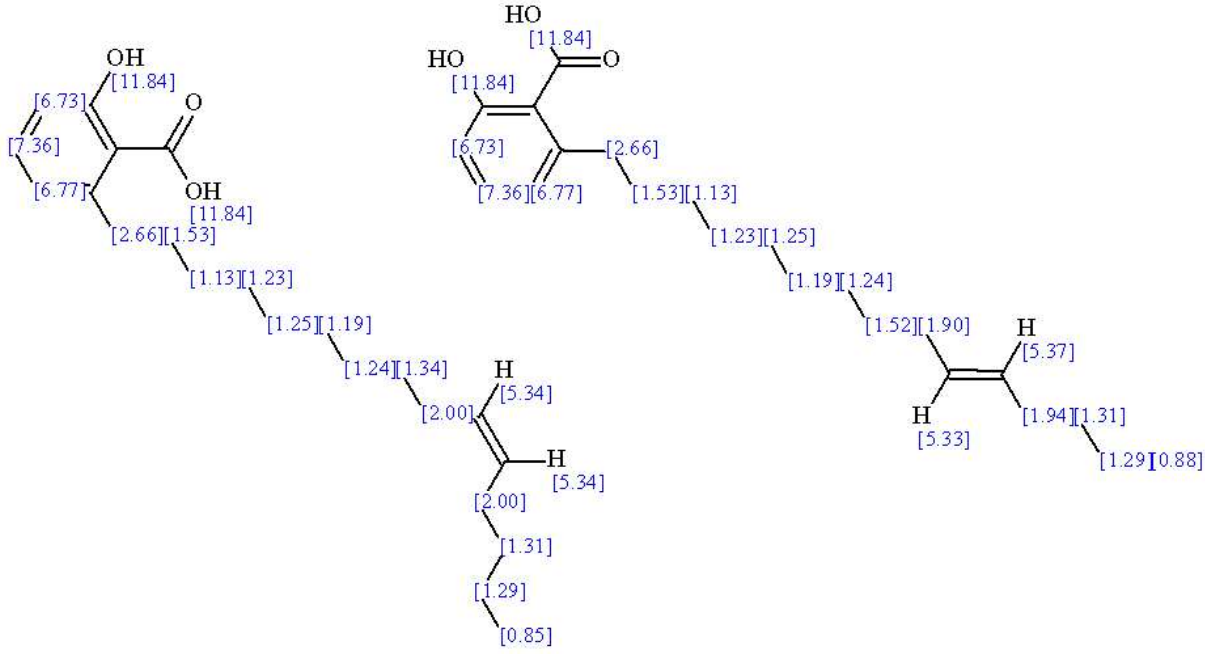

Figure S2. ^{1}H-NMR shifts for *E* and *Z* isomers of compound **1** (DMSO-d_6, 500 MHz), as calculated by ACDLabs software.

3.3. Validation of UHPLC-MS/MS methods for the determination of kaempferol and its metabolite 4-hydroxyphenyl acetic acid, and application to *in vitro* blood-brain barrier and intestinal drug permeability studies

Fahimeh Moradi-Afrapoli, Mouhssin Oufir, Fruzsina R. Walter, Maria A. Deli, Martin Smiesko, Volha Zabela, Veronika Butterweck, Matthias Hamburger

Journal of Pharmaceutical and Biomedical Analysis, 128 (2016) 264–274, **DOI:** 10.1016/j.jpba.2016.05.039

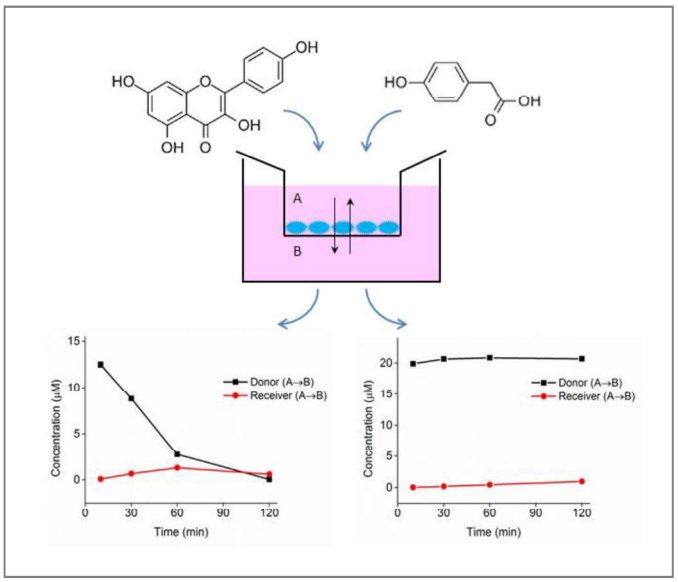

Kaempferol (KMF) is a positive $GABA_A$ receptor modulator. Through oral administration, KMF is metabolized by the intestinal microflora to phenolic acids. Oral application of KMF and intraperitoneal administration of its major intestinal metabolite, 4-hydroxyphenylacetic acid (4-HPAA), induce anxiolytic activities in mice.

In the present study, the ability of KMF and 4-HPAA to cross intestinal and blood-brain barriers was predicted *in silico* and assessed in cell-based models. Intestinal transport studies were performed with Caco-2 cells, and blood-brain barrier transports were studied with an immortalized mono-culture human model and a primary triple-co-culture rat model. For quantification of KMF and 4-HPAA in two transport buffers (RHB and HBSS) UHPLC–MS/MS methods were developed and fully validated according to EMA and FDA guidelines. Data obtained with all barrier models showed high intestinal and blood-brain barrier permeation of KMF, and no permeability of 4-HPAA, when compared to barrier integrity markers. KMF showed decreasing recovery in the Caco-2 model suggesting extensive metabolism of the compound in the cells that would result in poor bioavailability after oral administration.

My contributions to this publication: development and validation of the UPLC-MS/MS method in the RHB and HBSS*, performing the intestinal transport studies with Caco-2 cells and the BBB transport experiments with the mono-culture HBMEC model, sample preparation and analysis, writing the manuscript draft, and preparation of figures and tables.*

Fahimeh Moradiafrapoli

Journal of Pharmaceutical and Biomedical Analysis 128 (2016) 264–274

Contents lists available at ScienceDirect

Journal of Pharmaceutical and Biomedical Analysis

journal homepage: www.elsevier.com/locate/jpba

Validation of UHPLC–MS/MS methods for the determination of kaempferol and its metabolite 4-hydroxyphenyl acetic acid, and application to *in vitro* blood-brain barrier and intestinal drug permeability studies

Fahimeh Moradi-Afrapoli[a,b], Mouhssin Oufir[a], Fruzsina R. Walter[c], Maria A. Deli[c], Martin Smiesko[d], Volha Zabela[a], Veronika Butterweck[e,f], Matthias Hamburger[a,*]

[a] *Pharmaceutical Biology, Department of Pharmaceutical Sciences, University of Basel, Klingelbergstrasse 50, 4056 Basel, Switzerland*
[b] *Department of Pharmacognosy, Faculty of Pharmacy, Mazandaran University of Medical Sciences, Sari, Iran*
[c] *Institute of Biophysics, Biological Research Centre, Hungarian Academy of Sciences, Temesvari krt 62, 6726 Szeged, Hungary*
[d] *Division of Molecular Modeling, Department of Pharmaceutical Sciences, University of Basel, Klingelbergstrasse 50, 4056 Basel, Switzerland*
[e] *Department of Pharmaceutics, College of Pharmacy, University of Florida, 1345 Gainesville, FL, USA*
[f] *School of Life Sciences Institute for Pharma Technology, Gründenstrasse 40,CH-4132 Muttenz, Switzerland*

ARTICLE INFO

Article history:
Received 17 December 2015
Received in revised form 21 May 2016
Accepted 23 May 2016
Available online 24 May 2016

Keywords:
Kaempferol
4-HPAA
LC–MS/MS
Method validation
Caco-2 model
Blood-brain barrier

ABSTRACT

Sedative and anxiolytic-like properties of flavonoids such as kaempferol and quercetin, and of some of their intestinal metabolites, have been demonstrated in pharmacological studies. However, routes of administration were shown to be critical for observing *in vivo* activity. Therefore, the ability to cross intestinal and blood-brain barriers was assessed in cell-based models for kaempferol (KMF), and for the major intestinal metabolite of KMF, 4-hydroxyphenylacetic acid (4-HPAA). Intestinal transport studies were performed with Caco-2 cells, and blood-brain barrier transport studies with an immortalized mono-culture human model and a primary triple-co-culture rat model. UHPLC–MS/MS methods for KMF and 4-HPAA in Ringer-HEPES buffer and in Hank's balanced salt solution were validated according to industry guidelines. For all methods, calibration curves were fitted by least-squares quadratic regression with $1/X^2$ as weighing factor, and mean coefficients of determination (R^2) were >0.99. Data obtained with all barrier models showed high intestinal and blood-brain barrier permeation of KMF, and no permeability of 4-HPAA, when compared to barrier integrity markers.

Abbreviations: 4-HPAA, 4-hydroxyphenyl acetic acid; ACN, acetonitrile; BSA, bovine serum albumin; Cal, calibrator; C_{CI}, cell layer capacitance; CNS, central nervous system; CV%, coefficient of variation; CPT-cAMP, 8-(4-chlorophenylthio)-adenosine-3′,5′-cyclic monophosphate sodium salt; DMEM, dulbecco's modified eagle's medium; EMA, european medicines agency; ER, efflux ratio; ESI, electro-spray ionization; FBS, fetal bovine serum; FDA, food and drug administration; hBMEC, immortalized human brain microvascular endothelial cell line; HC, hydrocortison; HEPES, (4-(2-hydroxyethyl)-1-piperazineethanesulfonic acid); HPLC, high-performance liquid chromatography; IS, internal standard; KMF, kaempferol; LLOQ, lower limit of quantification; LogP, logarithm of partitioning coefficient; LY, lucifer yellow vs dilithium salt; min, minute; MRM, multiple reaction monitoring; MW, molecular weight; Na-F, sodium fluorescein; Papp, apparent permeability coefficient; PSA, polar surface area; QC, quality control; QCH, quality control high; QCL, quality control low; QCM, quality control medium; RBEC, primary rat brain capillary endothelial cell; RE%, relative error; RHB, Ringer HEPES buffer; Rpm, revolutions per minute; RT, room temperature; SD, standard deviation; SEM, standard error of the mean; SS, stock solution; TEER, transendothelial electrical resistance; ULOQ, upper limit of quantification; UHPLC–MS/MS, ultra-high performance liquid chromatography with tandem mass spectrometric detection; VA, vanillic acid; WS, working solution.

* Corresponding author at: Institute of Pharmaceutical Biology, Department of Pharmaceutical Sciences, University of Basel, Klingelbergstrasse 50, CH-4056 Basel, Switzerland.
E-mail address: matthias.hamburger@unibas.ch (M. Hamburger).

http://dx.doi.org/10.1016/j.jpba.2016.05.039
0731-7085/

1. Introduction

Flavonoids are a large and widely occurring class of natural products which are found in fruits, vegetables, wine, beer [1], and in medicinal plants [2,3]. Flavonoids reportedly possess a broad spectrum of pharmacological activities, such as anti-inflammatory, antiallergic, neuroprotective, cardioprotective, and cancer chemopreventive properties [1,4–9]. Sedative and anxiolytic-like activities of flavonoid-containing medicinal plants [10–14] and of selected purified flavonoids [15–19] have been substantiated in pharmacological studies. However, the route of administration appeared to be decisive, given that widely occurring flavonols such as kaempferol (KMF) and quercetin induced anxiolytic activities in mice only after oral administration (p.o.), but not upon intraperitoneal (i.p.) application [10].

Flavonols are metabolized by the intestinal microflora to phenolic acids, such as *p*-hydroxyphenylacetic, 3-phenylpropionic, *m*-hydroxyphenylacetic, *p*-hydroxyphenylpropionic and 3,4-dihydroxyphenylacetic acids [20–23]. Interestingly, phenolic acid metabolites of flavonoids, such as *p*-hydroxyphenylacetic acid (4-HPAA) and 3,4-dihydroxyphenylacetic acid showed anxiolytic activities after i.p. application [24]. Moreover, in gut sterilized mice no antidepressant-like effects were observed upon oral administration of KMF and quercetin [24]. Taken together, these findings suggested that flavonoids by themselves might not be the pharmacologically active compounds, but rather their metabolites produced by the intestinal microflora. At the same time, some of the intestinal metabolites of flavonoids occur in plasma as endogenous trace acids generated by oxidative deamination of amines such as dopamine and tyramine [25]. Plasma levels of the trace acids may vary significantly in several psychological disorders. It has been shown that plasma levels of 4-HPAA were significantly decreased in patients suffering from schizophrenia [26] and agoraphobia [27], as well as in violent offender prisoners [27], while they were increased in isolated aggressive mice [28]. Also, increased 4-HPAA and 3-HPAA levels in the brain were found upon treatment with anxiolytic and antipsychotic drugs such as chlorpromazine and sulpiride [29].

Bioactive compounds need to cross several biological barriers in the human body to reach the target tissues. After oral administration they have to be absorbed from the gut via the intestinal epithelium into systemic circulation. Compounds acting as modulators of brain function subsequently need to cross the blood-brain barrier (BBB) to reach the central nervous system (CNS) [30]. However, the systemic distribution and brain penetration of flavonoids and their metabolites is not well understood. To date, only a limited number of studies on intestinal [31–35] and brain permeability [36–39] of flavonoids and flavonoid metabolites have been published. Barrington et al. [40] showed that in Caco-2 cells KMF undergoes extensive phase 2 metabolism to sulfate and glucuronide conjugates, and that only a small fraction of non-conjugated KMF penetrated Caco-2 cell monolayers. Very recently, Yang et al. [37] reported the permeation of KMF in Caco-2 cells, and in a rat cell-based BBB model. However, none of these studies were performed with quantitative methods validated according to international bioanalytical guidelines [41,42]. To date, no transport studies with 4-HPAA have been reported. Therefore, we here investigated the permeation of KMF and its main metabolite, 4-HPAA, in human and rat *in vitro* barrier models. Determination of KMF and 4-HPAA in corresponding transport media was carried out with UHPLC–MS/MS assays. Quantification methods were developed and validated according to international guidelines [41,42].

2. Materials and methods

2.1. Ethics statement

Animal studies for the establishment of primary cultures were done according to the 1998. XXVIII. Hungarian law about animal protection and welfare. Formal approvals for animal studies have been obtained from the local Hungarian animal health authorities (Permit number: XVI./834/2012).

2.2. Reagents and chemicals

KMF, 4-HPAA, vanillic acid (VA), Hank's balanced salt solution (HBSS, pH 7.4), sodium fluorescein (Na-F), hydrocortisone (HC), chlorophenylthio-adenosine-3′,5′-cyclic monophosphate (CPT-cAMP), bovine serum albumin (BSA) and Dulbecco's modified Eagle medium (DMEM) were obtained from Sigma-Aldrich (Germany). RO 201724 was from Roche (Switzerland). Fetal bovine serum (FBS) "Gold" was from PAA Laboratories (Austria). $^{13}C_{15}$-labeled KMF was purchased from IsoLife (Netherlands), and Lucifer Yellow VS dilithium salt (LY) was from Santa Cruz (Germany). Formic acid (99%), and acetic acid glacial were obtained from Biosolve (Netherlands). Ringer HEPES buffer (RHB) was prepared by dissolving the ingredients (all from Sigma-Aldrich) in water as follows: NaCl (150 mM), $CaCl_2$ (2.2 mM), $MgCl_2$ (0.2 mM), KCl (5.2 mM), $NaHCO_3$ (6.0 mM), 4-(2-hydroxyethyl) piperazine-1-ethanesulfonic acid HEPES (5 mM) and glucose (2.8 mM), adjusted to pH 7.4, filtered through 0.2 μm filter and stored at 4 °C. HPLC grade acetonitrile was from Scharlau (Spain), and UHPLC grade methanol was from Lab-Scan (Poland). High quality water was prepared using EASYpure II purification system (Barnstead, USA). Tissue culture inserts for the BBB models were from Greiner Bio-one® (Germany). The inserts used in the Caco-2 model were from Corning Costar® (USA).

2.3. UHPLC–MS/MS instrument and chromatographic conditions

UHPLC–MS/MS analyses were performed on an Agilent 6430 Triple Quadrupole MS system connected to a 1290 Infinity LC system consisting of binary capillary pump G4220A, column oven G1316C, cooling system G1330B, and autosampler G4226A. Quantitative analysis by MS was performed with electrospray ionization (ESI) in MRM mode. Desolvation and nebulization gas was nitrogen. MS/MS data were analyzed with Agilent MassHunter Workstation software version B.06.00. The temperature of the autosampler was set at 10 °C.

2.3.1. Quantification of KMF

A ZORBAX Eclipse Plus C18 column (2.1 × 50 mm, 1.8 μm, Agilent) was used. The mobile phase consisted of high purity water (solvent A) and acetonitrile (ACN) (solvent B) both containing 0.1% formic acid. The following gradient (A–B, v/v) was used: 75:25 (0–1 min), 75:25 to 72:28(1–2.6 min), 72:28 to 0:100 (2.6–2.7 min), 0:100 (2.7–3.7 min), 0:100 to 75:25 (3.7–3.8 min), hold for one min (flow rate: 0.4 ml/min). Column temperature was set at 55 °C. Injection solvent was water-ACN (65:35, v/v) both containing 1 mM acetic acid. The needle wash solvent consisted of a water-methanol mixture (1:1, v/v). Mass spectrometry detection was performed in positive ESI mode. MRM transitions of KMF and the IS, and the corresponding collision energies and fragmentor voltages are provided in Table 1. Capillary voltage was set at 5000 V. The desolvation gas temperature was 350 °C, the flow rate for desolvation gas was 13 l/min, and the nebulizer was set at 60 psi. The dwell time was automatically set at 250 msec.

Table 1
MS/MS parameters for quantification of KMF, 4-HPAA, and corresponding internal standards (ISs).

Compound	Precursor Ion (*m/z*)	Product Ion (*m/z*)	Fragmentor (V)	Collision Energy (V)	Polarity
KMF	287.0	153.0[a]	155	34	Positive
		69.1[b]		58	
$^{13}C_{15}$-labeled KMF (IS)	302.0	160.1	155	34	
4-HPAA	151.0	106.6[a]	62	2	Negative
		107.1[b]		10	
Vanillic acid (IS)	167.0	152.0	88	18	

[a] Quantifier.
[b] Qualifier.

2.3.2. Quantification of 4-HPAA

Separation was performed on a Kinetex XB-C18 column (2.1 × 100 mm, 1.7 μm, Phenomenex). The mobile phase consisted of water (solvent A) and ACN (solvent B) both containing 5 mM acetic acid. The following gradient (A–B, v/v) was used: 98:2 (0–1 min), 98:2 to 90:10 (1–4.6 min), 90:10 to 0:100 (4.6–4.7 min), 0:100 (4.7–5.9 min), 0:100 to 98:2 (5.9–6 min), hold for one min (flow rate: 0.5 ml/min). Column temperature was set at 55 °C. Injection solvent was water-ACN (65:35, v/v) containing 1 mM acetic acid. The needle wash solvent consisted of a mixture of water-methanol-isopropanol-ACN (1:1:1:1, v/v/v/v). Mass spectrometry detection was performed in negative ESI mode. MRM transitions and the corresponding collision energies and fragmentor voltages are provided in Table 1. Capillary voltage was set at 4000 V. The desolvation gas temperature was 350 °C, the flow rate for desolvation gas was 13 l/min and the nebulizer was set at 60 psi. The dwell time was automatically set at 200 msec.

2.4. Bioanalytical method validation

Quantification methods were validated according to the European Medicines Evaluation Agency (EMA) [42] and US Food and Drug Administration (FDA) industry guidelines for method validation [41]. Full validation in RHB (BBB transport medium) was followed by partial method validation in HBSS buffer (Caco-2 transport medium).

2.4.1. Standard solutions, calibrators and quality control samples

Stock solutions (SS) of analytes and ISs were prepared at 10 mg/ml in DMSO. Working solutions (WS) of analytes (100 μg/ml in water) and ISs (50 μg/ml in methanol) were obtained by serial dilution of the corresponding SSs. Seven calibration samples (Cals) in the range of 20.0–2000 ng/ml, and quality controls (QCs) at low, medium and high levels (QCL = 60.0 ng/ml, QCM = 1000 ng/ml, QCH = 1600 ng/ml) were prepared by serial dilution of WS of the analytes in corresponding matrices (RHB and HBSS). All solutions were stored below −65 °C. Prior to each experiment, a second WS (WS2) of IS was freshly prepared by further dilution of WS1 in methanol. $^{13}C_{15}$-labeled KMF (WS2: 500 ng/ml) served as IS for quantification of KMF in both RHB and HBSS. Vanillic acid (VA) at 2000 ng/ml and 4000 ng/ml (WS2) was used as IS for quantification of 4-HPAA in RHB and HBSS, respectively.

2.4.2. Sample extraction protocol

Aliquots (200 μl) of each buffer (RHB or HBSS) were added to a mixture of 100 μl WS2 of IS and 150 μl BSA (60 g/L), subjected to protein precipitation by adding 1000 μl ice-cold acetonitrile, and mixed (1400 rpm) for 10 min at room temperature (RT). The mixtures were centrifuged for 20 min at 13200 rpm and 10 °C. Supernatants (1200 μl) were transferred into 96-deep well plates and dried by a nitrogen evaporator (Evaporex EVX-96, Apricots Designs Inc, USA). The dried extracts were dissolved in 200 μl injection solvent (high quality water-acetonitrile (65:35, v/v) containing 1 mM acetic acid), and mixed for 45 min at 1500 rpm.

2.4.3. Calibration curves

Calibration curves were generated with seven calibrators ranging from 20.0–2000 ng/ml. Two sets of calibrators (Cal_1-Cal_7) accompanied with a blank sample spiked with only IS (Cal_0) and two double blank samples were submitted to UHPLC–MS/MS. The first set was submitted at the beginning of each analytical run, starting from the lower limit of quantification (LLOQ = 20.0 ng/ml = Cal_1) to the upper limit of quantification (ULOQ = 2000 ng/ml = Cal_7). The second set was similarly submitted at the end of the run. Furthermore, the analytical run was validated by duplicates of QCL, QCM and QCH which were inserted randomly between real samples.

2.4.4. Within- and between-series imprecision and inaccuracy

Six replicates of five levels QCs (LLOQ, QCL, QCM, QCH and ULOQ) were processed and analyzed within three validation runs on three different days. Within-series imprecision and inaccuracy were assessed in one run (n = 6) to determine the repeatability of the method. Between-series imprecision and inaccuracy were evaluated by the overall mean and standard deviation for each QC level calculated for the three analytical runs (n = 18) to evaluate the reproducibility of the method.

2.4.5. Carry-over

In each analytical run the response of analyte and IS were assessed in blank samples injected immediately after the ULOQ. Mean carry-over (n = 2) in the blank samples of the two sets of calibrators were then calculated.

2.4.6. Selectivity and specificity

Selectivity and specificity of the methods were evaluated in three different batches of buffers. Six samples at the LLOQ (duplicate in three batches) were placed within a validation run and both selectivity imprecision and inaccuracy were assessed. Specificity of the method was evaluated by a total of six blank samples (duplicates in three batches). The peak areas evaluated in the blank samples were not allowed to exceed 20% of the mean LLOQ peak area.

2.4.7. Extraction yield

Six replicates of QCs at low, medium and high levels (60, 1000, 1600 ng/ml) were extracted, and then spiked with exact amount of unprocessed IS (set 1). A batch of six blank samples were extracted and then spiked with exact amount of unprocessed IS plus unprocessed analyte equal to the three corresponding QC levels (set 2). To calculate the absolute recovery of the analyte, the peak area ratios obtained from set 1 were compared with those of set 2. To calculate the absolute recovery of the IS, six samples of IS were extracted and later spiked with exact amount of unprocessed analyte equal to level QCM (set 3). A batch of six blank replicates were extracted and then spiked with unprocessed IS plus analyte equal to level QCM (set 4). Finally, the peak area ratios obtained from set 3 were compared with those of set 4.

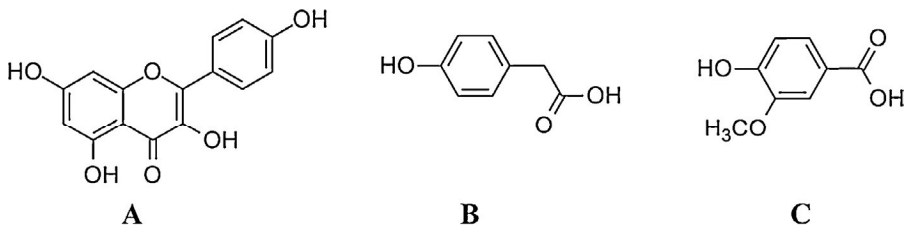

Fig. 1. Chemical structures of kaempferol (KMF) (A), 4-hydroxyphenylacetic acid (4-HPAA) (B), and vanillic acid (VA) (C).

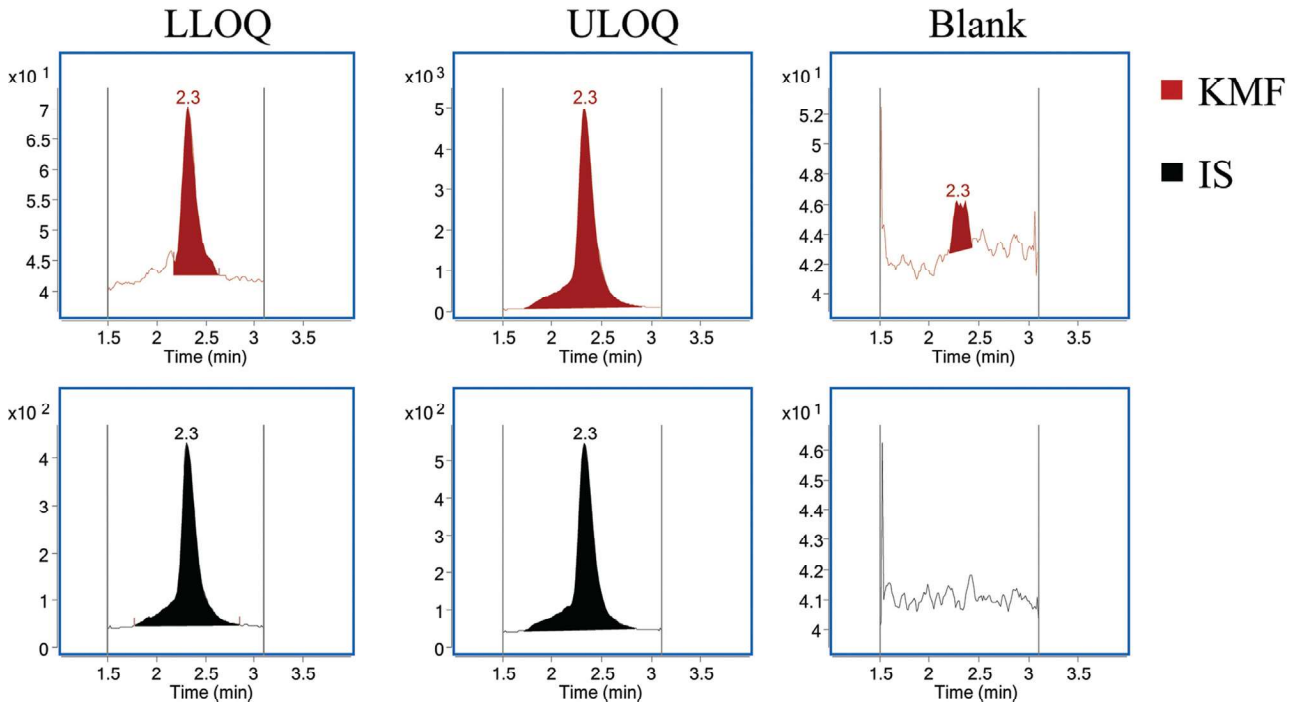

Fig. 2. Typical MRM chromatograms of kaempferol (KMF) and internal standard (IS, $^{13}C_{15}$ KMF) in both buffers spiked at 20.0 ng/ml (LLOQ) and 2000 ng/ml (ULOQ), and blank buffer immediately injected after ULOQ.

2.4.8. Dilution test

Samples at higher levels than ULOQ need to be diluted prior to analysis. However, the dilution should not affect the reliability of the method. To perform the dilution test, a sample of the analyte at 10000 ng/ml was prepared from the WS. This solution was further diluted 10X and 100X to give dilution-QCs at levels of 1000 ng/ml and 100 ng/ml, respectively. Six replicates of each dilution-QC were analyzed within an analytical run.

2.4.9. Short-term stability tests

Three sets of QCs each containing six replicates of QCL and QCH were prepared. The first set was stored on the bench for 4 h and then processed and analyzed in order to assess the compound's stability at room temperature. The freeze-thaw stability test was performed by exposing the QCs to three freeze (below −65 °C) and thaw (RT) cycles during three successive days. To evaluate the stability of processed samples in the UHPLC autosampler, a set of QCs was extracted and analyzed, then stored in the autosampler (set at 10 °C and protected from light) for at least 48 h, re-injected and re-analyzed within a freshly prepared analytical run.

2.4.10. Long-term stability test

Three replicates of freshly prepared QCL, QCM, and QCH were quantified at time 0 (t_0). Three other replicates of each level were stored below −65 °C for two (KMF) and three (4-HPAA) weeks (t_{test}) and then analyzed within a freshly prepared analytical run. The mean values of t_{test} were plotted in function of t_0 and a linear regression, forced through zero, was performed. To confirm the stability of the samples, the slope had to be within 1.00 ± 0.15.

2.4.11. Stock solution stability test

Stock solutions of analytes and ISs were stored below −65 °C for 30 days, and for approx. 6 h at RT. A working solution (10 μg/ml) of each corresponding stock solution was prepared in the injection solvent, and injected six times to the UHPLC–MS/MS system. Results were compared with the data obtained from freshly prepared SSs. Degradation should not exceed 5% for each compound.

2.5. Intestinal transport experiment

The Caco-2 human colorectal adenocarcinoma cell line was used as an *in vitro* model of the intestinal barrier [43]. Caco-2 cells of passages 60–65 were seeded in 6-well Transwell® plates (insert area: 4.7 cm^2, pore size: 0.4 μm, polycarbonate membrane) at a density of 3.58×10^5 cells/cm^2 (Fig. 4A). Culture medium was DMEM supplemented with FBS (10%), L-glutamate (200 mM) and non-essential amino acids (1%). A tight epithelial barrier was formed after 21 days. Integrity of the cell layer was evaluated by measurement of transepithelial electrical resistance (TEER) with the EVOM epithelial voltohmmeter (World Precision Instruments, USA). The transport study was performed when TEER values reached 400–600 Ωcm^2. Paracellular permeability was assessed

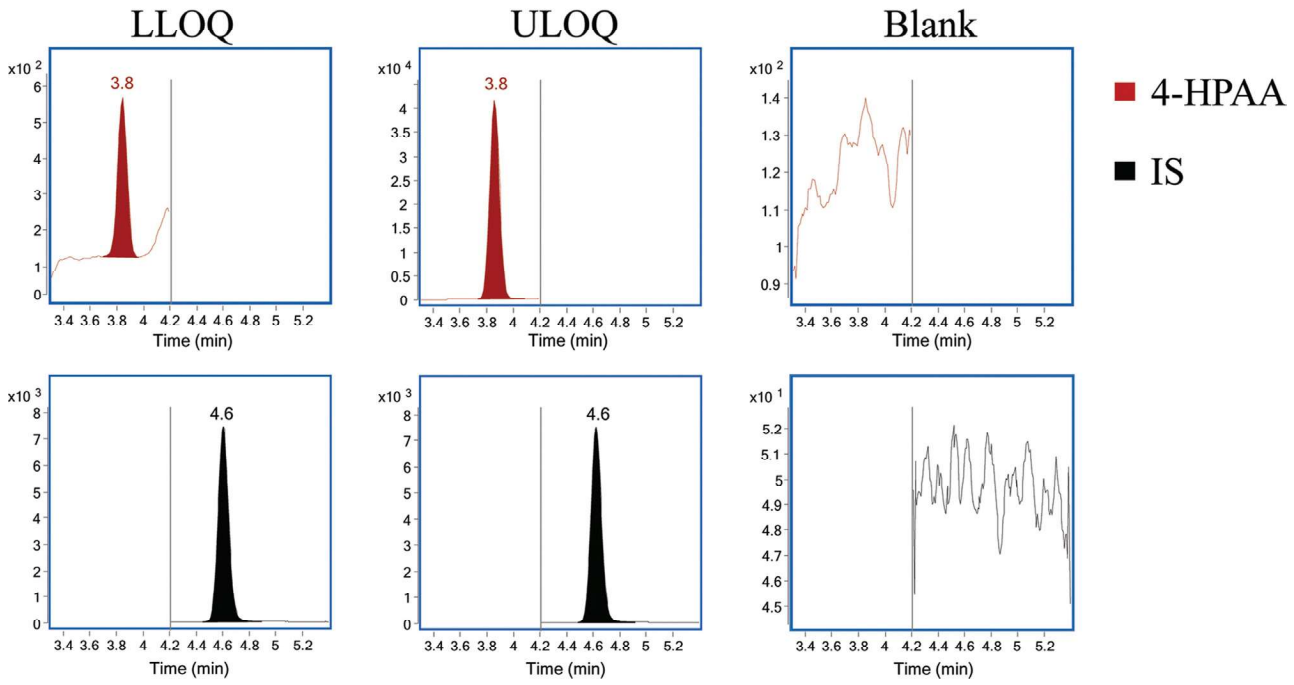

Fig. 3. Typical MRM chromatograms of 4-hydroxyphenylacetic acid (4-HPAA) and internal standard (IS, vanillic acid) in both buffers spiked at 20.0 ng/ml (LLOQ) and 2000 ng/ml (ULOQ), and blank buffer immediately injected after ULOQ.

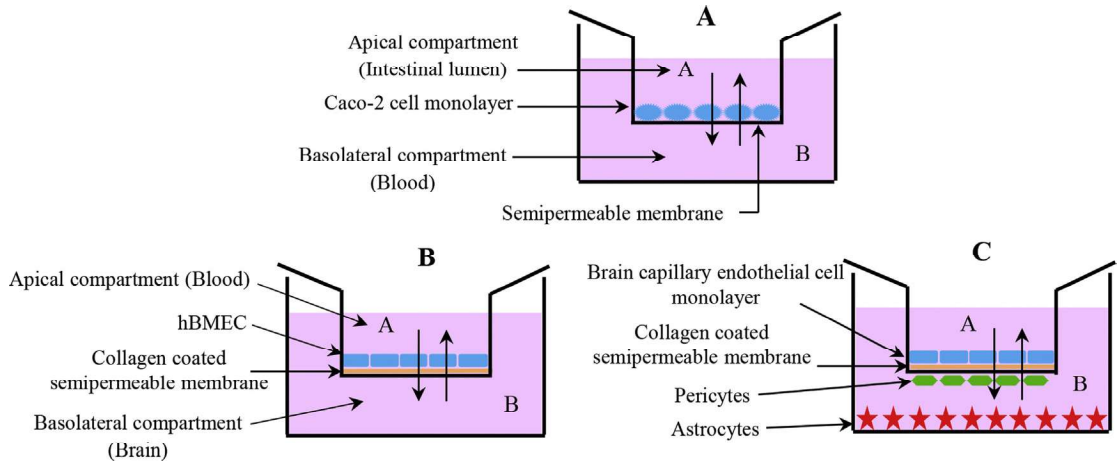

Fig. 4. General setup of permeability experiments. A) intestinal barrier model using Caco-2 cells in 6-well plates; B) human monoculture BBB model using hBMEC cells in 24-well plates; C) rat triple co-culture BBB model using primary rat brain endothelial cells, pericytes and astrocytes in 24-well plates.

using LY as fluorescent integrity marker. Paracellular permeability was asessed with LY as fluorescent integrity marker, since NaF has been shown to be not suited for the Caco-2 cells [44].To assess the apical-to-basolateral permeability (A–B), 1.6 ml of test solution consisting of 20 μM analyte plus 10 μg/ml LY in HBSS was added to the apical side, and 2.8 ml HBSS was added to the basolateral side. For measurement of the basolateral-to-apical permeability (B–A), 2.8 ml of the above test solution was added to the basolateral side (pH 7.4 in both compartments). Samples (200 μl) were taken from both sides at four time points of 10, 30, 60, and 120 min. All experiments were performed in triplicate, on an orbital shaker at 100 rpm, and at 37 °C. The TEER was evaluated after the experiment to ensure that the monolayer was not disturbed during the screening. The fluorescent marker in the samples was quantified using a microplate reader (Chameleon, Hidex, Finland), and the analytes were quantified by UHPLC–MS/MS. The apparent permeability coefficient (P_{app}) for both analyte and fluorescent marker, and recovery (%) were calculated according to the following equations:

$$P_{app}(\mathrm{cm/s}) = V_B/(AC_{A0}) \times (\Delta C_B/\Delta t)$$

$$Recovery(\%) = (C_{Af}V_A + C_{Bf}V_B)/(C_{A0}V_A) \times 100$$

where V_A and V_B are the volumes in the donor and receiver compartments, respectively, A is the surface area of the filter membrane, C_{A0} is the initial concentration in the donor compartment, $\Delta C_B/\Delta t$ is the change of concentration over time in the receiver compartment, and C_{Af} and C_{Bf} are the final concentrations of the compound in the donor and receiver compartments, respectively.

Efflux ratio (ER) was calculated as the ratio of P_{appB-A} to P_{appA-B}. A compound with a ratio greater than 2.0 is qualified as a substrate of the efflux mechanism [45].

$$ER = P_{appB-A}/P_{appA-B}$$

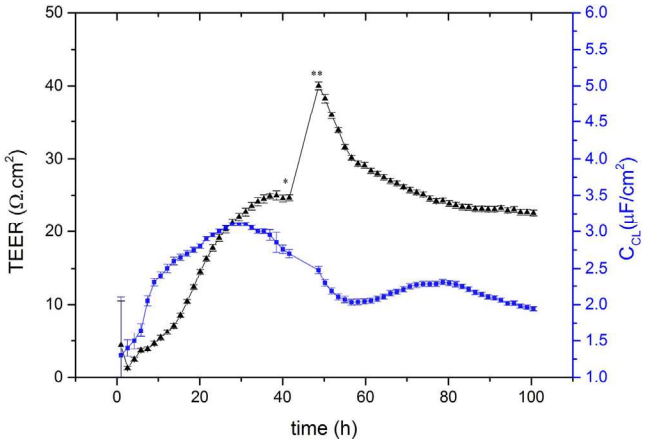

Fig. 5. Mean TEER values (▲) and C_{CL} values (■) for hBMEC cells grown on 24-well tissue culture inserts, with real-time recording in a CellZscope system. * Transfer of inserts to 24-well plate for permeability assay; ** transfer of inserts to CellZscope (37 °C) for a control of barrier integrity after the assay.

2.6. *In silico prediction of blood-brain barrier permeability*

Three-dimensional computer models of KMF and 4-HPAA were built in Maestro modeling environment (Maestro, version 9.3, Schrödinger, LLC, New York, NY, 2012), and the most favorable conformers were identified by the conformational search in MacroModel (MacroModel, version 9.9, Schrödinger, LLC, New York, NY, 2012) using the OPLS-2005 force-field, implicit solvent conditions (water), and 1000 iterations of the mixed serial/low mode sampling method. For each isomer, the conformers within 5 kcal/mol from the corresponding global minimum were used as input for the QikProp application (QikProp, version 3.5, Schrödinger, LLC, New York, NY, 2012), to evaluate various descriptors relevant for drug permeability. For comparison, the polar surface area (PSA) and the logarithm of partition coefficient (cLogP) descriptors were calculated also using the Calculator plugin of Chemaxon Marvin web-application (http://www.chemaxon.com/marvin/sketch/index.php, accessed on February 12, 2014) requiring only the 2D structural formula as input.

2.7. *Human* in vitro *BBB model*

We used an *in vitro* human model that had been previously established in our group, employing immortalized human brain microvascular endothelial cells (hBMEC cell line) [46–48]. Permeability screening was performed in 24-well plates. hBMEC cells of passages 20–25 were seeded at a density of 6.0×10^4 cells/cm^2 on the apical side of coated filter membranes of tissue culture inserts (Greiner Bio-one®, transparent PET membrane) to develop cell monolayers (Fig. 4B). Barrier tightness was calculated by real-time TEER measurements using a CellZscope system (NanoAnalytics, Germany). TEER values and cell layer capacitances (C_{CL}) were recorded every hour (Fig. 5). C_{CL} values in the range of 0.5–5.0 μF/cm^2 indicated cell confluency. After 44 h of incubation, TEER values of 26.6 ± 0.343 Ωcm^2 were reached, and the bidirectional permeability assays performed. Test solutions contained 5.0 μM analyte plus 10.0 μg/ml fluorescent marker (Na-F or LY) in RHB (pH 7.4). Samples were collected from apical and basolateral chambers at four time points of 10, 30, 60 and 120 min. All experiments were performed in triplicate, on an orbital shaker at

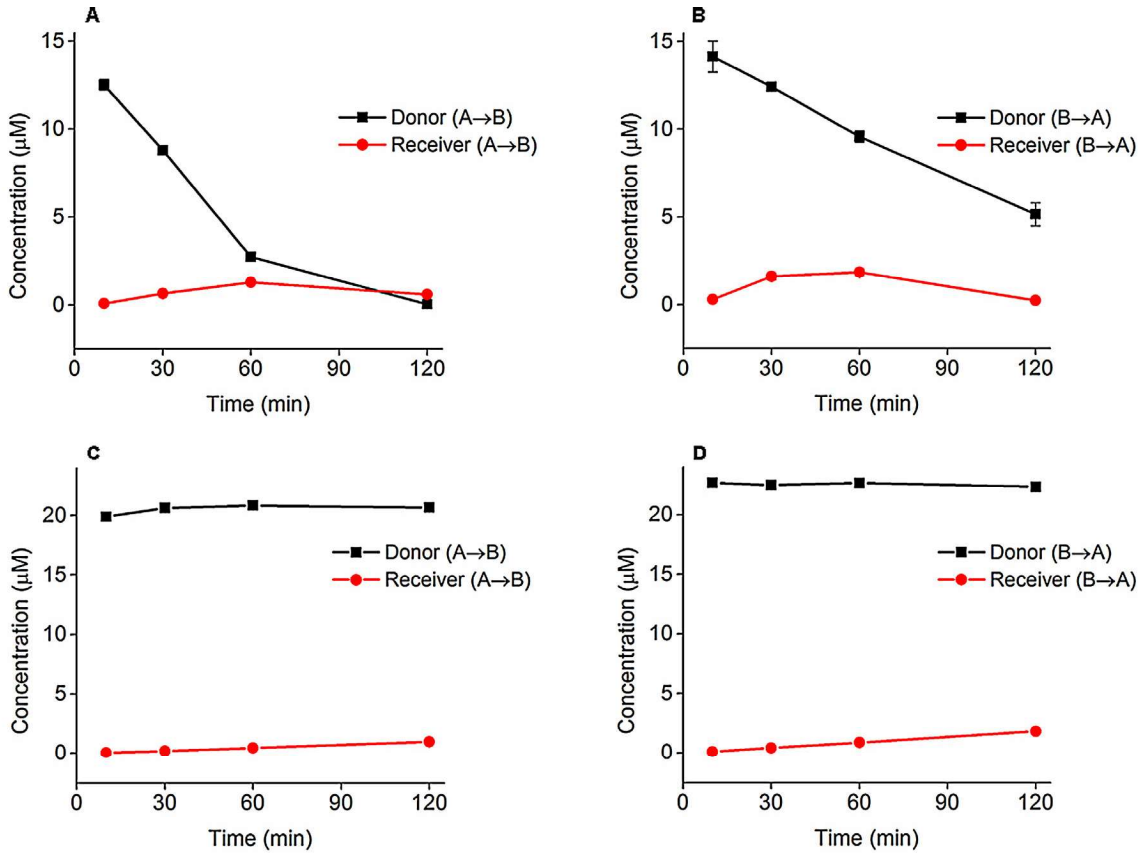

Fig. 6. Distribution of KMF (15 μM) and 4-HPAA (20 μM) in Caco-2 transport experiment; A) KMF was placed in apical compartment; B) KMF was placed in basolateral compartment; C) 4-HPAA was placed in the apical compartment; D) 4-HPAA was placed in the basolateral compartment.

100 rpm and 37 °C. The fluorescent markers in the samples were quantified with a microplate reader, and analytes were quantified by UHPLC–MS/MS. P_{app}, recovery (%) and ER were calculated as described in Section 2.5.

2.8. *Rat* in vitro *BBB model*

Primary brain microvessel endothelial cells (RBECs), glial cells and pericytes were isolated from Wistar rats as described earlier [47,49]. The primary triple co-culture BBB model based on these three cell types was used as previously described [47,50]. Briefly, to assemble the triple co-culture model the cell culture inserts (Greiner Bio-one®, transparent PET membrane) were put into 24-well plates (Greiner, Germany) containing glial cells at the bottom of the wells. Pericytes at passage number 3 were seeded to the bottom (abluminal) side of the inserts at a density of 1.5×10^4 cells/cm^2. RBECs were seeded to the upper side of the coated inserts (luminal) at a density of 7×10^4 cells/cm^2 (Fig. 4C). During the co-culture, the cell culture medium was supplemented with 550 nM HC [51]. One day before the permeability assay cells received CPT-cAMP (250 μM) and RO 201724 (17.5 μM) to tighten the intercellular junctions and elevate the resistance [52]. At a TEER value of 411.5 ± 21.8 Ωcm^2 (day 4 of co-culture), the permeability assay was performed in A–B and B–A directions. Working solutions contained 5.0 μM of KMF or 4-HPAA, plus Na-F as integrity marker (10.0 μg/ml) in RHB (pH 7.4) containing 0.1 % BSA. During the assay, the volumes in the apical and basolateral compartments were 300 μl and 700 μl, respectively. Test plates were incubated at 37 °C on a horizontal shaker at 100 rpm (Biosan, Latvia). Samples were collected from both apical and basolateral compartments after 60 min. Na-F was quantified with a fluorescent multiplate reader (Fluostar Optima, BMG Labtechnologies, Germany). Analyte concentrations were measured by UHPLC–MS/MS. P_{app}, recovery and ER were calculated as described in Section 2.5.

3. Results and discussion

3.1. *Method validation*

The fundamental parameters for a bioanalytical method validation are accuracy, precision, specificity, selectivity, sensitivity, repeatability, reproducibility, short-term and long-term stabilities. FDA/EMA guidances [41,42] stipulate that for all validation tests imprecision expressed by the coefficient of variation (CV%) should not exceed 15% (20% for the LLOQ) of the nominal values for all levels, and that the inaccuracy, expressed as the relative error (RE%), has to be within ±15% (±20% for the LLOQ) of the nominal values for all levels. All acceptance criteria for calibration standards and quality control samples were fulfilled by the four methods used.

Quantification range for KMF and 4-HPAA in RHB was 20.0–2000 ng/ml, and the calibration curves were fitted by least-squares quadratic regression with $1/X^2$ as weighing factor. The mean coefficient of determination (R^2) of the standard curve for KMF was 0.995, and 0.997 for 4-HPAA (Supporting Information, Tables S1 and S3). The curves met all the acceptance criteria of the international guidelines [29,30]. Calibration curves of KMF and 4-HPAA in HBSS were obtained by partial validation based on the method in RHB. Calibration curves were fitted by least-squares quadratic regression with weighing factor of $1/X^2$. R^2 of the standard curve was 0.997 for KMF, and 0.993 for 4-HPAA (Tables S2 and S4).

Within- and between-series impressions (CV%) of KMF in RHB were less than 5.86% of the nominal values at five QC levels. The inaccuracy (RE%) was between −3.46% and 10.2%, confirming both repeatability and reproducibility of the method (Table S5). Within and between-series imprecision (CV%) of 4-HPAA in RHB for the five QC levels was less than 5.27%, and inaccuracy (RE%) was within −6.23 to 2.93% of the nominal values (Table S6), and thus met the acceptance criteria for a validated method.

The mean carry-over of KMF was below 10.4% (<20% at LLOQ) and that of the IS ($^{13}C_{15}$-KMF) was less than 0.0866% (<5% of the signal at LLOQ) in both RHB and HBSS (Fig. 2, Tables S7 and S8). No carry-over of 4-HPAA and VA (IS) was detected in both buffers (Fig. 3, Tables S9 and S10). Hence, the carry-over did not impact the results [29,30].

Selectivity imprecision (CV%) for the six samples of KMF (duplicates, 3 different buffer batches) at the LLOQ was 9.82% in RHB, and 5.00% in HBSS (<20%). The inaccuracy (RE%) was −4.04% and 5.03% (within ±20%), respectively, indicating both methods were selective (Table S11). The quantification method of 4-HPAA was also shown to be selective in both RHB (CV% = 1.67%, RE% = −3.84%) and HBSS (CV% = 2.99%, RE% = 13.1%) (Table S11). Moreover, no peak area was present in the blank samples of RHB and HBSS (duplicates, 3 batches) for both KMF and 4-HPAA (data not shown), demonstrating that both methods were specific.

The absolute recovery of KMF from RHB was 56.7% at QCL, 58.1% at QCM, and 54.7% at QCH. An extraction yield of 70.4% was calculated for the IS ($^{13}C_{15}$-KMF) (Table S12). Absolute recovery of KMF from HBSS was 62.2% at QCL, 79.6% at QCM, and 84.6% at QCH, while 72.8% of the IS was recovered (Table S13).

Extraction recoveries of 4-HPAA from RHB at three levels of low, medium and high concentration were 89.8%, 96.4% and 95.3%, respectively. Recovery of the IS (VA) was 97.6% (Table S14). Absolute recoveries of 4-HPAA from HBSS were 77.0% at QCL, 88.4% at QCM, and 95.1% at QCH, while extraction yield of the IS was 101.3% (Table S15). No major variation of extraction was identified among the three levels of QCs samples.

Dilution tests for KMF and 4-HPAA in RHB and HBSS were carried out at two dilution levels (10 and 100 fold). The CV% for each QC series of the two analytes was below 15%, and the RE% was within ±15% of the nominal values (Tables S16 and S17). As a result, dilutions up to 100 fold did not impact precision and accuracy of all methods.

RHB and HBSS samples of KMF and 4-HPAA (QCL and QCH) were stable for up to 4 h at RT (Tables S18 and S19). The freeze-thaw stability of KMF in RHB was confirmed for two cycles. Stability of KMF in HBSS (QCL and QCH), and of 4-HPAA in both RHB and HBSS was established for three cycles (Tables S18 and S19). Processed samples of KMF (QCL and QCH) were stable in the autosampler (10 °C, protected from light) for up to 72 h, while those of 4-HPAA were stable for at least 156 h (Tables S18 and S19).

Long term stability test was performed after two weeks of storage below −65 °C for KMF. The results of t_{test} were plotted as a function of t_0, and a linear regression was performed. The slope of the calculated linear regression was 0.962 for RHB, and 0.974 for HBSS (Figs. S1 and S2), demonstrating the stability of the samples (acceptance criteria: 1.00 ± 0.15). Samples of 4-HPAA in both RHB and HBSS were stable for at least three weeks, as the slopes were 0.965 and 0.919, respectively (Figs. S3 and S4).

A stock solution of KMF stored below −65 °C was stable for at least 180 days, since the degradation expressed by the difference percentage was −3.13% (acceptance criteria: below 5%) (Table S20). Stock solution of 4-HPAA was stable for at least 35 days (degradation = 0.74%), and that of vanillic acid was stable for at least 190 days (degradation = 3.81%) (Tables S21 and S22).

3.2. *Intestinal barrier permeability assays*

Intestinal permeability of KMF was studied in Caco-2 cells, whereby bidirectional transport was assessed (apical to basolateral (A–B), and basolateral to apical (B–A)). Samples were taken

Table 2
Permeability data of KMF and 4-HPAA in the Caco-2 model (n = 3).

Analyte	Transport direction	Ät (min)	P_{app} of analyte ± SEM ($\times 10^{-6}$ cm/s)	Efflux ratio	Recovery ± SEM (%)	P_{app} of LY ($\times 10^{-6}$ cm/s)
KMF	A → B	10	4.83 ± 1.67		81.5 ± 1.94	0.937
		30	12.9 ± 1.70		64.7 ± 0.257	2.03
		60	11.9 ± 0.371		34.4 ± 1.93	2.14
		120	2.48 ± 0.199		8.68 ± 0.643	1.65
	B → A	10	11.2 ± 2.39	[a]	92.6 ± 4.03	2.19
		30	17.1 ± 1.27	[a]	86.0 ± 0.458	3.21
		60	8.45 ± 0.607	[a]	67.9 ± 2.11	2.94
		120	0.46 ± 0.125	[a]	34.0 ± 2.69	2.77
4-HPAA	A → B	10	–		87.6 ± 0.794	3.25
		30	2.45 ± 0.209		92.2 ± 0.341	2.51
		60	2.84 ± 0.170		95.7 ± 0.982	2.15
		120	2.58 ± 0.0921		100 ± 0.850	1.73
	B → A	10	–	–	100 ± 0.547	5.40
		30	2.98 ± 0.350	1.22	107 ± 0.757	3.16
		60	2.72 ± 0.312	0.955	101 ± 0.663	4.06
		120	2.35 ± 0.240	0.910	101 ± 1.72	3.93

[a] Not calculated due to changes in recovery rates.

Table 3
Permeability data of KMF and 4-HPAA obtained in the hBMEC BBB model (n = 3).

Analyte	Transport direction	Ät (min)	P_{app} of analyte ± SEM ($\times 10^{-6}$ cm/s)	Efflux ratio	Recovery ± SEM (%)	P_{app} of LY/Na-F[a] ($\times 10^{-6}$ cm/s)
KMF	A → B	10	–		99.1 ± 5.31	8.70
		30	34.4 ± 0.00		99.8 ± 7.17	7.40
		60	34.4 ± 4.12		102 ± 3.49	5.93
		120	34.0 ± 3.62		100 ± 1.48	5.94
	B → A	10	–	–	91.2 ± 6.41	4.35
		30	16.2 ± 0.728	0.594	102 ± 2.76	4.26
		60	23.0 ± 0.970	0.604	107 ± 7.47	5.77
		120	28.0 ± 2.15	0.894	105 ± 0.27	5.06
4-HPAA	A → B	10	–		108 ± 0.896	7.66
		30	–		105 ± 0.495	4.73
		60	–		84.7 ± 4.27	7.49
		120	8.32 ± 0.108		92.6 ± 1.68	6.50
	B → A	10	–	–	109 ± 0.441	6.59
		30	14.8 ± 0.610	–	106 ± 0.882	6.33
		60	7.13 ± 1.23	–	109 ± 3.10	7.20
		120	7.23 ± 0.601	0.869	106 ± 0.358	7.26

[a] LY was the low permeability reference compound for KMF assays; NaF was the reference compound for 4-HPAA assays.

at four time points (10, 30, 60, 120 min) (Fig. 6). When KMF was applied on the apical side (Fig. 6A), the concentration in the donor compartment decreased rapidly, while only a fraction of the compound appeared in the receiver compartment. A similar behavior was seen when the transport was performed in B–A direction (Fig. 6B). A–B permeation of KMF was detected after 10 min, as P_{appA-B} of KMF at t_{10} ($4.83 \pm 1.67 \times 10^{-6}$ cm/s) showed significant difference compared to that of low permeability reference compound LY (0.937×10^{-6} cm/s) (Table 2). The permeability rate increased to $12.9 \pm 1.70 \times 10^{-6}$ cm/s after 30 min. However, recovery of KMF gradually decreased during the experiment (from 81.5% at t_{10} to 8.68% at t_{120}). According to previous studies, flavonoids undergo phase 2 metabolism (sulfation and glucuronidation) in Caco-2 cells [28,40]. Therefore, the low recovery of KMF in this assay was possibly due to formation of these polar metabolites upon cellular uptake. Permeation of KMF in the reverse direction (B–A) followed a similar pattern, with a fast permeation detected after 10 min ($P_{appB-A} = 11.2 \pm 2.39 \times 10^{-6}$ cm/s) (Table 2). KMF showed some permeation as compared to the bidirectional permeability of LY (Papp from 0.937 to 3.21×10^{-6} cm/s).

Apparent permeability of 4-HPAA in A–B direction (Fig. 6C) was below 2.84×10^{-6} cm/s, while P_{appA-B} of LY was between 1.73×10^{-6} and 3.25×10^{-6} cm/s (Table 2). The permeability rate of 4-HPAA in the B–A direction (Fig. 6D) was between 2.35×10^{-6} and 2.98×10^{-6} cm/s. Compared to integrity marker LY, permeation of 4-HPAA was very low. The efflux ratio was below 2.0, and indicated absence of active transport processes in the net flux of the compound. Recovery of 4-HPAA was >87.6% in all experiments (Table 2).

3.3. *In silico prediction of blood-brain barrier permeability*

Physico-chemical properties of compounds were calculated for the 32 low energy conformers of KMF and the 3 low energy conformers of 4-HPAA, and averaged (Table S23). The data indicated that kaempferol fulfilled criteria for a good oral availability as defined by Lipinski (rule of 5) [53] and Veber [54]. The PSA of KMF (QikProp: 119 Å^2, Marwin: 107 Å^2) was somewhat above the upper limit of 90 Å^2 for BBB permeation [55]. However, the chromone carbonyl forms intramolecular hydrogen bonds with the two adjacent hydroxyl groups at C-3 and C-5, and thus lowers their effective contribution to PSA. At physiological pH (7.4) kaempferol is available to some 50% in the neutral form (experimental pKa 7.49 [56]). Therefore, it can be assumed that KMF can passively permeate across the BBB. Calculated data for 4-HPAA were indicative of good oral bioavailability, as defined by Lipinski (rule of 5) [53] and Veber [54].

Table 4
Permeability data of KMF and 4-HPAA obtained in the rat triple co-culture BBB model (n = 4).

Analyte	Transport direction	Ät (min)	P_{app} of analyte ± SEM ($\times 10^{-6}$ cm/s)	Efflux ratio	Recovery ± SEM (%)	P_{app} of NaF ($\times 10^{-6}$ cm/s)
KMF	A → B	60	28.0 ± 2.00		84.6 ± 2.4	0.55
	B → A	60	18.3 ± 0.737	0.670	91.4 ± 1.0	0.30
4-HPAA	A → B	60	–		78.8 ±1.0	1.68
	B → A	60	–	–	82.7 ± 1.3	0.55

However, given that the compound is negatively charged at physiological pH (experimental pKa = 4.25 [57]), the BBB permeation of 4-HPAA may be limited.

3.4. *Human* in vitro *BBB model*

Permeation of KMF from apical to basolateral (A–B) was detected after 30 min. The permeation rate was not time dependent, as P_{appA-B} of KMF remained at approx. 34×10^{-6} cm/s between t_{30} and t_{120} (Table 3). Compared to the integrity marker LY (P_{app} = 5.93–8.70 $\times 10^{-6}$ cm/s), KMF showed significantly higher permeability. The permeation rate of KMF in the B–A direction gradually increased from min 30 ($P_{appB-A} = 16.2 \pm 0.728 \times 10^{-6}$ cm/s) to min 120 ($P_{appB-A} = 28.0 \pm 2.15 \times 10^{-6}$ cm/s). The efflux ratio was below 2.0 and thus was not indicative of an active efflux mediated transport [50]. The recovery was above 91.2% in all experiments (Table 3).

Permeation of 4-HPAA in the A–B direction was detected after 120 min ($P_{appA-B} = 8.32 \pm 0.108 \times 10^{-6}$ cm/s), as concentrations from earlier time points were below the LLOQ (20.0 ng/ml). This was comparable to the Papp value of NaF (6.50×10^{-6} cm/s) and, considering the low TEER values (Fig. 5), we can conclude for no permeation of 4-HPAA. The highest B–A permeability was detected after 30 min ($P_{appB-A} = 14.8 \pm 0.610 \times 10^{-6}$ cm/s). The efflux ratio was below 2, suggesting no involvement of active transport [50]. Recovery of 4-HPAA was above 84.7%, and P_{app} of Na-F during the entire experiment was between 4.73 and 7.66×10^{-6} cm/s (Table 3).

3.5. *Rat* in vitro *BBB model*

The triple co-culture rat BBB model [58] showed high barrier tightness, with a TEER value of 411.5 ± 21.8 Ωcm^2 and a $P_{appA \rightarrow B}$ $0.77 \pm 0.62 \times 10^{-6}$ cm/s for Na-F. Permeability of KMF from apical to basolateral was $28.0 \pm 2.00 \times 10^{-6}$ cm/s, while that of Na-F was 0.55×10^{-6} cm/s (Table 4). P_{appB-A} of KMF was $18.3 \pm 0.737 \times 10^{-6}$ cm/s, and P_{appB-A} of Na-F was 0.30×10^{-6} cm/s. Compared to the flux of the integrity marker Na-F, KMF showed considerably higher permeability in the rat BBB model. These results are in line with the data from the human BBB model. Recovery of KMF in this experiment was above 84.6%. The efflux ratio was 0.670 (<2) and indicated absence of active efflux mediated transport (Table 4).

After the 60 min bidirectional transport study, concentrations of 4-HPAA in the receiver compartments were all below the LLOQ (20.0 ng/ml). This was indicative of no permeation of 4-HPAA in the rat BBB model, given that the recovery of the compound was >78.8%, and the P_{app} of Na-F between 0.55 and 1.68×10^{-6} cm/s (Table 4). The P_{app} values for Na-F indicating the barrier integrity, also showed absence of toxicity for the tested analyte at 5 μM.

4. Conclusion

UHPLC–MS/MS methods for quantification of KMF and its major metabolite, 4-HPAA, were developed and fully validated in two transport buffers (RHB and HBSS). Validation was performed according to EMA and FDA guidelines [41,42], and the methods were then used for *in vitro* studies in established models for intestinal and BBB permeability. KMF was found to cross the intestinal barrier and the BBB models to a certain extent, while 4-HPAA showed no permeation. KMF showed decreasing recovery in the Caco-2 model (from 81.5% at t_{10} to 8.68% at t_{120}). This suggests that KMF undergoes extensive metabolism that would result in poor bioavailability after oral administration.

The data obtained with the rat BBB model correlated with those from the human BBB model, and *in vitro* permeability of KMF was in accord with *in silico* predictions. However, *in silico* data of 4-HPAA did not correlate with the results from *in vitro* permeability assays. 4-HPAA is negatively charged at physiological pH (n.b. calculated logD7.4 = −1.86), and the lacking permeation in both *in vitro* BBB models might be due to a high desolvation and protonation penalty of the carboxyl group (required for entering the lipophilic environment of the plasma membrane).

The fact that i.p. application of 4-HPAA in mice induced behavioral changes [24] despite poor BBB permeability may have several explanations: First, 4-HPAA may act indirectly, e.g. via involvement of the gut-brain axis [59,60]. Second, metabolites of 4-HPAA may be responsible for the observed activity. 4-HPAA can be further metabolized by the colonic microflora into *p*-hydroxybenzoic acid, phenylacetic acid, and 4-methoxyphenylacetic acid [21,61]. Finally, *in vitro* models do not fully mimic an *in vivo* situation, since important differences exist, e.g. the lack of blood flow, and lower surface area in the *in vitro* models. These differences are particularly relevant for compounds with a rapid turnover rate [62].

Author contributions

Conceived the study: VB and MH. Conceived and designed the experiments: FM, FRW, MAD, MS, MH, and MO. Performed the experiments: FM, VZ, FRW, MS and MO. Analyzed the data: FM, FRW, MAD, MS, MH and MO. Contributed reagents/materials/analysis tools: FM, FRW, MAD, MS, MH, and MO. Wrote the paper: FM, FRW, MAD, MS, MO, VB and MH.

Acknowledgements

FM is grateful for the 2012 Dr. Willmar Schwabe Scholarship for Young Scientists of the Society of Medicinal Plant and Natural Product Research (GA). Financial support was provided by the Swiss National Science Foundation (project 105320_126888). Thanks are due to Prof. Georgios Imanidis for provision of Caco-2 cells, and to Ursula Thormann, Evelyn Jähne, and Daniela Eigenmann for providing training and support with the cell culture models. Orlando Fertig is acknowledged for technical assistance.

Appendix A. Supplementary data

Supplementary data associated with this article can be found, in the online version, at http://dx.doi.org/10.1016/j.jpba.2016.05.039.

References

[1] C.A. Rice-Evans, L. Packer, Flavonoids in Health and Disease, second ed., Marcel Dekker, Inc., New York, 2003.
[2] J.B. Harborne, C.A. Williams, Advances in flavonoid research since 1992, Phytochemistry 55 (2000) 481–504.
[3] R. Gu, Y. Wang, B. Long, E. Kennelly, S. Wu, B. Liu, P. Li, C. Long, Prospecting for bioactive constituents from traditional medicinal plants through ethnobotanical approaches, Biol. Pharm. Bull. 37 (2014) 903–915.
[4] D.F. Birt, S. Hendrich, W. Wang, Dietary agents in cancer prevention: flavonoids and isoflavonoids, Pharmacol. Therapeut. 90 (2001) 157–177.
[5] H. Chen, K. Yao, J. Nadas, A.M. Bode, M. Malakhova, N. Oi, H. Li, R.A. Lubet, Z. Dong, Prediction of molecular targets of cancer preventing flavonoid compounds using computational methods, PLoS One 7 (2012) e38261.
[6] N. Cook, S. Samman, Flavonoids-chemistry metabolism, cardioprotective effects, and dietary sources, J. Nutr. Biochem. 7 (1996) 66–76.
[7] M.A. Islam, R.W. Schmidt, S. Gunaseelan, A. Sanchez, An update on the cardiovascular effects of quercetin, a plant flavonoid, Curr. Nutr. Food Sci. 10 (2014) 36–48.
[8] M. Castell, F. Pérez-Cano, M. Abril-Gil, A. Franch, Flavonoids on allergy, Curr. Pharm. Des. 20 (2014) 973–987.
[9] K.J. Barnham, C.L. Masters, A.I. Bush, Neurodegenerative diseases and oxidative stress, Nat. Rev. Drug Discov. 3 (2004) 205–214.
[10] O. Grundmann, J.I. Nakajima, S. Seo, V. Butterweck, Anti-anxiety effects of *Apocynum venetum* L. in the elevated plus maze test, J. Ethnopharmacol. 110 (2007) 406–411.
[11] Z. Zhang-Jin, Therapeutic effects of herbal extracts and constituents in animal models of psychiatric disorders, Life Sci. 75 (2004) 1659–1699.
[12] E. Aguirre-Hernández, A. Martínez, M. González-Trujano, J. Moreno, H. Vibrans, M. Soto-Hernández, Pharmacological evaluation of the anxiolytic and sedative effects of *Tilia americana* L. var. mexicana in mice, J. Ethnopharmacol. 109 (2007) 140–145.
[13] S. Kumar, A. Sharma, Anti-anxiety activity studies of various extracts of *Turnera aphrodisiaca* Ward, J. Herb. Pharmacother. 5 (2005) 13–21.
[14] J.W. Jung, N.Y. Ahn, H.R. Oh, B.K. Lee, K.J. Lee, S.Y. Kim, J.H. Cheong, J.H. Ryu, Anxiolytic effects of the aqueous extract of *Uncaria rhynchophylla*, J. Ethnopharmacol. 108 (2006) 193–197.
[15] F. Chimenti, F. Cottiglia, L. Bonsignore, L. Casu, M. Casu, C. Floris, D. Secci, A. Bolasco, P. Chimenti, A. Granese, Quercetin as the active principle of *Hypericum hircinum* exerts a selective inhibitory activity against MAO-A: extraction, biological analysis, and computational study, J. Nat. Prod. 69 (2006) 945–949.
[16] B. Sloley, L. Urichuk, P. Morley, J. Durkin, J. Shan, P. Pang, R. Coutts, Identification of kaempferol as a monoamine oxidase inhibitor and potential neuroprotectant in extracts of *Ginkgo biloba* leaves, J. Pharm. Pharmacol. 52 (2000) 451–459.
[17] M. Marder, G. Estiú, L.B. Blanch, H. Viola, C. Wasowski, J.H. Medina, A.C. Paladini, Molecular modeling and QSAR analysis of the interaction of flavone derivatives with the benzodiazepine binding site of the GABA A receptor complex, Bioorgan. Med. Chem. 9 (2001) 323–335.
[18] J.H. Medina, H. Viola, C. Wolfman, M. Marder, C. Wasowski, D. Calvo, A.C. Paladini, Overview—flavonoids: a new family of benzodiazepine receptor ligands, Neurochem. Res. 22 (1997) 419–425.
[19] F. Wang, Y. Huen, S. Michael, S.Y. Tsang, H. Xue, Neuroactive flavonoids interacting with GABAA receptor complex, Curr. Drug Targets CNS Neurol. Disord. 4 (2005) 575–585.
[20] K. Keppler, E.M. Hein, H.U. Humpf, Metabolism of quercetin and rutin by the pig caecal microflora prepared by freeze-preservation, Mol. Nutr. Food Res. 50 (2006) 686–695.
[21] S. Labib, S. Hummel, E. Richling, H.U. Humpf, P. Schreier, Use of the pig caecum model to mimic the human intestinal metabolism of hispidulin and related compounds, Mol. Nutr. Food Res. 50 (2006) 78–86.
[22] M. Blaut, L. Schoefer, A. Braune, Transformation of flavonoids by intestinal microorganisms, Int. J. Vitam. Nutr. Res. 73 (2003) 79–87.
[23] L. Griffiths, G. Smith, Metabolism of myricetin and related compounds in the rat. Metabolite formation *in vivo* and by the intestinal microflora *in vitro*, Biochem. J. 130 (1972) 141–151.
[24] C. Vissiennon, K. Nieber, O. Kelber, V. Butterweck, Route of administration determines the anxiolytic activity of the flavonols kaempferol, quercetin and myricetin—are they prodrugs? J. Nutr. Biochem. 23 (2012) 733–740.
[25] L. Lindemann, M.C. Hoener, A renaissance in trace amines inspired by a novel GPCR family, Trends Pharmacol. Sci. 26 (2005) 274–281.
[26] A.A. Boulton, Some aspects of basic psychopharmacology: the trace amines, Prog. Neuro-Psychopharmacol. 6 (1982) 563–570.
[27] A.A. Boulton, B.A. Davis, H.Y. Peter, J.S. Wormith, D. Addington, Trace acid levels in the plasma and MAO activity in the platelets of violent offenders, Psychiatry Res. 8 (1983) 19–23.
[28] C.T. Dourish, B. Davis, L. Dyck, R. Jones, A. Boulton, Alterations in trace amine and trace acid concentrations in isolated aggressive mice, Pharmacol. Biochem. Behav. 17 (1982) 1291–1294.
[29] A. Juorio, P. McQuade, Effects of various antipsychotic drugs upon the striatal concentrations of para-hydroxyphenylacetic acid and meta-hydroxyphenylacetic acid in the mouse, Br. J. Pharmacol. 80 (1983) 581–585.
[30] W.M. Pardridge, Blood-brain barrier drug targeting: the future of brain drug development, Mol. Intervention 3 (2003) 90–105.
[31] J. Chen, H. Lin, M. Hu, Metabolism of flavonoids via enteric recycling: role of intestinal disposition, J. Pharmacol. Exp. Ther. 304 (2003) 1228–1235.
[32] M.R. Olthof, P.C. Hollman, T.B. Vree, M.B. Katan, Bioavailabilities of quercetin-3-glucoside and quercetin-4′-glucoside do not differ in humans, J. Nutr. 130 (2000) 1200–1203.
[33] Y. Konishi, Transepithelial transport of microbial metabolites of quercetin in intestinal caco-2 cell monolayers, J. Agr. Food Chem. 53 (2005) 601–607.
[34] K. Murota, S. Shimizu, S. Miyamoto, T. Izumi, A. Obata, M. Kikuchi, J. Terao, Unique uptake and transport of isoflavone aglycones by human intestinal caco-2 cells: comparison of isoflavonoids and flavonoids, J. Nutr. 132 (2002) 1956–1961.
[35] X.J. Tian, X.W. Yang, X. Yang, K. Wang, Studies of intestinal permeability of 36 flavonoids using caco-2 cell monolayer model, Int. J. Pharm. 367 (2009) 58–64.
[36] A. Faria, M. Meireles, I. Fernandes, C. Santos-Buelga, S. Gonzalez-Manzano, M. Dueñas, V. de Freitas, N. Mateus, C. Calhau, Flavonoid metabolites transport across a human BBB model, Food Chem. 149 (2014) 190–196.
[37] Y. Yang, L. Bai, X. Li, J. Xiong, P. Xu, C. Guo, M. Xue, Transport of active flavonoids, based on cytotoxicity and lipophilicity: an evaluation using the blood–brain barrier cell and caco-2 cell models, Toxicol. in vitro 28 (2014) 388–396.
[38] K.A. Youdim, M.Z. Qaiser, D.J. Begley, C.A. Rice-Evans, N.J. Abbott, Flavonoid permeability across an in situ model of the blood–brain barrier, Free Radic. Biol. Med. 36 (2004) 592–604.
[39] K.A. Youdim, M.S. Dobbie, G. Kuhnle, A.R. Proteggente, N.J. Abbott, C. Rice-Evans, Interaction between flavonoids and the blood–brain barrier: in vitro studies, J. Neurochem. 85 (2003) 180–192.
[40] R. Barrington, G. Williamson, R.N. Bennett, B.D. Davis, J.S. Brodbelt, P.A. Kroon, Absorption conjugation and efflux of the flavonoids, kaempferol and galangin, using the intestinal CaCo-2/TC7 cell model, J. Funct. Foods 1 (2009) 74–87.
[41] C. FDA, Guidance for Industry: Bioanalytical Method Validation. US Department of Health and Human Services, In, Food and Drug Administration, Center for Drug Evaluation and Research (CDER), Center for Veterinary Medicine (CV), 2001.
[42] EMA, Guideline on bioanalytical method validation, in, European Medicines Agency (EMEA/CHMP/EWP/192217/2009), London, 2011.
[43] S.B. Kapitza, B.R. Michel, P. van Hoogevest, M.L. Leigh, G. Imanidis, Absorption of poorly water soluble drugs subject to apical efflux using phospholipids as solubilizers in the caco-2 cell model, Eur. J. Pharm. Biopharm. 66 (2007) 146–158.
[44] Y. Konishi, K. Hagiwara, M. Shimizu, Transepithelial transport of fluorescein in caco-2 cell monolayers and use of such transport in vitro evaluation of phenolic acid availability, Biosci. Biotech. Biochem. 66 (2002) 2449–2457.
[45] M. Kanaan, Y. Daali, P. Dayer, J. Desmeules, Uptake/efflux transport of tramadol enantiomers and O-desmethyl-tramadol: focus on P-glycoprotein, Basic Clin. Pharmacol. 105 (2009) 199–206.
[46] D.E. Eigenmann, G. Xue, K.S. Kim, A.V. Moses, M. Hamburger, M. Oufir, Comparative study of four immortalized human brain capillary endothelial cell lines, hCMEC/D3, hBMEC, TY10, and BB19 and optimization of culture conditions, for an in vitro blood–brain barrier model for drug permeability studies, Fluids Barriers CNS 10 (2013) 1–17.
[47] E.A. Jähne, D.E. Eigenmann, M. Culot, R. Cecchelli, F.R. Walter, M.A. Deli, R. Tremmel, G. Fricker, M. Smiesko, M. Hamburger, M. Oufir, Development and validation of a LC–MS/MS method for assessment of an anti-inflammatory indolinone derivative by in vitro blood-brain barrier models, J. Pharm. Biomed. Anal. 98 (2014) 235–246.
[48] D.E. Eigenmann, E.A. Jähne, M. Smiesko, M. Hamburger, Mouhssin Oufir, Validation of an immortalized human (hBMEC) in vitro blood-brain barrier model, Anal. Bioanal. Chem. 8 (2016) 2095–2107.
[49] S. Veszelka, A.E. Tóth, F.R. Walter, Z. Datki, E. Mózes, L. Fülöp, Z. Bozsó, É. Hellinger, M. Vastag, B. Orsolits, Docosahexaenoic acid reduces amyloid-β induced toxicity in cells of the neurovascular unit, J. Alzheimers Dis. 36 (2013) 487–501.
[50] S. Nakagawa, M.A. Deli, H. Kawaguchi, T. Shimizudani, T. Shimono, A. Kittel, K. Tanaka, M. Niwa, A new blood–brain barrier model using primary rat brain endothelial cells, pericytes and astrocytes, Neurochem. Int. 54 (2009) 253–263.
[51] N. Perriere, P. Demeuse, E. Garcia, A. Regina, M. Debray, J.P. Andreux, P. Couvreur, J.M. Scherrmann, J. Temsamani, P.O. Couraud, Puromycin-based purification of rat brain capillary endothelial cell cultures. Effect on the expression of blood–brain barrier-specific properties, J. Neurochem. 93 (2005) 279–289.
[52] M.A. Deli, C.S. Ábrahám, Y. Kataoka, M. Niwa, Permeability studies on in vitro blood–brain barrier models: physiology, pathology, and pharmacology, Cell. Mol. Neurobiol. 25 (2005) 59–127.
[53] C.A. Lipinski, F. Lombardo, B.W. Dominy, P.J. Feeney, Experimental and computational approaches to estimate solubility and permeability in drug discovery and development settings, Adv. Drug Deliv. Rev. 64 (2012) 4–17.
[54] D.F. Veber, S.R. Johnson, H.Y. Cheng, B.R. Smith, K.W. Ward, K.D. Kopple, Molecular properties that influence the oral bioavailability of drug candidates, J. Med. Chem. 45 (2002) 2615–2623.
[55] H. van de Waterbeemd, G. Camenisch, G. Folkers, J.R. Chretien, O.A. Raevsky, Estimation of blood-brain barrier crossing of drugs using molecular size and shape, and H-bonding descriptors, J. Drug Targeting 6 (1998) 151–165.

[56] I. Matei, C. Tablet, S. Ionescu, M. Hillebrand, Close-lying pKa values of kaempferol determined by second-derivative synchronous fluorescence, Rev. Roum. Chim. 59 (2014) 401–405.
[57] R.M. Smith, A.E. Martell, Critically selected stability constants of metal complexes, NIST Stand. Reference Database 46 (2004) 8.
[58] M. Ott, M. Huls, M.G. Cornelius, G. Fricker, St. John's wort constituents modulate P-glycoprotein transport activity at the blood-brain barrier, Pharm. Res. 27 (2010) 811–822.
[59] J.A. Foster, K.A. McVey Neufeld, Gut–brain axis: how the microbiome influences anxiety and depression, Trends Neurosci. 36 (2013) 305–312.
[60] S. Reardon, Gut-brain link grabs neuroscientists, Nature 515 (2014) 175–177.
[61] A. Serra, A. Macià, M.P. Romero, J. Reguant, N. Ortega, M.J. Motilva, Metabolic pathways of the colonic metabolism of flavonoids (flavonols, flavones and flavanones) and phenolic acids, Food Chem. 130 (2012) 383–393.
[62] M.L. Chen, G.L. Amidon, L.Z. Benet, H. Lennernas, L.X. Yu, The BCS BDDCS, and regulatory guidances, Pharm. Res. 28 (2011) 1774–1778.

Supporting Information

Journal of Pharmaceutical and Biomedical Analysis

Validation of UHPLC-MS/MS methods for the determination of kaempferol and its metabolite 4-hydroxyphenyl acetic acid, and application to *in vitro* blood-brain barrier and intestinal drug permeability studies

Fahimeh Moradi-Afrapoli[a,b], Mouhssin Oufir[a], Fruzsina R. Walter[c], Maria A. Deli[c], Martin Smiesko[d], Volha Zabela[a], , Veronika Butterweck[e,f], and Matthias Hamburger[a*]

[a]Pharmaceutical Biology, Department of Pharmaceutical Sciences, University of Basel, Klingelbergstrasse 50, 4056 Basel, Switzerland

[b]Department of Pharmacognosy, Faculty of Pharmacy, Mazandaran University of Medical Sciences, Sari, Iran

[c]Institute of Biophysics, Biological Research Centre, Hungarian Academy of Sciences, Temesvari krt 62, 6726 Szeged, Hungary

[d]Division of Molecular Modeling, Department of Pharmaceutical Sciences, University of Basel, Klingelbergstrasse 50, 4056 Basel, Switzerland

[e]Department of Pharmaceutics, College of Pharmacy, University of Florida, 1345 Gainesville, Florida, USA

[f]School of Life Sciences Institute for Pharma Technology, Gründenstrasse 40,CH- 4132 Muttenz, Switzerland

*corresponding author: Prof. Matthias Hamburger, Institute of Pharmaceutical Biology, Department of Pharmaceutical Sciences, University of Basel, Klingelbergstrasse 50, CH-4056 Basel, Switzerland, Phone: +41-61-267-1425 Fax: +41-61-267-1474
E-Mail: matthias.hamburger@unibas.ch

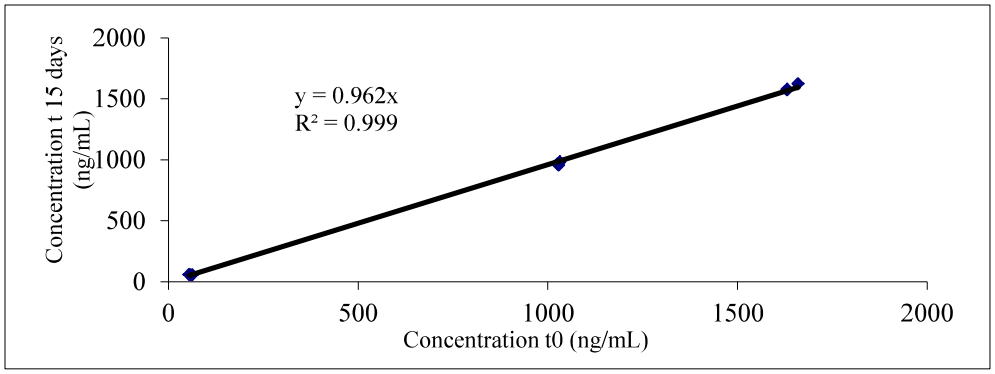

Figure S1: Long-term stability of KMF in RHB for 15 days below -65°C.

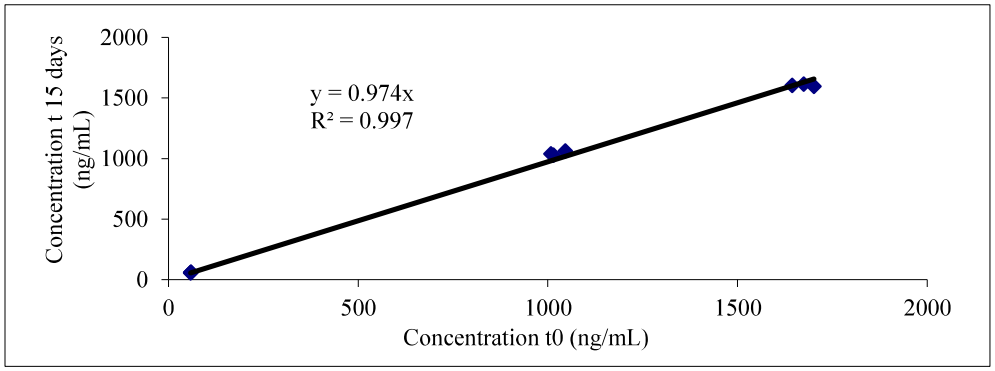

Figure S2: Long-term stability of KMF in HBSS for 15 days below -65°C.

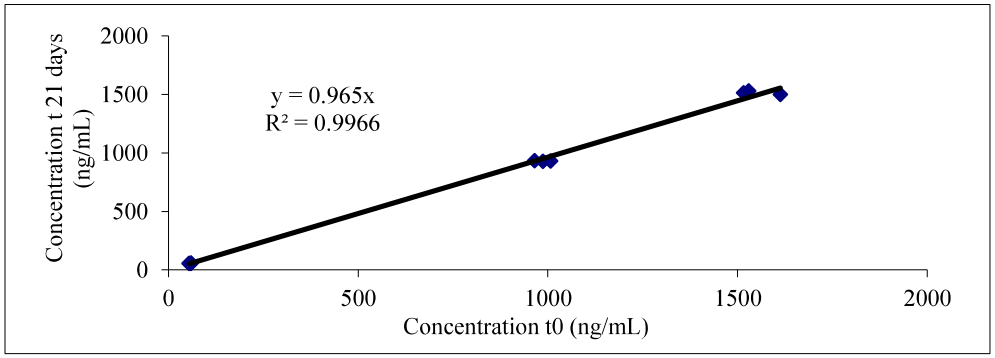

Figure S3: Long-term stability of 4-HPAA in RHB for 21 days below -65°C.

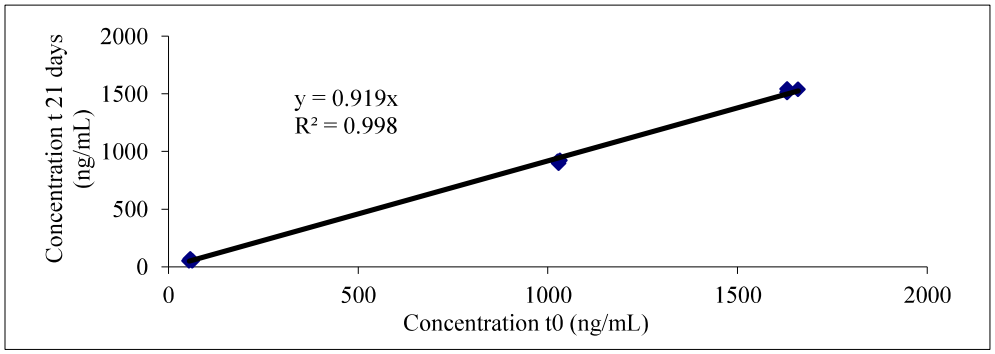

Figure S4: Long-term stability of 4-HPAA in HBSS for 21 days below -65°C

Table S1: Calibrators and calibration curve parameters for the determination of KMF in RHB. Response: A × Conc.^{2} + B × Conc. + C, Quadratic regression, $1/X^2$ weighting

Run No.	Nominal concentration (ng/mL)							Regression parameters			
	20.0	**50.0**	**100**	**250**	**500**	**1000**	**2000**	**A**	**B**	**C**	**R^2**
1	18.4	48.3	96.8	252	492	1065	1942	0.236	3.48	-0.0265	0.994
	22.7	45.3	99.9	247	521	1083	1921				
2	19.2	48.0	91.6	249	529	1082	1912	0.0954	3.98	-0.0219	0.994
	21.8	48.4	92.8	248	534	1074	1900				
3	19.3	44.7	97.4	251	542	1033	1959	0.291	3.44	-0.00520	0.995
	22.1	47.1	94.7	254	530	1018	1944				
4	20.7	48.0	93.9	237	538	1033	1917	0.0413	3.71	0.0113	0.996
	20.1	49.1	96.0	244	555	1050	1943				
Mean	20.6	47.4	95.4	247	530	1054	1929	0.166	3.65	-0.0106	0.995
S.D.	1.55	1.58	2.69	5.50	18.3	24.6	20.0	0.117	0.249		
CV%	7.54	3.33	2.82	2.22	3.45	2.34	1.04				
RE%	2.79	-5.28	-4.62	-0.953	6.00	5.47	-3.51				

Table S2: Calibrators and calibration curve parameters for the determination of KMF in HBSS. Response: A × Conc.^{2} + B × Conc. + C, Quadratic regression, $1/X^2$ weighting

Run No.	Nominal concentration (ng/mL)							Regression parameters			
	20.0	**50.0**	**100**	**250**	**500**	**1000**	**2000**	**A**	**B**	**C**	**R^2**
1	21.1	50.2	98.9	244	530	996	2001	0.000000485	0.00864	-0.0429	0.998
	19.4	46.5	99.8	249	521	1083	1974				
2	20.1	46.0	99.0	241	489	996	1981	0.000000795	0.00839	-0.0504	0.998
	20.3	51.6	106	253	531	1037	1981				
3	20.7	48.0	93.9	237	538	1033	1917	0.0413	3.71	0.0113	0.996
	20.1	49.1	96.0	244	555	1050	1943				
Mean	20.3	48.6	99.0	244	527	1032	1966	0.0138	1.24	-0.0273	0.997
S.D.	0.587	2.17	4.27	5.68	21.9	33.3	30.3	0.0238	2.14		
CV%	2.89	4.47	4.31	2.32	4.16	3.23	1.54				
RE%	1.47	-2.89	-1.00	-2.20	5.42	3.23	-1.69				

Table S3: Calibrators and calibration curve parameters for the determination of 4-HPAA in RHB.

Response: A × Conc.^{2} + B × Conc. + C, Quadratic regression, 1/X^2 weighting

Run No.	Nominal concentration (ng/mL)							Regression parameters			
	20.0	**50.0**	**125**	**250**	**500**	**1000**	**2000**	**A**	**B**	**C**	**R^2**
1	21.3	47.7	122	256	513	985	1943	0.855	6.54	-0.0113	0.997
	19.6	46.2	128	253	529	972	2056				
2	18.1	*41.2	115	250	512	1013	2013	0.776	8.76	-0.0221	0.998
	22.7	45.6	126	261	534	998	1938				
3	21.3	43.7	124	257	527	1066	1945	1.26	8.40	0.0431	0.996
	20.5	45.6	115	257	532	1029	1925				
Mean	20.6	45.8	122	255	524	1010	1970	0.966	7.90	-0.0255	0.997
S.D.	1.61	1.40	5.49	3.86	9.78	33.6	52.3	0.262	1.19		
CV%	7.83	3.07	4.51	1.51	1.87	3.33	2.66				
RE%	2.85	-8.47	-2.57	2.23	4.90	1.05	-1.50				

* value outside acceptance criteria (>15%), not used in calculations

Table S4: Calibrators and calibration curve parameters for determination of 4-HPAA in HBSS.

Response: A × Conc.^{2} + B × Conc. + C, Quadratic regression, 1/X^2 weighting

Run No.	Nominal Concentration (ng/mL)							Regression parameters			
	20.0	**50.0**	**100**	**250**	**500**	**1000**	**2000**	**A**	**B**	**C**	**R^2**
1	23.9	51.7	117	237	505	958	1807	0.000000458	0.00228	-0.0175	0.986
	16.3	*37.6	115	254	542	1115	2113				
2	19.4	50.0	121	239	479	948	1936	0.0000000132	0.00412	-0.00895	0.998
	20.4	51.1	132	256	513	1042	2082				
3	21.8	47.1	116	237	475	950	1873	0.000000289	0.00361	-0.0211	0.994
	18.7	49.5	131	269	540	1079	2088				
Mean	20.1	49.9	122	249	509	1015	1983	0.000000253	0.00334	-0.0158	0.993
S.D.	2.62	1.77	7.66	13.1	28.8	73.2	129	0.000000225	0.000952		
CV%	13.0	3.55	6.28	5.27	5.65	7.21	6.50				
RE%	0.416	-0.243	-2.45	-0.567	1.82	1.53	-0.846				

* value outside acceptance criteria(>15%), not used in calculations

Table S5: Within- and between-run imprecision (expressed as CV%) and inaccuracy (expressed as RE%) of KMF samples in RHB based on 3 series of 6 replicates at 5 different levels

Nominal concentration (ng/ml)	20.0	60.0	1000	1600	2000
Within-run Mean	21.3	60.4	1097	1608	1984
S.D.	1.25	1.38	7.45	18.3	22.8
CV%	5.86	2.28	0.679	1.14	1.15
RE%	6.50	0.58	9.73	0.475	-0.788
Between-run Mean	20.2	57.9	1102	1575	1950
S.D.	0.665	2.36	17.1	16.0	21.2
CV%	3.29	4.07	1.55	1.02	1.14
RE%	0.939	-3.46	10.2	-1.54	-2.49

Table S6: Within- and between-run imprecision (expressed as CV%) and inaccuracy (expressed as RE%) of 4-HPAA samples in RHB based on 3 series of 6 replicates at 5 different levels

Nominal concentration (ng/ml)	20.0	60.0	1000	1600	2000
Within-run Mean	20.2	57.4	995	1560	1993
S.D.	1.07	2.15	16.4	35.9	15.4
CV%	5.27	3.75	1.65	2.30	0.774
RE%	1.04	-4.40	-0.492	-2.50	-0.330
Between-run Mean	20.5	56.3	1029	1581	1969
S.D.	1.05	1.93	20.1	28.6	32.1
CV%	5.13	3.43	1.95	1.81	1.63
RE%	2.30	-6.23	2.93	-1.19	-1.55

Table S7: Carry-over assessment for KMF and $^{13}C_{15}$-labeled KMF (IS) in RHB

Run No.	Replicate	Peak response (counts)				Carry-over (%)		Mean Carry-over (%)	
		Blank sample		LLOQ					
		Analyte	IS	Analyte	IS	Analyte	IS	Analyte	IS
1	1	0.200	2.20	448	11928	0.04	0.0184	3.25	0.0617
	2	45.3	14.0	702	13329	6.45	0.105		
2	1	80.4	4.12	747	14241	10.8	0.0289	10.6	0.0938
	2	68.0	16.0	656	10082	10.4	0.159		
3	1	0.00	4.80	923	15029	0.00	0.0319	7.17	0.112
	2	164	31.0	1144	16112	14.3	0.192		
4	1	72.5	4.70	849	12939	8.54	0.0363	9.57	0.788
	2	79.3	14.3	748	11795	10.6	0.121		
					Mean	7.64	0.0866		

Table S8: Carry-over assessment for KMF and $^{13}C_{15}$-labeled KMF (IS) in HBSS

Run No.	Replicate	Peak response (counts)				Carry-over (%)		Mean Carry-over (%)	
		Blank sample		LLOQ					
		Analyte	IS	Analyte	IS	Analyte	IS	Analyte	IS
1	1	31.0	0.00	688	4917	4.51	0.00	9.02	0.169
	2	98.6	19.7	729	5829	13.5	0.338		
2	1	88.0	0.00	548	4621	16.1	0.00	17.5	0.00233
	2	134	0.274	710	5893	18.9	0.00		
3	1	0.00	0.00	99.0	686	0.00	0.00	5.51	0.00
	2	27.0	0.00	245	1888	11.0	0.00		
4	1	72.5	4.70	849	12939	8.54	0.0400	9.75	0.0788
	2	79.3	14.3	748	11795	10.6	0.121		
					Mean	10.4	0.0625		

Table S9: Carry-over assessment for 4-HPAA and vanillic acid (IS) in RHB.

Run No.	Replicate	Peak response (counts)				Carry-over (%)		Mean Carry-over (%)	
		Blank sample		LLOQ					
		Analyte	IS	Analyte	IS	Analyte	IS	Analyte	IS
1	1	0.00	0.00	126	1996	0.00	0.00	0.00	0.00
	2	0.00	0.00	106	2108	0.00	0.00		
2	1	0.00	0.00	51.3	899	0.00	0.00	0.00	0.00
	2	0.00	0.00	75.0	967	0.00	0.00		
3	1	0.00	0.00	54.1	1163	0.00	0.00	0.00	0.00
	2	0.00	0.00	59.1	1377	0.00	0.00		
					Mean	0.00	0.00		

Table S10: Carry-over assessment for 4-HPAA and vanillic acid (IS) in HBSS.

Run No.	Replicate	Peak response (counts)				Carry-over (%)		Mean Carry-over (%)	
		Blank sample		LLOQ					
		Analyte	IS	Analyte	IS	Analyte	IS	Analyte	IS
1	1	0.00	0.00	1840	49470	0.00	0.00	0.00	0.00
	2	0.00	0.00	1681	85202	0.00	0.00		
2	1	0.00	0.00	51.3	899	0.00	0.00	0.00	0.00
	2	0.00	0.00	75.0	967	0.00	0.00		
3	1	0.00	0.00	54.1	1163	0.00	0.00	0.00	0.00
	2	0.00	0.00	59.1	1377	0.00	0.00		
					Mean	0.00	0.00		

Table S11: Selectivity test at the LLOQ (20.0 ng/ml) based on three different buffer batches (n=6)

	KMF		4-HPAA	
	RHB	**HBSS**	**RHB**	**HBSS**
Mean concentration (ng/ml)	19.2	21.0	19.2	22.6
S.D.	1.88	1.05	0.320	0.675
CV%	9.82	5.00	1.67	2.99
RE%	-4.04	5.03	-3.84	13.1

Table S12: Absolute recovery of KMF and $^{13}C_{15}$KMF (IS) from RHB (n=6)

	Analyte			IS
	QCL	**QCM**	**QCH**	
Nominal concentration (ng/mL)	**60.0**	**1000**	**1600**	**206.9**
Absolute recovery (%)	56.7	58.1	54.7	70.4
CV%	9.44	11.4	15.8	11.6
SD	5.35	6.63	8.64	8.16

Table S13: Absolute recovery of KMF and $^{13}C_{15}$KMF (IS) from HBSS (n=6)

	Analyte			IS
	QCL	**QCM**	**QCH**	
Nominal concentration (ng/mL)	**60.0**	**1000**	**1600**	**206.9**
Absolute recovery (%)	62.2	79.6	84.6	72.8
CV%	3.91	2.25	1.70	7.08
SD	2.43	1.79	1.43	5.15

Table S14: Absolute recovery of 4-HPAA and vanillic acid (IS) from RHB (n=6)

	Analyte			IS
	QCL	**QCM**	**QCH**	
Nominal concentration (ng/mL)	**60.0**	**1000**	**1600**	**827.6**
Absolute recovery (%)	89.8	96.4	95.3	97.6
CV %	15.8	3.73	2.41	1.10
SD	14.2	3.59	2.29	1.08

Table S15: Absolute recovery of 4-HPAA and vanillic acid (IS) from HBSS (n=6)

	Analyte			IS
	QCL	**QCM**	**QCH**	
Nominal concentration (ng/mL)	**60.0**	**1000**	**1600**	**1655**
Absolute recovery (%)	77.0	88.4	95.1	101
CV%	5.09	2.74	4.26	4.71
SD	3.92	2.42	4.05	4.77

Table S16: Dilution test of KMF in RHB and HBSS at nominal concentration of 10000 ng/ml (n=6)

	RHB		HBSS	
Dilution factor	**10X**	**100X**	**10X**	**100X**
Mean	11441	10005	10213	10350
S.D.	66.6	254	531	619
CV%	0.582	2.53	5.20	5.98
RE%	14.4	0.0517	2.13	3.50

Table S17: Dilution test of 4-HPAA in RHB and HBSS at nominal concentration of 10000 ng/ml (n=6)

	RHB		HBSS	
Dilution factor	**10X**	**100X**	**10X**	**100X**
Mean	10299	9377	11339	10088
S.D.	138	365	146	171
CV%	1.34	3.89	1.29	1.70
RE%	2.99	-6.23	13.4	0.880

Table S18: Short-term stability of KMF in RHB and HBSS during storage in various conditions (n=6), expressed as RE%

	RHB		HBSS	
Nominal concentration (ng/mL)	**60.0**	**1600**	**60.0**	**1600**
Freeze/thaw cycles below -65°C*	-9.22	-7.07	-5.93	-7.76
Stored for 4 h at RT	-9.59	-5.42	0.763	4.54
Processed samples stored in autosampler for 72 h at 10°C	-13.2	0.653	-	-

*two F/T cycles for RHB and three cycles for HBSS

Table S19: Short term stability of 4-HPAA in RHB and HBSS during storage in various conditions (n=6), expressed as RE%

	RHB		HBSS	
Nominal concentration (ng/mL)	**60.0**	**1600**	**60.0**	**1600**
Three successive freeze/thaw cycles below -65°C	-6.26	-3.18	7.58	4.08
Stored for 4 h at RT	-10.5	-4.28	-10.9	6.99
Processed samples stored in autosampler for 156 h at 10°C	-4.12	2.96	-	-

Table S20: Stock solution (SS) stability of KMF in DMSO, stored below -65°C for 180 days (n=6)

	KMF SS stored below -65°C for 180 days with freshly prepared IS SS	KMF SS freshly prepared with freshly prepared IS SS
Mean peak area ratio	2.70	2.61
S.D.	0.0122	0.0118
CV%	0.45	0.45
Difference%	-3.13	

Table S21: Stock solution (SS) stability of 4-HPAA in DMSO, stored below -65°C for 35 days (n=6)

	4-HPAA SS stored below -65°C for 35 days with freshly prepared IS SS	4-HPAA SS freshly prepared with freshly prepared IS SS
Mean peak area ratio	628	632
S.D.	15.3	30.1
CV%	2.43	4.76
Difference%	0.742	

Table S22: Stock solution (SS) stability of vanillic acid (VA) in DMSO, stored below -65°C for 190 days (n=6)

	VA SS stored below -65°C for 190 days with freshly prepared 4-HPAA SS	VA SS freshly prepared with freshly prepared 4-HPAA SS
Mean peak area ratio	229	238
S.D.	17.4	5.30
CV%	7.58	2.23
Difference%	3.81	

Table S23: Mean values of the most relevant *in silico* pharmacokinetic descriptors for KMF and 4-HPAA

QikProp descriptors (3D)								Chemaxon Marvin (2D)	
Compound	**MW**	**Donor HB**	**Accpt HB**	**$LogP_{o/w}$**	**LogBB**	**Human Oral Absorption (%)**	**PSA [Å^2]**	**$LogP_{o/w}$**	**PSA[Å^2]**
KMF	286	3.00	4.50	1.09	-1.82	64.8	119	2.46	107
4-HPAA	152	2.00	2.75	1.27	-0.860	68.7	72.9	1.31	60.4

Table S23: Mean values of the most relevant *in silico* and experimental pharmacokinetic descriptors for KMF and 4-HPAA

	QikProp descriptors (3D)							Chemaxon Marvin (2D)			Exp.
Com-pound	**MW**	**Donor HB**	**Accpt HB**	**$LogP_{o/w}$**	**LogBB**	**Human Oral Absorption (%)**	**PSA [Å^2]**	**$LogP_{o/w}$**	**$LogD_{7.4}$**	**PSA [Å^2]**	**pK_a**
KMF	286	3.00	4.50	1.09	-1.82	64.8	119	2.46	1.31	107	7.49, 7.96
4-HPAA	152	2.00	2.75	1.27	-0.86	68.7	73	1.31	-1.86	60	4.25, 9.98

4. Conclusion and Outlook

To accelerate HPLC-based discovery and de-replication process of allosteric $GABA_A$ receptor modulators from natural sources, an in-house assay was developed with zebrafish larvae. PTZ-provoked locomotor-activity assay was established using 7dpf larvae in a 96-well format, and automated tracking of larval locomotion with an IR-sensitive camera. PTZ concentration, number of larvae, incubation time of larvae with test solutions, duration of the experiment, as well as data capturing and analysis were defined as the main assay parameters relevant for the quality of data, which had not been validated in previous publications.

PTZ effect on zebrafish larvae was concentration-dependent. A direct-linear correlation was found between the 25-min total locomotion and PTZ concentrations up to 10 mM. However, the concentration-activity dependency at higher PTZ levels (between 10 and 20 mM) was rather reflected by variations of latency to different seizure stages. A faster transition of seizure behavior to the last stage (body stiffening) resulted in reduction of total locomotion and therefore, an inverse concentration-activity relationship. It has been concluded that the concentration of PTZ being used in the bioassay considerably impacts the outcome of the screenings for $GABA_A$ receptor modulators, and unoptimized PTZ concentrations may easily result in false-positive/negative data.

Patterns of PTZ-provoked locomotion were visualized by plotting movement *vs*. time, whereby total locomotion was summed in 5-min intervals. Variations of the latency to different seizure stages could be tracked with the aid of the locomotion patterns and were taken into account for data interpretation, along with the total larval locomotion (mm). In previous publications, total larval locomotion (mm) during the tracking period was employed for quantitative analysis of the seizure behavior, independently. This could increase the tendency of the bioassay to pick false positive results.

With respect to concentrations of test samples, a maximum tolerable concentration (MTC) was determined for each compound/extract, which was then used as the highest test concentration. Monitoring the signs of toxicity for 24 h revealed that a 3-hour exposure would suffice absorption of the compounds to exhibit toxicity, as well as activity. A longer incubation of larvae with test solutions has been avoided to minimize the risk of decomposition of test compounds in the aqueous medium, and also their metabolism in the organism body. Both of which, may either wipe out the activity or lead to the appearance of more active artifacts.

In conclusion, the final assay protocol included incubation of larvae with the test samples for 3 h, induction of larval locomotion by 10 mM PTZ, identification of $GABA_A$ receptor

modulators through a decrease in total larval locomotion during 25 min tracking period, and confirmation of the data interpretation with the patterns of larval locomotion. The statistical significance of data was ensured with employment of an appropriate number of larvae in the experiment (n = 16 per test sample), and by consideration of minimum two replicates for each examination.

Given that in zebrafish larvae the test compounds have to be absorbed and systemically distributed to reach the target tissues at relevant concentrations, the model is reasonably exclusive for drug-like compounds. This has been corroborated with examination of a series of $GABA_A$-receptor agonistic natural products which have been purified from our in-house extract library including: sophoraflavanone G (isolated from roots of *Sophora flavescens*) [1], sanggenon C (isolated from roots of *Morus alba*) [2], dehydroabietic acid (isolated from *Boswellia thurifera* resin) [3] and sandaracopimaric acid (identified in *Biota orientalis* leaves). [4] Lowering of locomotor activity was found for these compounds with exception of sanggenone C. Various descriptors relevant to blood-brain-barrier (BBB) permeability of the compounds (PSA, cLogP, number of H-donor and acceptor sites, and number of rotatable bonds) were calculated *in silico*. The calculated physicochemical properties of sanggenone C predicted a lack of permeability of the compound across the BBB. Lack of activity in this example was indicative of the presence of a functional and size-exclusive BBB in the zebrafish larvae.

The zebrafish locomotor-activity assay was successfully translated into the HPLC-based activity profiling approach. Applicability of the protocol to localize the active compounds in analytical HPLC separations of extracts was confirmed with EtOAc extracts from *Magnolia officinalis* and *Valeriana officinalis* which previously showed activity in the same bioassay. The validated protocol was finally employed for discovery of new scaffolds targeting the $GABA_A$ receptor.

It is known that PTZ-induced seizures in zebrafish larvae may also be prevented by compounds acting on other targets than $GABA_A$ receptors. [5-7] Therefore, we used the functional assay with *Xenopus* oocyte model for the primary screening of extract libraries. A selection of extracts from South African medicinal plants, traditionally used for treatment of epilepsy and other neurological disorders, were screened in the *Xenopus* oocyte assay. The extracts with promising *in vitro* activities were submitted to the zebrafish larval assay described herein. Among these, a DCM extract from *S. pyroides* leaves had the ability of lowering PTZ-provoked larval locomotion. HPLC-based profiling followed by targeted

isolation of phytochemicals in the active time-window, revealed identification of the active constituents as anacardic acid derivatives. The GABAergic activity of pure compounds has been confirmed with both zebrafish larvae and *Xenopus* oocytes assays. This was the first report on pharmacological active principles of *S. pyroides*.

Application of the in-house zebrafish behavioral model has accelerated the discovery process of $GABA_A$ receptor modulating NPs by reduction of the turnaround time of the activity data. The *Xenopus* oocytes assay, as our external bioactivity model, was used as the primary screening method for the extract library to obtain hit extracts that were active and specifically acting on $GABA_A$ receptors while being excluded from the HPLC-based profiling step of the discovery process.

Rather than the extract of *S. pyroides*, some additional plant extracts have been examined and showed differing levels of activity in the zebrafish model. These extracts have the potential to be investigated in the future as a source of "drug-like" $GABA_A$ receptor modulating scaffolds. Moreover, the validated protocol has been transferred to the University of the Free State in South Africa and would be applied to discovery of further GABAergic NPs in future studies.

The zebrafish larvae locomotor activity assay can logically serve as a bridging model between high-throughput *in vitro* assays and lower-scale *in vivo* mammalian models. We previously identified a series of allosteric $GABA_A$ receptor agonists with the aid of *in vitro* electrophysiological assay. Following the *in vitro* target-based studies, examination of the promising active molecules with the new larval zebrafish model will enable access to the compounds that perform well *in vivo*.

Last but not least, plant extracts are complex cocktails of phytochemicals. Some might be mixtures of both anti- and proconvulsive constituents. Interestingly, the zebrafish locomotor activity model can localize both types of pharmacological activities in the HPLC profile of extracts, simultaneously. Proconvulsive activity of NPs can be tracked by either "increase of total larval locomotion" or "reduction of latency to the larval seizure stages". This aspect of the assay needs to be validated by detailed investigations prior to further applications.

The next part of this research on CNS-active natural products addressed ADME properties of selected compounds as definitive parameters for their route of administration. Intestinal barrier and BBB permeability, the main ADME challenges for orally administered neuroactive compounds, were studied for KMF and 4-HPAA in cell-based models. Caco2 cells were employed in the intestinal permeability model, while BBB transport studies were

performed with a human immortalized hBMEC cell model along with a primary triple co-culture (RBECs, pericytes and glial cells) rat model.

The compounds had to be analyzed in transport media for determination of their permeability coefficients across the cell monolayers. Therefore, specific, selective, accurate, and precise UHPLC-MS/MS methods for quantification of KMF and 4-HPAA were developed and validated in the corresponding transport media (RHB and HBSS). Method validation was according to EMA and FDA guidelines. The range of quantification for both compounds was 20.0 – 2000 ng/ml and the standard calibration curves were quadratic with a weighting factor of $1/X^2$ and $R^2 > 0.99$, for all methods. Following the stability assessments of KMF and 4-HPAA in biological samples, 4 h of sample collection and handling at RT, two weeks storage below -65°C, and maximum two freeze-thaw cycles were defined as the acceptable maintenance conditions to prevent alteration of the compounds and ensure reliability of results. The processed samples could be stored in the autosampler (10°C) for at least 48 hours. Sample dilution up to 100-fold did not impact the precision and accuracy of the method.

The validated methods were applied for *in vitro* membrane permeability studies. KMF was found to cross the intestinal barrier and the BBB to a significant extent, while 4-HPAA showed only slow permeation. KMF had a time-dependent decreasing recovery in the intestinal barrier model. This suggested that KMF would undergo an extensive metabolism by the intestinal cells which may result in poor bioavailability after oral administration. Efflux ratios (< 2) and the calcein-AM uptake assay in PBCEC indicated that KMF and 4-HPAA were neither P-gp substrates nor P-gp inhibitors. Our *in vitro* data supported the previously described *in vivo* CNS effects of KMF while the role of 4-HPAA needs to be elucidated in further studies.

The fact that i.p. application of 4-HPAA in mice induced behavioral changes [8] despite poor BBB permeability may have several explanations. For instance, 4-HPAA may indirectly impact the CNS *via* involvement of the gut-brain axis. [9] Also considering that *in vitro* models do not fully mimic an *in vivo* situation, it can be speculated that a slow penetration of 4-HPAA into the brain (lower than the detection ability of *in vitro* assays) may be sufficient for exerting its pharmacological activity. Some of the differences, including the lack of blood flow, and lower surface area, in *in vitro* models are crucial for compounds with a rapid turnover rate. [10] Moreover, metabolites of 4-HPAA might be responsible for the observed activity given that 4-HPAA undergoes further metabolism by colonic microflora into p-hydroxybenzoic acid, phenylacetic acid, and 4-methoxyphenylacetic acid. [11, 12] The role of

these corresponding metabolites, in anxiolytic performance of 4-HPAA, needs to be further studied in the future.

References:

[1] Yang, X., Baburin, I., Plitzko, I., Hering, S., Hamburger, M., HPLC-based activity profiling for $GABA_A$ receptor modulators from the traditional Chinese herbal drug Kushen (*Sophora flavescens* root), Molecular Diversity. 15 (2011) 361-72.

[2] Kim, H. J., Baburin, I., Zaugg, J., Ebrahimi, S. N., Hering, S., Hamburger, M., HPLC-based activity profiling--discovery of sanggenons as $GABA_A$ receptor modulators in the traditional Chinese drug Sang bai pi (*Morus alba* root bark), Planta Medica. 78 (2012) 440-7.

[3] Rueda, D. C., Raith, M., De Mieri, M., Schöffmann, A., Hering, S., Hamburger, M., Identification of dehydroabietc acid from *Boswellia thurifera* resin as a positive $GABA_A$ receptor modulator, Fitoterapia. 99 (2014) 28-34.

[4] Zaugg, J., Khom, S., Eigenmann, D., Baburin, I., Hamburger, M., Hering, S., Identification and characterization of $GABA_A$ receptor modulatory diterpenes from *Biota orientalis* that decrease locomotor activity in mice, Journal of Natural Products. 74 (2011) 1764-72.

[5] Baraban, S., Taylor, M., Castro, P., Baier, H., Pentylenetetrazole induced changes in zebrafish behavior, neural activity and c-fos expression, Neuroscience. 131 (2005) 759-68.

[6] Afrikanova, T., Serruys, A. S. K., Buenafe, O. E., Clinckers, R., Smolders, I., de Witte, P. A., et al., Validation of the zebrafish pentylenetetrazol seizure model: locomotor versus electrographic responses to antiepileptic drugs, PLoS One. 8 (2013) e54166.

[7] Baxendale, S., Holdsworth, C. J., Santoscoy, P. L. M., Harrison, M. R. M., Fox, J., Parkin, C. A., et al., Identification of compounds with anti-convulsant properties in a zebrafish model of epileptic seizures, Disease Models and Mechanisms. 5 (2012) 773-84.

[8] Vissiennon, C., Nieber, K., Kelber, O., Butterweck, V., Route of administration determines the anxiolytic activity of the flavonols kaempferol, quercetin and myricetin – are they prodrugs?, Journal of Nutritional Biochemistry. 23 (2012) 733-40.

[9] Reardon, S., Gut-brain link grabs neuroscientists, Nature. 515 (2014) 175-7.

[10] Chen, M. L., Amidon, G. L., Benet, L. Z., Lennernas, H., Lawrence, X. Y., The BCS, BDDCS, and regulatory guidances, Pharmaceutical Research. 28 (2011) 1774.

[11] Labib, S., Hummel, S., Richling, E., Humpf, H. U., Schreier, P., Use of the pig caecum model to mimic the human intestinal metabolism of hispidulin and related compounds, Molecular Nutrition & Food Research. 50 (2006) 78-86.

[12] Serra, A., Macià, A., Romero, M. P., Reguant, J., Ortega, N., Motilva, M. J., Metabolic pathways of the colonic metabolism of flavonoids (flavonols, flavones and flavanones) and phenolic acids, Food Chemistry. 130 (2012) 383-93.

Acknowledgments

I would like to thank Prof. Matthias Hamburger for giving me the opportunity to join his research group, for his support, advices and encouragement during my entire PhD program.

My sincere appreciation goes to Dr. Veronica Butterweck and Dr. Mouhssin Oufir for the great support in ADME and bioanalytical studies of my PhD.

I would like to express my gratitude to Dr. Muriel Cuendet who accepted to be the co-referee of my PhD examination.

Thanks to Dr. Maria de Meri for the assistance in structure elucidation of natural compounds, to Dr. Henry Beltig for giving me the access to the zebrafish facility, to Hannes van der Merwe and Anke Wilhelm for their fruitful cooperation in Zebrafish studies.

A big thank to Orlando and Manuela for the assistance in the laboratory and administration issues.

Also, I would like to thank my dear Teresa for proof-reading my thesis and my dear Justine for being a great accompany when finalizing my writings.

My warm thanks to all friends, current and former colleagues at the Division of Pharmaceutical Biology in Basel for their friendship and constant support, for the great atmosphere in the lab, at the coffee breaks, by weekly planning's, bowling, fondue, cookie and movie parties, and for much other small happiness which made me always feeling at home.

Finally, very special thanks to my family for their love, support and encouragement.